HYBRID INORGANIC-ORGANIC, ORGANIC CHARGE TRANSFER, AND RADICAL BASED COMPOUNDS WITH CHALCOFULVALENE DONORS AND ORGANIC ACCEPTORS

A Dissertation

by

ERIC WADE REINHEIMER

Submitted to the Office of Graduate Studies of
Texas A&M University
in partial fulfillment of the requirements for the degree of

DOCTOR OF PHILOSOPHY

December 2007

Major Subject: Chemistry

HYBRID INORGANIC-ORGANIC, ORGANIC CHARGE TRANSFER, AND RADICAL BASED COMPOUNDS WITH CHALCOFULVALENE DONORS AND ORGANIC ACCEPTORS

A Dissertation

by

ERIC WADE REINHEIMER

Submitted to the Office of Graduate Studies of
Texas A&M University
in partial fulfillment of the requirements for the degree of

DOCTOR OF PHILOSOPHY

Approved by:

Chair of Committee,	Kim R. Dunbar
Committee Members,	Francois P. Gabbaï
	Raymond E. Schaak
	Donald G. Naugle
Head of Department,	David H. Russell

December 2007

Major Subject: Chemistry

ABSTRACT

Hybrid Inorganic-Organic, Organic Charge Transfer, and Radical Based Compounds with Chalcofulvalene Donors and Organic Acceptors**.** (December 2007)

Eric Wade Reinheimer, B.S., California State Polytechnic University, Pomona;

M.S., California State Polytechnic University, Pomona

Chair of Advisory Committee: Dr. Kim R. Dunbar

The primary focus of this dissertation is the electrochemical preparation of radical cation salts utilizing the donor *o*-4,4'-dimethyltetrathiafulvalene (*o*-Me_2TTF) and spherical, tetrahedral, octahedral, bimetallic, cyanometallate, and polyoxometallate anions. Other donors, such as tetramethyl(tetraselenafulvalene) (TMTSF), tetramethyl(tetrathiafulvalene) (TMTTF), bis(ethylenedithio)tetrathiafulvalene (BEDT-TTF or ET), and bis(propylenedithio)tetrathiafulvalene (BPDT-TTF or PT) also found use in the preparation of salts in the course of this study. X-ray structural characterization of these salts revealed stacking between donor molecules containing significant S•••S interactions in the solid state. Various salts were subjected to either conductivity or molecular magnetism measurements in order to determine the level of itinerant electron density and magnetic contribution from paramagnetic charge compensating anions. In order to expand the library of TTF-containing hybrid materials prepared through metathesis, salts of other tetrathiafulvalenium radicals have also been prepared and characterized crystallographically and by select spectroscopic methods.

In an effort to gain further information on formation of organic charge transfer complexes, TTF was combined with nitrofluorenone family of acceptors as well as the organocyanide acceptors HAT-$(CN)_6$ (HAT-$(CN)_6$ = 1,4,5,8,9,12-hexaazatriphenylene-hexacarbonitrile) and TCNB (TCNB = 1,2,4,5-tetracyanobenzene). The complexes were characterized using X-ray crystallography, infrared spectroscopy, and molecular magnetism. All of these techniques showed that all compounds underwent little to no charge transfer.

Commencing in 2003, the combined work of Dunbar and Omary revealed that systems combining inorganic donors with chelating, sulfur-based ligands and organic acceptors could have their spectroscopic response tuned to display low-energy charge transfer bands extending into the near-IR making them suitable candidates as photosensitizing dyes for semiconductors. In keeping with this idea, new layered charge transfer compounds combining the nitrofluorenone family of acceptors and the inorganic donor Pt(dbbpy)(tdt) (tdt = 3,4-toluenedithiolate) were prepared. The resulting complexes were characterized utilizing X-ray crystallography as well as both spectroscopic and electrochemical methods. Similar analyses were also conducted on various platinum/terpyridine salts and illustrated a level of spectroscopic tunability to that observed for the supramolcular systems composed of inorganic donors and organic acceptors.

To My Family and Friends:

You have all made me a better person and have encouraged me to be the best person I could everyday. I love you all!

ACKNOWLEDGEMENTS

First and foremost, I would like to thank my mother Jill Reinheimer and brother Todd Reinheimer who encouraged me and listened to me whenever I hit the dry times during my doctoral studies. They were the rock that I supported myself against whenever times got tough. The road to the end has been paved with their love and support.

I also need to extend a hand of thanks to the Thorne family who came into my life through the marriage of their daughter Michelle to my brother. They have always asked how I've been doing in the work I've done and along with my mom, provided me a nice place to visit and some great food when on vacation.

Thanks, next, to Kerrie Gath, who served as another lifeline for support while in Texas. Some of the best times at Texas A&M University have been had with her whenever we had a chance to cook dinner together and share our feelings.

Many, many thanks must also go to my advisor Prof. Kim Dunbar, who encouraged and inspired me to achieve results in chemistry that I never dreamed possible.

I also extend thanks to my graduate committee of Dr. Gabbaï, Dr. Schaak, and Dr. Naugle for their assistance in the learning process.

Thank you to my friends Brent, Jared, Adriana, and Billy who became more to me than just friends, they became my family.

Thanks also to my Texas parents: Michael and Elaine Koehn and Charlene Campbell. You have all taken care of me and done your part to treat me as a son. My thanks and love for you transcends words.

Thanks to my friends and labmates who preceded me: Brad, Karn, Eric Schelter, Curtis, Mijeong, and Alfredo. I thank you all for the example you set and research trails you blazed. Your instruction and guidance were invaluable.

Merv, you left us all before your time, and you took me under your wing and trained me. You were a great friend and are sorely missed. We will argue more about Star Trek someday and in case you forgot, Captain Kirk was always the better starship captain.

Thank you to the current members of the Dunbar group: Mashalle, Ben, Brandi, Carolina, Matt, Helen, Ferdi, Ed, Kristen, Nazario, Dafhne, Ian, and Sofi, for all of the camaraderie you have supplied over the years. I wish you all the best with everything that you do.

I thank Mike and Han for their assistance with the X-ray crystallography of some of the compounds presented in this dissertation and Andrew for assistance with some of the magnetic measurements. I thank Dr. Jose-Ramon Galán-Mascarós for teaching me how to conduct electrocrystallization experiments and Profs. Marc Fourmigué and Patrick Batail for valuable discussions regarding the salts prepared using electrocrystallization. Thanks also go to Prof. Mohammad Omary, Joshua Hudson, and Joyce Chen for valuable discussions regarding our collaborative projects.

Despite his rough exterior, I would also like to acknowledge radio disk jockey Howard Stern for providing some hilarious radio to listen to during the writing process.

TABLE OF CONTENTS

LIST OF FIGURES

FIGURE Page

FIGURE Page

FIGURE Page

FIGURE Page

FIGURE Page

FIGURE Page

FIGURE Page

FIGURE Page

FIGURE Page

FIGURE Page

LIST OF TABLES

TABLE Page

TABLE Page

TABLE Page

TABLE Page

NOMENCLATURE

Å	Angstrom
Ag/AgCl	silver-silver chloride reference
BEDO-TTF	bis(ethylenedioxo)tetrathiafulvalene
BEDT-TTF or ET	bis(ethylenedithio)tetrathiafulvalene
BEDT-TSF or BETS	bis(ethylenedithio)tetraselenafulvalene
BEDS-TTF or BEST	bis(ethylenediseleno)tetrathiafulvalene
BET-TTF	bis(ethylenethia)tetrathiafulvalene
BMDT-TTF or MT	bis(methylenedithio)tetrathiafulvalene
BPDT-TTF or PT	bis(propylenedithio)tetrathiafulvalene
bpy	2,2'-bipyridine
cbt	4-chlorobenzenethiolate anion
cm^{-1}	wavenumbers
Cp*	pentamethylcyclopentadiene
CT	charge transfer
CV	cyclic voltammetry
dbbpy	4,4'-di-*tert*-butyl-2,2'-bipyridine
dcbpy	4,4'-dicarboxy-2,2'-bipyridine
dmbpy	4,4'-dimethyl-2,2'-bipyridine
dmbt	3,4-dimethylbenzenethiolate anion
dmeobt	2,5-dimethoxybenzenethiolate anion
dmid	1,3-dithiole-2-one-4,5-dithiolate anion
DMSO	dimethyl sulfoxide

DMDPTTF	dimethyldiphenyltetrathiafulvalene
DNF	2,7-dinitro-9-fluorenone
dpphen	4,7-dimethyl-1,10-phenanthroline
ecda	1-(ethoxycarbonyl)-1-cyanoethylene-2,2-dithiolate anion
E-Me_2TTF	*E*-4,4'-dimethyltetrathiafulvalene
ε	molar extinction coefficient
HAT-$(CN)_6$	1,4,5,8,9,11-hexaazatriphenylenehexacarbonitrile
HOMO	highest occupied molecular orbital
ILCT	intraligand charge transfer
K	Kelvin
λ	wavelength
LLCT	ligand-to-ligand charge transfer
LUMO	lowest unoccupied molecular orbital
M	molar concentration (# mol solute/L solvent)
MM'LLCT	mixed metal/ligand-to-ligand charge transfer
Me	methyl group ($-CH_3$)
mbt	4-methylbenzenethiolate anion
MLCT	metal-to-ligand charge transfer
mnt	maleonitriledithiolate anion
SOMO	singly-occupied molecular orbitals
o-Me_2TTF	*o*-4,4'-dimethyltetrathiafulvalene
ox	oxalate dianion ($[C_2O_4]^{2-}$)
TBA	tetra-*n*-butylammonium cation ($N[n\text{-}Bu]_4]^+$)

tbtrpy	4,4',4''-*t*-butyl-2,2';6',2''-terpyridine
tdt	3,4-toluenedithiolate
TCNB	1,2,4,5-tetracyanobenzene
TCNE	tetracyanoethylene
TCNQ	7,7,8,8'-tetracyanoquinodimethane
$TCNQF_4$	2,3,5,6-tetrafluoro-7,7',8,8'-tetracyanoquinodimethane
TEA	tetra-*n*-ethylammonium ($N[CH_2CH_3]_4^+$)
TENF	2,4,5,7-tetranitro-9-fluourenone
THF	tetrahydrofuran
TMTTF	tetramethyltetrathiafulvalene
TMTSF	tetrametheyltetraselenafulvalene
TTF	tetrathiafulvalene
TRNF	2,4,7-trinitro-9-fluorenone
trpy	2,2';6',2''-terpyridine
TPTTF	tetraphenyltetrathiafulvalene

CHAPTER I

INTRODUCTION: SULFUR-BASED CHARGE TRANSFER SYSTEMS

For the last three decades, the design of materials exhibiting tunable conducting, magnetic, or optoelectronic properties has been a focus of great interest in the chemistry community. Typically, organic and inorganic chemists have undertaken the pursuit of these goals separately.[1] Recent results have demonstrated that the highest probability of preparing "hybrid" materials that exhibit a combination of the aforementioned properties in one material exists at the interface of these chemical disciplines.[2] Two excellent illustrations of this fact are the discovery of superconducting charge-transfer salts composed of BEDT-TTF radicals and paramagnetic metal-based anions, and conducting charge-transfer salts with ferromagnetic ordering.[3,4] Also, research in the area of organic radicals has led to the discovery of materials with properties once considered to be mutually exclusive in one material, namely superconductivity and magnetism.

The co-existence of these properties has been found to be accessible with the lanthanide metals as well as with the donor-acceptor organic and metal systems.[5,6,7] These discoveries are paving the way for continued research to prepare dual-property materials capable of behaving both as conductors and magnets.

This dissertation follows the style and format of *Journal of the American Chemical Society*.

The origins of the field of conducting materials can be traced back to the discovery of the molecule tetrathiafulvalene (TTF). This molecule was first synthesized in 1970 by Fred Wudl and coworkers and was found to be capable of undergoing two reversible oxidations.[8] TTF behaves as an electron donor and the radical form is stabilized by extended π-orbital overlap in the material. Density-functional calculations carried out on TTF with optimized D_2h symmetry revealed that the HOMO (highest occupied molecular orbital) and LUMO (lowest unoccupied molecular orbital) have the symmetries b_{1u} and b_{2g} respectively, that the highest level of electron density resides on the TTF core, and that the HOMO has nodes on the C-S bonds.[9] A new field of research was opened when solutions of TTF were mixed with the organocyanide acceptor 7,7,8,8-tetracyanoquinodimethane (TCNQ) (Figure 1). The material TTF-TCNQ is the first all-organic system to display metallic conductivity.[10] The material displays a room temperature conductivity of 500 $S \bullet cm^{-1}$ and a maximum conductivity of 10^4 $S \bullet cm^{-1}$ at 66K. This high level of conductivity is a consequence of partial electron transfer between the TTF donor and TCNQ acceptors of approximately 0.55-0.59 electrons per donor molecule; the result is a high level of conductivity caused by the formation of partially-occupied valence shells.[11]

Networks of oxidized stacks of TTF (or its donors) are important for the formation of conducting materials because of the tendency of oxidized donors to stack in the solid-state. With the presence of diffuse π-orbitals, the donor molecules can engage in intermolecular interactions. Favorable overlap occurs between orbitals of similar symmetry and energy which are in close proximity; this scenario is most often observed in segregated stacks of donors and acceptors.

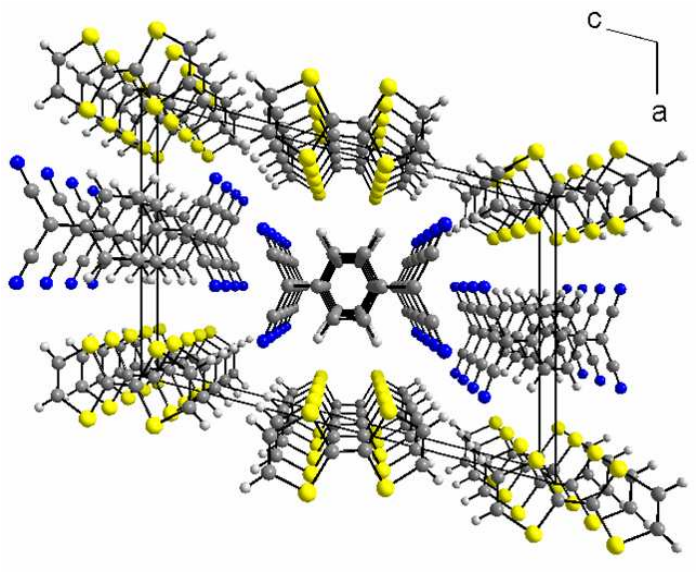

Figure 1. Structure of TTF-TCNQ.

With favorable orbital overlap, electron density can be delocalized throughout the stacks, which when coupled with redox-active molecules, can lead to the formation of fractionally-occupied valence shells. High levels of conductivity arise when the solid-state packing allows for the close orientation of molecules of similar symmetry such that electronic diffusion can occur throughout the stacks resulting in the formation of a band structure for the TTF molecules.[12]

Two paradigms have gained universal acceptance for the preparation of charge transfer systems. The most popular method for the preparation of these materials is to combine independent donors and acceptors to form charge transfer materials. A second avenue for preparing hybrid charge-transfer materials that has gained a following in the recent years is the direct coordination of acceptors to donors through intervening

heteroatoms such as a nitrogen, phosphorus, or sulfur atom. This has been the approach used by groups such as Dunbar, Fourmigué, and Kobayashi to prepare interesting coordination compounds wherein TTF donors are ligated to transition metal atoms through various donor atoms.[13]

Since the discovery of TTF-TCNQ, various derivatives of TTF have been prepared, and materials containing those donors in their oxidized forms have been synthesized. Oxidation of these donors was first achieved by chemical means using oxidizers such as TCNQ and iodine. Later, after the preparation of the Bechgaard series of salts, the method of electrochemical oxidation was found to be a suitable method for preparing materials containing partially-oxidized chalcofulvalene moieties.[14] With this technique, an anion and neutral donor molecule are dissolved and exposed to a slight anodic current. The exposure of the neutral donor to this current slowly oxidizes the donor to its radical cation resulting in the formation of salts where the TTF (or its derivatives) aggregate in stacks and the corresponding anions are evenly distributed throughout the crystalline lattice.

As stated previously, electrochemical oxidation has been demonstrated as a successful technique for the preparation of systems containing oxidized chalcofulvalene donors after the initial report by Bechgaard and coworkers of the one-dimensional organic mixed-valence cation-radical salt $(TMTSF)_2PF_6$ (Figure 2).[14] This salt, and its counterparts with $[BF_4]^-$, $[AsF_6]^-$, $[SbF_6]^-$, and $[NO_3]^-$ are interesting examples of the results obtained via this technique, as they are the first examples of organic superconductors.

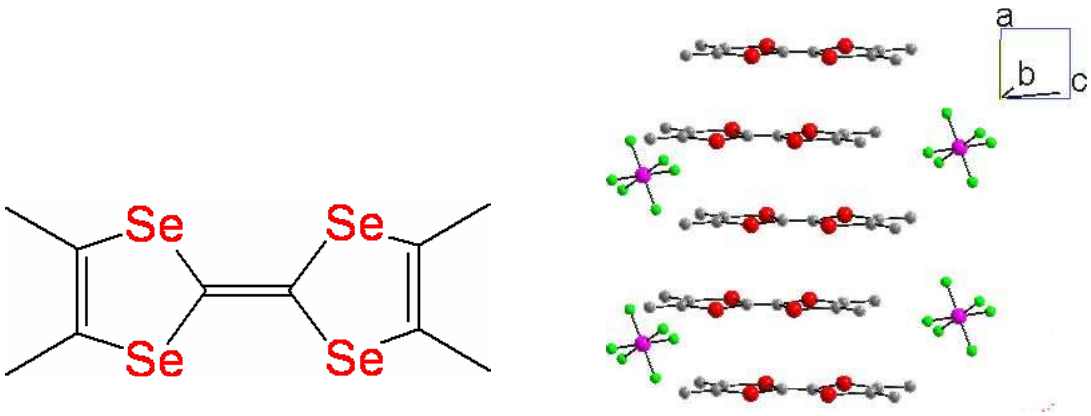

Figure 2. Schematic representations of TMTSF and the X-ray crystal structure of the superconducting Bechgaard salt $(TMTSF)_2PF_6$.

After the discovery of the Bechgaard salts which enter a superconducting state at temperatures below 0.9 K, a search began for methods to prepare higher temperature superconductors.[15] The discovery of the donor molecule bis(ethylenedithio)tetrathia-fulvalene and its incorporation into superconducting systems led to the next generation of superconductors. The temperatures at which the onset of super-conductivity was observed were approximately a magnitude higher than those in the Bechgaard salts. In all sulfur- or selenium-containing organic molecules, the temperature at which superconductivity is observed, (Tc), is strongly dependent upon the stacking motif as well as the pressure and/or chemically-induced stabilization of the corresponding anion.[16] Several phases of BEDT-TTF have been shown to exist and their corresponding observed properties are strongly dependent on the intermolecular sulfur-sulfur inter-actions.[17] The ability of these molecules to engage in inter-stack interactions leads to increased dimensionality in the solid-state and a resultant stabilization of the super-conducting state. These intermolecular interactions and their ability to increase the solid-state

dimensionality also decreases the possibility of observing a spin-Peierls distortion which interrupts electronic delocalization over the entire system by forming isolated units such as dimers which leads to charge localization.

Part 1: Hybrid Conducting Systems Prepared by Electrochemical Synthesis

The preparation of higher temperature superconductors is only one of the advances in the field of charge transfer chemistry. Another interest of chemists is to prepare materials in which mutually-exclusive properties such as super or metallic conductivity, magnetism, or optoelectronic responses can be engendered in a single material. In an attempt to prepare materials that exhibited both a superconducting and magnetic response, Day and coworkers combined BEDT-TTF with $[Fe(C_2O_4)_3]^{3-}$ to yield the salt $[(BEDT\text{-}TTF)]_4(H_2O)Fe(C_2O_4)_3 \bullet C_6H_5CN$ which is the first material to exhibit superconductivity in the presence of paramagnetic metal anions (Figure 3).[3]

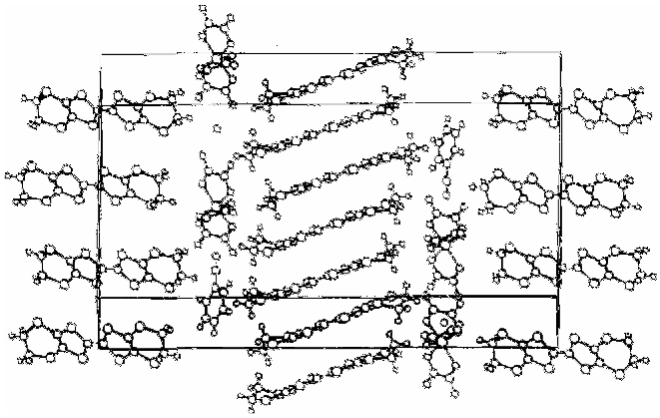

Figure 3. X-ray crystal structure of the superconducting salt $(BEDT\text{-}TTF)_4(H_2O)Fe(C_2O_4)_3 \bullet C_6H_5CN$.[3]

Later, work by Coronado and coworkers involved the concept of designing multi-functional materials by combining BEDT-TTF with a paramagnetic oxalate-bridged layer network to yield the first molecular-metal ferromagnet reported in the year 2000 (Figure 4).[4]

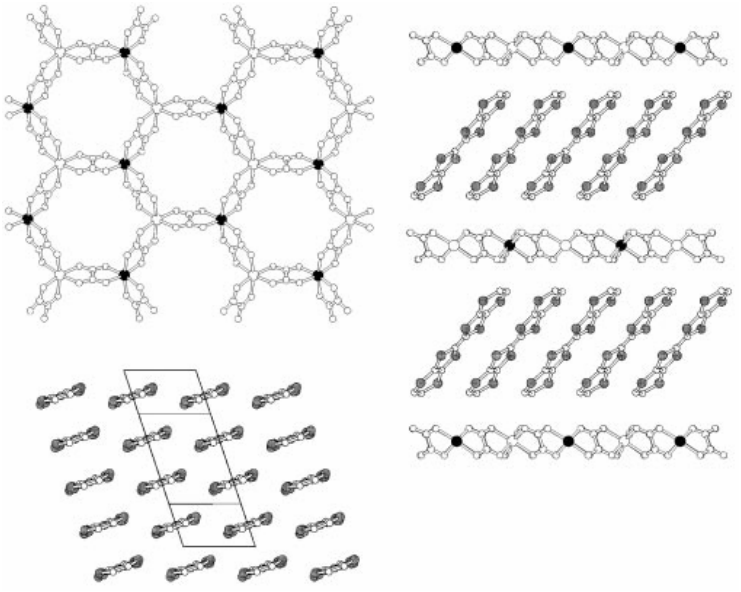

Figure 4. X-ray crystal structure of the molecular-metal ferromagnet (BEDT-TTF)$_3$[MnCr(ox)$_3$]•CH_2Cl_2.[4]

Later in 2003, the same group reported a similar result with bis(ethylenedithio)-tetraselenafulvalene (BEDT-TSF or BETS).[18] The compound with BEDT-TTF is metallic down to 0.3 K, while with BETS, the salt is metallic down to about 150 K. This is believed to be related to the differences in the packing of the organic donors in the crystals (Figure 5).

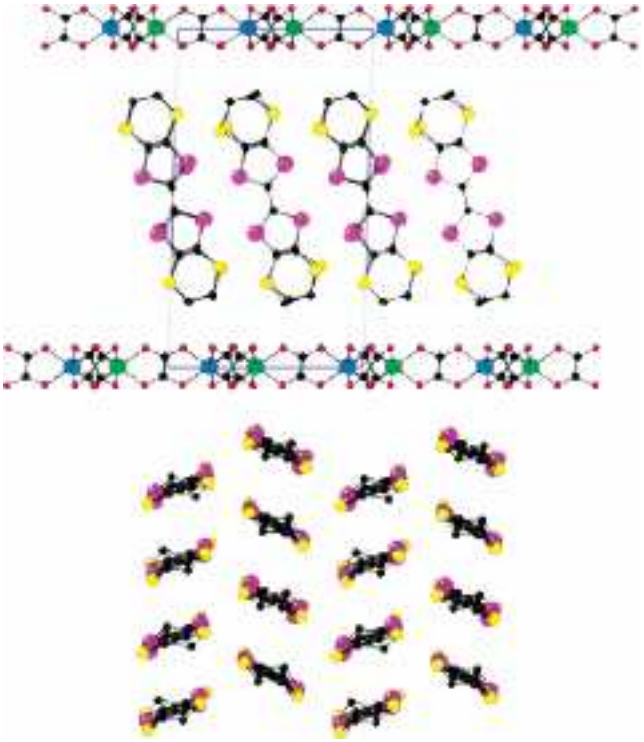

Figure 5. X-ray crystal structure of the molecular-metal ferromagnet $(BETS)_3[MnCr(ox)_3]\bullet CH_2Cl_2$.[18]

Interesting results have been obtained not only with paramagnetic oxalate-based layer compounds, but several strong semiconductors, metals, and superconductors have also been reported with the chalcofulvelene donors BEDT-TTF and BETS and metal salts. Among these results are those from Kurmoo and coworkers who reported the salt $(BEDT\text{-}TTF)_3[CuCl_4]\bullet H_2O$ which is a paramagnetic metal.[19] Coronado and coworkers were also successful in using the donor bis(ethylenethia)tetrathifulvalene (BET-TTF) (Figure 6) with $[FeCl_4]^-$ to prepare the salt $(BET\text{-}TTF)_2[FeCl_4]$ which displays metallic conductivity down to ~30 K (Figure 7).[20]

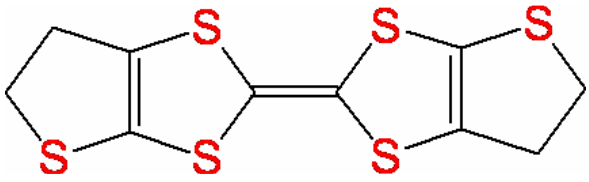

Figure 6. Schematic representation of BET-TTF.

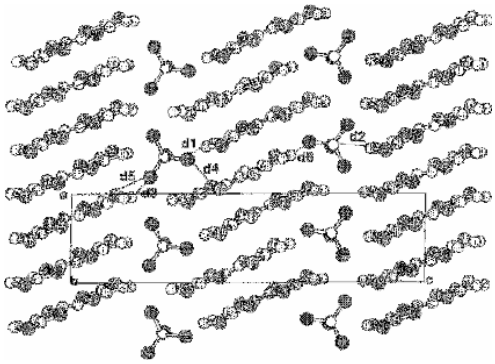

Figure 7. X-ray crystal structure of the conducting salt $(BET\text{-}TTF)_2[FeCl_4]$.[20]

An important discovery in this vein is the combination of tetrahedral transition metal anions in combinations with chalcofulvalene donors such as the salts $(BETS)_2[FeX_4]$ (X = Cl^- and Br^-) reported by Kobayashi and coworkers which exhibited antiferromagnetism and superconductivity (Figure 8).[21]

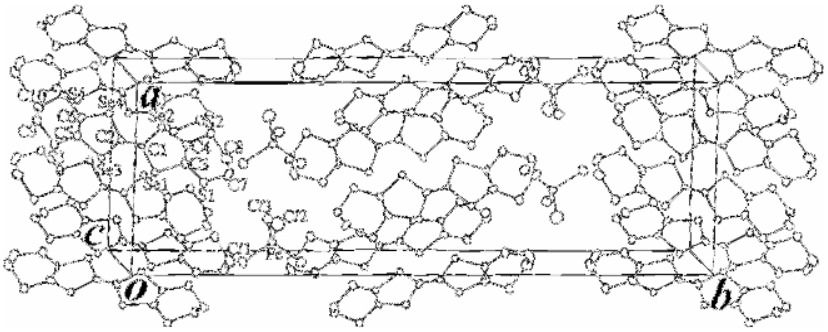

Figure 8. X-ray crystal structure of the superconducting salt κ-$(BETS)_2[FeCl_4]$.[21]

Another group of anions that has found considerable use in the preparation of potential dual-property materials are the octahedral anions hexacyanoferrate $[Fe(CN)_6]^{3-}$, hexacyanocobaltate $[Co(CN)_6]^{3-}$, and nitroprusside $[Fe(CN)_5NO]^{2-}$. The donors that have seen the most use in the preparation of salts based on these anions are BEDT-TTF, BET-TTF, the BEDT-TTF-like donor bis(ethylenediseleno)tetrathiafulvalene (BEST-TTF or BEST), as well as, to a limited extent, TTF which was used by Ouahab and coworkers to prepare the salt $(TTF)_{11}[Fe(CN)_6]_3 \cdot 5H_2O$.[22-26] This compound is the first cyanometallate salt to be prepared with TTF or any of its derivatives (Figure 9). Analysis of the transport properties revealed that this salt is a semiconductor. When the donor was changed to BEDT-TTF and combined with hexacyanoferrate, cobaltate, and chromate, the isolated phases were found to be much better semiconductors (0.02 - 10 $S \cdot cm^{-1}$ vs. 10^{-3} $S \cdot cm^{-1}$ for the TTF.

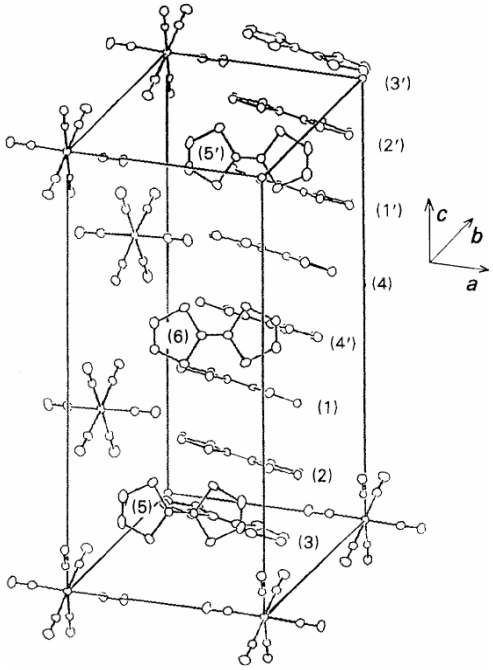

Figure 9. X-ray crystal structure of the radical cation salt $(TTF)_{11}[Fe(CN)_6]_3 \bullet 5H_2O$.[22]

Another interest in the field of dual-property materials has been to prepare systems combining a conductive organic sublattice with an inorganic sublattice capable of exhibiting an optical response. The nitroprusside anion is an interesting candidate for incorporation into potential dual-property materials because it exhibits a photoinduced transition to an extremely long-lived metastable state upon irradiation with light in the range 350-580 nm at temperatures below 160 K.[23,24b] Upon exposure to this radiation, nitroprusside undergoes linkage isomerism first going from the nitrosyl through an η^2-NO intermediate and finally to the isonitrosyl isomer.[26] It is speculated that these excitations produce geometrical changes in the anion that could facilitate light-induced alterations of the TTF radical cation lattice which affect the conductive properties of the salt. Prior to

the electrochemical synthesis of nitroprusside salts with TTF-related cations, the only known salts containing nitroprusside were those that contained alkali-metal, alkaline-earthmetal, or tetra-alkylammonium cations. These salts did not exhibit any interesting conductive properties, however, as the cations are electronically "innocent" and do not form a conducting sublattice.

The salt $(BEDT\text{-}TTF)_4K[Fe(CN)_5NO]_2$, prepared by Yu and Zhu in 1997, represents the first example of a nitroprusside with a conducting sublattice (Figure 10).[27] Initial studies of the transport properties of this salt reported a transition to a superconducting state at 7 K, which was later refuted by another study in 1999.[28] While the superconducting transition was contributed to an impurity, it was found that the salt displayed metallic behavior at room temperature of 60-200 $S \bullet cm^{-1}$.[29]

Later, efforts by Coronado and coworkers yielded salts of nitroprusside with TTF, BET-TTF, and BEST.[23-24,29] All of these materials were found to be semiconductors. A semiconducting material was also prepared by Yagubskii and coworkers using the donor (ethylenedithio)tetrathiafulvalene (EDT-TTF) (Figure 11).[30] These same authors were successful in preparing a material with metallic behavior when nitroprusside was combined with bis(ethylenedioxy)tetrathiafulvalene (BEDO-TTF) (Figure 11) to yield a system with a room temperature conductivity of 40-100 $S \bullet cm^{-1}$.[30]

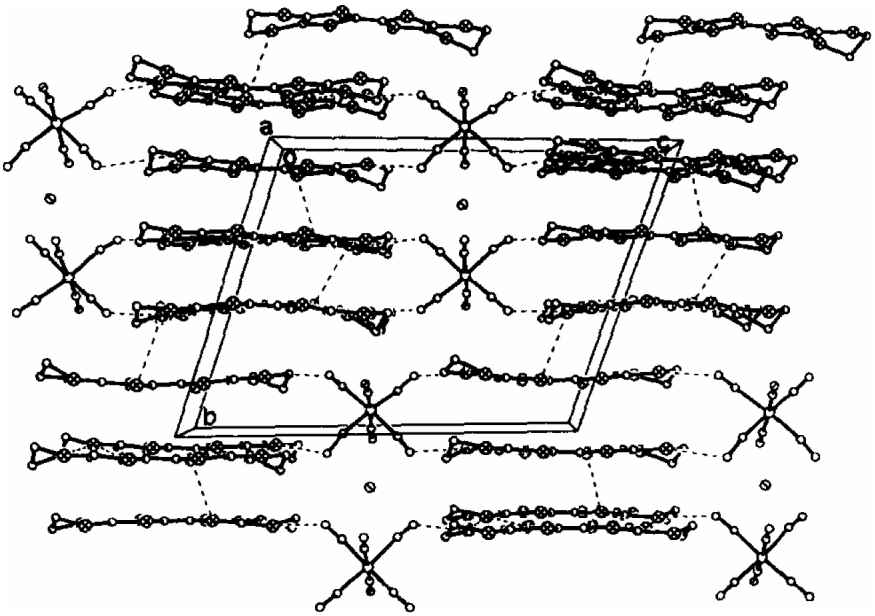

Figure 10. X-ray crystal structure of the radical cation salt of (BEDT-TTF)$_4$K[Fe(CN)$_5$NO]$_2$.[27]

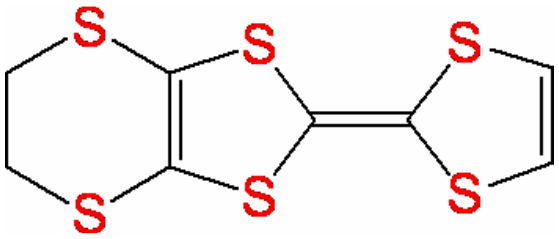

(**a**)

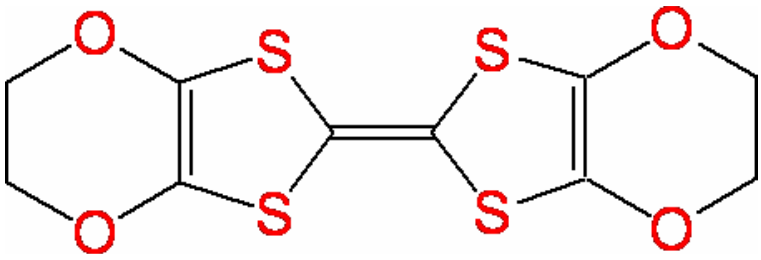

(**b**)

Figure 11. Schematic representations of EDT-TTF (**a**) and BEDO-TTF (**b**).

Octahedral transition metal anions are not the only anions that have been studied in the preparation of radical cation salts of the TTF-type donors. In an effort to further study how novel lattice architectures and physical properties resulting from the association of organic radical cations can be affected by large anions or anions possessing properties such as localized magnetic moments, attention has turned to the use of large polyoxometallate clusters that present several characteristics which make them attractive counterions in the preparation of new radical cation salts:

(I) Polyoxometallate clusters are often prepared as tetraalkylammonium salts which engenders a high level of solubility for these clusters in aqueous or nonaqueous solutions. Their solubility in polar solvents is particularly important, as this provides a means to obtain solid-state associations of these large clusters with organic donors using electro-crystallization, the preferred method for obtaining single-crystals of sufficient quality to obtain structural and physical characterizations.[30]

(II) The bulky clusters exhibit variable charges, shapes, and sizes which induces different packings of the radical cations in the solid-state which can cause alterations in the band structure. The crystal structures of hybrid materials are the result of the tendency of the planar, oxidized radical cations to aggregate in stacks and for the inorganic clusters to adopt closed-packed lattices. The possibility of varying the anionic charge on the polyoxometallate clusters results in control of the electronic band filling of the resulting salt which can directly influence its physical properties.[30]

(III) In some instances, polyoxometallates can be reduced by one or more electrons. The well known α-Keggin polyxometallate $[PMo_{12}O_{40}]^{3-}$ can be reduced in some instances to the mixed-valence cluster $[PMo_{12}O_{40}]^{4-}$. This enables the formation of

hybrid materials wherein delocalized electrons coexist in both the organic network and the inorganic clusters.[30]

(IV) The polyoxometallate clusters themselves can be prepared with one or more magnetically-active transition metal ions at specific sites in the polyoxanion structure. By introducing magnetic character into the polyanion, it becomes possible to prepare materials wherein delocalized electrons in the organic sublattice coexist with localized magnetic moments in the anion which allows for the further investigation of materials combining magnetism and conductivity.[30]

With polyoxometallate clusters, several different organic acceptors have been used, such as TTF, TMTTF, TMTSF, BEDT-TTF, BEST, BET-TTF, TPTTF (tetraphenyltetrathiafulvalene), and DMDPTTF (dimethyldiphenyltetrathiafulvalene).[32-40] Most of the prepared salts are semiconductors, but a few salts of the compounds exhibit metallic conductivities. Among them are the 5:1 phases between BEDT-TTF and the substituted Lindqvist anions $[VW_5O_{19}]^{3-}$ reported by Ouhab and coworkers in 1993 which exhibits a room temperature conductivity of 14 $S \cdot cm^{-1}$ which increases to a maximum of ~30 $S \cdot cm^{-1}$ at 250 K (Figure 12).[41] Later in 1996, Coronado and coworkers were successful in preparing the salt $[BEDT\text{-}TTF]_{11}[P_2W_{18}O_{62}] \cdot 3H_2O$ with the complex Dawson-Wells anion $[P_2W_{18}O_{62}]^{6-}$. This salt exhibits metallic-like behavior characterized by an increase from ~5 $S \cdot cm^{-1}$ at room temperature to 5.5 $S \cdot cm^{-1}$ at 230 K (Figure 13).[42]

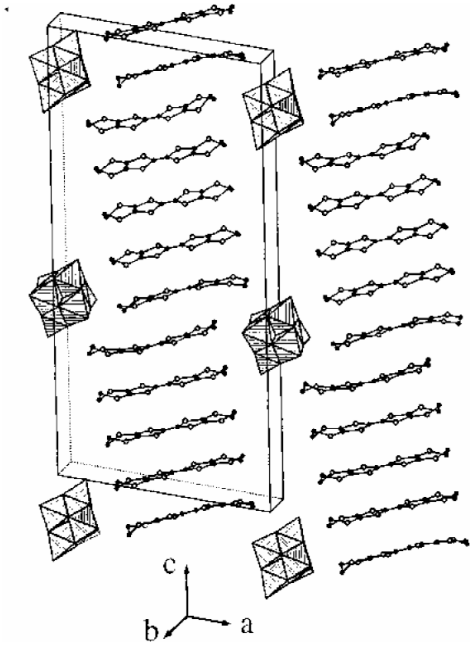

Figure 12. X-ray crystal structure of the radical cation salt (BEDT-TTF)$_5$[VW_5O_{19}]•6H_2O.[41]

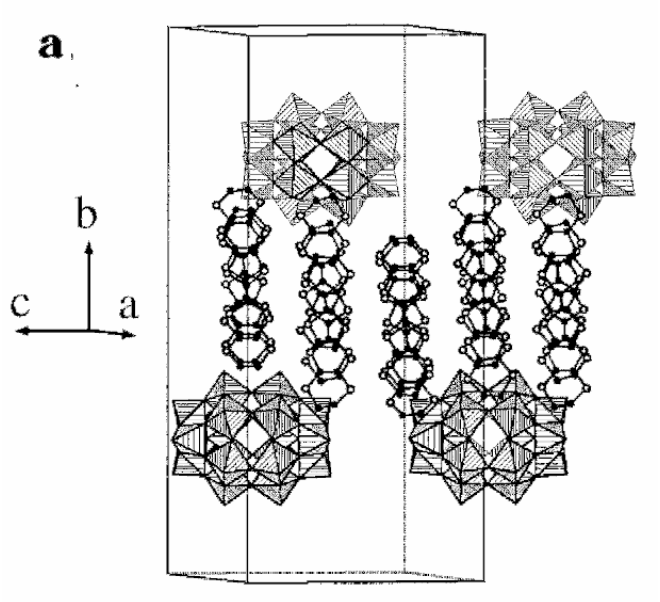

Figure 13. X-ray crystal structure of the radical cation salt (BEDT-TTF)$_{11}$[$P_2W_{18}O_{62}$]•3H_2O.[42]

Hybrid Conducting Systems Prepared by Metathetical Techniques

While the bulk of hybrid inorganic/organic materials are prepared using electrochemical techniques, a little studied facet of research related to the preparation of these systems has been their preparation using metathesis reactions. Electrochemical oxidation is the preferred method by which partially-oxidized chalcofulvalene donors can be generated and form segregated stacks essential to the establishment of band structures and high levels of conductivity, but groups have also been exploring the use of stable salts of oxidized TTF-like donors in order to introduce electronically non-innocent cations into hybrid inorganic/organic salts via metathetical techniques.

The potential of using metathesis reactions to prepare hybrid materials has long been the focus of research for groups in the field of materials science. Organometallic cations such as $[(Cp^*)_2Co]^+$ and $[(Cp^*)_2Fe]^+$ have found use instead of standard tetraalkylammonium cations in salts with polyoxometallates and layered, bimetallic oxalate networks.[43] Given that stable salts are formed when organometallic cations were used in reactions had been successfully utilized, the possibility of introducing TTF radical cations in a similar manner appears to be plausible.

The only known salt containing TTF radicals is $(TTF)_3[BF_4]_2$, first synthesized by Wudl in 1975.[44] X-ray structural data for the salt was later reported by Cassoux and coworkers in 1983.[45] At first glance, this salt appears to possess partially-oxidized segregated stacks of TTF radicals with uniform stacking between the radical cations, structural features often illustrative of systems displaying high levels of conductivity. A measurement of the conductive properties revealed insulating properties with a room temperature conductivity of 2×10^{-5} $S \cdot cm^{-1}$.[45] Closer inspection of the X-ray structure

revealed that two of the donors are completely ionized to an integral oxidation state and are dimerized, thus leading to strong charge localization and therefore consequently low conductivity for the salt. While this salt of the TTF radical cation is stable, it does not exhibit the requisite electronic features to render it a strong conductor.[45]

To date, $(TTF)_3[BF4]_2$ (Figure 14) has been used extensively to prepare various hybrid materials. Among the materials prepared are the $[M^{II}(mnt)_2]^{2-}$ salts where M^{II} = Pt, Cu, Co, and Ni.[44]

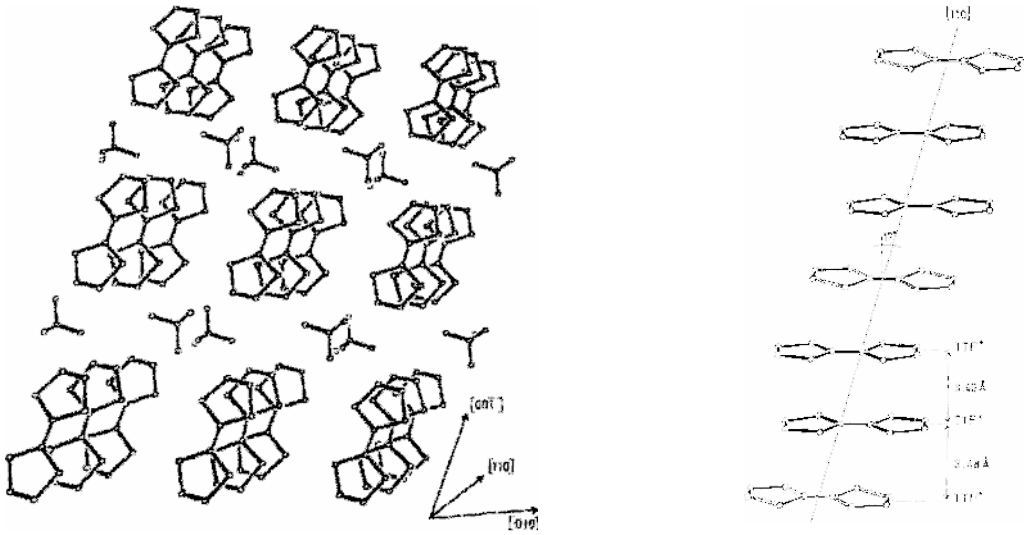

Figure 14. X-ray crystal structure for the salt $(TTF)_3[BF_4]_2$.[44]

Much like the salt of the radical cation from which they were derived, the $[M^{II}(mnt)_2]^{2-}$ salts exhibit low conductivities presumably due to the high charge localization originating from the strongly dimerized TTF radical cations in the tetrafluoroborate salt.[45]

The $(TTF)_3[BF4]_2$ salt has been used for the preparation of salts of general formula $(TTF)_4\{M^{II}(H_2O)_2[M^{III}(ox)_3]_2\}\bullet nH_2O$ where M^{II} = Mn, Fe, Co, Ni, Cu, and Zn; M^{III} = Cr and Fe (Figure 15).[46] Layered two-dimensional bimetallic phases with tetra-*n*-

butyl-ammonium cations have been known since 1995 and are known to exhibit ferro- or ferri-magnetic behavior with critical temperatures ranging from 1.7K to 44K.[47] Similar materials with the dithiooxalate (dto) anion were also prepared and found to behave as ferromagnets.[47] In the case of the TTF salts prepared using $[Cr(ox)_3]^{3-}$ all of the compounds, except for the copper and zinc analogues, which display antiferromagnetic and paramagnetic behavior respectively, exhibit ferromagnetic interactions. In the case of the $[Fe(ox)_3]^{3-}$ analogues, all salts show antiferromagnetic interactions except for the zinc salt which behaves as a paramagnet.[47]

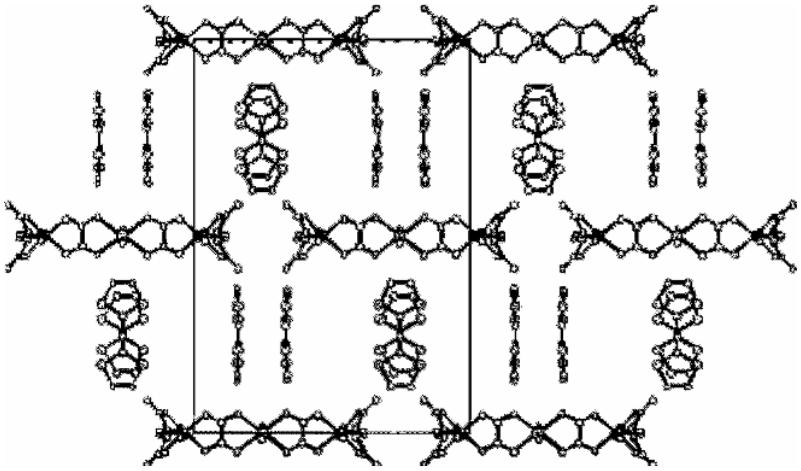

Figure 15. View of the unit cell for the TTF salt $(TTF)_4\{Mn(H_2O)_2[Cr(C_2O_4)_3]_2\}$.[46]

Compounds Composed of Organic Donor and Acceptors

As mentioned earlier, one of the most exciting discoveries in the field of organic materials science is the discovery of metallic conductivity in TTF-TCNQ as a result of partial electron transfer between the TTF donor and the TCNQ acceptor of ~0.55-0.59 electrons per donor molecule. Since this initial report, similar materials have been reported using different derivatives of both TTF and TCNQ, where similar properties have been reported.[10]

In 1989, a charge transfer compound was prepared between TTF and the organic acceptor 2,7-dinitro-9-fluorenone (DNF) by Toscano and coworkers.[48] Later spectroscopic studies in 1993 by the same group of authors reported that spontaneous charge transfer occurred between the donor and acceptor molecules whereby the charge on TTF was ~ +0.2 as determined by infrared spectroscopy.[49] This spontaneous charge transfer occurred despite the large disparity between the first oxidation potential of TTF which occurs at +0.33 V and the first reduction potential of DNF which occurs -0.78 V.[50] Based on the hypothesis that a similarity between the redox potentials of the individual components is essential for spontaneous electron transfer, it was rationalized that the tetranitrofluorenone (TENF) acceptor, with a larger number of electron withdrawing nitro groups would be a more suitable acceptor because its first reduction potential (+0.14 V) is much closer to the first oxidation potential of TTF.[51] Chapter IV outlines the preparation and solid-state structures for the charge transfer complex between TTF and and members of the nitrofluorenone family of acceptors. In addition, charge transfer complexes between TTF and TMTTF with trinitrofluorenone (TRNF) were prepared and

will be presented. Complexes between TTF and *o*-Me_2TTF and HAT-$(CN)_6$ (Figure 16) were prepared and the potential for charge transfer was probed.

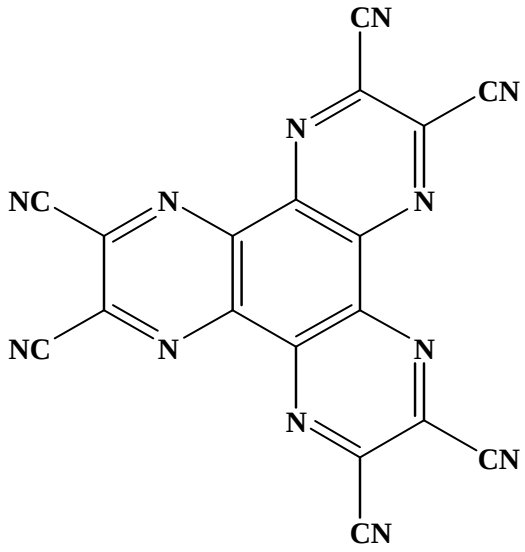

Figure 16. Schematic drawing of the organocyanide acceptor HAT-$(CN)_6$.

Part II: Square Planar Platinum(II) Molecules

Research involving transition metal complexes has dominated inorganic photochemistry for the past twenty years.[52] Interest in this field has increased as promising results using inorganic coordination compounds have led to applications such as solar energy conversion, photocatalysis, nonlinear optics, photonic molecular devices, and photoluminescent probes for biological systems.[53-57] Considerable work has been devoted to the development of synthetic strategies for the preparation of new complexes demonstrating a high level of stability as well as spectroscopic properties which can be easily varied by systematic alterations of the molecular structure. In the late 1980s, the

inorganic systems that were most often the subject of spectroscopic studies were the homoleptic Ru(II) tris-diimine complex $[Ru(bpy)_3]^{2+}$ and its derivatives as well as related complexes of Fe(II) and Os(II). The high level of stability and synthetic control of the Ru(II) complexes prompted Grätzel and coworkers to use the complex $Ru(dcbpy)_2(NCS)_2$ where dcbpy = 4,4'-dicarboxy-2,2'bipyridine as a photosensitizing dye for solar cells based on the colloidal semiconductor TiO_2.[58] To date, this compound achieves the highest level of reported energy conversion, rivaling those levels observed in solar cells based on highly-crystalline silicon wafers. Several studies have been conducted using various chelating heteroatom ligands such as phen where phen = 1,10-phenanthroline to analyze the effect of altering the chelating heteroatom ligand on the performance of the dye. To date no alterations of the original system have led to significant improvement in performance.

Complexes Containing Chelating Diimine and Dithiolate Ligands

Beginning in 1989, Eisenberg and coworkers reported that a series of platinum diimine complexes containing 1,1- and 1,2-dithiolate ligands exhibited solution luminescence.[59] It was found that platinum complexes based on diimine and dithiolate liagnds were not the only systems that exhibit this luminescence, as compounds with phenyl, phenylacetylide, cyanide, and chelating diphospine ligands were also emitters.[60-63] Larger complexes with heteroaromatic chelates and divalent platinum species also exhibit solution luminescent properties.[64-66] All of these heteroaromatic ligands possess low-lying π^*-orbitals which are involved in charge-transfer (CT) processes in the respective complexes. Various charge-transfer processes can exist in these complexes

due to the variety of orbitals present. Among the charge-transfer processes reported are intra-ligand charge-transfer (ILCT), metal-to-ligand charge transfer (MLCT) and ligand-to-ligand charge transfer (LLCT). In the square planar complexes containing diimine and dithiolate ligands coordinated to a platinum atom, the HOMO is a hybrid orbital containing contributions from the metal atom and dithiolate ligands, and the LUMO is centered on the heteroaromatic chelating ligand. Calculations revealed that the dominant charge transfer process in the square planar complexes is a mixed metal/ligand-to-ligand charge transfer (MM'LLCT) band.

The first square planar diimine dithiolate molecules to display interesting spectroscopic properties are the complexes Pt(dmbpy)(ecda) and Pt(dpphen)(mnt), where dmbpy = 4,4'-dimethyl-2,2'-bipyridine, ecda = 1-(ethoxycarbonyl)-1-cyanoethylene-2,2dithiolate, dpphen = 4,7-diphenyl-1,10-phenanthroline, and mnt = maleonitrile-dithiolate (Figure 17). Later in 1996, Cummings and Eisenberg reported a systematic study on the Pt diimine dithiolate complexes which revealed that the spectroscopic response of these molecules could be tuned to higher or lower energies by changing the identity of the diimine or dithiolate ligand; this was achieved by adding electron-withdrawing or electron-donating substituents to the diimine ligand, or by changing the polarity of the solvent used for the dissolution of the complex.[67]

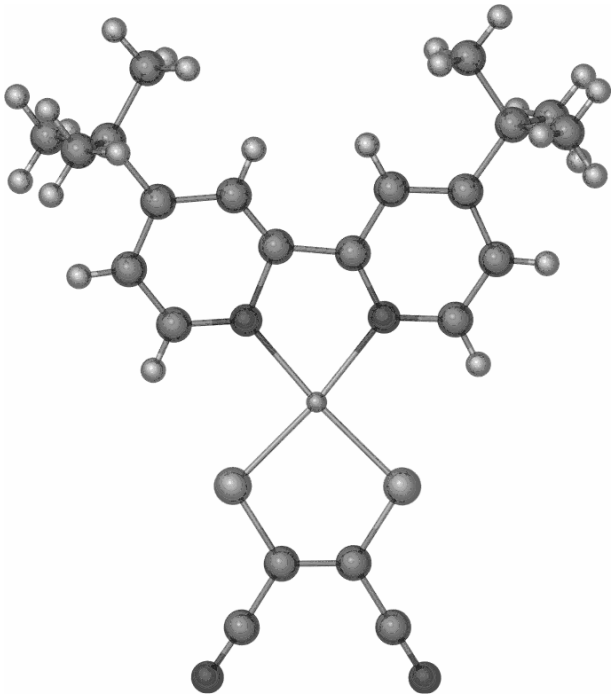

Figure 17. Representative X-ray crystal structure for the M(dbbpy)(mnt) family of compounds.

It was this high level of synthetic control that prompted the investigation of Pt dimiine dithiolate and complexes as potential photosensitizing dyes for solar cells based on colloidal semiconductors. In 2001, Arakawa and coworkers probed the use of various Pt(dcbpy)(dithiolate) complexes for solar cells based on TiO_2. Unlike the dye prepared by Grätzel and coworkers, the dyes prepared by Arakawa did not show the same level of photovoltaic activity, but the results revealed that the incorporation of dithiolate ligands into the coordination sphere of the platinum complexes leads to the onset of charge-transfer bands that are red-shifted from complexes lacking these ligands.[68]

Later in 2003, Dunbar and Omary made an important discovery in the field of Pt diimine dithiolate compounds. In this report, M(dbbpy)(dmid) (Figure 18) where dmid =

1,3-dithiole-2-one-4,5-dithiolate and M = Pt and Pd was combined with the organo-cyanide acceptors TCNQ, TCNE, and $TCNQ_4$ to yield donor/acceptor systems capable of sensitizing TiO_2.[69] The previous work of Grätzel and Arakawa had indicated that carboxylate groups present on the chelating diimine ligands were essential for attaching the dye molecules to the surface and for facilitating electron injection into the conduction band of the semiconductor, but the new studies revealed that an outer sphere molecule was capable of assisting the binding of the dye molecules to TiO_2.[58]

In the traditional complexes of the type in Pt(dbbpy)(dmid), there are no linking groups available for surface adsorption. The inclusion of the organocyanide acceptors into the material is novel from a twofold standpoint: First, organocyanide acceptors exhibit low-lying π-π^* absorption bands in the near-IR, which allows for the donor/acceptor systems to absorb lower energy radiation. Secondly, despite the lack of traditional adsorbing groups on the metal complex itself, the systems are able to adsorb to the surface the TiO_2 semiconductor using the cyanide group of the acceptor molecule. Ultimately, however, these donor/acceptor systems did not present optimal functionality as photosensitizing dyes presumably due to the lack of efficient electron injection into the conduction band of the semiconductor. In order to function as photosensitizing dyes, the first-reduction potential for the complex must be more negative than the conduction band of the semiconductor. Since neutral acceptors were being used in the preparation of the donor/acceptor systems, a large disparity existed between the acceptor and semiconductor-based reduction potentials which presents a large limiting factor for their use as functional photosensitizing dyes.

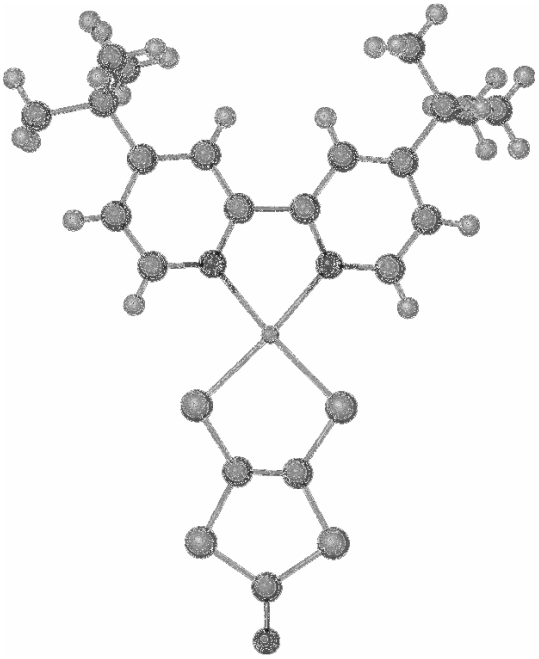

Figure 18. X-ray crystal structure of Pt(dbbpy)(dmid).

Chapter V outlines the preparation of new inorganic/organic donor acceptor systems using the nitrofluourenone family of acceptors, work that demonstrates these acceptors, much like the organocyanide acceptors, allows for materials containing them to show a spectral response at lower energies.[69]

Complexes Containing Tris-chelating Terpyridine Ligands

In 1994, McMillin and coworkers reported an interesting addition to the field of square planar platinum molecules by illustrating the use of tris-chelating heteroatom ligands in the preparation of platinum molecules with tunable spectroscopic properties.[64] The complexes $[Pt(trpy)X]^+$ where terpy = 2,2':6',2''-terpyrdine exhibit intraligand π-π* ILCT transitions due to the presence of an extended π-electron system on the terpy ligand. The terpyridine ligand, beside facilitating the presence of intraligand charge

transfer bands, also allows for the prevention of radiationless decay of the spectroscopic signal because of the rigid planarity which limits distortions that cause reduced spectroscopic performance via this mechanism.[64] The terpyridine ligand can also be functionalized with various groups, and "X" can be varied to yield a family of compounds whose properties can be probed systematically. Due to their variable spectroscopic behavior, terpyridine complexes of platinum have already seen use as probes for DNA intercalation.

In their first report, McMillin and coworkers were able to classify some of the charge-transfer processes occurring in the platinum-terpy salts.[70] All of the platinum salts studied showed high-energy absorption bands at wavelengths less than 350 nm. These high-energy bands were attributed to intraligand π-π^* transitions from the coordinated terpy-ligand. Lower energy bands at longer wavelengths >350 nm were the subject of debate until their relative intensity was considered; since their molar absorptivity was ~1000 $M^{-1} \cdot cm^{-1}$, the bands were assigned to be metal-to-ligand charge transfer transitions. Studies are still being conducted to further establish if this metal-to-ligand charge transfer band has mixed parentage similar to that encountered in platinum complexes containing diimine and dithiolate, but it is believed that, like the previously studied compounds, platinum salts containing chelating terpyridine ligands also have a hybrid HOMO with metal contribution.

To date, the group of Yam and coworkers have carried out most of the research on the electrochemical and spectroscopic properties of platinum-terpyridine salts. Also, along with the electrochemical and spectroscopic studies, this group has also reported a large number of solid-state structures as determined by X-ray crystallography.[71] While

this group has studied complexes where the ancillary ligands are various acetylide and substituted acetylides as they relate to biological applications, this group has not considered using these complexes for materials applications where a tailored photochemical response could be considered advantageous. In analyzing the work of Yam and coworkers, it can be seen that the addition of electron-donating or electron-withdrawing groups on either the terpyridine or platinum-coordinated ligand can affect the spectroscopic response by altering the energy of the charge transfer band across the HOMO-LUMO gap.[72] This alteration leads to either a red- or blue-shift in their photochemical response. With such a high level of tunability, these complexes are excellent candidates for use in applications such as photosensitizing dyes for solar cells. Chapter VI outlines electrochemical and crystallographic studies on platinum terpyridine complexes incorporating thiolate-ligands which show a spectroscopic response at energies lower than those encountered by McMillan and Yam. Their potential use as photosensitizing dyes for solar cells is discussed.

CHAPTER II

PREPARATION OF CHALCOFULVALENIUM SALTS VIA ELECTROCHEMICAL METHODS

Introduction

The preparation of stable chalcofulvalenium salts by electrochemical methods is a fundamental approach to preparing interesting conducting and even superconducting materials. One particularly exciting initiative is the synthesis of materials that can display multifunctionality, whereby on a molecular level, molecular materials combine, in the same crystal, two or more physical properties which are difficult, or even impossible, to achieve in continuous lattice solids. In order to overcome this barrier, cation/anion salts where each framework contributes distinct properties to the solid have been prepared. This approach can give rise to materials that exhibit a coexistence of properties, or those exhibiting novel properties due to the mutual interaction between the individual components. Among these materials are those that combine organic, conducting sublattices of the TTF (tetrathiafulvalene) with a secondary inorganic sublattice with interesting magnetic or optical properties can originate. Of particular interest are those materials that combine both magnetism and conductivity, especially ferromagnetism and superconductivity as those properties are considered to be mutually exclusive. The coexistence of these materials in a single material has been the subject of intense debate among physicists and has been thoroughly investigated from both experimental and theoretical viewpoints.

Planar organic donors and acceptors have been used extensively to prepare molecular conductors and superconductors. Among these early examples involves the reaction between TTF and TCNQ, whereby spontaneous, partial electron transfer between the donor and acceptor molecules leads to the formation of segregated stacks of partially-ionized species in the solid state which displayed metallic conductivity. The formation of the segregated stacks is critical as the overlap of orbitals of similar energy and symmetry leads to the formation of delocalized electron energy bands essential for metallic conductivity to occur.[10,11]

Electron delocalization was also discovered in solids formed by the ion-radicals of TTF or its derivatives resulting from its oxidation and subsequent pairing with charge-compensating counterions. These cation-radical salts, of the general formula $[donor]_mX_n$ have offered the most widely studied examples of molecular conductors and superconductors. The Bechgaard family of salts, first reported in 1980, combined TMTSF with anions such as $[BF_4]^-$, $[AsF_6]^-$, $[SbF_6]^-$, $[NO_3]^-$, and $[PF_6]^-$ to yield a family of one-dimensional organic mixed-valence cation-radical salts which represent the first organic superconductors.[14]

Inorganic chemistry offers an extensive library of metal complexes of various nuclearities and dimensionalities that can be used as charge-compensating counterions for conducting radical-cation salts. Among those anions encountered are simple mononuclear anions, large polyoxometallate clusters, bimetallic oxalate-bridged anions, and substituted dithiolate anions. Among the most dramatic results in the field of electrochemically-prepared radical cation salts is the salt $(BEDT\text{-}TTF)_4(H_2O)Fe(C_2O_4)_3 \cdot C_6H_5CN$ which was the first salt to combine superconductivity with paramagnetic metal

anions and the salts $(BETS)_2[FeX_4]$ (X = Cl^- and Br^-) reported by Kobayashi and coworkers which combined antiferromagnetism with superconductivity.[19,21] These results were among the most interesting, as the properties of superconductivity and ferromag-netism were once considered inimical by physicists. The roots of this argument lie in the fundamental difference between superconductivity and normal metallic conductivity. In the superconducting state, the current carriers are pairs of electrons (Cooper pairs), while in metallic conductivity the electrons move independently.[73] In the superconducting state, interaction between the electrons and lattice vibrations are the most common means of overcoming Coulombic repulsion, resulting in the formation of an attractive potential. The presence of a magnetic field disrupts the pairing energy and causes the superconductor to return to the normal state. External magnetic fields are not the only fields effective in disrupting the superconducting state; a fact discovered upon studying ferromagnetic compounds revealed that an internal field is generated due to the ordering of magnetic moments thus fields generated by ferromagnetic should be sufficient enough to disrupt the superconducting state. Local fields are also generated by antiferromagnets and paramagnets, but their effect on the disruption of the superconducting is negligible when compared to ferromagnets. To date, no ferromagnetic superconductor with a chalcofulvalene origin has been prepared.

Several results obtained via the electrochemical oxidation of chalcofulvalene have been previoulsly discussed in the introduction; however, other results, including those obtained with dimeric anions, have yet to be considered. Dimeric anions, have seen limited use in radical cation salts. The anion $[Fe_2(C_2O_4)_5]^{4-}$ has been combined with the donors TTF, TMTTF, and BEDT-TTF, yielding salts where the anion dominates the

magnetic behavior. The use of TTF with the above anion yields two salts; the first is of the formula $(TTF)_5$ $[Fe_2(C_2O_4)_5]$•2PhMe•$4H_2O$ and the second is $(TTF)_7[Fe_2(C_2O_4)_5]$ •$4H_2O$.[74] The solid-state structure of the former is dominated by chains of donors surrounded by the dimeric anions and orthogonal TTF dimers. In the latter salt, TTF donors are packed in chains surrounded by four orthogonal dimers of TTF molecules and the $[Fe(C_2O_4)_3]^{3-}$ anion. Other salts such as $(TMTTF)_4[Fe_2(C_2O_4)_5]$ •PhCN•H_2O consists of stacks of donors and anions in a "checkerboard" arrangement.[74] The salt (BEDT-TTF)$_4$ $[Fe_2(C_2O_4)_5]$ exhibits closely-spaced radical cation dimers, forming a checkboard arrangement similar to the network seen previously in the salt (BEDT-TTF)$_2$[Ge$(C_2O_4)_3$]•PhCN.[75]

Other salts containing oxalate-bridged dimeric anions include the salts (BEDT-TTF)$_5$[MM'$(C_2O_4)(NCS)_8$] where MM' is either CrFe or CrCr.[76] The inclusion of NCS^- in this salt is interesting because it presents the opportunity for cation-anion S•••S interactions. The magnetic response in both systems is dominated by the dimeric anion. [76] In the CrFe case there appears to be ferromaganetic intra-dimer exchange between the metal centers to yield an S = 4 ground state.[76] In the case of the CrCr system a second salt with the formula (BEDT-TTF)$_8$[CrCr$(C_2O_4)(NCS)_8$] was isolated which shows metallic conductivity. In both CrCr cases, the magnetic response is dominated by an antiferromagnetic interaction between the Cr centers. [76]

While oxalate-bridged dimeric anions have yielded interesting results for the preparation of stable, radical cation salts, there have been few studies of bimetallic systems that possess metal-metal bonds. Salts of BEDT-TTF with $[Re_2(NCS)_{10}]^{n-}$ (n = 2, 3) have been prepared which show differences in their solid-state structure facilitated by

alteration of the anion's charge.[77] The structure of the n = 3 analog consists of layers containing both cations and anions with several short S•••S contacts. Despite the presence of several short sulfur contacts, there is no network of continuous ET radicals, which results in a low conductivity for the salt. The magnetic susceptibility of the resulting salt has been best modeled as a sum of the contributions from the anion and BEDT-TTF dimers.[77] A salt has also been prepared with the donor DMDPTTF and $[Re_2Cl_8]^{2-}$ which showed layers of $[Re_2Cl_8]^{2-}$ separated by eclipsed dimers of fully-ionized donors.[78]

Planar metallocomplex anions of the metal-bisdithiolene family tend to form one-dimensional stacks in the solid-state when combined with suitable cations. In this context, metal bis-maleonitriledithiolate anions $[M(mnt)_2]^-$ (M(III) = Ni, Cu, Au, Pt, Pd, Co, and Fe) have been combined with perylene to form organic charge-transfer solids $Per_2M(mnt)_2$.[79] The organic donor perylene is one of the most well-studied donors and has been used in the preparation of highly conducting solids, but because of the lack of sulfur atoms on perylene, all systems are strongly one-dimensional and suffer from the traditional electronic instabilities associated with 1-D systems. All of the salts with perylene as the donor show metallic conductivity to low temperatures before undergoing a metal-to-insulator transition. Very little work has been devoted to the study of the metal bis-maleonitriledithiolate anions with chalcofulvalenium radical cations. The structure and transport properties of the (BEDT-TTF)$[Pt(mnt)_2]$ have been reported and reveal that this salt is an extremely weak semiconductor.[80] The structures and transport properties of two phases of (BEDT-TTF)$[Ni(mnt)_2]$ have been reported and, much like the platinum salt, show reduced conductivity.[81] The transport properties of (BEDT-

TTF)[Cu(mnt)$_2$] have been reported, showing room temperature conductivity values of $<10^{-6}$ S•cm^{-1}, but no structure was reported.[82] Salts of the general formula (TTF)$_2$[M(mnt)$_2$] where M = Ni, Cu, Au, Pt, Pd, Co, and Fe have been prepared via metathesis methods using the oxidized tetrathiafulvalenium salt (TTF)$_3$[BF$_4$]$_2$ and *n*-tetrabutylammonium salts of the metal bis-maleonitriledithiolate anions. As expected, because of the strong dimerization of the fully-ionized TTF radicals, the resulting salts are insulators.[45]

This chapter outlines the results of electrochemical syntheses of stable chalcofulvalenium salts. Among the salts prepared are those which incorporate the metal-metal bonded dianion [Re$_2$Cl$_8$]$^{2-}$ with BEDT-TTF, TMTTF, TMTSF, and *o*-Me$_2$TTF (Figure 19). Some work involving the [Cu(mnt)$_2$]$^-$ anion is also presented including the structure of its salt with ET. A salt with the donor TMTTF was also prepared. In an effort to fully establish a family of salts for a single donor, electrochemical methods were used to prepare radical cation salts between *o*-Me$_2$TTF and several anions, including Cl$^-$, Br$^-$, I$^-$, [BF$_4$]$^-$, [PF$_6$]$^-$, and [I$_3$]$^-$. Other salts with this donor and some members of the polyoxometallate and cyanometallate family of anions were also prepared. Finally, a few salts were prepared with other donors such as BPDT-TTF and TTF (Figure 19) including its salts with [Co(CN)$_6$]$^{3-}$ and [Fe^{III}(CN)$_6$]$^{3-}$.

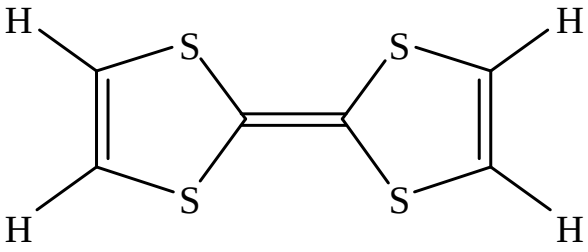

(**a**)

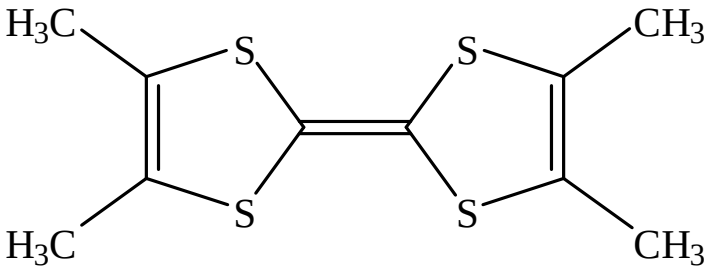

(**b**)

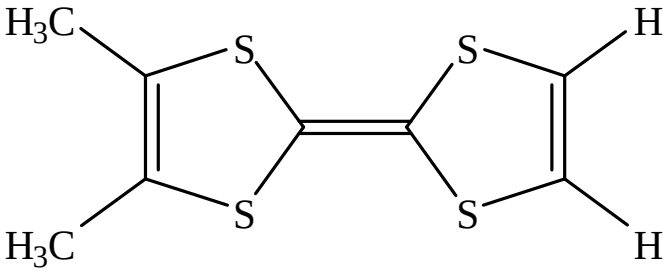

(**c**)

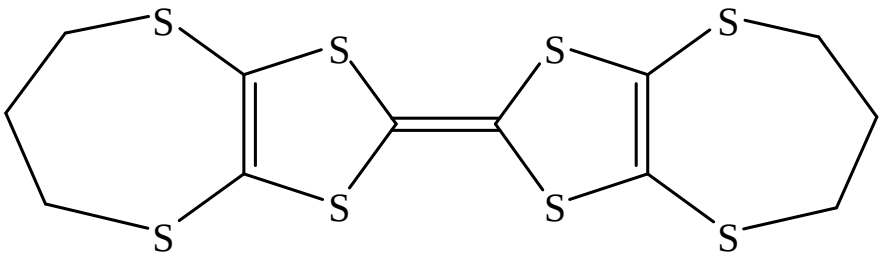

(**d**)

Figure 19. The chalcofulvalene donors TTF (**a**), TMTTF (**b**), *o*-Me_2TTF (**c**), and BPDT-TTF (**d**).

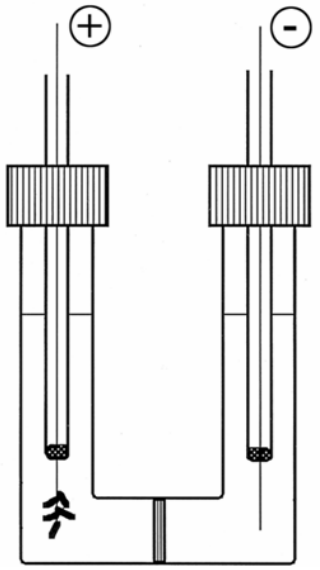

Figure 20. Diagram of cell used in the preparation of salts containing oxidized chalcofulvalene moieties via electrochemical methods.

Experimental Section

Preparation of Compounds

For all electrochemical preparations, solvents were not previously dried. In fact, the preparation of salts containing cyanometallate charge compensating anions formed higher quality crystals upon the addition of few drops of water. For all radical cation salts, crystals formed on platinum electrodes in the anodic compartment of a standard U- or H-cell (Figure 20) under the conditions of the application of a low constant current. All syntheses were performed at room temperature with the exception of **10**, which formed on the electrode after submersion in an ethanol bath at -10°C. TTF and BEDT-TTF were purchased from TCI and TMTSF was purchased from Acros and were used as received without further purification. TMTTF, *o*-Me_2TTF, and BPDT-TTF were provided by Prof. Marc Fourmigué and used without additional purification.[83] The salts

$P(Ph)_4Cl$, $P(Ph)_4Br$, TBAI, $TBABF_4$, $TBAPF_6$, $TBAI_3$, $(TBA)_3[Fe(CN)_6]$, $K_3[Fe(CN)_6]$, and $K_3[Co(CN)_6]$ were all purchased from Aldrich or Acros and used as received. The salts $(TBA)_2[Re_2Cl_8]$, $(TBA)_2[W_6O_{19}]$, and $(TBA)_2[Mo_6O_{19}]$ were prepared according to literature procedures.[84,85] The crown ether Dibenzo-18-crown-6 was purchased from Acros and used as received without further purification.

Table 1. Synthetic conditions for $(BEDT\text{-}TTF)_2[Re_2Cl_8]$ (**1**), $(TMTTF)_3[Re_2Cl_8]\bullet 2CH_3CN$ (**2•2CH$_3$CN**), $(TMTSF)_5[Re_2Cl_8]_2\bullet 3CH_2Cl_2$ (**3•3CH$_2$Cl$_2$**), and $(o\text{-}Me_2TTF)_2[Re_2Cl_8]$ (**4**). All reactions were performed at a constant current of 0.5 μA.

salt	anode		cathode
$(BEDT\text{-}TTF)_2[Re_2Cl_8]$ (**1**)	BEDT-TTF (25 mg) $(TBA)_2[Re_2Cl_8]$ (150 mg) PhCN (10 mL)		 $(TBA)_2[Re_2Cl_8]$ (150 mg) PhCN (10 mL)
$(TMTTF)_3[Re_2Cl_8]\bullet 2CH_3CN$ (**2**)	TMTTF (20 mg) $(TBA)_2[Re_2Cl_8]$ (100 mg) CH_3CN (10 mL)		 $(TBA)_2[Re_2Cl_8]$ (100 mg) CH_3CN (10 mL)
$(TMTSF)_5[Re_2Cl_8]_2\bullet 3CH_2Cl_2$ (**2**)	TMTSF (20.2 mg) $(TBA)_2[Re_2Cl_8]$ (102 mg) CH_2Cl_2 (10 mL)		 $(TBA)_2[Re_2Cl_8]$ (102 mg) CH_2Cl_2 (10 mL)
$(o\text{-}Me_2TTF)_2[Re_2Cl_8]$ (**4**)	$o\text{-}Me_2TTF$ (12 mg) $(TBA)_2[Re_2Cl_8]$ (100 mg) CH_3CN (10 mL)		 $(TBA)_2[Re_2Cl_8]$ (100 mg) CH_3CN (10 mL)

$(BEDT\text{-}TTF)_2[Re_2Cl_8]$ (1). As outlined in Table 1, into both compartments of the electrochemical cell, ~150 mg (0.131 mmol) of $(TBA)_2[Re_2Cl_8]$ was added and combined in each compartment with 10 mL of PhCN. BEDT-TTF (0.025 g, 0.061 mmol) was added to the anodic compartment and the entire cell was attached to a potentiostat to insure that a constant oxidative current biased to a low potential of 0.5 μA was applied to the system. After a period of two months, small black block crystals of the title

compound had formed on the electrode surface. The crystals were removed from the electrode surface, washed with PhCN, and dried in air.

$(TMTTF)_3[Re_2Cl_8]•2CH_3CN$ ($2•2CH_3CN$). As in the case of **1**, the synthesis for this salt is outlined in Table 1. $(TBA)_2[Re_2Cl_8]$ (0.100 g, 0.088 mmol) was added to each compartment of the electro-chemical cell where each added mass was combined in each compartment with 10 mL of CH_3CN. TMTTF (0.020 g, 0.077 mmol) was added to the anodic compartment and subjected to a low current potential of 0.5 μA. After a period of two weeks, black block crystals of the salt had formed on the electrode surface which were later removed, washed with MeCN, and dried in air.

$(TMTSF)_5[Re_2Cl_8]_2•3CH_2Cl_2$ ($3•3CH_2Cl_2$). Like the previous salts, the synthesis for this salt is outlined in Table 1. $(TBA)_2[Re_2Cl_8]$ (0.102 g, 0.090 mmol) was added to each compartment of the electrochemical cell where each added mass was combined in each compartment with 10 mL of CH_2Cl_2. TMTSF (0.020 g, 0.044 mmol) was added to the anodic compartment and subjected to a low current density of 0.5 μA. After a period of one week, small black needle crystals of the salt had formed on the electrode surface which were later removed, washed with CH_2Cl_2, and allowed to dried in air.

(o-$Me_2TTF)_2[Re_2Cl_8]$ (4). To a standard electrochemical cell, $(TBA)_2[Re_2Cl_8]$ (0.100 g, 0.088 mmol) was added to each compartment of the electrochemical cell where each added mass was dissolved in 10 mL of CH_3CN. To the anodic compartment was added o-Me_2TTF (0.012 g, 0.052 mmol) and the cell was subjected to a low current density of

0.5 μA. After a period of two weeks, small black needle crystals of the salt had formed on the electrode surface which were later removed, washed with CH_3CN, and dried in air.

Table 2. Synthetic conditions for (BEDT-TTF)[Cu(mnt)$_2$] (**5**) and (TMTTF) [Cu(mnt)$_2$] (**6**). Both syntheses were performed at a constant current of 0.7 μA.

salt		anode		cathode
(BEDT-TTF)[Cu(mnt)$_2$] (**5**)		BEDT-TTF (10 mg) $(TBA)_2$[Cu(mnt)$_2$] (50 mg) 1,1,2-trichloroethane (15 mL)		$(TBA)_2$[Cu(mnt)$_2$] (50 mg) 1,1,2-trichloroethane (15 mL)
(TMTTF)[Cu(mnt)$_2$] (**6**)		TMTTF (10 mg) $(TBA)_2$[Cu(mnt)$_2$] (100 mg) CH_3CN (15 mL)		$(TBA)_2$[Cu(mnt)$_2$] (100 mg) CH_3CN (15 mL)

(BEDT-TTF)[Cu(mnt)$_2$] (**5**)**.** As outlined in Table 2, $(TBA)_2$[Cu(mnt)$_2$] (0.050 g, 0.060 mmol) was added to both compartments of a standard electrochemical cell which was later dissolved by adding 10 mL of 1,1,2-trichloroethane to those compartments. Into the anodic compartment was added BEDT-TTF (0.010 g, 0.026 mmol). The entire cell was exposed to low oxidizing current density of 0.7 μA which facilitated the deposition of black block crystals of the radical cation salt on the electrode surface after two weeks. The crystals were removed from the electrode, washed with 1,1,2-trichloroethane and CH_3CN and dried in air.

(TMTTF)[Cu(mnt)$_2$] (**6**)**.** In a manner similar to that reported for **5** in Table 2, $(TBA)_2$[Cu(mnt)$_2$] (0.100 g, 0.121 mmol) was added to both compartments of a standard electrochemical cell and dissolved by adding 10 mL of CH_3CN into the compartments. Into the anodic compartment was added TMTTF (0.010 g, 0.038 mmol) and oxidized at a

low current density of 0.7 μA in the presence of the electrolyte solution to yield small black needle crystals of the title salt after a period of two weeks. The crystals were removed from the electrode, washed with CH_3CN and dried in air.

Table 3. Synthetic conditions for (*o*-$Me_2TTF)_2$[Cl] (**7**), (*o*-$Me_2TTF)_2$[Br] (**8**), and (*o*-$Me_2TTF)_2$[I] (**9**). All reactions were performed at a constant current of 0.5 μA.

salt		anode		cathode
(*o*-$Me_2TTF)_2$[Cl] (**7**)		*o*-Me_2TTF (9.6 mg) $P(Ph)_4Cl$ (105 mg.) CH_3CN (10 mL)		 $P(Ph)_4C$ l(105 mg.) CH_3CN (10 mL)
(*o*-$Me_2TTF)_2$[Br] (**8**)		*o*-Me_2TTF (10.1 mg) $P(Ph)_4Br$ (105 mg.) CH_3CN (10 mL)		 $P(Ph)_4Br$ (105 mg.) CH_3CN (10 mL)
(*o*-$Me_2TTF)_2$[I] (**9**)		*o*-Me_2TTF (9.4 mg) TBAI (105 mg.) CH_3CN (10 mL)		 TBAI (105 mg.) CH_3CN (10 mL)

(*o*-$Me_2TTF)_2$[Cl] (7). As reported in Table 3, $P(Ph)_4Cl$ (0.105 g, 0.281 mmol) was added to both compartments of a standard electrochemical cell and dissolved by adding 10 mL of CH_3CN into the compartments. Into the anodic compartment was added *o*-Me_2TTF (0.010 g, 0.043 mmol) and oxidized at a low current density of 0.5 μA in the presence of the electrolyte solution to yield small black needle crystals of the title salt which were harvested from the electrode surface after a period of two weeks. The crystals were removed from the electrode, washed with CH_3CN and dried in air.

(*o*-$Me_2TTF)_2$[Br] (8). Into a standard electrochemical cell, $P(Ph)_4Br$ (0.105 g, 0.251 mmol) was added to both compartments where each added mass was dissolved in 10 mL of CH_3CN. Into the anodic compartment was added *o*-Me_2TTF (0.010 g, 0.043 mmol)

and oxidized at a low current potential of 0.5 μA in the presence of the electrolyte solution. Black needle crystals of the title salt had formed on the electrode surface after a period of a few hours and were later harvested after a period of two weeks. The crystals were removed from the electrode, washed with CH_3CN and dried in air.

(*o*-Me_2TTF)$_2$[I] (9). Into a standard electrochemical cell, TBAI (0.105 g, 0.284 mmol) was added to both compartments. The salt added to each compartment was dissolved in 10 mL of CH_3CN. The *o*-Me_2TTF donor (0.010 g, 0.043 mmol), which was added to the anodic compartment, was oxidized at a 0.5 μA in the presence of the electrolyte. Black needle crystals of the title salt formed on the electrode surface after a period of a few hours, but grew larger over the period of two weeks and were later harvested. The harvested crystals were washed with CH_3CN and dried in air.

Table 4. Synthetic conditions for (*o*-Me_2TTF)$_2$[BF_4] (**10**), (*o*-Me_2TTF)$_2$[PF_6] (**11**), and (*o*-Me_2TTF)[I_3] (**12**). All reactions were performed at a constant current of 0.5 μA.

salt		anode		cathode
(*o*-Me_2TTF)$_2$[BF_4] (**10**)		*o*-Me_2TTF (9.6 mg) (TBA)BF_4 (100 mg) CH_3CN (12 mL)		(TBA)BF_4 (100 mg) CH_3CN (12 mL)
(*o*-Me_2TTF)$_2$[PF_6] (**11**)		*o*-Me_2TTF (10.1 mg) (TBA)PF_6 (105 mg) CH_3CN (12 mL)		(TBA)PF_6 (105 mg) CH_3CN (12 mL)
(*o*-Me_2TTF)[I_3] (**12**)		*o*-Me_2TTF (9.8 mg) (TBA)I_3 (105 mg) CH_3CN (12 mL)		(TBA)I_3 (105 mg) CH_3CN (12 mL)

(*o*-Me_2TTF)$_2$[BF_4] (10). Into both compartments of a standard electrochemical cell, $TBABF_4$ (0.100 g, 0.304 mmol) was added to both compartments. The salt added to each

compartment was dissolved in 12 mL of CH_3CN and oxidized in the presence of the *o*-Me_2TTF donor (0.0096 g, 0.041 mmol) at a low current density of 0.5 μA. Small black needle crystals of the title salt formed on the electrode surface after a period of a few weeks at -10°C. The intense dark green solution was then allowed to slowly evaporate in air yielding more needle-like black crystals after an additional week. All harvested crystals were washed with CH_3CN and dried in air. The synthesis of this salt was outlined in Table 4.

(*o*-$Me_2TTF)_2[PF_6]$ (11). Into a standard electrochemical cell, $TBAPF_6$ (0.105 g, 0.271 mmol) was added to both compartments and dissolved in 12 mL of CH_3CN. The donor *o*-Me_2TTF (0.0101 g, 0.044 mmol), which was also added to the anodic compartment was oxidized at a low constant current of 0.5 μA in the presence of the electrolyte solution to yield black block crystals of the title salt on the surface of the electrode which were harvested after a period of two weeks. The harvested crystals were washed with CH_3CN and dried in air. The synthesis of this salt is outlined in Table 4.

(*o*-$Me_2TTF)[I_3]$ (12). Into both compartments of a standard electrochemical H-cell, $TBAI_3$ (0.105 g, 0.169 mmol) was added and later dissolved in 12 mL of CH_3CN. The donor *o*-Me_2TTF (0.0098 g, 0.042 mmol) was combined with the electrolyte solution in the anodic compartment and exposed to a weak current density of 0.5 μA to yield black block-like crystals on the electrode surface which were harvested after a period of two weeks, washed with CH_3CN, and dried in air.

Table 5. Synthetic conditions for (*o*-$Me_2TTF)_2[W_6O_{19}]$ (**13**), (*o*-$Me_2TTF)_2[Mo_6O_{19}]$ (**14**) and $(BPDT\text{-}TTF)_2[W_6O_{19}]$ (**15**). All reactions were done at a constant current of 1.0 μA.

salt		anode		cathode
(*o*-$Me_2TTF)_2[W_6O_{19}]$ (**13**)		*o*-Me_2TTF (9.6 mg) $(TBA)_2[W_6O_{19}]$ (107 mg) CH_3CN (10 mL)		$(TBA)_2[W_6O_{19}]$ (107 mg) CH_3CN (10 mL)
(*o*-$Me_2TTF)_2[Mo_6O_{19}]$ (**14**)		*o*-Me_2TTF (9.8 mg) $(TBA)_2[Mo_6O_{19}]$ (110 mg) CH_3CN (10 mL)		$(TBA)_2[Mo_6O_{19}]$ (110 mg) CH_3CN (10 mL)
$(BPDT\text{-}TTF)_2[W_6O_{19}]$ (**15**)		BPDT-TTF (12 mg) $(TBA)_2[W_6O_{19}]$ (107 mg) CH_3CN/1,1,2-TCE (10 mL)		$(TBA)_2[W_6O_{19}]$ (107 mg) CH_3CN/1,1,2-TCE (10 mL)

(*o*-$Me_2TTF)_2[W_6O_{19}]$ (13). As outlined in Table 5, into both compartments of a standard electrochemical H-cell, $(TBA)_2[W_6O_{19}]$ (0.107 g, 0.057 mmol) was added and dissolved in 10 mL of CH_3CN. The donor *o*-Me_2TTF (0.0096 g, 0.041 mmol) was combined with the electrolyte solution in the anodic compartment and exposed to a constant current density of 1.0 μA to yield black block-like crystals on the electrode surface which were harvested after a period of two weeks, washed with CH_3CN, and dried in air.

(*o*-$Me_2TTF)_2[Mo_6O_{19}]$ (14). Into a standard electrochemical cell, $(TBA)_2[Mo_6O_{19}]$ (0.110 g, 0.080 mmol) was added to both compartments and dissolved in 10 mL of CH_3CN. The donor *o*-Me_2TTF (0.0098 g, 0.042 mmol), which was also added to the anodic compartment, was oxidized at a constant current of 1.0 μA in the presence of the electrolyte solution to yield black needle crystals of the title salt on the surface of the electrode which were harvested after a period of two weeks. The crystals were washed with CH_3CN and dried in air. The synthesis of this salt is outlined in Table 5.

(BPDT-TTF)$_2$[W$_6$O$_{19}$] (15). As outlined in Table 5, into both compartments of a standard electrochemical H-cell, (TBA)$_2$[W$_6$O$_{19}$] (0.107 g, 0.057 mmol) was added and dissolved in 10 mL of a mixed CH_3CN/1,1,2-trichloroethane solution. The donor BPDT-TTF (0.010 g, 0.024 mmol) was combined with the electrolyte solution in the anodic compartment and exposed to a constant current density of 1.0 μA to yield black block-like crystals on the electrode surface which were harvested after a period a month, washed with CH_3CN and 1,1,2-trichloroethane and dried in air.

Table 6. Synthetic conditions for (*o*-Me$_2$TTF)$_8$[Fe^{III}(CN)$_6$]$_3$•2H$_2$O (**16•2H$_2$O**), (*o*-Me$_2$TTF)$_8$ [Co(CN)$_6$]2•8H$_2$O (**17•8H$_2$O**), (TTF)$_{11}$[Fe^{III}(CN)$_6$]$_3$•8H$_2$O (**18•8H$_2$O**),and (TTF)$_{11}$[Co(CN)$_6$]$_3$•8H$_2$O (**19•8H$_2$O**). All reactions were performed at a constant current of 0.9 μA.

salt		anode		cathode
(*o*-Me$_2$TTF)$_8$[Fe^{III}(CN)$_6$]$_3$•2H$_2$O (**16•2H$_2$O**)		*o*-Me$_2$TTF (10.1 mg) (TBA)$_3$[Fe(CN)$_6$] (115 mg) CH_3CN (10 mL)		(TBA)$_3$[Fe(CN)$_6$] (115 mg) CH_3CN (10 mL)
(*o*-Me$_2$TTF)$_8$[Co(CN)$_6$]•8H$_2$O (**17•8H$_2$O**)		*o*-Me$_2$TTF (10.1 mg) K$_3$[Co(CN)$_6$] (102 mg) Dibenzo-18-crown-6 (150 mg) CH_3CN (10 mL) H$_2$O (1 mL)		K$_3$[Co(CN)$_6$] (102 mg) Dibenzo-18-crown-6 (150 mg) CH_3CN (10 mL) H$_2$O (1 mL)
(TTF)$_{11}$[Fe^{III}(CN)$_6$]$_3$•8H$_2$O (**18•8H$_2$O**)		TTF (9.8 mg) K$_3$[Fe(CN)$_6$] (102 mg) Dibenzo-18-crown-6 (150 mg) CH_3CN (10 mL) H$_2$O (1 mL)		K$_3$[Fe(CN)$_6$] (102 mg) Dibenzo-18-crown-6 (150 mg) CH_3CN (10 mL) H$_2$O (1 mL)
(TTF)$_{11}$[Co(CN)$_6$]$_3$•8H$_2$O (**19•8H$_2$O**)		TTF (10.3 mg) K$_3$[Co(CN)$_6$] (102 mg) Dibenzo-18-crown-6 (150 mg) CH_3CN (10 mL) H$_2$O (1 mL)		K$_3$[Co(CN)$_6$] (102 mg) Dibenzo-18-crown-6 (150 mg) CH_3CN (10 mL) H$_2$O (1 mL)

(*o*-Me$_2$TTF)$_8$[Fe^{III}(CN)$_6$]$_3$•2H$_2$O (16•2H$_2$O). As outlined in Table 6, into both compartments of a standard electrochemical H-cell, (TBA)$_3$[Fe(CN)$_6$] (0.115 g, 0.122

mmol) was added and dissolved in 10 mL of CH_3CN. The donor *o*-Me_2TTF (0.0101 g, 0.044 mmol) was combined with the electrolyte solution in the anodic compartment and exposed to a constant current density of 0.9 μA to yield black needle crystals on the electrode surface which were harvested after a period a month, washed with CH_3CN, and dried in air.

(*o*-$Me_2TTF)_8[Co(CN)_6]_2 \cdot 8H_2O$ (17•$8H_2O$). As outlined in Table 6, into both compartments of a standard electrochemical H-cell, $K_3[Co(CN)_6]$ (0.105 g, 0.316 mmol) and dibenzo-18-crown-6 (0.150 g, 0.416 mmol) were added and dissolved in 10 mL of CH_3CN and 1 mL of H_2O. The donor *o*-Me_2TTF (0.0101 g, 0.044 mmol) was added to the anodic compartment and exposed to a constant current density of 0.9 μA to yield black block-like crystals on the electrode surface which were harvested after a period a month, washed with H_2O and CH_3CN, and dried in air.

$(TTF)_{11}[Fe^{III}(CN)_6] \cdot 8H_2O$ (18•$8H_2O$). As outlined in Table 6, into both compartments of a standard electrochemical H-cell, $K_3[Fe(CN)_6]$ (0.102 g, 0.310 mmol) and dibenzo-18-crown-6 (0.150 g, 0.416 mmol) were added and combined with 10 mL of CH_3CN and 1 mL of H_2O. The donor TTF (0.0098 g, 0.048 mmol) was added to the anodic compartment and the entire assembly was exposed to a constant current density of 0.9 μA which yielded black block-like crystals on the electrode surface which were harvested after a period of one month, washed with H_2O and CH_3CN, and dried in air.

$(TTF)_{11}[Co(CN)_6]_3 \cdot 8H_2O$ ($19 \cdot 8H_2O$). As described previously in Table 6, into both compartments of a standard electrochemical H-cell, $K_3[Co(CN)_6]$ (0.102 g, 0.307 mmol) and dibenzo-18-crown-6 (0.150 g, 0.416 mmol) were added and combined with 10 mL of CH_3CN and 1 mL of H_2O. The donor TTF (0.0103 g, 0.051 mmol) was added to the anodic compartment after which time the cell was subjected to an oxidative current density of 0.9 μA to yield black block-like crystals on the electrode surface which were harvested after a period a month, washed with H_2O and CH_3CN, and dried in air.

X-ray Crystallographic Details and Structure Solution

X-ray data for salts **2** and **5** were collected on a Bruker SMART CCD diffractometer at 110±2 K with graphite monochromated Mo-Kα (λ = 0.71073 Å) radiation. The data used to solve structures for **3** and **6, 15,** were collected on a Bruker D8 GADDS system at 110±2K with graphite monochromated Cu-Kα (λ = 1.54178 Å) radiation. Data for the remaining salts were collected on a Bruker APEX II diffractometer using graphite monochromated Mo-Kα (λ = 0.71073 Å) radiation. The data were corrected for Lorentz and polarization effects. The Bruker SAINT software package was used to integrate the frames and the data were corrected for absorption using the SADABS program.[86,87] Space groups were unambiguously assigned by analysis of symmetry and systematic absences determined by XPREP.[88] The structures were solved by direct methods by the use of the SHELXS-97 program in the Bruker SHELXTL v5.1 software package.[89,90] The final refinements were carried out with anisotropic thermal parameters for all non-hydrogen atoms. Figures for the crystallographic structures were generated using the XSEED program.[91]

Other Physical Measurements

Magnetic measurements were performed on a Quantum Design SQUID, MPMS-XL magnetometer. Magnetic susceptibility measurements in the DC mode were carried out at an applied field of 0.1 T in the 2-300 K range. Electrical conductivity was measured with the four probe technique using a Quantum Design PPMS equipment in the temperature range 300-220 K on single crystals of samples **1** and **3.** The contacts between the platinum wires (25 μm diameter) and the crystals were done using graphite paste. The samples were measured with cooling and warming rates of 0.5 $K.min^{-1}$ and with a D.C. intensity current of 0.1 μA. Theoretical band diagrams were calculated using the program CAESAR.[92]

X-ray Structures

The crystals for all of the radical cation salts were grown by electrochemical oxidation of various chalcofulvalene donors in the presence of solutions of various charge compensating anions. It has been well established in various literature reports that, in the absence of any inter-molecular contacts such as π-π or S ••• S interactions, neutral chalcofulvalene donors are non-planar, often exhibiting significant bends of up to 30° along intra-molecular dithiole or diseleno bridges.[12] Upon oxidation of the donor, structural alterations accompanying the formation of the radical cation occur, which includes the adoption of a planar conformation followed by a lengthening of the central C=C bond and a shortening of the C-S bonds in the central TTF core.[93]

The central C=C bond and C-S bonds are the most susceptible to the oxidation state of the donor and have been used by Coppens and coworkers to develop an empirical relationship that can be used to calculate the overall oxidation state of the donor molecule.[94] With the presence of planar, radical cation salts of TTF-like molecules, another intermolecular interaction occurs in the solid state. Planar, radical cations, such as TTF, have a strong tendency to form dimers in the solid-state via a two-electron bond through direct overlap of their singly-occupied molecular orbitals (SOMOs). An important characteristic of the tetrathiafulvalene molecule is the shape of its SOMO, which is an orbital whose π-character covers the central C_2S_4 motif. The approach of two such radical cations into a face-to-face eclipsed arrangement corresponds to the formation of σ bonding and σ* antibonding combinations of the two SOMOs (Figure 21). With an electron occupancy of two, a strong σ bond between the radicals is formed and the dyadic, dicationic entity becomes fully diamagnetic.[95]

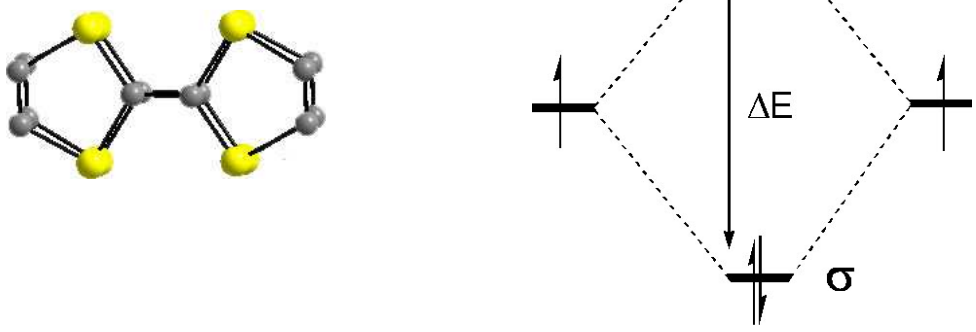

Figure 21. Face-to face arrangement in dimers of TTF and corresponding molecular orbital diagram description of the diamagnetic nature of this entity.

*(BEDT-TTF)$_2$[Re$_2$Cl$_8$] (**1**), (TMTTF)$_3$[Re$_2$Cl$_8$]•2CH$_3$CN (**2•2CH$_3$CN**), (TMTSF)$_5$[Re$_2$Cl$_8$]•3CH$_2$Cl$_2$ (**3•3CH$_2$Cl$_2$**), and (o-Me$_2$TTF)$_2$ [Re$_2$Cl$_8$] (**4**)*

The salt (BEDT-TTF)$_2$[Re$_2$Cl$_8$] (**1**) crystallizes in the triclinic space group *P-1* and is dominated by the formation of strong σ-type dimers between fully oxidized radical cations of BEDT-TTF. The oxidation state for both radicals has been determined to be +1 via calculation using the Coppens formula. Closer inspection of the intradimer S-S contacts along the (1,1,1) stacking axis reveal separations of 3.463 and 3.476 Å between neighboring sulfur atoms in the TTF core of the BEDT-TTF molecules. Since the separation between the neighboring atoms is <3.6 Å, the sum of the van der Waals radii for overlapped sulfur p-orbitals, it can be postulated that a dimer has formed between the BEDT-TTF radical cations, which would lead to the onset of strong charge localization. No S-S contacts are found to exist between peripheral sulfur atoms on the ethylenedithio bridges as the intradimer contacts between these sulfur atoms are >3.8 Å. There are also significant bends in these ethylenedithio bridges around the sp^3-hybridized carbons, a direct consequence of the tetrahedral geometry of these carbon atoms. The solid-state structure and selected bnond distances for **1** are shown in Figures 22 and 23 and Table 7.

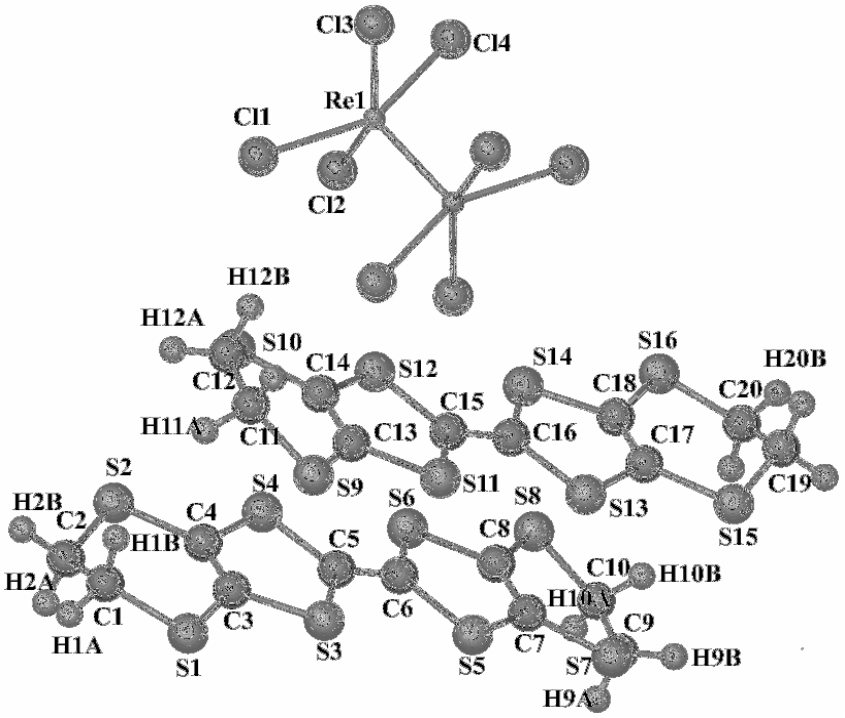

Figure 22. X-ray crystal structure of $(BEDT\text{-}TTF)_2[Re_2Cl_8]$ (**1**).

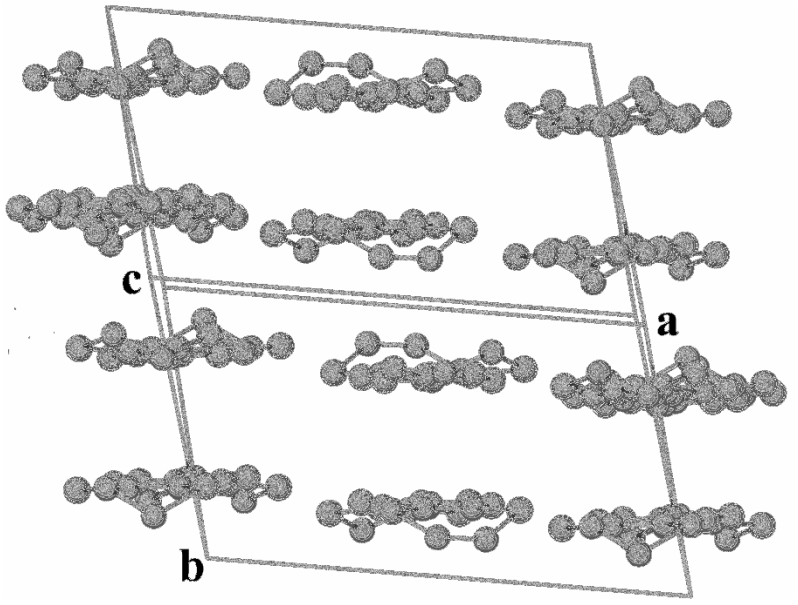

Figure 23. Solid-state packing of the BEDT-TTF donor molecules in **1** illustrating the formation of stacks of the BEDT-TTF donor molecules.

Table 7. Bond distances for (BEDT-TTF)$_2$[Re_2Cl_8] (**1**) in Å.

Re(1)-Re(1)	2.231(19)	S(9)-C(11)	1.72(3)
Re(2)-Re(2)	2.222(18)	S(9)-C(13)	1.74(2)
Re(1)-Cl(1)	2.337(5)	S(10)-C(12)	1.73(3)
Re(1)-Cl(2)	2.340(5)	S(10)-C(14)	1.72(2)
Re(1)-Cl(3)	2.335(5)	S(11)-C(13)	1.74(2)
Re(1)-Cl(4)	2.318(5)	S(11)-C(15)	1.70(2)
Re(2)-Cl(5)	2.334(5)	S(12)-C(14)	1.77(2)
Re(2)-Cl(6)	2.335(5)	S(12)-C(15)	1.73(2)
Re(2)-Cl(7)	2.308(6)	S(13)-C(16)	1.72(2)
Re(2)-Cl(8)	2.334(6)	S(13)-C(17)	1.75(2)
S(1)-C(1)	1.81(2)	S(14)-C(16)	1.74(2)
S(1)-C(3)	1.72(2)	S(14)-C(18)	1.76(2)
S(2)-C(2)	1.80(3)	S(15)-C(17)	1.748(18)
S(2)-C(4)	1.78(2)	S(15)-C(19)	1.79(3)
S(3)-C(3)	1.77(2)	S(16)-C(18)	1.76(2)
S(3)-C(5)	1.70(2)	S(16)-C(20)	1.73(3)
S(4)-C(4)	1.74(2)	C(1)-C(2)	1.44(3)
S(4)-C(5)	1.731(19)	C(3)-C(4)	1.31(3)
S(5)-C(6)	1.706(19)	C(5)-C(6)	1.41(3)
S(5)-C(7)	1.76(2)	C(7)-C(8)	1.42(3)
S(6)-C(6)	1.73(2)	C(9)-C(10)	1.45(3)
S(6)-C(8)	1.71(2)	C(11)-C(12)	1.33(4)
S(7)-C(7)	1.71(2)	C(13)-C(14)	1.33(3)
S(7)-C(9)	1.83(2)	C(15)-C(16)	1.39(3)
S(8)-C(8)	1.71(2)	C(17)-C(18)	1.32(3)
S(8)-C(10)	1.79(2)	C(19)-C(20)	1.38(4)

Upon initial observation analysis of **2**, it appears that mixed-valence chalcofulvalene donors essential to the onset of enhanced conductivity may be present. Upon closer inspection of the C=C and C-S bond distances, it appears that two of the three TMTTF donor molecules have been completely ionized to the +1 state while the third remains neutral. The stacking motif which exists along the (1,1,1) axis is dominated by close S-S contacts between neighboring sulfur atoms at distances <3.6 Å, indicating the presence of a potential strong σ-type dimer between the tetramethyltetrathiafulvalenium cations. The intra-atomic distances between the sulfur atoms of one TMTTF radical cation and the neutral donor are >3.6 Å leading to a non-uniform stacking motif along the stacking axis. Another interesting feature found in the structure is the presence of weak hydrogen bonds between the nitrogen atom (N2) of an interstitial acetonitrile molecules and a single sp^3-hybridized carbon atom (H24B) of a tetramethyltetrathiafulvalenium cation. The solid-state structure and selected bnond distances for (**2•2CH$_3$CN**) are shown in Figures 24 and 25 and Table 8.

The solid state structure of **3** gives the initial appearance of a mixed-valence system. A key difference between **2** and **3** is the substitution of selenium atoms into the molecular environment of the chalcofulvalenium donor. Much like S-S contacts at distances <3.6 Å, Se-Se overlap at distances <4.0 Å indicate strong inter-atomic interactions. These strong interactions are essential to the formation of a facile pathway for the transfer of itinerant electrons. Upon closer analysis of the critical bond distances, it appears that four of the five TMTSF donors, labeled as A-E, have been ionized to their +1 state.

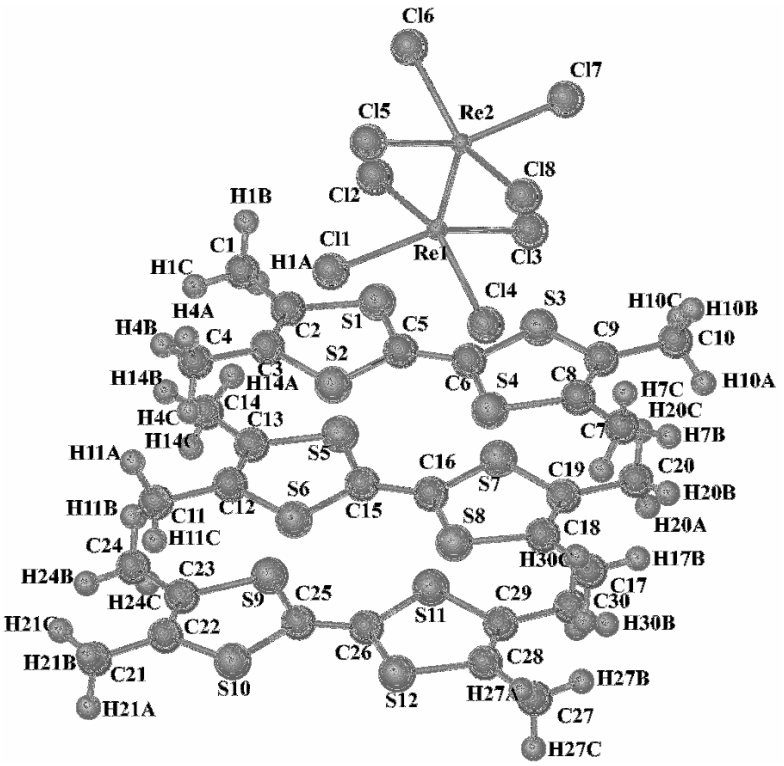

Figure 24. X-ray crystal structure of $(TMTTF)_3[Re_2Cl_8]\bullet 2CH_3CN$ (**$2\bullet CH_3CN$**). Interstitial acetonitrilemolecules have been omitted for the sake of clarity.

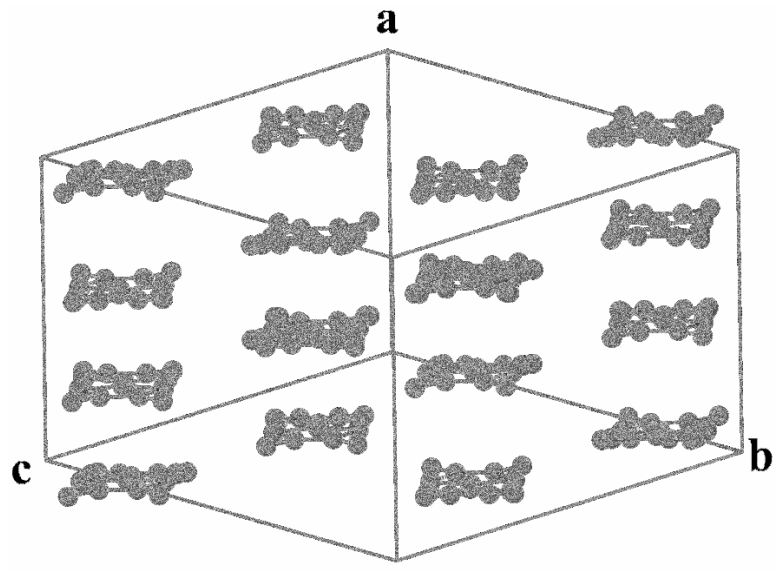

Figure 25. Solid-state packing of the TMTTF donor molecules in **$2\bullet 2CH_3CN$** illustrating their formation of a one-dimensional stacking motif in the organic sublattice.

Table 8. Bond distances for $(TMTTF)_3[Re_2Cl_8]\bullet 2CH_3CN$ (**2•2CH$_3$CN**) in Å.

Re(1)-Re(2)	2.2253(8)	S(11)-C(26)	1.718(4)
Re(1)-Cl(1)	2.3230(12)	S(11)-C(29)	1.751(4)
Re(1)-Cl(2)	2.3271(12)	S(12)-C(26)	1.726(4)
Re(1)-Cl(3)	2.3317(14)	S(12)-C(28)	1.742(4)
Re(1)-Cl(4)	2.3304(11)	C(1)-C(2)	1.505(6)
Re(2)-Cl(5)	2.3186(14)	C(2)-C(3)	1.338(6)
Re(2)-Cl(6)	2.3344(11)	C(3)-C(4)	1.507(6)
Re(2)-Cl(7)	2.3367(12)	C(5)-C(6)	1.357(6)
Re(2)-Cl(8)	2.3263(13)	C(7)-C(8)	1.499(6)
S(1)-C(2)	1.760(4)	C(8)-C(9)	1.341(6)
S(1)-C(5)	1.750(4)	C(9)-C(10)	1.492(6)
S(2)-C(3)	1.761(4)	C(11)-C(12)	1.500(6)
S(2)-C(5)	1.751(4)	C(12)-C(13)	1.362(6)
S(3)-C(6)	1.752(4)	C(13)-C(14)	1.491(6)
S(3)-C(8)	1.758(4)	C(15)-C(16)	1.399(5)
S(4)-C(6)	1.748(4)	C(17)-C(18)	1.506(6)
S(4)-C(9)	1.755(4)	C(18)-C(19)	1.350(6)
S(5)-C(12)	1.738(4)	C(19)-C(20)	1.499(5)
S(5)-C(15)	1.721(4)	C(21)-C(22)	1.499(6)
S(6)-C(13)	1.740(4)	C(22)-C(23)	1.360(6)
S(6)-C(15)	1.716(4)	C(23)-C(24)	1.496(6)
S(7)-C(16)	1.716(4)	C(25)-C(26)	1.392(5)
S(7)-C(19)	1.732(4)	C(27)-C(28)	1.489(6)
S(8)-C(16)	1.713(4)	C(28)-C(29)	1.352(6)
S(8)-C(18)	1.731(4)	C(29)-C(30)	1.491(6)
S(9)-C(22)	1.729(4)	C(31)-C(32)	1.438(8)
S(9)-C(25)	1.725(4)	C(33)-C(34)	1.442(8)
S(10)-C(23)	1.737(4)	C(32)-N(1)	1.136(7)
S(10)-C(25)	1.710(4)	C(34)-N(2)	1.137(8)

Close inspection of the inter- and intra-atomic bond distances reveal that the Se-Se contacts between selenium atoms in A and B are <4.0 Å, indicating the formation of a strong dimer of the σ-type. Intermolecular bond distances between B and C show contacts at distances ranging from a minimum of 3.933 Å to a maximum of 4.188 Å. The lack of contact between selenium atoms at distances >4.0 Å between donors B and C indicate the existence of a dimer between donors A and B instead of a trimer composed of A-C. The onset of short Se-Se contacts between selenium atoms in C and D are <4.0 Å, indicating the formation of a strong σ-dimer between these donors. The final set of intermolecular contacts, those between D and E show inter-atomic distances similar to those between B and C, primarily that they are >4.0 Å ranging from a minimum of 3.933 Å to a maximum of 4.188 Å. In accordance with charge neutrality dictated by the presence of two $[Re_2Cl_8]^{2-}$ dianions, it can be concluded that the organic sublattice is composed of a dimer of TMTSF radical cation dimers. The solid-state structure and selected bond distances for (**3•3CH$_2$Cl$_2$**) are shown in Figures 26 and 27 and Table 9.

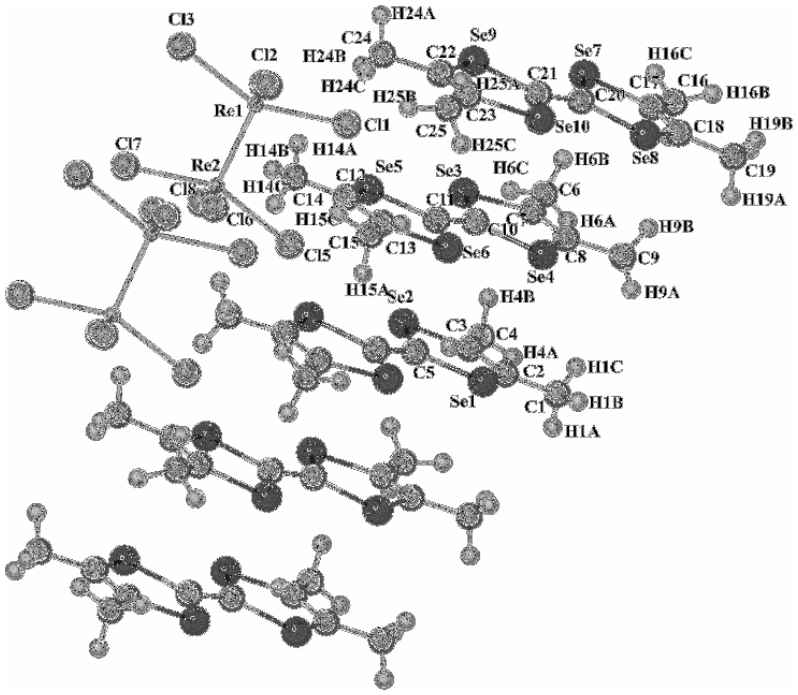

Figure 26. X-ray crystal structure of $(TMTSF)_5[Re_2Cl_8]_2 \cdot 3CH_2Cl_2$ (**3•3CH$_2$Cl$_2$**). Interstitial dichloromethane molecules have been omitted for the sake of clarity.

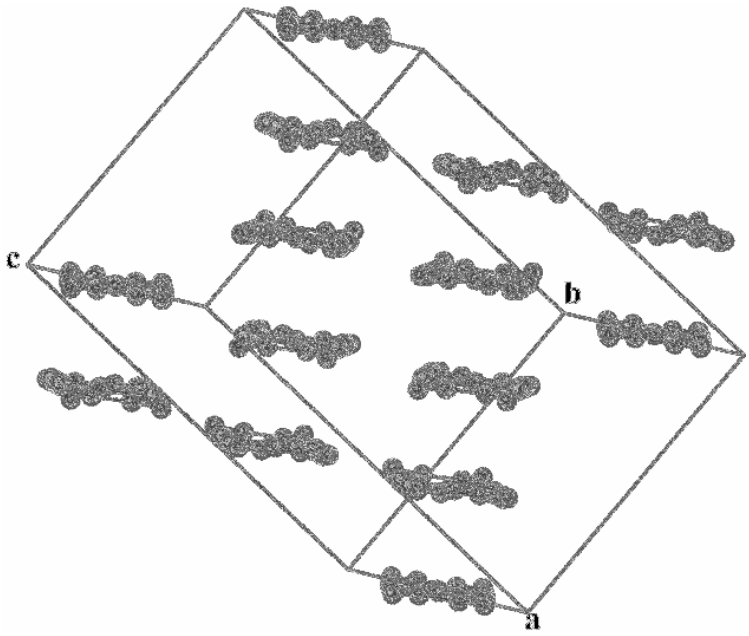

Figure 27. Solid-state packing of the TMTSF donor molecules in **3•3CH$_2$Cl$_2$** illustrating the formation of a one-dimensional stacking motif in the organic sublattice.

Table 9. Bond distances for $(TMTSF)_5[Re_2Cl_8]_2 \cdot 3CH_2Cl_2$ (**3•3CH_2Cl_2**) in Å.

Re(1)-Re(2)	2.257(16)	Se(9)-C(22)	1.89(2)
Re(1)-Cl(1)	2.340(5)	Se(10)-C(21)	1.87(2)
Re(1)-Cl(2)	2.320(5)	Se(10)-C(23)	1.86(2)
Re(1)-Cl(3)	2.329(5)	C(1)-C(2)	1.47(3)
Re(1)-Cl(4)	2.329(5)	C(2)-C(3)	1.36(3)
Re(2)-Cl(5)	2.327(5)	C(3)-C(4)	1.53(5)
Re(2)-Cl(6)	2.327(5)	C(5)-C(5)	1.40(4)
Re(2)-Cl(7)	2.331(5)	C(6)-C(7)	1.52(3)
Re(2)-Cl(8)	2.330(5)	C(7)-C(8)	1.32(3)
Se(1)-C(3)	1.84(2)	C(8)-C(9)	1.50(3)
Se(1)-C(5)	1.87(2)	C(10)-C(11)	1.38(3)
Se(2)-C(2)	1.90(2)	C(12)-C(13)	1.37(3)
Se(2)-C(5)	1.85(2)	C(12)-C(15)	1.50(3)
Se(3)-C(7)	1.88(2)	C(13)-C(14)	1.48(3)
Se(3)-C(10)	1.87(2)	C(16)-C(17)	1.43(3)
Se(4)-C(8)	1.91(2)	C(17)-C(18)	1.36(3)
Se(4)-C(10)	1.86(2)	C(18)-C(19)	1.50(3)
Se(5)-C(11)	1.87(2)	C(20)-C(21)	1.38(3)
Se(5)-C(12)	1.88(2)	C(22)-C(23)	1.39(3)
Se(6)-C(11)	1.90(2)	C(22)-C(25)	1.47(3)
Se(6)-C(13)	1.89(2)	C(26)-Cl(9)	1.76(3)
Se(7)-C(17)	1.90(2)	C(26)-Cl(10)	1.75(3)
Se(7)-C(20)	1.86(2)	C(27)-Cl(11)	1.72(3)
Se(8)-C(18)	1.868(19)	C(27)-Cl(12)	1.78(3)
Se(8)-C(20)	1.89(2)	C(28)-Cl(13)	1.77(3)
Se(9)-C(21)	1.86(2)	C(28)-Cl(14)	1.64(3)

The solid-state structure of **4** crystallizes in the triclinic space group *P-1* and is dominated by short S-S contacts at distances <3.6 Å between the neighboring sulfur atoms of the *o*-Me_2TTF donor which reside along the tetrathiafulvalenium stacks which coincide with the (1,1,1) axis. These short interatomic bond distances combined with the presence of +1 charges on the radical cations should lead to the formation of strong σ-type dimers which could lead to the onset of charge localization. Among other structural details of the structure is a Re-Re bond distance of 2.225 Å consistent with the existence of a quadruple bond between the rhenium atoms, as expected.[96] The solid-state structure and selected bond distances for **4** are shown in Figures 28 and 29 and Table 10. X-ray crystallographic and refinement and the calculated valences for the chalcofulvalenium radical cations for **1-4** are listed in Tables 11 and 12.

*(BEDT-TTF)[Cu(mnt)$_2$] (**5**) and (TMTTF) [Cu(mnt)$_2$] (**6**)*

The solid state structure of **5**, which crystallizes in the triclinic space group *P-1*, and is dominated by integrated stacks of BEDT-TTF donors and $[Cu(mnt)_2]^-$ anions. Unlike the structures, with one-dimensional stacks of donor molecules, the structure of **5** shows 1:1 stacks of molecules of dissimilar symmetry which stack along the (1,1/2,1) plane.

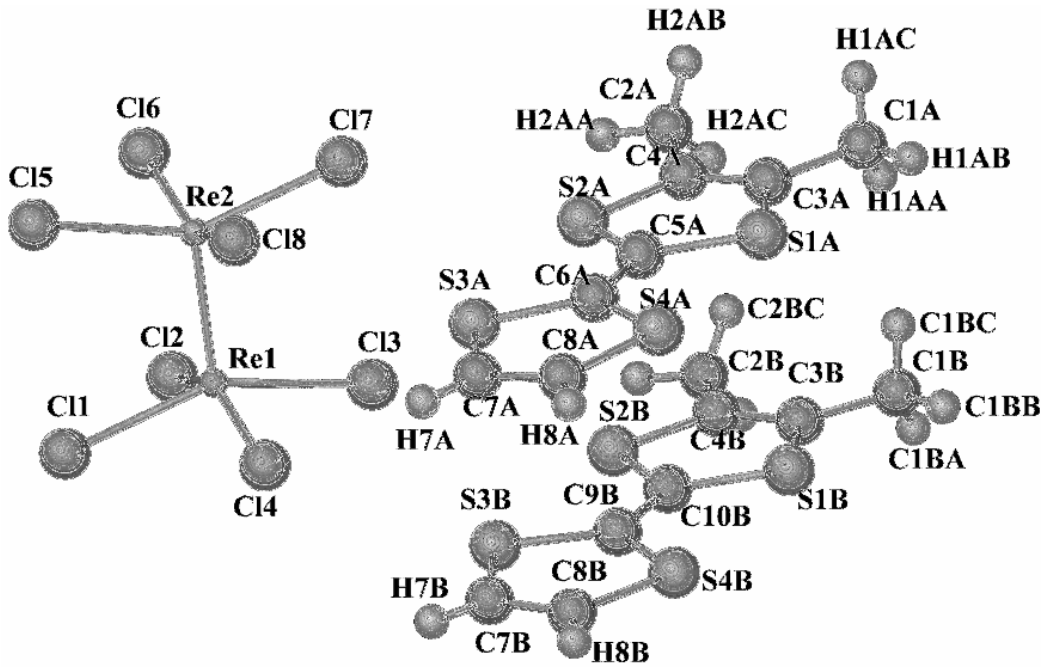

Figure 28. X-ray crystal structure of (*o*-Me_2TTF)$_2$[Re_2Cl_8] (**4**).

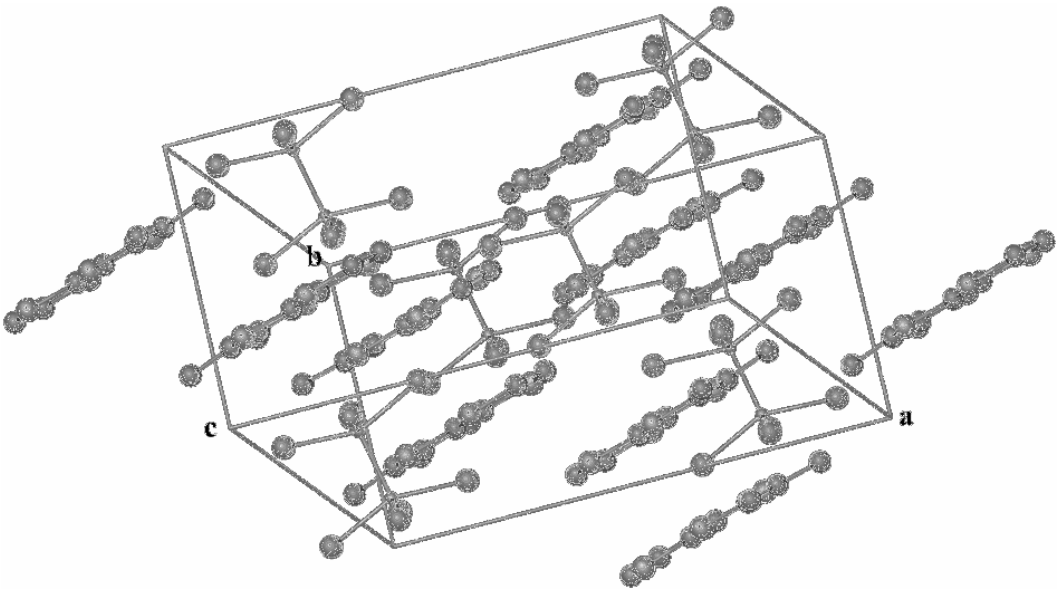

Figure 29. Extended solid-state structure of **4** illustrating the formation of eclipsed head-to-head dimers of the *o*-Me_2TTF donor.

Table 10. Bond distances for (*o*-$Me_2TTF)_2[Re_2Cl_8]$ (**4**) in Å.

Re(1)-Re(2)	2.2249(4)
Re(1)-Cl(8)	2.3071(18)
Re(1)-Cl(5)	2.3267(17)
Re(1)-Cl(60	2.3385(16)
Re(1)-Cl(7)	2.3411(18)
Re(2)-Cl(3)	2.3158(18)
Re(2)-Cl(2)	2.3254(16)
Re(2)-Cl(4)	2.3279(18)
Re(2)-Cl(1)	2.3378(17)
S(1A)-C(5A)	1.722(7)
S(1A)-C(3A)	1.742(7)
S(2A)-C(5A)	1.702(7)
S(2A)-C(4A)	1.728(7)
S(3A)-C(6A)	1.712(7)
S(3A)-C(7A)	1.727(8)
S(4A)-C(8A)	1.700(8)
S(4A)-C(6A)	1.724(7)
C(1A)-C(3A)	1.502(9)
C(2A)-C(4A)	1.508(9)
C(3A)-C(4A)	1.337(9)
C(5A)-C(6A)	1.401(8)
C(7A)-C(8A)	1.342(11)
S(1B)-C(5B)	1.713(7)
S(1B)-C(3B)	1.746(7)
S(2B)-C(4B)	1.727(7)
S(2B)-C(5B)	1.727(6)
S(3B)-C(7B)	1.717(9)
S(3B)-C(6B)	1.718(7)
S(4B)-C(6B)	1.718(7)
S(4B)-C(8B)	1.719(10)
C(1B)-C(3B)	1.485(10)
C(2B)-C(4B)	1.491(9)
C(3B)-C(4B)	1.356(10)

Table 11. X-ray crystallographic and refinement data for radical salts **1-4**.

Compound	(BEDT-TTF)$_2$[Re_2Cl_8] (**1**)	(TMTTF)$_3$[Re_2Cl_8]•2CH_3CN (**2**)	(TMTSF)$_5$[Re_2Cl_8]$_2$•3CH_2Cl_2 (**3**)	(*o*-Me_2TTF)$_2$[Re_2Cl_8] (**4**)
Formula	$C_{20}S_{16}Re_2Cl_8$	$C_{34}H_{42}S_{12}N_2Re_2Cl_8$	$C_{53}H_{66}Se_{20}Re_4Cl_{22}$	$C_{16}H_{16}S_8Re_2Cl_8$
formula weight	1409.28	1515.66	3817.98	1117.56
Space group	P-1	P-1	P-1	P-1
a, Å	10.404(2)	10.542(2)	13.042(3)	8.7469(4)
b, Å	12.843(3)	13.786(3)	14.022(3)	10.6444(5)
c, Å	15.622(3)	19.664(4)	15.283(3)	16.5506(8)
α, deg	97.16(3)	100.64(3)	93.84(3)	79.058(2)
β, deg	105.25(3)	104.87(3)	103.51(3)	81.276(2)
γ, deg	100.91(3)	107.66(3)	109.76(3)	88.963(2)
volume, Å^3	1943.75	2522.82	2524.91	1495.34(12)
Z	3	4	4	4
μ, mm^{-1}	11.48	10.76	25.53	9.372
Temp.	110(2)	110(2)	110(2)	110(2)
Reflns. collected	4955	11560	11339	6810
Reflns. I>2σ	3461	10068	8429	5330
Parameters	410	537	467	307
Restraints	0	0	0	0
R1[a]	0.0735	0.0339	0.0992	0.0410
wR2[b]	0.1038	0.0930	0.2746	0.0898
Goodness-of-fit[c]	1.014	1.042	1.064	1.081

[a] $R1 = \sum||F_o| - |F_c||/\sum|F_o|$. [b] $wR2 = [\sum [w(F_o^2-F_c^2)^2]/ \sum [w(F_o^2)^2]^{1/2}$

[c] Goodness-of-fit = $[\sum w(|F_o|-|F_c|)^2/(N_{obs}-N_{parameter})]^{1/2}$

Table 12. Estimated degree of ionicity for the donor molecules for **1,** (**2•2CH$_3$CN**)**,** (**3•3CH$_2$Cl$_2$**)**,** and **4**.

salt	**molecule**	**A**[a]	**B**[b]	**Q**[c]
(ET)$_2$[Re_2Cl_8] (**1**)	A	1.408(6) Å	1.717(5) Å	+1.29
	B	1.385(7) Å	1.725(6) Å	+0.89
(TMTTF)$_3$[Re_2Cl_8]•2CH_3CN (**2•2CH$_3$CN**)	A	1.392(8) Å	1.728(4) Å	+0.95
	B	1.399(3) Å	1.717(5) Å	+1.17
	C	1.357(5) Å	1.750(3) Å	+0.25
(TMTSF)$_5$[Re_2Cl_8]$_2$•3CH_2Cl_2 (**3•3CH$_2$Cl$_2$**)	A	1.377(9) Å	1.859(8) Å	+1.10
	A	1.377(9) Å	1.859(8) Å	+1.10
	B	1.381(5) Å	1.877(4) Å	+1.10
	B	1.381(5) Å	1.877(4) Å	+1.10
	C	1.401(8) Å	1.872(7) Å	+1.40
(*o*-Me_2TTF)$_2$[Re_2Cl_8] (**4**)	A	1.401(3) Å	1.715(3) Å	+1.22
	B	1.373(2) Å	1.717(4) Å	+0.82

[a] Central C=C bond distance.

[b] Mean central C-S bond distance.

[c] Q = charge estimated with the formula Q = -17.92 + 23.43*(A/B) from Ref. 94.

As is evidenced by the C=C and average C-S bond distances of the BEDT-TTF donor (1.402 and 1.724 Å respectively), its valence using the Coppens formula has been calculated to be in the +1 state.[94] In order to balance the charge in the salt, the $[Cu(mnt)_2]^{2-}$ anion, introduced as its tetrabutylammonium salt, has also undergone oxidation to the -1 state. The Cu-S bond distances, determined crystallographically to be 2.191 and 2.195 Å are similar to isostructural M-S bond distances in analogous metal-dithiolene systems where the anion has undergone oxidation.[81-83] Close S-S contacts are found to exist in the side-to-side regime unlike the previous charge-transfer salts where the close contacts exist along the stacking axis. These close contacts with distances of 3.489 and 3.579 Å are <3.6 Å and indicate the presence of close interplanar S-S contacts in the plane formed by the BEDT-TTF donors. No cation-anion S-S contacts between the donor and acceptor exist along the stacking axis, as the closest interatomic contact between their neighboring sulfur atoms is 3.787 Å. This is longer than the sum of each sulfur atom's individual atomic radius and indicates no significant interactions. The solid-state structure and selected bond distances for **5** are shown in Figures 30 and 31 and Table 13.

The solid-state structure for **6** crystallizes in the triclinic space group *P-1* and shows similar features to **5**. Based on the C=C and average C-S bond distances of the for TMTTF donor, the overall charge has been calculated to be +1. Also, much like the BEDT-TTF salt, the charge was balanced by the anion which showed oxidation to the -1 state.[81-83]

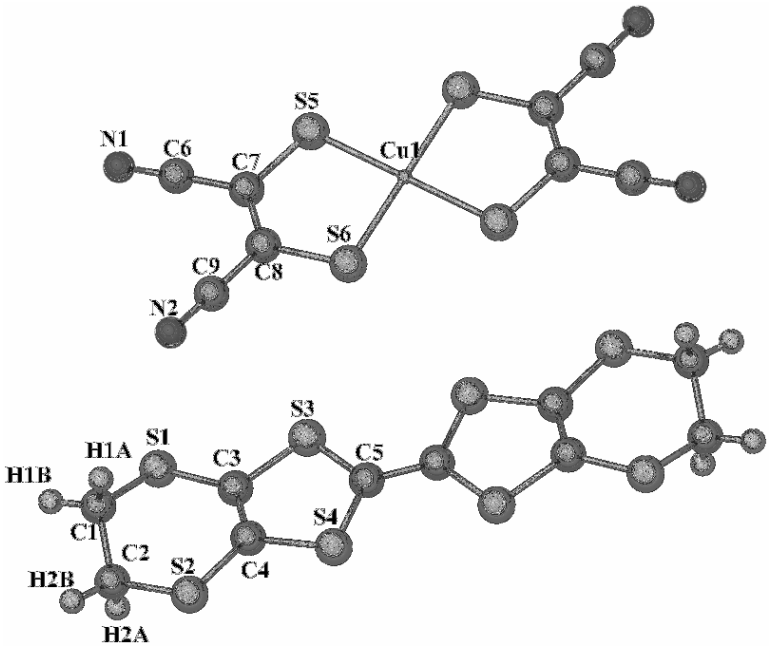

Figure 30. X-ray crystal structure of (BEDT-TTF)[Cu(mnt)$_2$] (**5**).

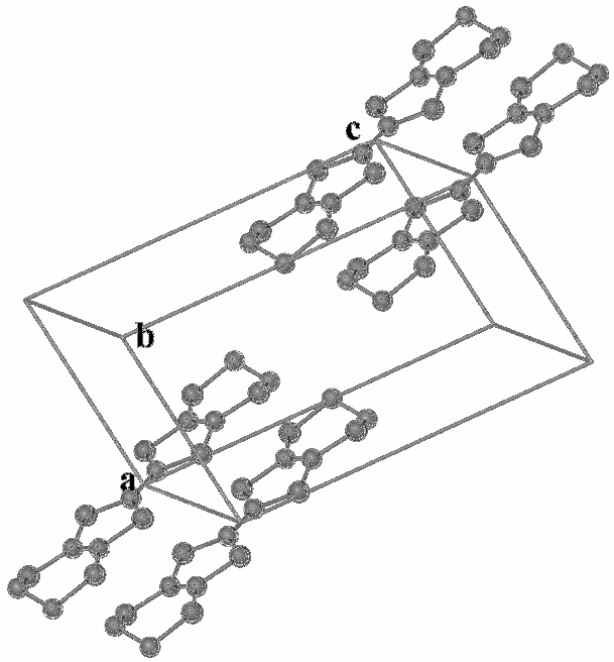

Figure 31. Symmetry-generated representation for the organic sublattice of **5** illustrating the formation of donor molecule sheets in the crystal lattice. Hydrogen atoms on the BEDT-TTF donors have been omitted for the sake of clarity.

Table 13. Bond distances for (BEDT-TTF)[Cu(mnt)$_2$] (**5**) in Å.

Cu(1)-S(5)	2.1909(15)
Cu(1)-S(6)	2.1950(15)
S(1)-C(1)	1.817(6)
S(1)-C(3)	1.736(6)
S(2)-C(2)	1.814(6)
S(2)-C(4)	1.751(6)
S(3)-C(3)	1.755(6)
S(3)-C(5)	1.726(5)
S(4)-C(4)	1.744(6)
S(4)-C(5)	1.722(5)
S(5)-C(8)	1.750(6)
S(6)-C(7)	1.758(5)
N(1)-C(6)	1.160(7)
N(2)-C(9)	1.151(7)
C(1)-C(2)	1.524(8)
C(3)-C(4)	1.373(8)
C(5)-C(5)	1.402(11)
C(6)-C(7)	1.435(8)
C(7)-C(8)	1.344(8)
C(8)-C(9)	1.437(8)

Unlike the previously discussed BEDT-TTF salt, along the stacking axis, which coincides with the unit cell's b-axis, the stacks are dominated by 2:1 stacks of integrated donor and acceptor molecules. Separate integrated stacks are related to one another by translation along the c-glide plane in a sinusoidal wave pattern. Also of note is the occurrence of strong σ-type dimers of fully-oxidized TMTTF donors as evidenced by close S-S contacts of 3.365 and 3.471 Å between sulfur atoms of the TMTTF donors which could lead to the onset of charge localization. Upon close inspection, there are no transverse S-S interactions between the cations and anions, as the interatomic distances are >3.8 Å. The solid-state structure and selected bond distances for **5** are shown in Figure 32 and Table 14. X-ray crystallographic and refinement and the calculated valences for the chalcofulvalenium radical cations for **5** and **6** are listed in Tables 15 and 16.

*$(o\text{-}Me_2TTF)_2[Cl]$ (**7**), $(o\text{-}Me_2TTF)_2[Br]$ (**8**), $(o\text{-}Me_2TTF)_2[I]$ (**9**), $(o\text{-}Me_2TTF)_2[BF_4]$ (**10**), $(o\text{-}Me_2TTF)_2[PF_6]$ (**11**) and $(o\text{-}Me_2TTF)[I_3]$ (**12**)*

The solid-state structures of **7-10** are isostructural and crystallize in the highly-symmetric tetragonal space group $I4_2d$. All of the radical cation charges, which according to calculations using the Coppens' method of valence calculation, were determined to be +0.5 indicating the presence of donors in genuine, non-integral oxidation states and stack along the c-axis in a head-to-tail manner. This pattern is unlike the traditional formation of strong eclipsed dimers between fully-ionized TTF radical cations which align in a face-to-face arrangement to form σ-bonding and σ*-antibonding combinations of the two SOMOs.

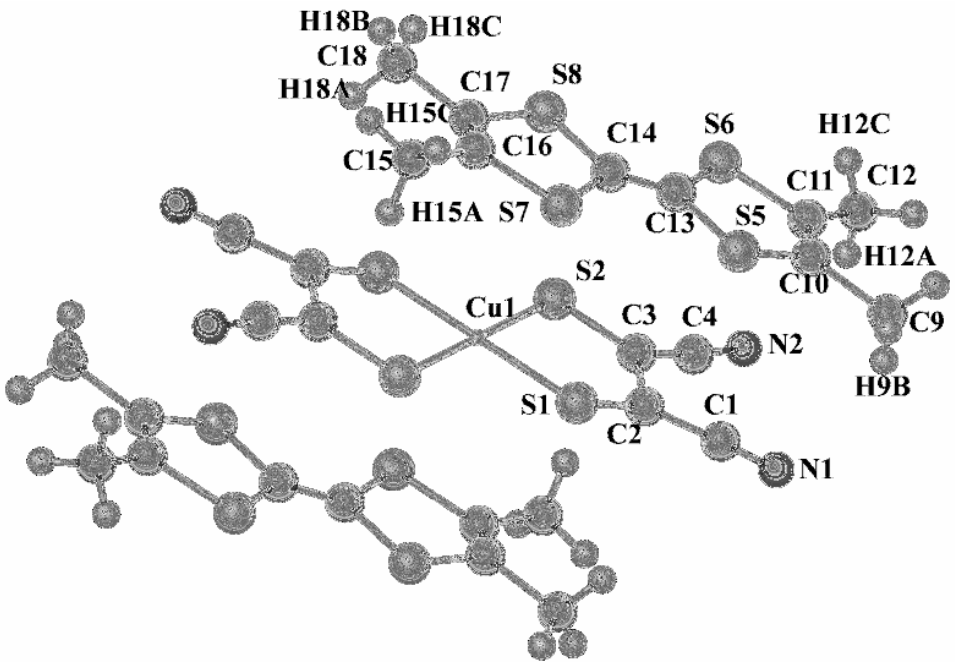

Figure 32. X-ray crystal structure of (TMTTF)[Cu(mnt)$_2$] (**6**).

Table 14. Bond distances for (TMTTF)[Cu(mnt)$_2$] (**6**) in Å.

Cu(1)-S(1)	2.197(7)	C(1)-N(1)	1.122(4)
Cu(1)-S(2)	2.194(3)	C(4)-N(2)	1.095(2)
S(1)-C(2)	1.699(5)	C(1)-C(2)	1.264(6)
S(2)-C(3)	1.736(4)	C(2)-C(3)	1.517(5)
S(5)-C(10)	1.749(2)	C(3)-C(4)	1.445(7)
S(5)-C(13)	1.727(7)	C(9)-C(10)	1.493(2)
S(6)-C(11)	1.741(3)	C(10)-C(11)	1.356(4)
S(6)-C(13)	1.724(5)	C(11)-C(12)	1.490(5)
S(7)-C(14)	1.725(4)	C(13)-C(14)	1.392(8)
S(7)-C(16)	1.731(2)	C(15)-C(16)	1.487(9)
S(8)-C(14)	1.736(3)	C(16)-C(17)	1.358(3)
S(8)-C(17)	1.724(5)	C(17)-C(18)	1.497(6)

Table 15. X-ray crystallographic and refinement data for **5** and **6**.

Compound	(BEDT-TTF)[Cu(mnt)$_2$] (**5**)	(TMTTF)[Cu(mnt)$_2$] (**6**)
Formula	$C_{18}H_8CuN_4S_{12}$	$C_{18}H_{12}CuN_4S_8$
formula weight	728.54	602.81
Space group	P-1	P-1
a, Å	6.7987(14)	13.079(3)
b, Å	7.2713(15)	11.205(2)
c, Å	13.705(3)	23.691(5)
***α*, deg**	80.23(3)	89.97(3)
β, deg	89.91(3)	95.94(3)
γ, deg	71.54(3)	89.97(3)
volume, Å^3	632.3(2)	3453.2(12)
Z	1	4
μ, mm^{-1}	1.875	1.663
Temp.	110(2)	110(2)
Reflns. collected	1696	11089
Reflns. I>2σ	1408	7564
Parameters	632	568
Restraints	0	0
R1[a]	0.0455	0.055
wR2[b]	0.1258	0.1499
Goodness-of-fit[c]	1.034	0.984

[a] $R1 = \sum||F_o| - |F_c||/\sum|F_o|$. [b] $wR2 = [\sum [w(F_o^2-F_c^2)^2]/ \sum [w(F_o^2)^2]]^{1/2}$

[c] Goodness-of-fit = $[\sum w(|F_o|-|F_c|)^2/(N_{obs}-N_{parameter})]^{1/2}$

Table 16. Estimated degree of ionicity for the donor molecules for **5** and **6.**

salt	**molecule**	**A**[a]	**B**[b]	**Q**[c]
(BEDT-TTF)[Cu(mnt)$_2$] (**5**)	A	1.402 Å	1.724 Å	+1.13
(TMTTF)[Cu(mnt)$_2$] (**6**)	A	1.392 Å	1.728 Å	+0.95

[a] Central C=C bond distance.
[b] Mean central C-S bond distance.
[c] Q = charge estimated with the formula Q = -17.92 + 23.43*(A/B) from Ref. 94.

In contrast to the strong dyadic, dicationic $(TTF)_2^{2+}$, which becomes fully diamagnetic, the head-to-tail non-integral donors can be considered as the elementary building block for extended one- and two-dimensional structures found to exist in conducting systems. The formation of bonding and antibonding orbital combinations also captures the essence of the mixed valence dyadic system $[TTF]_2^{\bullet+}$, leads to a singly-occupied σ* orbital.[95] The solid-state structures and selected bond distances for **5** are shown in Figure 32 and Table 14.

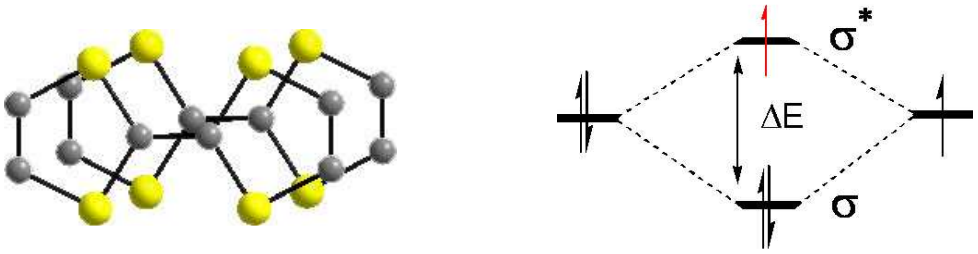

Figure 33. Formation of bond over ring arrangement in mixed-valence dimers of TTF and corresponding molecular orbital diagram description of the paramagentic nature of this entity.

In this configuration, the net bond formation is weaker but the intraction is still present. Due to this decreased interaction, the plane-to-plane distance increases and the molecules shift from the eclipsed conformation in the dicationic dyad to the bond-over-ring conformation. This conformation is described above in Figure 33 and is similar to those encountered in extended structures, where an infinite number of partially-occupied SOMOs interact to form the energy bands of a metal.

The solid-state structure and selected bond distances for **7-10** are shown in Figure 34-37. The solid-state structures for are dominated by infinite stacks of donors conforming to the bond-over-ring scenario wherein the mixed-valence donors are separated by equivalent interplanar distances along the length of the stacks are imposed by the crystallographic symmetry of the unit cell. As expected, a corresponding change in the unit cell's volume accompanies the anionic alteration. The unit cell for the chloride-containing system, the corresponding unit cell contains an interstitial volume of 1944.46 $Å^3$, which increases to a maximum of 2149.70 $Å^3$ with the iodide system after reaching an intermediate volume of 2061.96 $Å^3$ with the bromide anion.

When spherical halide anions are substituted by the smallest tetrahedral anion $[BF_4]^-$, the corresponding volume of the unit cell remains close to that of the iodide salt, crystallizing with a volume of 2148.65 $Å^3$. Prior to the present work with *o*-Me_2TTF, the only related structure is the 1:1 insulating salt (*o*-Me_2TTF)$[ReO_4]$ which crystallizes in the orthorhombic space group *Cmca* with an interstitial volume of 2605.80 $Å^3$.[97] In going from the small tetrahedral anion $[BF_4]^-$ to the significantly larger $[ReO_4]^-$ anion, the uniform, bond-over-ring stacking motif encountered in the tetragonal salts, which is indicative of potentially highly-conducting systems, is disrupted resulting in integrated salts of cations and anions in uniform stoichiometries wherein the fully-ionized TTF radical cations form strong face-to-face arrangements which result in the insulating behavior encountered in the $[ReO_4]^-$ salt.

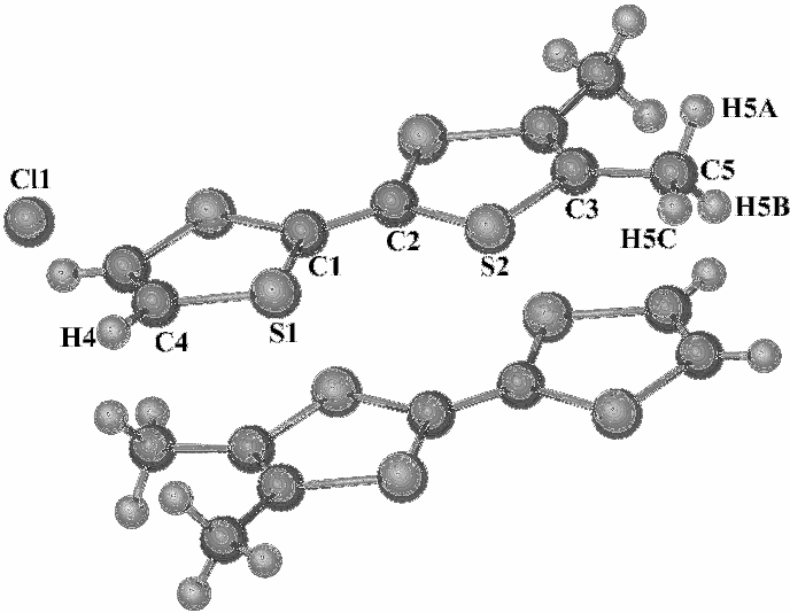

Figure 34. X-ray crystal structure of (*o*-Me_2TTF)$_2$[Cl] (**7**).

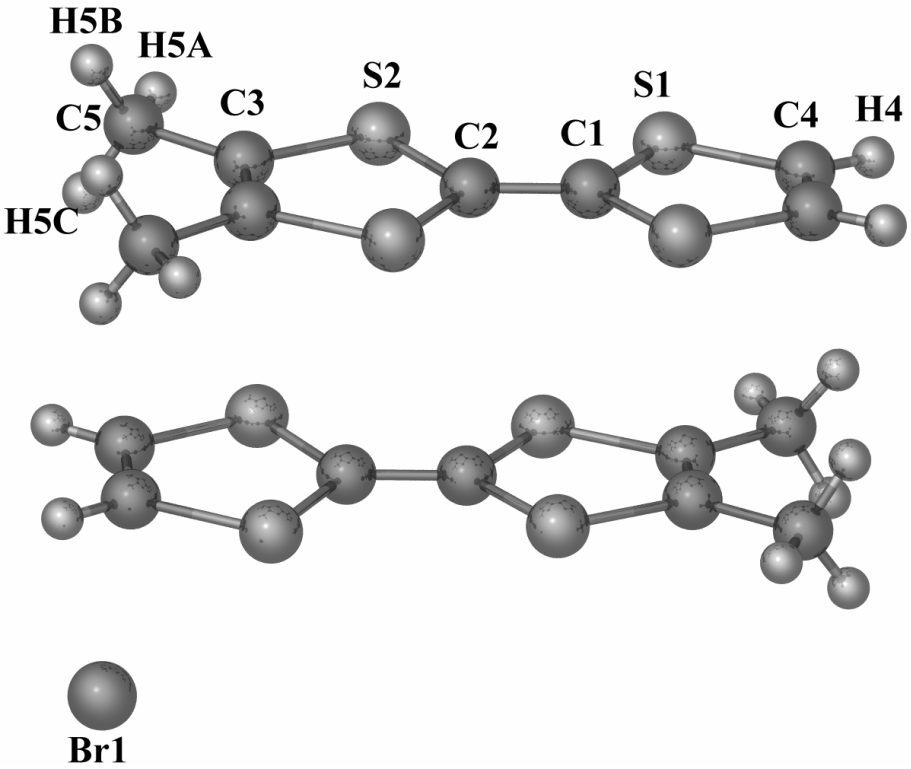

Figure 35. X-ray crystal structure of (*o*-Me_2TTF)$_2$[Br] (**8**).

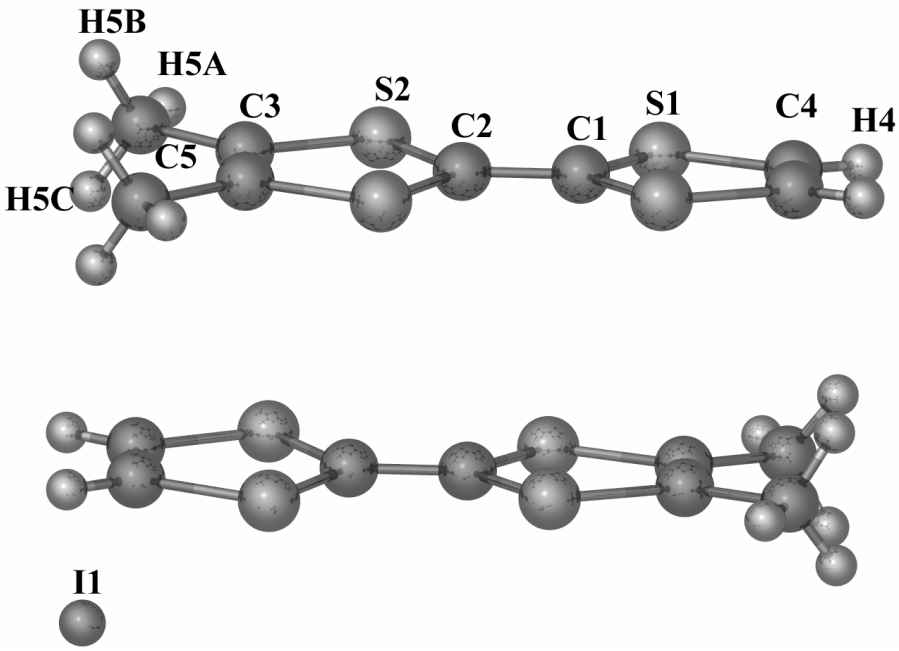

Figure 36. X-ray crystal structure of (*o*-$Me_2TTF)_2$[I] (**9**).

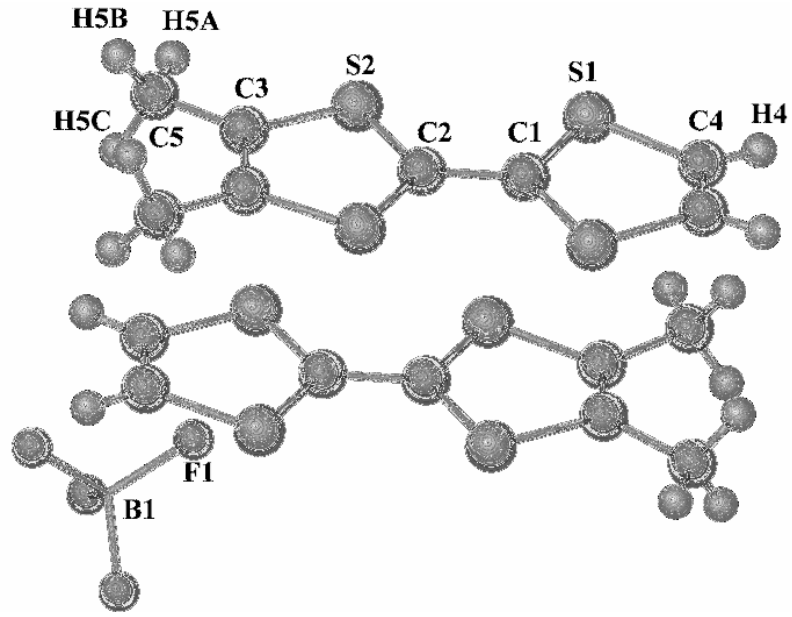

Figure 37. X-ray crystal structure of (*o*-$Me_2TTF)_2[BF_4]$ (**10**).

In going from the small tetrahedral anion $[BF_4]^-$ to the significantly larger $[ReO_4]^-$ anion, the uniform, bond-over-ring stacking motif encountered in the tetragonal salts, which is indicative of potentially highly-conducting systems, is disrupted resulting in integrated salts of cations and anions in uniform stoichiometries wherein the fully-ionized TTF radical cations form strong face-to-face arrangements which result in the insulating behavior encountered in the $[ReO_4]^-$ salt. Representations of the one-dimensional, uniform stacking in **7-10** are shown in Figures 38 and 39. Selected bond distances for **7-9** as well as X-ray crystallographic and refinement data and the calculated valences for their chalcofulvalenium radical cations are listed in Tables 17-21.

The structure for **11** crystallizes in the triclinic space group *P-1* and forms a structure reminiscent of the famous Bechgaard series of salts which exhibit super-conducting properties under applied pressure.[13] The solid-state structure of **11**, much like the previous four salts, forms segregated stacks of cations and anions, but, because of the crystallographic symmetry imposed by the triclinic symmetry, the inversion center leads to incongruent interplanar separations of ~3.659 and ~3.733 Å between the three radical cations which lie coincident to the unit cell's b-axis.

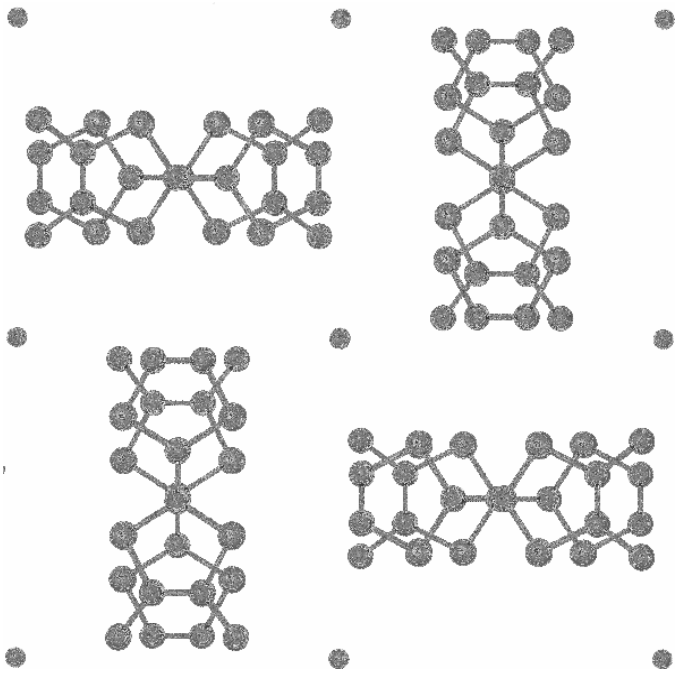

Figure 38. One-dimensional, uniform stacks of *o*-Me_2TTF donor molecules looking down the c-axis in the solid-state structures for **7-9**.

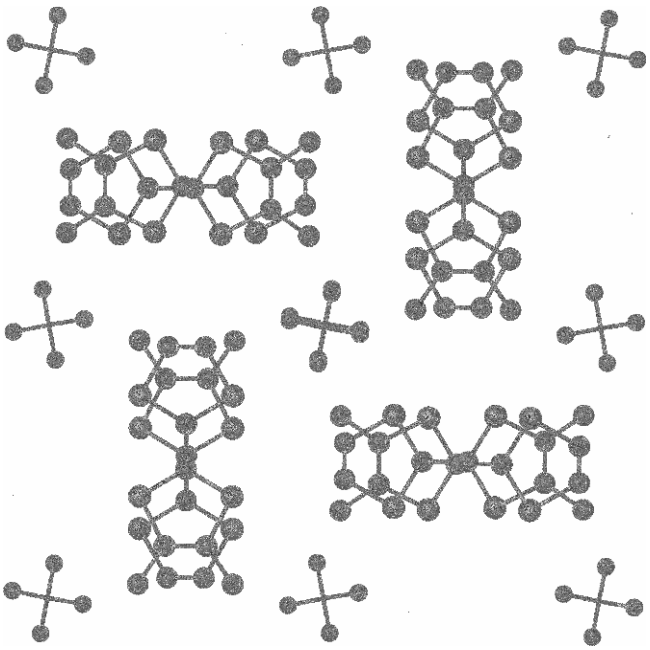

Figure 39. One-dimensional, uniform stacks of *o*-Me_2TTF donor molecules looking down the c-axis in the solid-state structures for **10**.

Table 17. Bond distances for (*o*-$Me_2TTF)_2$[Cl] (**7**) in Å.

S(1)-C(4)	1.731(5)
S(1)-C(1)	1.740(4)
S(2)-C(2)	1.728(4)
S(2)-C(3)	1.749(5)
C(1)-C(2)	1.365(10)
C(3)-C(3)	1.340(11)
C(3)-C(5)	1.493(7)
C(4)-C(4)	1.348(11)

Table 18. Bond distances for (*o*-$Me_2TTF)_2$[Br] (**8**) in Å.

S(1)-C(4)	1.736(3)
S(1)-C(1)	1.743(2)
S(2)-C(2)	1.738(2)
S(2)-C(3)	1.750(3)
C(1)-C(2)	1.356(5)
C(3)-C(3)	1.338(6)
C(3)-C(5)	1.506(4)
C(4)-C(4)	1.330(6)

Table 19. Bond distances for (*o*-$Me_2TTF)_2$[I] (**9**) in Å.

S(1)-C(4)	1.732(3)
S(1)-C(1)	1.742(2)
S(2)-C(2)	1.734(2)
S(2)-C(3)	1.746(3)
C(1)-C(2)	1.365(6)
C(3)-C(3)	1.348(6)
C(3)-C(5)	1.506(4)
C(4)-C(4)	1.336(6)

Table 20. X-ray crystallographic and refinement data for radical salts **7-9**.

Compound	(*o*-Me_2TTF)$_2$[Cl] (**7**)	(*o*-Me_2TTF)$_2$[Br] (**8**)	(*o*-Me_2TTF)$_2$[I] (**9**)
Formula	$C_{16}H_{16}S_8Cl$	$C_{16}H_{16}S_8Br$	$C_{16}H_{16}S_8I$
formula weight	498.87	542.82	590.81
Space group	$I4_2d$	$I4_2d$	$I4_2d$
a, Å	16.807(2)	17.0920(3)	17.4031(2)
b, Å	16.807(2)	17.0920(3)	17.4031(2)
c, Å	6.8835(14)	7.0582(2)	7.09780(10)
α, deg	90	90	90
β, deg	90	90	90
γ, deg	90	90	90
volume, Å^3	1944.5(6)	2061.96(8)	2149.70(5)
Z	8	4	4
μ, mm^{-1}	1.055	2.803	2.266
Temp.	110(2)	110(2)	110(2)
Reflns. collected	1127	1192	1226
Reflns. I>2σ	938	1124	1197
Parameters	59	60	59
Restraints	0	0	0
R1[a]	0.0578	0.0278	0.0247
wR2[b]	0.1386	0.0721	0.0647
Goodness-of-fit[c]	1.143	1.132	1.082

[a] $R1 = \sum||F_o| - |F_c||/\sum|F_o|$. [b] $wR2 = [\sum [w(F_o^2-F_c^2)^2]/\sum [w(F_o^2)^2]^{1/2}$

[c] Goodness-of-fit = $[\sum w(|F_o|-|F_c|)^2/(N_{obs}-N_{parameter})]^{1/2}$

Table 21. Estimated degree of ionicity for the donor molecules for **7-9.**

salt	**molecule**	**A**[a]	**B**[b]	**Q**[c]
(*o*-Me_2TTF)$_2$[Cl] (**7**)	A	1.365(4) Å	1.734(5) Å	+0.52
	A	1.365(4) Å	1.734(5) Å	+0.52
(*o*-Me_2TTF)$_2$[Br] (**8**)	A	1.356(7) Å	1.741(6) Å	+0.33
	A	1.356(7) Å	1.741(6) Å	+0.33
(*o*-Me_2TTF)$_2$[I] (**9**)	A	1.365(5) Å	1.738(4) Å	+0.48
	A	1.365(5) Å	1.738(4) Å	+0.48

[a] Central C=C bond distance.
[b] Mean central C-S bond distance.
[c] Q = charge estimated with the formula Q = -17.92 + 23.43*(A/B) from Ref. 94.

Despite the presence of *o*-Me_2TTF radical cations in fractional oxidation states, incongruent interplanar separations can lead to a Peirls distortion in the radical cation stacks, which is responsible for diminished charge delocalization contributing to the resistivity of the mixed-valence salts with TMTTF radical cations. Despite the incongruent interplanar distances that exist between the TMTSF radical cations, the use of selenium atoms and their larger Van der Waals radii lead to side-to-side interactions with neighboring stacks which can lead to the stabilization of the metallic state. The smaller sulfur orbital radii in the TMTTF family of radical cation salts do not engage in homologous interactions between stacks, leading to reduced itinerant electron response and high resistivity.

The X-ray structure for **12** is dominated by fully ionized *o*-Me_2TTF radical cations that stack along the b-axis and crystallize in the monoclinic space group $P2_1/n$. Like the salt between *o*-Me_2TTF and $[Re_2Cl_8]^{2-}$, the radical cations align themselves in a manner essential to form strong σ-type dimers between the singly-occupied SOMOs of the respective cations. Using the Coppens' method, the valence of the *o*-Me_2TTF cations were determined to be +1.[94] Upon inspection of the packing diagram of **12**, it can be seen that separate layers of *o*-Me_2TTF dimers and I_3^- anions lie along the a-axis. In those separate layers, both the cation dimers and anions form an undulating pattern which translates along the c-axis. The solid-state structures for **11** and **12** as well are shown in Figures 40 and 41. Selected bond distances for **10-12** as well as X-ray crystallographic and refinement data and the calculated valences for their chalcofulvalenium radical cations are listed in Tables 22-26.

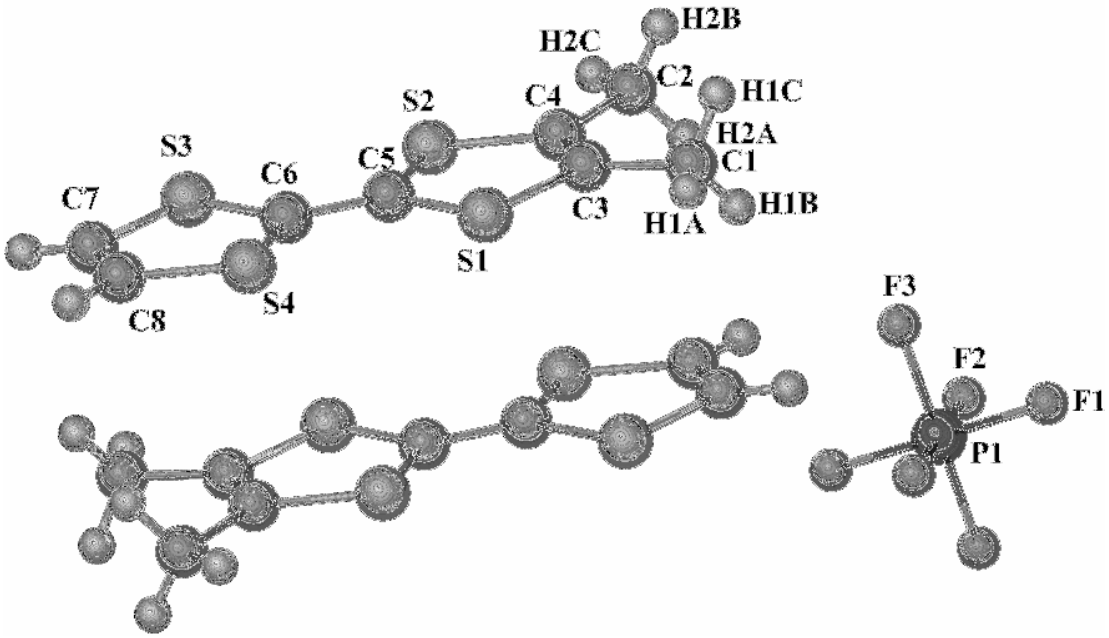

Figure 40. X-ray crystal structure of (*o*-Me_2TTF)$_2$[PF_6] (**11**).

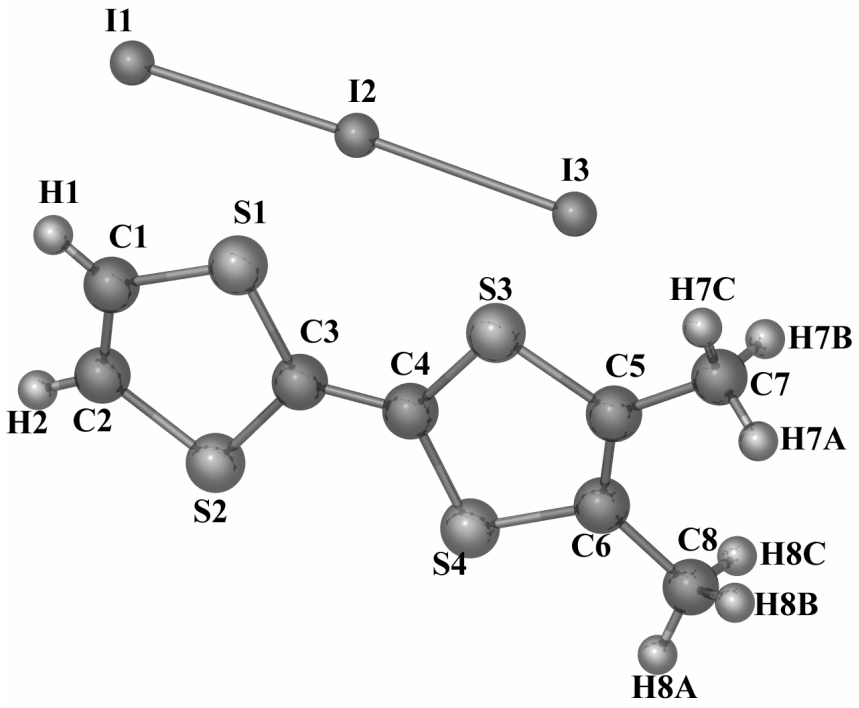

Figure 41. X-ray crystal structure of (*o*-Me_2TTF)[I_3] (**12**).

Table 22. Bond distances for (*o*-$Me_2TTF)_2[BF_4]$ (**10**).

S(1)-C(4)	1.733(3)
S(1)-C(1)	1.736(2)
S(2)-C(2)	1.734(2)
S(2)-C(3)	1.744(3)
C(1)-C(2)	1.364(6)
C(3)-C(3)	1.345(6)
C(3)-C(5)	1.504(4)
C(4)-C(4)	1.332(6)
B(1)-F(1)	1.417(3)

Table 23. Bond distances for (*o*-$Me_2TTF)_2[PF_6]$ (**11**) in Å.

S(1)-C(5)	1.731(3)
S(1)-C(3)	1.742(3)
S(2)-C(5)	1.727(3)
S(2)-C(4)	1.746(3)
S(3)-C(7)	1.733(4)
S(3)-C(6)	1.737(3)
S(4)-C(8)	1.728(4)
S(4)-C(6)	1.736(3)
C(1)-C(3)	1.497(4)
C(2)-C(4)	1.506(4)
C(3)-C(4)	1.345(4)
C(5)-C(6)	1.380(5)
C(7)-C(8)	1.330(5)
P-F(1)	1.577(2)
P-F(2A)	1.564(9)
P-F(3A)	1.513(10)
P-F(2B)	1.528(11)
P-F(3B)	1.537(17)

Table 24. Bond distances for (*o*-Me_2TTF)[I_3] (**12**) in Å.

I(1)-I(3)	2.9011(5)
I(1)-I(2)	2.9587(4)
S(1)-C(3)	1.729(4)
S(1)-C(1)	1.741(5)
S(2)-C(3)	1.722(4)
S(2)-C(2)	1.723(5)
S(3)-C(4)	1.719(4)
S(3)-C(6)	1.739(5)
S(4)-C(4)	1.716(4)
S(4)-C(5)	1.737(5)
C(1)-C(2)	1.340(7)
C(3)-C(4)	1.401(6)
C(5)-C(6)	1.354(7)
C(5)-C(8)	1.494(6)
C(6)-C(7)	1.496(6)

Table 25. X-ray crystallographic and refinement data for radical salts **10**-**12**.

Compound	(*o*-Me_2TTF)$_2$[BF_4] (**10**)	(*o*-Me_2TTF)$_2$[PF_6] (**11**)	(*o*-Me_2TTF)[I_3] (**12**)
Formula	$C_{16}H_{16}S_8BF_4$	$C_{16}H_{16}S_8PF_6$	$C_8H_8S_4I_3$
formula weight	550.90	608.87	612.66
Space group	$I4_2d$	P-1	$P2_1/n$
a, Å	17.4714(17)	6.7281(3)	7.5960(3)
b, Å	17.4714(17)	7.3860(4)	16.2668(5)
c, Å	7.039(11)	12.1431(6)	12.9152(4)
α, deg	90	85.614(2)	90
β, deg	90	82.102(2)	102.815(2)
γ, deg	90	85.022(2)	90
volume, Å^3	2148.65(4)	594.18(5)	1556.09(9)
Z	4	1	4
μ, mm^{-1}	1.705	0.870	6.533
Temp.	110(2)	110(2)	110(2)
Reflns. collected	2870	2710	3552
Reflns. I>2σ	2037	1930	2990
Parameters	153	161	137
Restraints	0	0	0
R1[a]	0.0457	0.0559	0.0246
wR2[b]	0.1396	0.1572	0.0551
Goodness-of-fit[c]	1.078	1.051	1.089

[a] $R1 = \sum||F_o| - |F_c||/\sum|F_o|$. [b] $wR2 = [\sum [w(F_o^2-F_c^2)^2]/ \sum [w(F_o^2)^2]^{1/2}$

[c] Goodness-of-fit = $[\sum w(|F_o|-|F_c|)^2/(N_{obs}-N_{parameter})]^{1/2}$

Table 26. Estimated degree of ionicity for the donor molecules for **10-12.**

salt	molecule	A[a]	B[b]	Q[c]
(*o*-Me_2TTF)$_2$[BF_4] (**10**)	A	1.364(3) Å	1.736(5) Å	+0.49
	A	1.364(3) Å	1.736(5) Å	+0.49
(*o*-Me_2TTF)$_2$[PF_6] (**11**)	A	1.380(2) Å	1.733(6) Å	+0.73
	A	1.380(2) Å	1.733(6) Å	+0.73
(*o*-Me_2TTF)[I_3] (**12**)	A	1.401(5) Å	1.722(4) Å	+1.14

[a] Central C=C bond distance.
[b] Mean central C-S bond distance.
[c] Q = charge estimated with the formula Q = -17.92 + 23.43*(A/B) from Ref. 94.

*(o-Me_2TTF)$_2$[W_6O_{19}] (**13**), (o-Me_2TTF)$_2$ [Mo_6O_{19}] (**14**), and (BPDT-TTF)$_2$[W_6O_{19}] (**15**)*

Several crystallized examples of charge-transfer salts with polyoxometallate anions have been resolved by low-temperature X-ray diffraction methods. Among the many chalcofulvalene donors used are TMTTF, TPTTF, BEDT-TT, BET-TTF, TMTSF, and TTF with the Linqvist family of anions ($[Mo_6O_{19}]^{2-}$, $[W_6O_{19}]^{2-}$, and $[MW_5O_{19}]^{3-}$ where M = V, Nb).[39] Among this family of salts are the TTF salts which offer salts that contain not only strong σ-dimers of fully-ionized TTF, but also those which contain a combination of neutral and oxidized donors and mixed valence donors. An example of system which contains a combination of neutral and oxidized donors is the salt (TMTSF)$_3$[Mo_6O_{19}]•2DMF; this lies in contrast to the initial belief that this salt contained donors in non-integral oxidation states.[33] All of systems prepared between fully-ionized chalcofulvalene donors and the dianionic Lindqvist anions are all weak semiconductors or insulators, due to the strong dimerization of the radical cations in the solid state. Despite the large number of donors utilized in the preparation of radical cation salts, the use of the donors *o*-Me_2TTF and BPDT-TTF has not been explored with these large

anionic clusters in an attempt to evaluate the onset of interesting properties obtained in these systems.

The solid-state structures for **13** and **14** represent initial attempts to prepare charge-transfer salts between the little researched donor *o*-Me_2TTF and the dianionic Lindqvist anions. Despite their crystallization in the triclinic space group *P-1*, the solid state structures of both salts are quite different, as the salt with $[Mo_6O_{19}]^{2-}$ crystallizes in a larger unit cell. This crystallographic fact lies in contrast to the ET family of salts which are isostructural despite the identity of the transition metal in the coordination sphere of the polyoxometallate clusters. For both salts, the *o*-Me_2TTF donors are in their monocationic states and, as judged by short interatomic distances between neighboring sulfur atoms at distances <3.6 Å, strong σ-type dimers between these radical cations have formed in the solid state. Another interesting structural behavior present in structures containing polyoxometallate anion clusters is the presence of short hydrogen bonding interactions between the hydrogen atoms of TTF-like donors and the bridging or terminal oxygen atoms of the polyoxometallate clusters. The solid-state structures for **13** and **14** are shown in Figures 42 and 43.

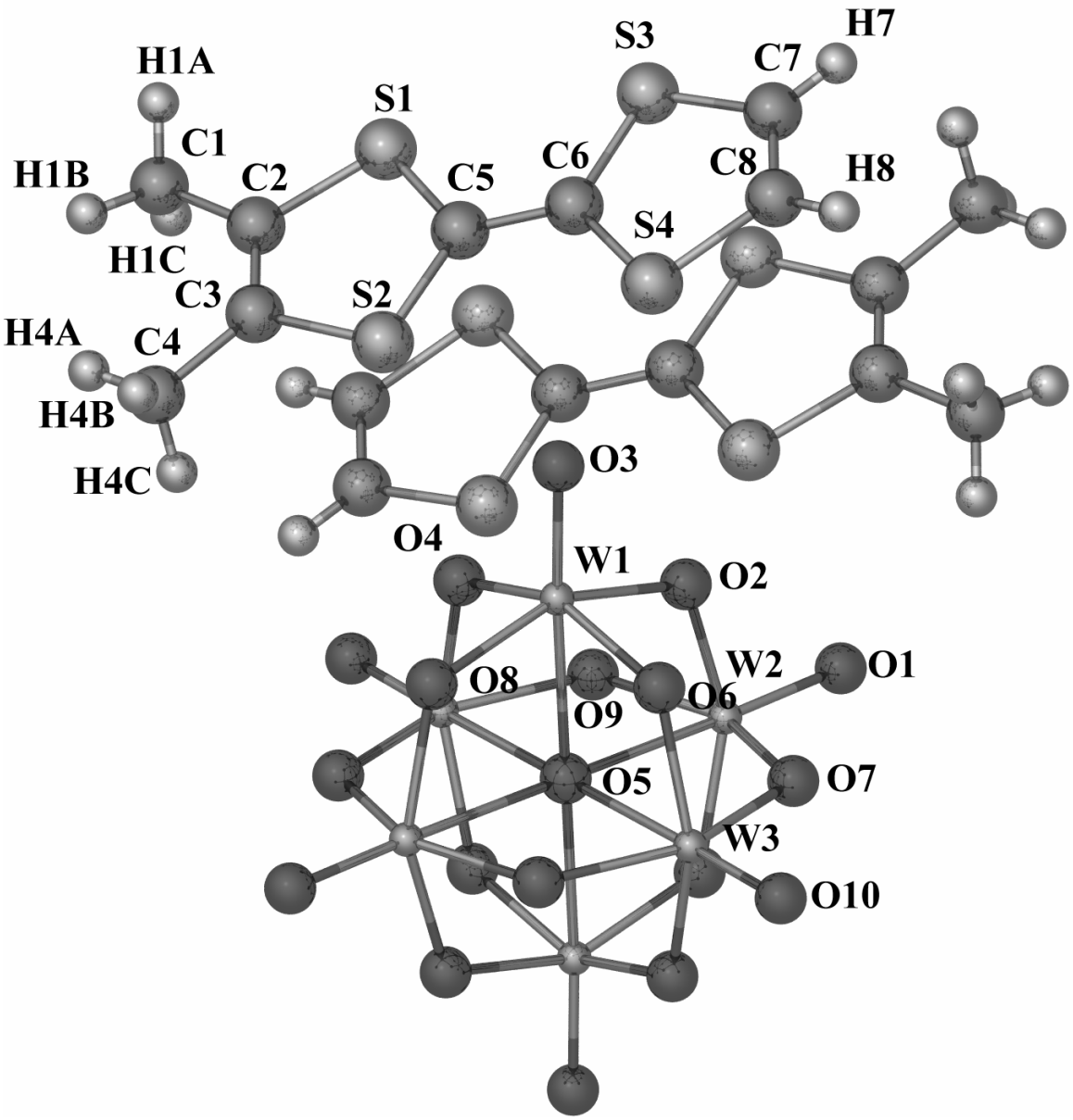

Figure 42. X-ray crystal structure of (*o*-$Me_2TTF)_2[W_6O_{19}]$ **(13).**

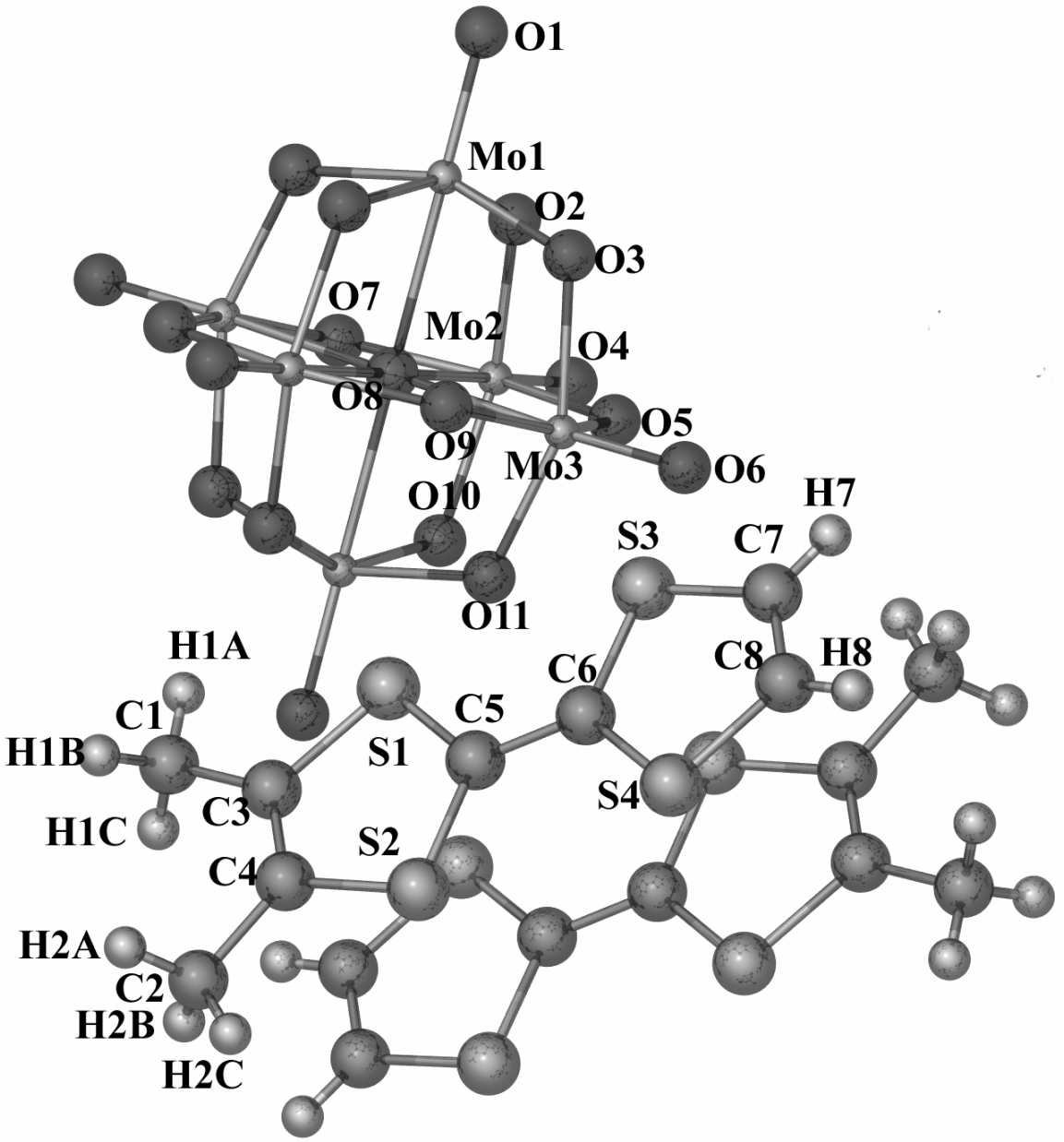

Figure 43. X-ray crystal structure of (*o*-$Me_2TTF)_2[Mo_6O_{19}]$ (**14**).

A 1999 report by Batail and coworkers demonstrated, by the use of by electrostatic potential maps, that bridging oxygen atoms in clusters are more basic than those in terminal positions.[101] In **13**, a short C_{sp2}-O interaction of 2.296 Å exists between H8-O9, a bridging oxygen atom in the tungsten cluster. In the molybdenum analogue (**14**), a longer hydrogen bonding interaction of 2.363 Å exists between a C_{sp3}-hybrdized hydrogen atom (H2A3) of one *o*-Me_2TTF donor and a terminal oxygen atom (O6) of one of the anionic clusters. Despite the presence of hydrogen bonding interactions in both salt structures, the shorter, hydrogen bonding interaction in **13** can be rationalized based on the increased basicity of the bridging oxygen.

Unlike the structures between BEDT-TTF and the Linqvist dianions, the formation of a charge-transfer salt between BPDT-TTF and $[W_6O_{19}]^{2-}$ (**15**) yields a structure dominated by slipped dimers of fully oxidized donors which crystallize in the triclinic space group *P-1*. An interesting feature of the topology in the structure is that, due to the sp^3-hybrid-ized carbon atoms in the structure, there are significant bends in the propylene-dithio-bridge facilitated by the necessity to preserve the ~109° bond angles found in systems with tetrahedral symmetry. The solid-state structure for **15** is shown in Figure 44.

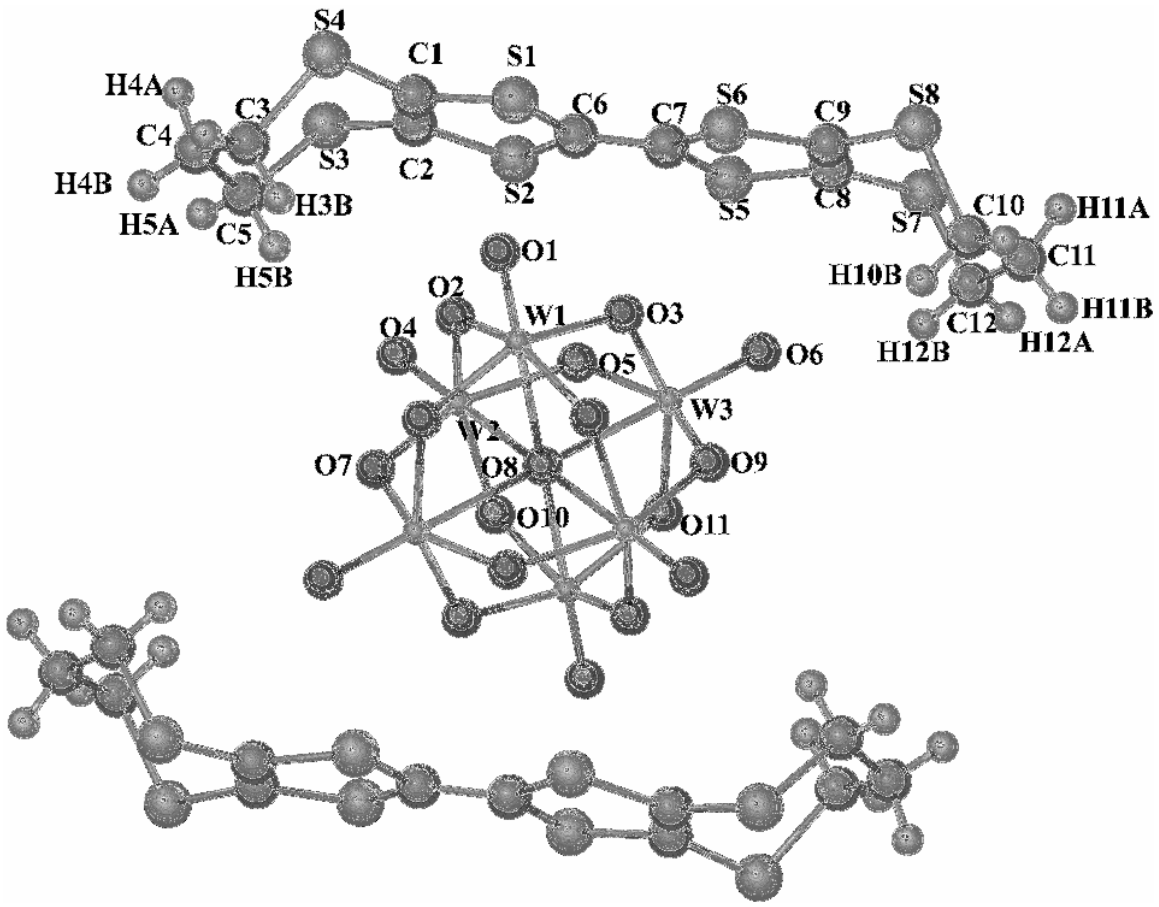

Figure 44. X-ray crystal structure of $(BPDT\text{-}TTF)_2[W_6O_{19}]$ (**15**).

As in the case of the *o*-Me_2TTF donor and the Lindqvist anions, hydrogen bonding interactions are present. The first interaction involves H12B and a terminal oxygen (O11) at a distance of 2.495 Å while a second exists between H5B and a bridging oxygen (O23) at a distance of 2.482 Å. The extent of the hydrogen bonding interaction can be rationalized in a fashion to those previously encountered in the *o*-Me_2TTF salts. Not only does a difference exist between the basic environments in the polyoxometallate clusters, but hydrogen atoms bound to carbon atoms directly ligated to sulfur atoms on the periphery of the BPDT-TTF donor should become relatively acidic because of the electron-withdrawing properties of the sulfur atom. All of the hydrogen bonding interactions discussed above involve these weakly-acidic hydrogen atoms. Selected bond distances for **13-15** as well as X-ray crystallographic and refinement data and the calculated valences for their chalcofulvalenium radical cations are listed in Tables 27-31.

Table 27. X-ray crystallographic and refinement data for radical salts **13-15**.

Compound	(*o*-$Me_2TTF)_2[W_6O_{19}]$ (**13**)	(*o*-$Me_2TTF)_2[Mo_6O_{19}]$ (**14**)	$(BPDT\text{-}TTF)_2[W_6O_{19}]$ (**15**)
Formula	$C_{16}H_{16}S_8W_6O_{19}$	$C_{16}H_{16}S_8Mo_6O_{19}$	$C_{20}H_{16}S_{16}W_6O_{19}$
formula weight	1871.51	1355.24	2175.29
Space group	P-1	P-1	P-1
a, Å	7.6211(7)	8.14330(10)	10.9266(15)
b, Å	9.5231(9)	13.3359(2)	11.9041(15)
c, Å	12.2148(11)	15.9318(2)	12.6604(17)
α, deg	105.5870(10)	97.1989(10)	101.261(5)
β, deg	106.8340(10)	93.7457(10)	115.174(5)
γ, deg	95.6950(10)	103.6209(8)	114.434(5)
volume, Å^3	802.10(13)	1660.16	1211.4(3)
Z	1	2	1
μ, mm^{-1}	22.034	2.78	14.944
Temp.	110(2)	110(2)	110(2)
Reflns. collected	3708	14130	5478
Reflns. I>2σ	3614	9673	4197
Parameters	227	445	295
Restraints	0	0	0
R1[a]	0.0241	0.0555	0.0525
wR2[b]	0.0625	0.1462	0.1322
Goodness-of-fit[c]	1.055	1.189	1.041

[a] $R1 = \sum||F_o| - |F_c||/\sum|F_o|$. [b] $wR2 = [\sum [w(F_o^2-F_c^2)^2]/ \sum [w(F_o^2)^2]]^{1/2}$

[c] Goodness-of-fit = $[\sum w(|F_o|-|F_c|)^2/(N_{obs}-N_{parameter})]^{1/2}$

Table 28. Bond distances for (o-$Me_2TTF)_2[W_6O_{19}]$ (**13**) in Å.

W(1)-O(1)	1.694(4)	W(3)-O(9)	1.930(4)
W(1)-O(2)	1.927(4)	W(3)-O(10)	1.708(4)
W(1)-O(4)	1.919(4)	S(1)-C(2)	1.737(6)
W(1)-O(5)	2.324(2)	S(1)-C(5)	1.708(5)
W(1)-O(7)	1.916(4)	S(2)-C(3)	1.741(5)
W(1)-O(9)	1.926(4)	S(2)-C(5)	1.721(5)
W(2)-O(2)	1.911(4)	S(3)-C(6)	1.721(5)
W(2)-O(3)	1.706(4)	S(3)-C(8)	1.716(6)
W(2)-O(4)	1.929(4)	S(4)-C(6)	1.717(5)
W(2)-O(5)	2.327(2)	S(4)-C(7)	1.725(6)
W(2)-O(6)	1.911(4)	C(1)-C(2)	1.505(7)
W(2)-O(8)	1.933(4)	C(2)-C(3)	1.334(8)
W(3)-O(5)	2.322(3)	C(3)-C(4)	1.498(7)
W(3)-O(6)	1.925(4)	C(5)-C(6)	1.387(7)
W(3)-O(7)	1.911(4)	C(7)-C(8)	1.332(8)
W(3)-O(8)	1.919(4)		

Table 29. Bond distances for (o-$Me_2TTF)_2[Mo_6O_{19}]$ (**14**) in Å.

Mo(1)-O(a)	2.326(7)	S(1A)-C(3A)	1.741(6)
Mo(1)-O(1)	1.681(3)	S(1A)-C(5A)	1.717(4)
Mo(1)-O(12)	2.003(5)	S(2A)-C(4A)	1.748(3)
Mo(1)-O(13)	1.966(9)	S(2A)-C(5A)	1.716(5)
Mo(1)-O(21)	1.885(4)	S(3A)-C(6A)	1.719(6)
Mo(2)-O(a)	2.324(2)	S(3A)-C(7A)	1.731(4)
Mo(2)-O(2)	1.695(3)	S(4A)-C(6A)	1.714(5)
Mo(2)-O(12)	2.003(6)	S(4A)-C(8A)	1.715(6)
Mo(2)-O(23)	1.918(4)	S(1B)-C(3B)	1.739(7)
Mo(2)-O(32)	1.911(2)	S(1B)-C(5B)	1.712(8)
Mo(3)-O(a)	2.316(3)	S(2B)-C(4B)	1.746(2)
Mo(3)-O(3)	1.675(3)	S(2B)-C(5B)	1.717(3)
Mo(3)-O(23)	1.939(8)	S(3B)-C(6B)	1.713(8)
Mo(3)-O(31)	1.989(5)	S(3B)-C(7B)	1.726(4)
Mo(4)-O(4)	1.687(2)	S(4B)-C(6B)	1.718(5)
Mo(4)-O(45)	1.961(6)	C(1A)-C(3A)	1.502(7)
Mo(4)-O(54)	1.900(8)	C(2A)-C(4A)	1.493(9)
Mo(4)-O(64)	1.910(4)	C(3A)-C(4A)	1.354(6)
Mo(5)-O(5)	1.693(2)	C(5A)-C(6A)	1.397(4)
Mo(5)-O(45)	1.880(4)	C(7A)-C(8A)	1.341(3)
Mo(5)-O(56)	2.000(3)	C(1B)-C(3B)	1.485(10)
Mo(5)-O(65)	1.871(6)	C(2B)-C(4B)	1.491(9)
Mo(6)-O(b)	2.323(4)	C(3B)-C(4B)	1.341(6)
Mo(6)-O(6)	1.683(8)	C(5B)-C(6B)	1.404(8)
Mo(6)-O(46)	1.903(5)	C(7B)-C(8B)	1.323(6)
Mo(6)-O(56)	1.872(6)		

Table 30. Bond distances for $(BPDT\text{-}TTF)_2[W_6O_{19}]$ (**15**) in Å.

W(1)-O(11)	1.696(10)	S(2)-C(1)	1.726(13)
W(1)-O(13)	1.916(8)	S(3)-C(2)	1.742(13)
W(1)-O(12)	1.924(9)	S(3)-C(5)	1.811(15)
W(1)-O(31)	1.931(9)	S(4)-C(1)	1.737(13)
W(1)-O(21)	1.932(9)	S(4)-C(3)	1.818(15)
W(1)-O(C)	2.3224(6)	S(5)-C(7)	1.728(12)
W(2)-O(22)	1.688(10)	S(5)-C(8)	1.729(13)
W(2)-O(32)	1.914(9)	S(6)-C(7)	1.717(13)
W(2)-O(12)	1.918(8)	S(6)-C(9)	1.730(13)
W(2)-O(23)	1.920(9)	S(7)-C(8)	1.741(13)
W(2)-O(21)	1.922(9)	S(7)-C(12)	1.821(17)
W(2)-O(C)	2.3309(6)	S(8)-C(9)	1.746(14)
W(3)-O(33)	1.705(9)	S(8)-C(10)	1.799(15)
W(3)-O(13)	1.903(9)	C(1)-C(2)	1.361(18)
W(3)-O(23)	1.913(10)	C(3)-C(4)	1.50(2)
W(3)-O(31)	1.923(9)	C(4)-C(5)	1.53(2)
W(3)-O(32)	1.929(10)	C(6)-C(7)	1.384(17)
W(3)-O(C)	2.3250(5)	C(8)-C(9)	1.355(19)
S(1)-C(6)	1.711(13)	C(10)-C(11)	1.50(2)
S(1)-C(2)	1.711(13)	C(11)-C(12)	1.51(2)
S(2)-C(6)	1.724(13)		

Table 31. Estimated degree of ionicity for the donor molecules for **13-15.**

salt	molecule	A[a]	B[b]	Q[c]
(*o*-$Me_2TTF)_2[W_6O_{19}]$ (**13**)	A	1.387 Å	1.717 Å	+1.01
	A	1.387 Å	1.717 Å	+1.01
(*o*-$Me_2TTF)_2[Mo_6O_{19}]$ (**14**)	A	1.404 Å	1.715 Å	+1.26
	B	1.397 Å	1.717 Å	+1.14
$(BPDT\text{-}TTF)_2[W_6O_{19}]$ (**15**)	A	1.384 Å	1.720 Å	+0.93
	A	1.384 Å	1.720 Å	+0.93

[a] Central C=C bond distance.
[b] Mean central C-S bond distance.
[c] Q = charge estimated with the formula Q = -17.92 + 23.43*(A/B) from Ref. 94.

(o-Me$_2$TTF)$_8$[Fe(CN)$_6$]$_3$•2H$_2$O ***(16•2H$_2$O)***, *(o-Me$_2$TTF)$_8$ [Co(CN)$_6$]2•8H$_2$O* ***(17•8H$_2$O)***, *(TTF)$_{11}$[Fe(CN)$_6$]$_3$•8H$_2$O* ***(18•8H$_2$O)*** *and (TTF)$_{11}$[Co(CN)$_6$]$_3$•8H$_2$O* ***(19•8H$_2$O)***

Compound (**16•2H$_2$O**) crystallizes in the triclinic space group *P-1* and adds to the library of charge transfer salts incorporating cyanometallate anions and chalcofulvalene donors. This salt is the first to incorporate the unsymmetrical donor *o*-Me$_2$TTF donor into this category of materials. The structure is characterized by head-to-tail stacks of donor molecules along the b-axis of the unit cell. Separate stacks are related to one another via translations along the c-axis. Three donor molecules form the repeating stacked unit consisting of two of the constituent donor molecules have been ionized to +0.85 and +0.76 while the third has been oxidized to +0.18. The two *o*-Me$_2$TTF radical cations are strongly dimerized as evidenced by interatomic interactions between neighboring sulfur atoms at distances <3.6 Å. The third donor molecule is offset from this dimer in a pattern reminiscent of the X-ray structure of (TTF)$_3$[BF$_4$]$_2$.[45] A plane along the a-axis between stacks of donor molecules contains the $[Fe^{III}(CN)_6]^{3-}$ charge compensating anions, interstitial water molecules and the fourth *o*-Me$_2$TTF cation. Also inclusive in this plane is an interstitial water molecule which forms a strong hydrogen bonding interaction of 2.179 Å with a hydrogen atom from one of the sp^2-hybridized carbon atoms of an *o*-Me$_2$TTF donor. The final feature of this plane is the fourth *o*-Me$_2$TTF radical, which according to bond distance calculations using the Coppens' method, exists with a charge of +1.58 which is the highest charge observed for this donor.[94] The solid-state structures illustrating the one-dimensional stacking of *o*-Me$_2$TTF donors and the hybrid organic-inorganic sheets are shown in Figures 45 and 46.

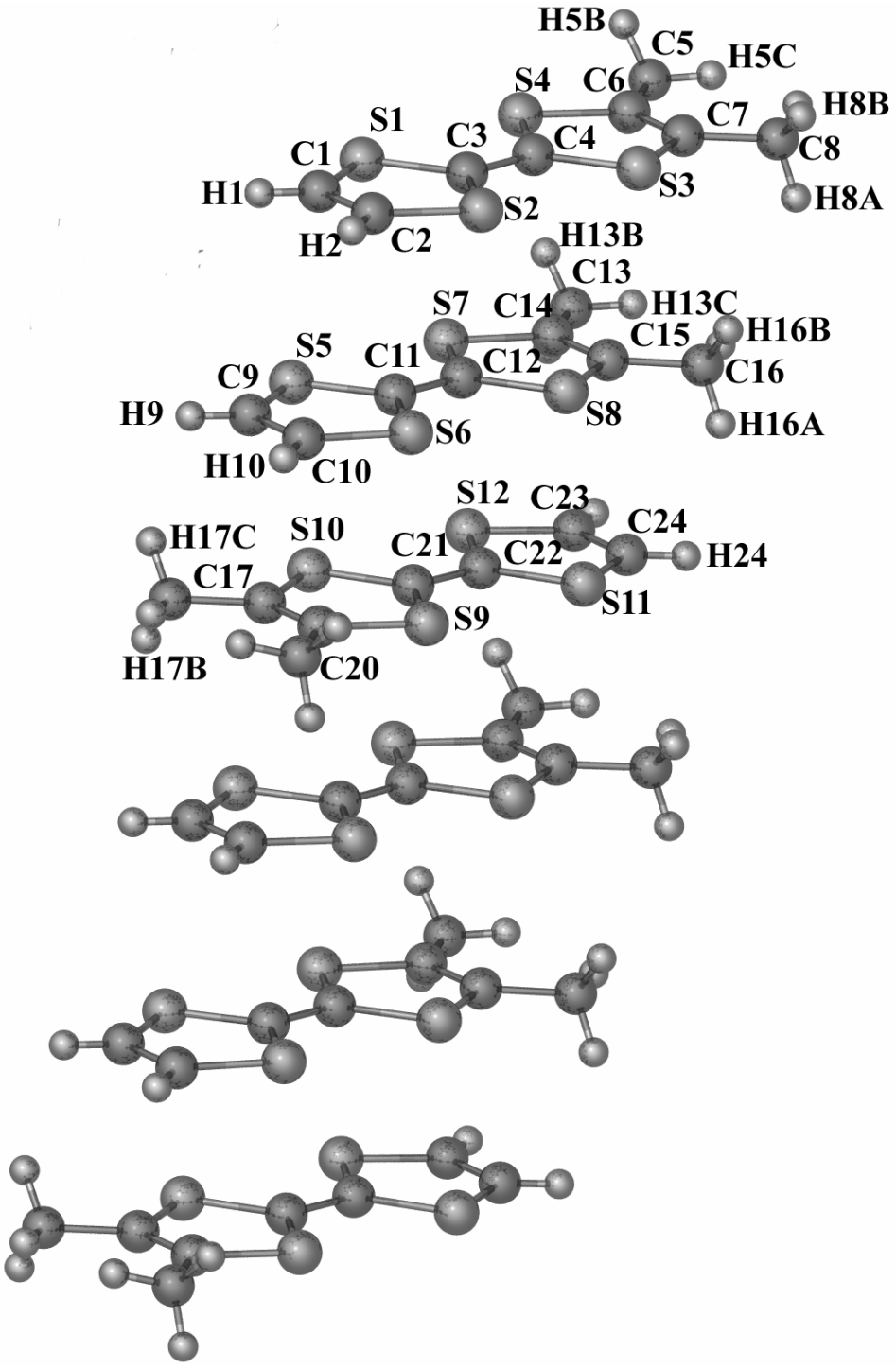

Figure 45. X-ray crystal structure of (*o*-$Me_2TTF)_8[Fe^{III}(CN)_6]_3$•$2H_2O$ **(16•2H_2O),** illustrating the one-dimensional stacking of the *o*-Me_2TTF donor molecules. Interstitial water molecules have been omitted for the sake of clarity.

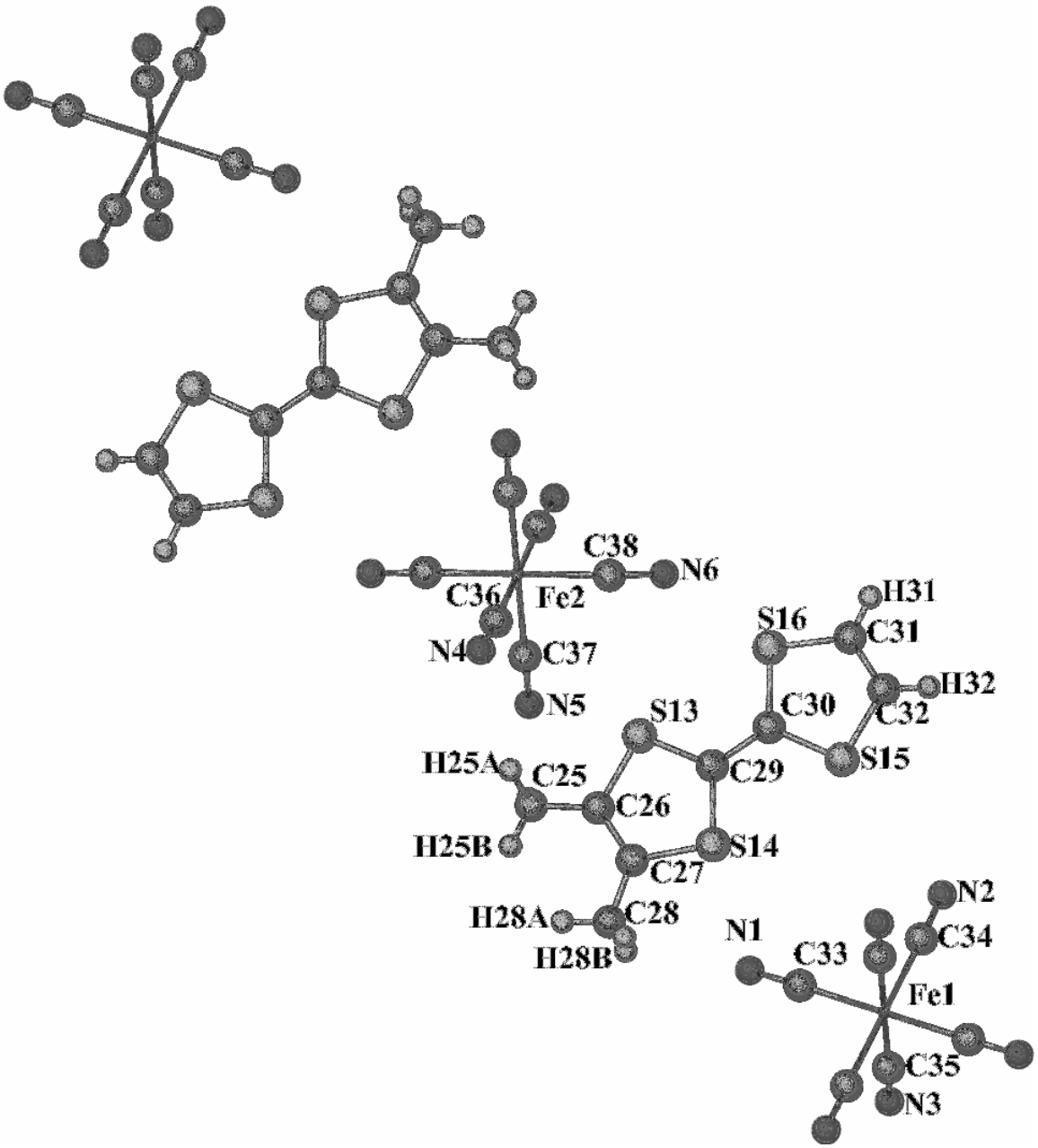

Figure 46. X-ray crystal structure of (o-$Me_2TTF)_8[Fe^{III}(CN)_6]_3$•$2H_2O$ (**16•2H$_2$O**), illustrating the hybrid organic-inorganic sheets lying between the one-dimensional stacks of o-Me_2TTF donors. Interstitial water molecules have been omitted for the sake of clarity.

The X-ray structure of (**17•8H_2O**) crystallizes in the monoclinic space group *$P2_1/n$* and consists of eight independent *o*-Me_2TTF donors which stack in the (1,1,0) plane in the head-to-tail stacking motif observed in other salts composed of *o*-Me_2TTF radical cations. The stacks of *o*-Me_2TTF radical cations form along the (1,0,1) plane rotated ~45° from the unit cell origin. Upon close inspection of the stacks, the donors labeled as A-H form trimers of *o*-Me_2TTF donors separated by a strong σ-dimer between fully oxidized radical cations. Due to the lack of extended S-S overlap between the donors and the presence of neutral donor molecules, this system should display weakly-conducting properties. Salts that combine organic donors of the chalcofulvalene family with inorganic cyanometallate charge-compensating anions are considered "hybrid" systems as they introduce separate organic and inorganic com-ponents into the crystalline matrix. The solid-state structure of this "hybrid" salt consists of separate planes of organic and inorganic components extending out in an alternating pattern along the b-axis of the unit cell. In various literature reports, the stacking pattern of oxidized chalcofulvalene donors in hybrid systems form the basis upon which each system's structural features are often discussed. The structure for (**17•8H_2O**) is very interesting because, unlike other hybrid salts containing a potentially conducting organic sublattice, interesting features are seen in the inorganic sublattice because of a network of hydrogen-bonding interactions composed of two, alternating sets of interactions involving water molecules and hexacyanocobaltate anions. In each group of four water molecules, hydrogen bonding interactions exist between the water molecules and the hexacyano-cobaltate anions. In the first group, hydrogen bonds between 1.9 and 2.0 Å in distance exist in a four-fold fashion between the hydrogen atoms of the water molecules and both

the oxygen atom of another water molecule and nitrogen atom from a cyanide group in the hexacyanocobaltate. The second set of hydrogen bonding interactions form a square pattern where one vertex of the square is an oxygen atom. The corresponding hydrogen atoms from this oxygen form two hydrogen bonds with oxygen atoms at opposite vertices of the square. The hydrogen atoms from these latter oxygen atoms also form hydrogen bonds with two nitrogen atoms from cyanide ligands of different cyanometallates. The fourth corner of this square hydrogen bonding network forms interactions that mirror the former water and its constituent oxygen atom. The interactions are in the range of 1.9-2.0 Å. The solid-state structures illustrating the hybrid organic-inorganic repeat units as well as the overall structure's the hybrogen bonding network and constituent motifs are shown in Figures 47-49.

The salt structures for (**18•8H_2O**) and (**19•8H_2O**) are isostructural and are dominated by eight TTF radical cations which stack along the (1,1,1/2) plane. Inspection of the radical cations, indicate that four strong σ-dimers form from these eight cations. The dimers stack in a stair-step fashion reminiscent of the pattern observed for the $(TTF)_3[BF_4]_2$ salt, in which the $TTF^{\bullet+}$ radical cation dimers are separated by neutral TTF donors.[45] In a manner similar to (**18•8H_2O**), stacks of oxidized TTF donors form segregated stacks with $[Co(CN)_6]^{3-}$ anions. Despite the presence of segregated organic and inorganic lattices in (**18•8H_2O**), the inorganic packing of (**19•8H_2O**) shows the presence of interpenetrated TTF donors. The bond distances of the donors and their corresponding bond distances, according to the Coppens' formula, indicate that two of the three donors are neutral while the third has been oxidized to the +1 state.[94]

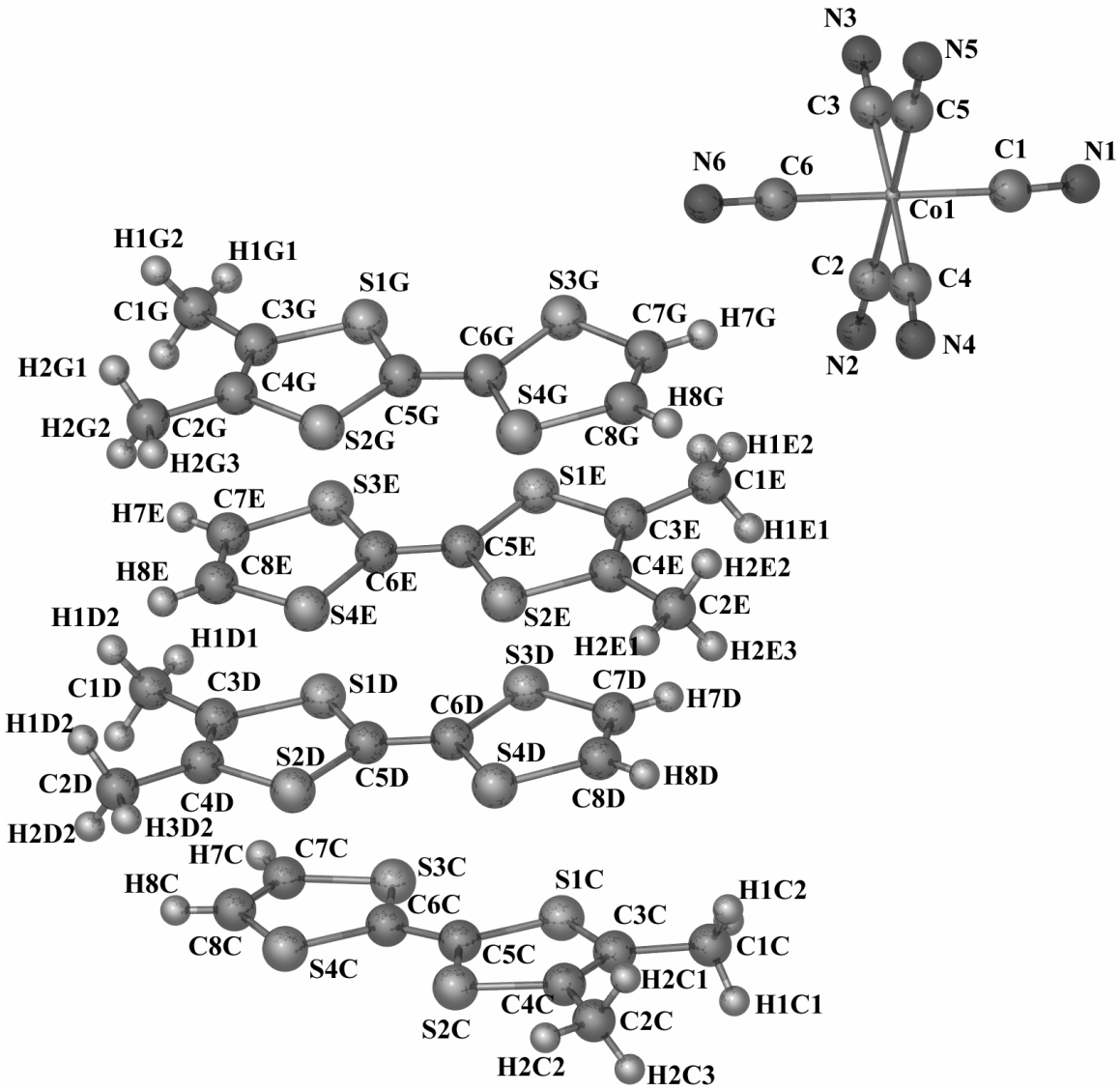

Figure 47. X-ray crystal structure of (*o*-$Me_2TTF)_8[Co(CN)_6]_2$•$8H_2O$ (**17•8H_2O**) illustrating one, independent hybrid inorganic-organic repeating unit of four *o*-Me_2TTF donors and one hexacyanocobaltate anion. Interstitial water molecules have been omitted for the sake of clarity.

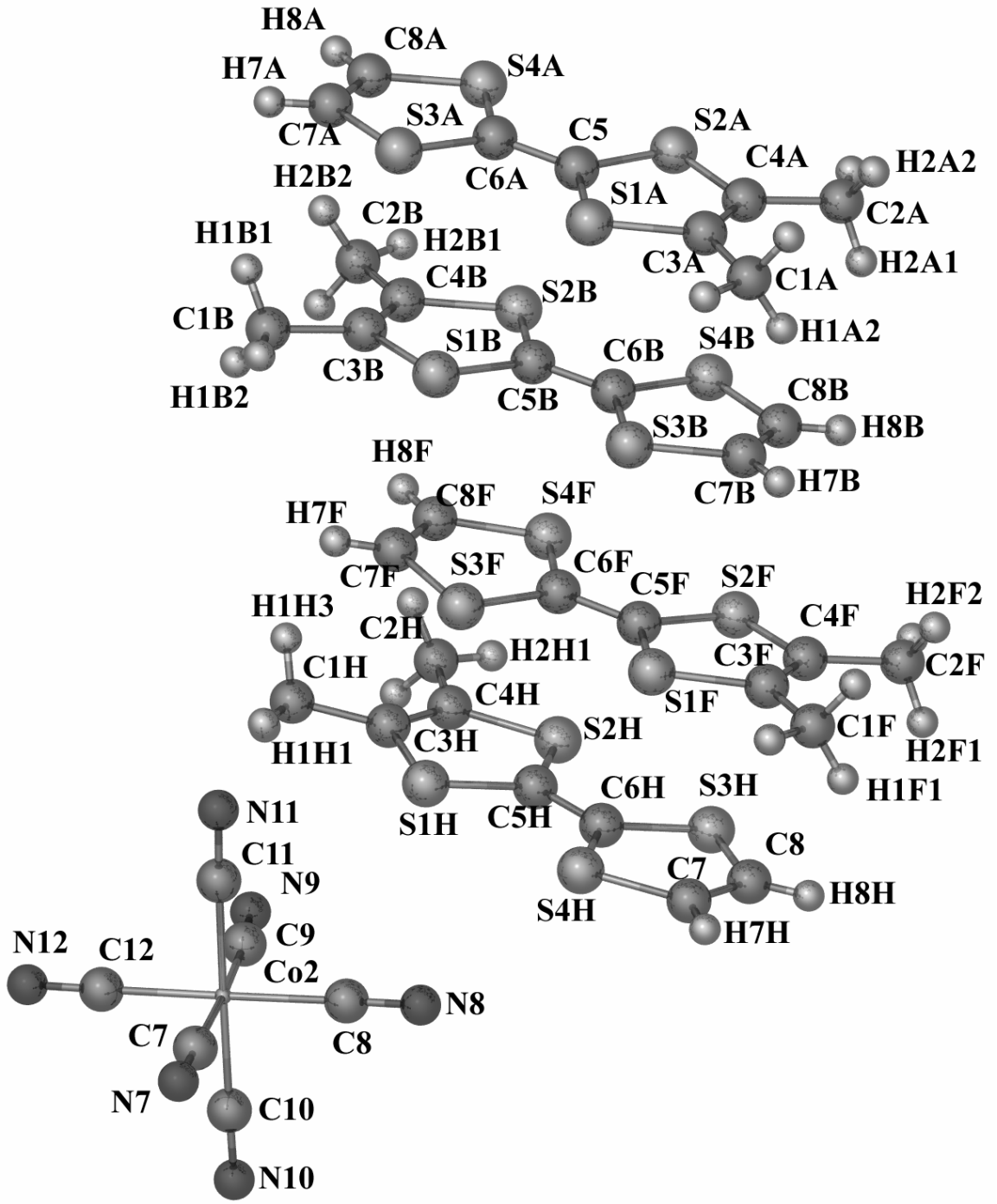

Figure 48. X-ray crystal structure of (o-$Me_2TTF)_8[Co(CN)_6]_2$•$8H_2O$ (**17•8H$_2$O**) illustrating the second hybrid inorganic-organic unit containing four o-Me_2TTF donors and one hexacyanocobaltate anion. Interstitial water molecules have been omitted for the sake of clarity.

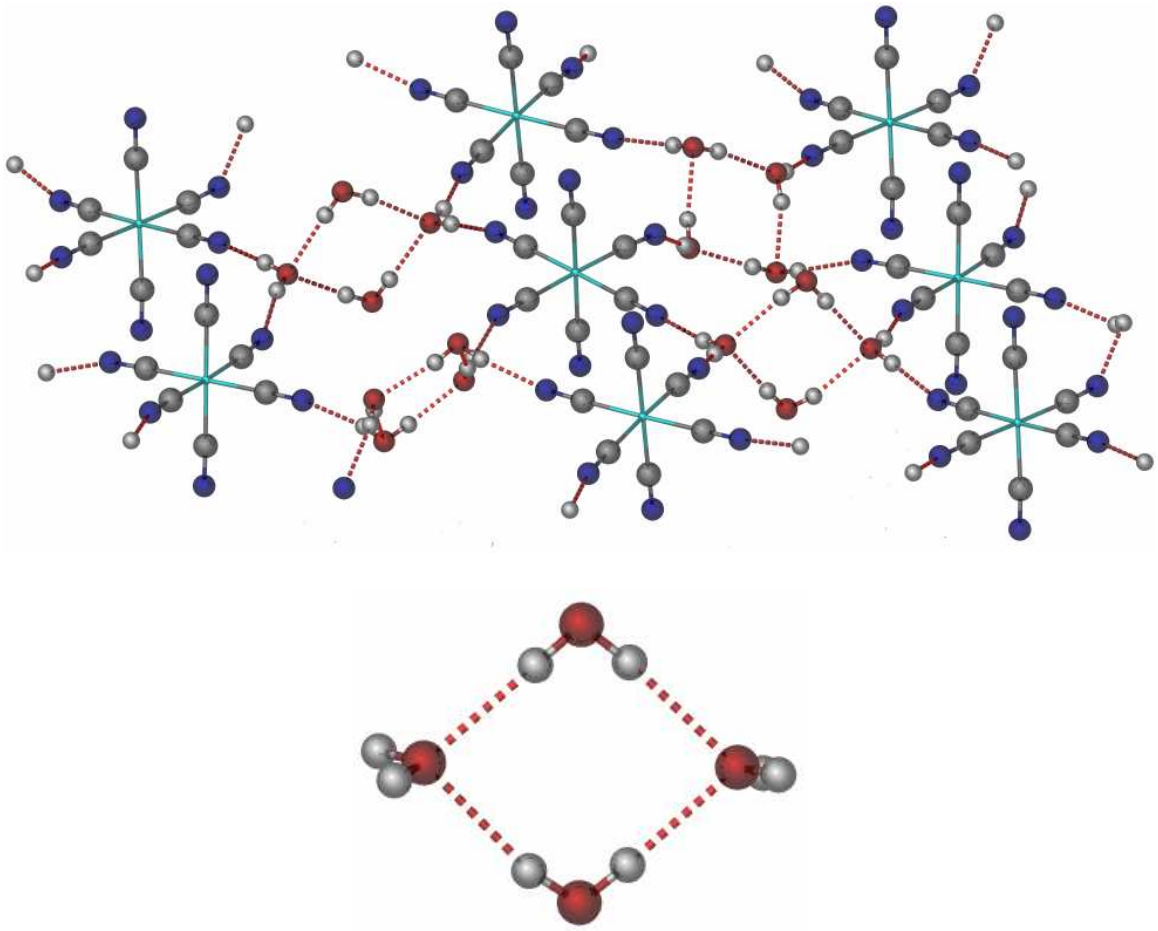

(**a**)

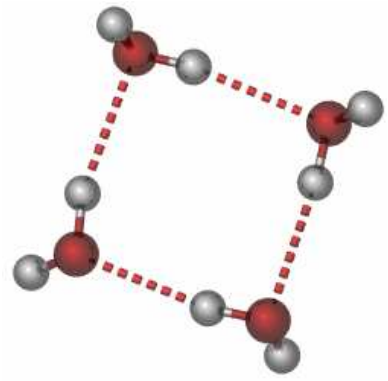

(**b**)

Figure 49. Solid-state packing of the extended unit cell for (**18•8H_2O**) illustrating the hydrogen bonding networks involving interstitial water molecules and hexacyano-cobaltate. The individual hydrogen-bonding motifs (**a**) and (**b**) are also shown.

A hydrogen bonding network also exists in this hybrid network in a sinusoidal pattern along the c-axis of the unit cell, by forming bridging, hydrogen bonding interactions between 1.9 and 2.0 Å among hydrogen atoms of interstitial water molecules and nitrogen atoms from the cyanide ligands of different hexacyanocobaltate anions. Due to their presence of similar structural features, the solid-state structure for (**19•8H_2O**) will be presented as a representative example of the radical cation salts obtained between TTF and the cyanometallate family of anions. Figures representing the one-dimensional stacking of TTF donor molecues, the hybrid organic-inorganic layers, and the hydrogen bonding network in this pair of salts are shown in Figures 50-52. Selected bond distances for (**16•2H_2O**), (**17•8H_2O**), (**18•8H_2O**), and (**19•8H_2O**) as well as X-ray crystallographic and refinement data and the calculated valences for their chalcofulvalenium radical cations are listed in Tables 32-39.

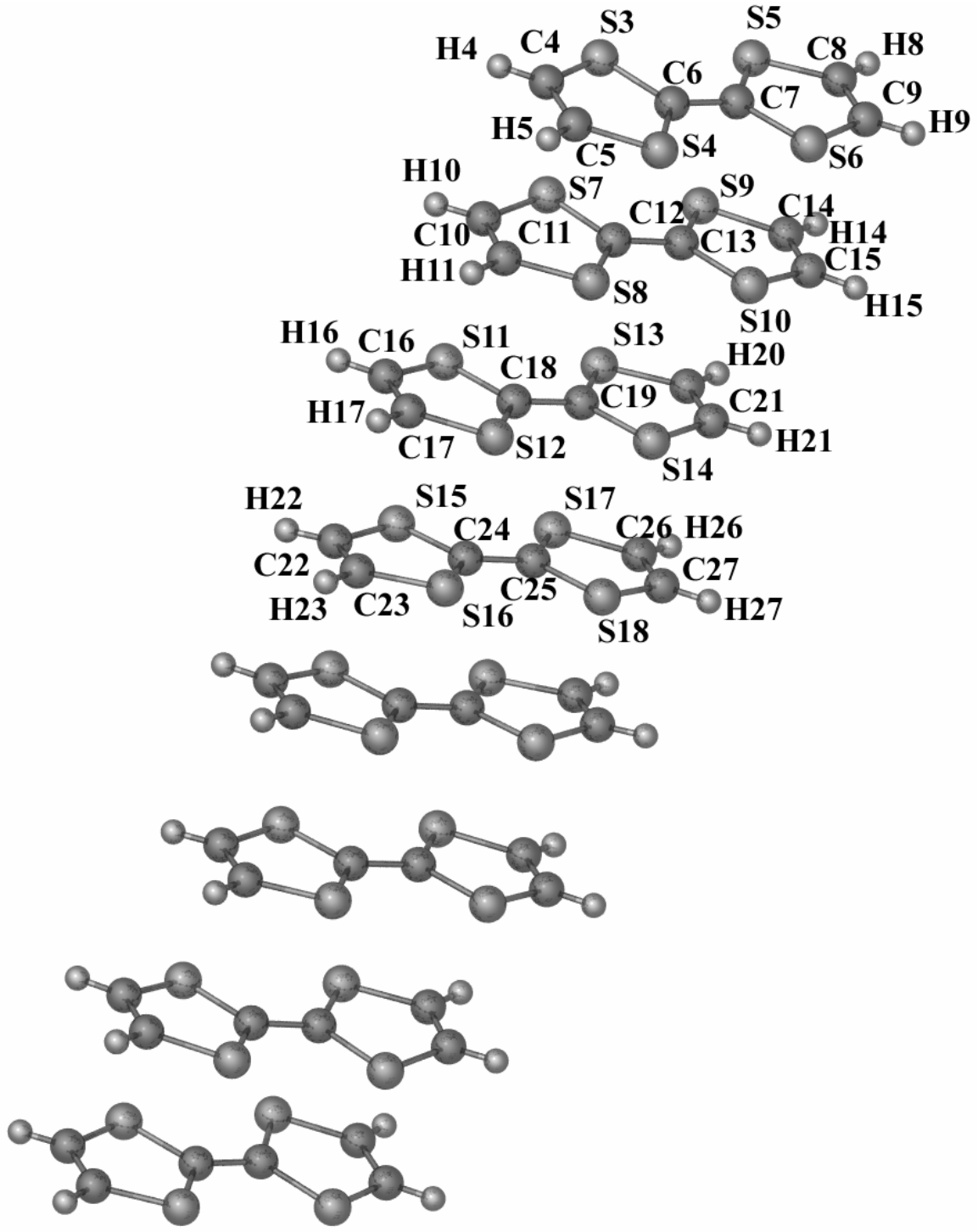

Figure 50. X-ray crystal structure of $(TTF)_{11}[Co(CN)_6]_3 \bullet 8H_2O$ (**19•8H$_2$O**), illustrating the one-dimensional stacking of the TTF donor molecules in the TTF-hexacyanometallate family of salts. Interstitial water molecules have been omitted for the sake of clarity.

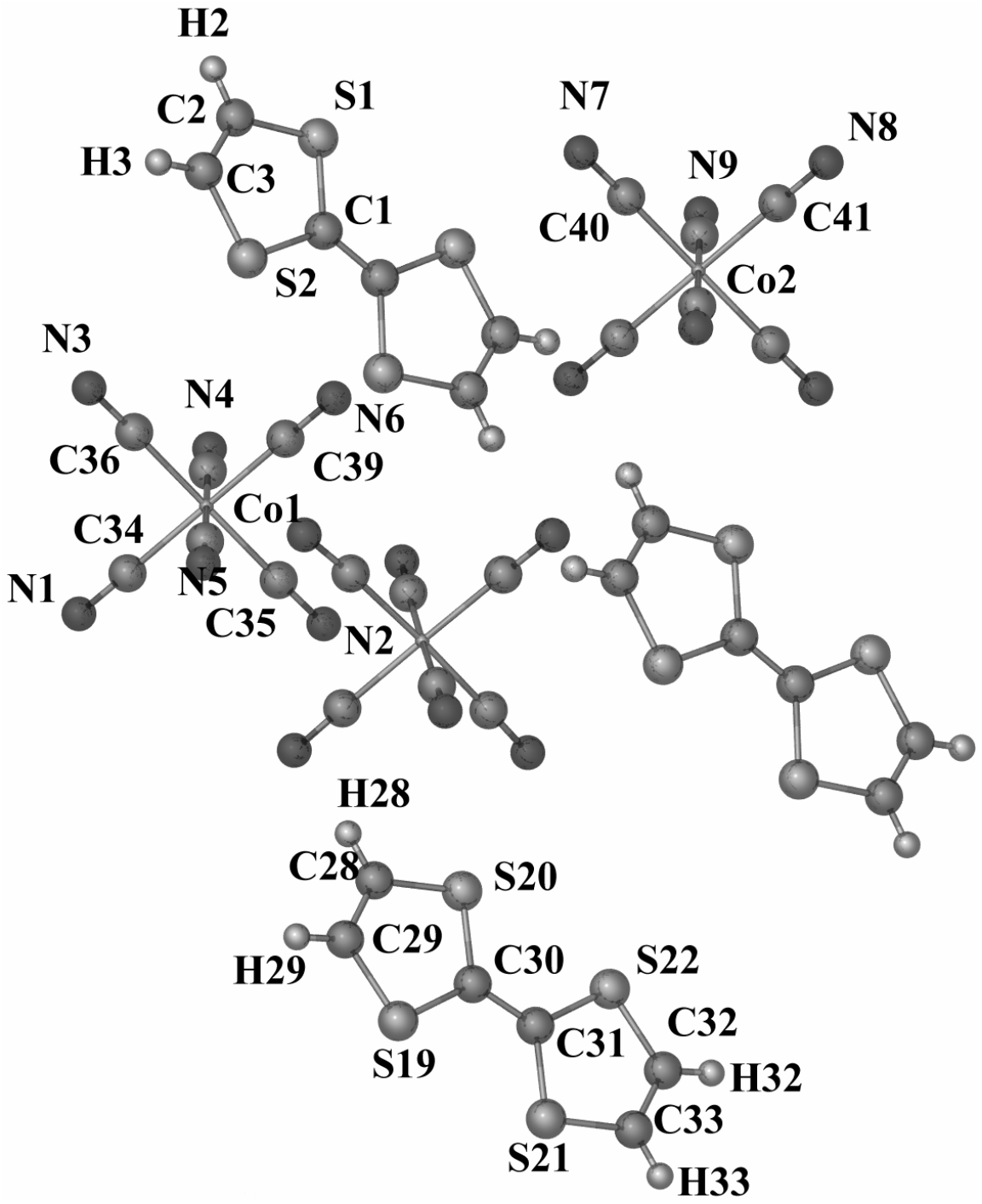

Figure 51. X-ray crystal structure of $(TTF)_{11}[Co(CN)_6]_3 \bullet 8H_2O$ (**19•8H$_2$O**), illustrating the hybrid organic-inorganic layers lying between the one-dimensional stacks of TTF in the TTF-hexacyanometallate family of salts. Interstitial water molecules have been omitted for the sake of clarity.

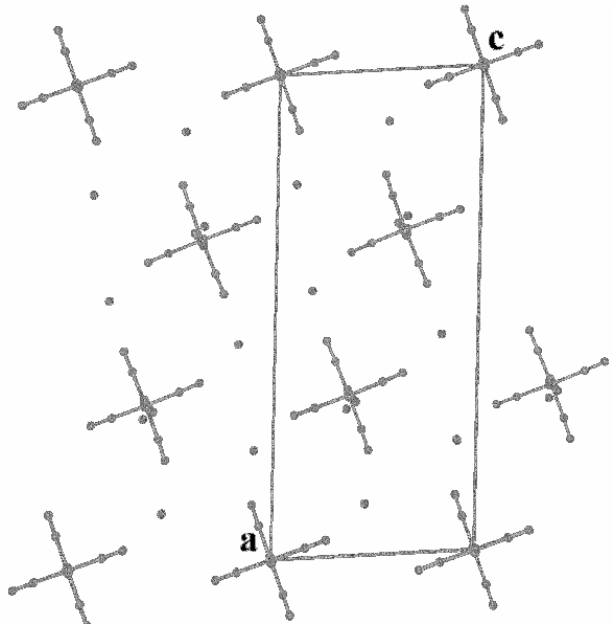

(**a**)

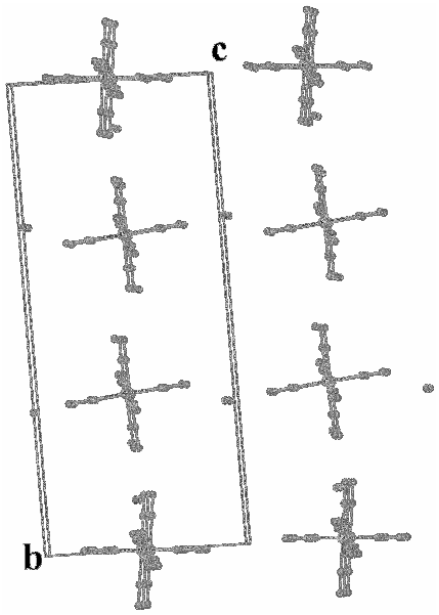

(**b**)

Figure 52. Solid-state packing of the extended unit cell for (**19•8H_2O**) illustrating the formation of hydrogen bonding networks involving interstitial water molecules and hexacyanocobaltate from the top (**a**) and side (**b**) in the TTF-hexacyanometallate family of salts.

Table 32. X-ray crystallographic and refinement data for radical salts (**16•2H_2O**) and (**17•8H_2O**).

Compound	(*o*-$Me_2TTF)_8[Fe^{III}(CN)_6]_3$•2$H_2O$ (**16•2H_2O**)	(*o*-$Me_2TTF)_8[Co(CN)_6]_2$•8H_2O (**17•8H_2O**)
Formula	$C_{82}H_{68}S_{32}N_{18}Fe_3O_2$	$C_{76}H_{80}S_{32}Co_2N_{12}O_8$
formula weight	2527.49	2429.59
Space group	P-1	$P2_1/n$
a, Å	10.294(2)	19.2319(9)
b, Å	10.372(2)	25.2366(12)
c, Å	22.539(5)	21.1081(10)
α, deg	80.11(3)	90
β, deg	85.73(3)	92.629(3)
γ, deg	81.82(3)	90
volume, Å^3	2343.4(8)	10234.0(8)
Z	1	4
μ, mm^{-1}	1.076	1.034
Temp.	110(2)	110(2)
Reflns. collected	6275	23426
Reflns. I>2σ	5075	19426
Parameters	570	1235
Restraints	0	16
R1[a]	0.0586	0.0359
wR2[b]	0.1465	0.0991
Goodness-of-fit[c]	1.044	1.079

[a] $R1 = \sum||F_o| - |F_c||/\sum|F_o|$. [b] $wR2 = [\sum [w(F_o^2-F_c^2)^2]/ \sum [w(F_o^2)^2]^{1/2}$

[c] Goodness-of-fit = $[\sum w(|F_o|-|F_c|)^2/(N_{obs}-N_{parameter})]^{1/2}$

Table 33. X-ray crystallographic and refinement data for radical salts (**18•8H$_2$0**) and (**19•8H$_2$O**).

Compound	$(TTF)_{11}[Fe^{III}(CN)_6]_3$•$8H_2O$ (**18•8H$_2$O**)	$(TTF)_{11}[Co(CN)_6]_3$•$8H_2O$ (**19•8H$_2$O**)
Formula	$C_{84}H_{60}S_{44}Fe_3N_{18}O_8$	$C_{84}H_{60}S_{44}Co_3N_{18}O_8$
formula weight	3023.06	3032.05
Space group	P-1	P-1
a, Å	10.759(2)	10.745(2)
b, Å	10.797(2)	10.798(2)
c, Å	25.110(5)	25.186(5)
α, deg	85.68(3)	90.53(3)
β, deg	89.86(3)	93.96(3)
γ, deg	80.23(3)	99.82(3)
volume, Å^3	2866.1(10)	2871.8(10)
Z	1	1
μ, mm^{-1}	1.238	1.290
Temp.	110(2)	140(2)
Reflns. collected	12915	13420
Reflns. I>2σ	11051	10351
Parameters	689	689
Restraints	0	0
R1[a]	0.0321	0.0393
wR2[b]	0.0833	0.1007
Goodness-of-fit[c]	1.034	1.084

[a] $R1 = \sum||F_o| - |F_c||/\sum|F_o|$. [b] $wR2 = [\sum [w(F_o^2-F_c^2)^2]/ \sum [w(F_o^2)^2]^{1/2}$

[c] Goodness-of-fit = $[\sum w(|F_o|-|F_c|)^2/(N_{obs}-N_{parameter})]^{1/2}$

Table 34. Bond distances for (*o*-$Me_2TTF)_8[Fe^{III}(CN)_6]_3 \cdot 2H_2O$ (**16•2H$_2$O**) in Å.

Fe(1)-C(33)	1.949(7)	S(14)-C(27)	1.741(7)
Fe(1)-C(34)	1.957(10)	S(14)-C(29)	1.704(7)
Fe(1)-C(35)	1.951(7)	S(15)-C(30)	1.719(9)
Fe(2)-C(36)	1.957(7)	S(15)-C(32)	1.707(12)
Fe(2)-C(37)	1.957(7)	S(16)-C(30)	1.708(9)
Fe(2)-C(38)	1.951(7)	S(16)-C(31)	1.697(12)
S(1)-C(1)	1.713(6)	N(1)-C(33)	1.150(8)
S(1)-C(3)	1.725(6)	N(2)-C(34)	1.136(10)
S(2)-C(2)	1.735(6)	N(3)-C(35)	1.143(8)
S(2)-C(3)	1.730(6)	N(4)-C(36)	1.150(8)
S(3)-C(4)	1.727(6)	N(5)-C(37)	1.148(8)
S(3)-C(7)	1.740(6)	N(6)-C(38)	1.149(8)
S(4)-C(4)	1.730(6)	C(1)-C(2)	1.335(9)
S(4)-C(6)	1.741(6)	C(3)-C(4)	1.378(9)
S(5)-C(9)	1.744(6)	C(5)-C(6)	1.492(9)
S(5)-C(11)	1.751(6)	C(6)-C(7)	1.356(9)
S(6)-C(10)	1.749(6)	C(7)-C(8)	1.507(8)
S(6)-C(11)	1.759(6)	C(9)-C(10)	1.327(8)
S(7)-C(12)	1.756(6)	C(11)-C(12)	1.355(8)
S(7)-C(14)	1.764(6)	C(13)-C(14)	1.501(8)
S(8)-C(12)	1.749(6)	C(14)-C(15)	1.333(9)
S(8)-C(15)	1.764(6)	C(15)-C(16)	1.499(9)
S(9)-C(19)	1.747(6)	C(17)-C(18)	1.499(8)
S(9)-C(21)	1.717(6)	C(18)-C(19)	1.344(8)
S(10)-C(18)	1.744(6)	C(19)-C(20)	1.506(8)
S(10)-C(21)	1.726(6)	C(21)-C(22)	1.382(8)
S(11)-C(22)	1.727(6)	C(23)-C(24)	1.333(9)
S(11)-C(24)	1.716(6)	C(25)-C(26)	1.437(11)
S(12)-C(22)	1.730(6)	(C26)-C(27)	1.382(12)
S(12)-C(23)	1.714(6)	C(27)-C(28)	1.388(11)
S(13)-C(26)	1.744(8)	C(29)-C(30)	1.425(11)
S(13)-C(29)	1.716(7)	C(31)-C(32)	1.350(17)

Table 35. Bond distances for (*o*-$Me_2TTF)_8[Co(CN)_6]_2 \cdot 8H_2O$ (**17•8H_2O**) in Å.

Co(1)-C(6)	1.887(3)	S(2E)-C(5E)	1.725(3)
Co(1)-C(4)	1.898(3)	S(2E)-C(4E)	1.744(3)
Co(1)-C(3)	1.906(3)	S(3E)-C(7E)	1.727(3)
Co(1)-C(1)	1.906(3)	S(3E)-C(6E)	1.731(3)
Co(1)-C(2)	1.907(3)	S(4E)-C(8E)	1.728(3)
Co(1)-C(5)	1.911(3)	S(4E)-C(6E)	1.729(3)
C(1)-N(1)	1.156(4)	C(1E)-C(3E)	1.497(4)
C(2)-N(2)	1.150(3)	C(2E)-C(4E)	1.504(4)
C(3)-N(3)	1.153(4)	C(3E)-C(4E)	1.351(4)
C(4)-N(4)	1.159(4)	C(5E)-C(6E)	1.388(4)
C(5)-N(5)	1.148(3)	C(7E)-C(8E)	1.342(4)
C(6)-N(6)	1.162(4)	S(1F)-C(5F)	1.726(3)
Co(2)-C(12)	1.889(3)	S(1F)-C(3F)	1.749(3)
Co(2)-C(9)	1.896(3)	S(2F)-C(5F)	1.725(3)
Co(2)-C(10)	1.905(3)	S(2F)-C(4F)	1.740(3)
Co(2)-C(11)	1.908(3)	S(3F)-C(6F)	1.728(3)
Co(2)-C(8)	1.909(3)	S(3F)-C(7F)	1.730(3)
Co(2)-C(7)	1.911(3)	S(4F)-C(6F)	1.731(3)
C(7)-N(7)	1.155(4)	S(4F)-C(8F)	1.733(3)
C(8)-N(8)	1.158(4)	C(1F)-C(3F)	1.499(4)
C(9)-N(9)	1.156(4)	C(2F)-C(4F)	1.501(4)
C(10)-N(10)	1.155(4)	C(3F)-C(4F)	1.349(4)
C(11)-N(11)	1.159(4)	C(5F)-C(6F)	1.393(4)
C(12)-N(12)	1.154(4)	C(7F)-C(8F)	1.343(4)
S(1A)-C(5A)	1.726(3)	S(1G)-C(5G)	1.736(3)
S(1A)-C(3A)	1.749(3)	S(1G)-C(3G)	1.758(3)
S(2A)-C(5A)	1.720(3)	S(2G)-C(5G)	1.727(3)
S(2A)-C(4A)	1.744(3)	S(2G)-C(4G)	1.754(3)
S(3A)-C(6A)	1.730(3)	S(3G)-C(6G)	1.737(3)
S(3A)-C(7A)	1.739(3)	S(3G)-C(7G)	1.743(3)
S(4A)-C(6A)	1.730(3)	S(4G)-C(8G)	1.737(3)
S(4A)-C(8A)	1.733(3)	S(4G)-C(6G)	1.741(3)

Table 35. Continued.

C(1A)-C(3A)	1.504(4)	C(1G)-C(3G)	1.500(4)
C(2A)-C(4A)	1.501(4)	C(2G)-C(4G)	1.501(4)
C(3A)-C(4A)	1.356(4)	C(3G)-C(4G)	1.353(4)
C(5A)-C(6A)	1.395(4)	C(5G)-C(6G)	1.385(4)
C(7A)-C(8A)	1.343(4)	C(7G)-C(8G)	1.338(4)
S(1B)-C(5B)	1.744(3)	S(1H)-C(5H)	1.720(3)
S(1B)-C(3B)	1.766(3)	S(1H)-C(3H)	1.749(3)
S(2B)-C(5B)	1.749(3)	S(2H)-C(5H)	1.722(3)
S(2B)-C(4B)	1.761(3)	S(2H)-C(4H)	1.742(3)
S(3B)-C(7B)	1.747(3)	S(3H)-C(8H)	1.735(3)
S(3B)-C(6B)	1.757(3)	S(3H)-C(6H)	1.738(3)
S(4B)-C(8B)	1.744(3)	S(4H)-C(6H)	1.719(3)
S(4B)-C(6B)	1.750(3)	S(4H)-C(7H)	1.724(3)
C(1B)-C(3B)	1.501(4)	C(1H)-C(3H)	1.499(4)
C(2B)-C(4B)	1.503(4)	C(2H)-C(4H)	1.509(4)
C(3B)-C(4B)	1.345(4)	C(3H)-C(4H)	1.350(4)
C(5B)-C(6B)	1.358(4)	C(5H)-C(6H)	1.396(4)
C(7C)-C(8C)	1.345(4)	C(7H)-C(8H)	1.344(4)
S(1D)-C(5D)	1.742(3)	C(7B)-C(8B)	1.322(5)
S(1D)-C(3D)	1.754(3)	S(1C)-C(5C)	1.728(3)
S(2D)-C(5D)	1.732(3)	S(1C)-C(3C)	1.747(3)
S(2D)-C(4D)	1.751(3)	S(2C)-C(5C)	1.723(3)
S(3D)-C(7D)	1.739(3)	S(2C)-C(4C)	1.736(3)
S(3D)-C(6D)	1.742(3)	S(3C)-C(6C)	1.726(3)
S(4D)-C(8D)	1.739(3)	S(3C)-C(7C)	1.727(3)
S(4D)-C(6D)	1.751(3)	S(4C)-C(8C)	1.728(3)
C(1D)-C(3D)	1.508(4)	S(4C)-C(6C)	1.732(3)
C(2D)-C(4D)	1.501(4)	C(1C)-C(3C)	1.499(4)
C(3D)-C(4D)	1.348(4)	C(2C)-C(4C)	1.491(4)
C(5D)-C(6D)	1.370(4)	C(3C)-C(4C)	1.362(4)
C(7D)-C(8D)	1.337(4)	C(5C)-C(6C)	1.393(4)

Table 36. Bond distances for $(TTF)_{11}[Fe^{III}(CN)_6]_3 \cdot 8H_2O$ (**18•8H$_2$O**) in Å.

Fe(1)-C(35)	1.934(2)	S(16)-C(22)	1.758(2)
Fe(1)-C(36)	1.935(2)	S(17)-C(25)	1.735(2)
Fe(1)-C(37)	1.941(2)	S(17)-C(27)	1.730(2)
Fe(1)-C(38)	1.953(3)	S(18)-C(26)	1.722(3)
Fe(1)-C(39)	1.945(3)	S(18)-C(27)	1.727(2)
Fe(1)-C(40)	1.933(3)	S(19)-C(28)	1.726(2)
Fe(2)-C(41)	1.953(2)	S(19)-C(29)	1.728(3)
Fe(2)-C(42)	1.946(3)	S(20)-C(28)	1.733(2)
Fe(2)-C(43)	1.935(2)	S(20)-C(30)	1.721(3)
S(1)-C(1)	1.720(3)	S(21)-C(31)	1.731(3)
S(1)-C(3)	1.727(3)	S(21)-C(33)	1.730(2)
S(2)-C(2)	1.716(3)	S(22)-C(32)	1.726(3)
S(2)-C(3)	1.718(3)	S(22)-C(33)	1.733(2)
S(3)-C(4)	1.717(2)	N(1)-C(35)	1.151(3)
S(3)-C(5)	1.724(3)	N(2)-C(36)	1.153(3)
S(4)-C(4)	1.729(3)	N(3)-C(37)	1.153(3)
S(4)-C(6)	1.715(3)	N(4)-C(380	1.158(3)
S(5)-C(7)	1.732(2)	N(5)-C(39)	1.159(3)
S(5)-C(9)	1.730(2)	N(6)-C(40)	1.151(3)
S(6)-C(8)	1.727(2)	N(7)-C(41)	1.157(3)
S(6)-C(9)	1.722(2)	N(8)-C(42)	1.153(3)
S(7)-C(10)	1.722(2)	N(9)-C(43)	1.156(3)
S(7)-C(11)	1.722(2)	C(1)-C(2)	1.339(4)
S(8)-C(10)	1.728(2)	C(3)-C(4)	1.391(4)
S(8)-C(12)	1.728(2)	C(5)-C(6)	1.334(4)
S(9)-C(13)	1.719(2)	C(7)-C(8)	1.336(3)
S(9)-C(15)	1.720(2)	C(9)-C(10)	1.396(3)
S(10)-C(14)	1.723(2)	C(11)-C(12)	1.338(3)
S(10)-C(15)	1.717(2)	C(13)-C(14)	1.343(3)
S(11)-C(16)	1.723(2)	C(15)-C(16)	1.400(3)
S(11)-C(17)	1.724(2)	C(17)-C(18)	1.344(3)
S(12)-C(16)	1.723(2)	C(19)-C(20)	1.323(4)
S(12)-C(18)	1.728(2)	C(21)-C(22)	1.358(3)
S(13)-C(19)	1.750(3)	C(23)-C(24)	1.318(4)
S(13)-C(21)	1.754(2)	C(25)-C(26)	1.333(3)
S(14)-C(20)	1.734(3)	C(27)-C(28)	1.387(3)
S(14)-C(21)	1.758(2)	C(29)-C(30)	1.342(4)
S(15)-C(23)	1.742(3)	C(31)-C(32)	1.334(4)
S(15)-C(22)	1.754(2)	C(33)-C(33')	1.380(4)
S(16)-C(24)	1.749(3)		

Table 37. Bond distances for $(TTF)_{11}[Co(CN)_6]_3 \cdot 8H_2O$ (**19•8H$_2$O**) in Å.

Co(1)-C(34)	1.896(3)	S(16)-C(24)	1.723(3)
Co(1)-C(35)	1.887(3)	S(17)-C(25)	1.720(3)
Co(1)-C(36)	1.898(3)	S(17)-C(26)	1.711(4)
Co(1)-C(37)	1.899(3)	S(18)-C(25)	1.723(3)
Co(1)-C(38)	1.897(3)	S(18)-C(27)	1.714(3)
Co(1)-C(39)	1.888(3)	S(19)-C(29)	1.730(3)
Co(2)-C(40)	1.894(3)	S(19)-C(30)	1.750(3)
Co(2)-C(41)	1.899(3)	S(20)-C(28)	1.737(3)
Co(2)-C(42)	1.896(3)	S(20)-C(30)	1.752(3)
S(1)-C(1)	1.738(3)	S(21)-C(31)	1.748(3)
S(1)-C(2)	1.727(3)	S(21)-C(33)	1.733(4)
S(2)-C(1)	1.734(3)	S(22)-C(31)	1.754(3)
S(2)-C(3)	1.729(4)	S(22)-C(32)	1.730(4)
S(3)-C(4)	1.712(3)	N(1)-C(34)	1.148(4)
S(3)-C(6)	1.727(3)	N(2)-C(35)	1.149(4)
S(4)-C(5)	1.722(3)	N(3)-C(36)	1.147(4)
S(4)-C(6)	1.725(3)	N(4)-C(37)	1.151(4)
S(5)-C(7)	1.721(3)	N(5)-C(38)	1.147(4)
S(5)-C(8)	1.711(3)	N(6)-C(39)	1.146(4)
S(6)-C(7)	1.724(3)	N(7)-C(40)	1.153(4)
S(6)-C(9)	1.729(3)	N(8)-C(41)	1.153(4)
S(7)-C(10)	1.724(3)	N(9)- C(42)	1.150(3)
S(7)-C(12)	1.722(3)	C(1)-C(1)	1.371(6)
S(8)-C(11)	1.719(3)	C(2)-C(3)	1.331(5)
S(8)-C(12)	1.719(3)	C(4)-C(5)	1.338(5)
S(9)-C(13)	1.717(3)	C(6)-C(7)	1.384(4)
S(9)-C(14)	1.717(3)	C(8)-C(9)	1.350(4)
S(10)-C(13)	1.720(3)	C(10)-C(11)	1.340(4)
S(10)-C(15)	1.717(3)	C(12)-C(13)	1.394(4)
S(11)-C(16)	1.725(3)	C(14)-C(15)	1.342(4)
S(11)-C(18)	1.721(3)	C(16)-C(17)	1.335(4)
S(12)-C(17)	1.720(3)	C(18)-C(19)	1.395(4)
S(12)-C(18)	1.721(3)	C(20)-C(21)	1.336(4)
S(13)-C(19)	1.718(3)	C(22)-C(23)	1.336(4)
S(13)-C(20)	1.723(3)	C(24)-C(25)	1.383(4)
S(14)-C(19)	1.726(3)	C(26)-C(27)	1.337(5)
S(14)-C(21)	1.720(3)	C(28)-C(290	1.315(5)
S(15)-C(22)	1.714(3)	C(30)-C(31)	1.352(4)
S(15)-C(24)	1.719(3)	C(32)-C(33)	1.312(5)
S(16)-C(23)	1.718(3)		

Table 38. Estimated degree of ionicity for the donor molecules for (**16•2H$_2$O**) and (**17•8H$_2$O**).

salt	molecule	A[a]	B[b]	Q[c]
(*o*-Me$_2$TTF)$_8$[Fe^{III}(CN)$_6$]$_3$•2H$_2$O (**16•2H$_2$O**)	A	1.425(5)Å	1.712(8) Å	+1.58
	A	1.425(5)Å	1.712(8) Å	+1.58
	B	1.382(4) Å	1.725(3) Å	+0.85
	B	1.382(4) Å	1.725(3) Å	+0.85
	C	1.355(6) Å	1.754(2) Å	+0.18
	C	1.355(6) Å	1.754(2) Å	+0.18
	D	1.378(7) Å	1.728(6) Å	+0.76
	D	1.378(7) Å	1.728(6) Å	+0.76
(*o*-Me$_2$TTF)$_8$[Co(CN)$_6$]$_2$•8H$_2$O (**17•8H$_2$O**)	A	1.393(7) Å	1.727(5) Å	+0.98
	B	1.370(2) Å	1.742(3) Å	+0.51
	C	1.388(4) Å	1.727(5) Å	+0.91
	D	1.385(5) Å	1.733(7) Å	+0.81
	E	1.396(4) Å	1.725(8) Å	+1.04
	F	1.393(6) Å	1.728(6) Å	+0.97
	G	1.358(3) Å	1.750(4) Å	+0.26
	H	1.395(4) Å	1.727(3) Å	+1.01

[a] Central C=C bond distance.
[b] Mean central C-S bond distance.
[c] Q = charge estimated with the formula Q = -17.92 + 23.43*(A/B) from Ref. 94.

Table 39 Estimated degree of ionicity for the donor molecules for (**18•8H_2O**) and (**19•8H_2O**).

salt	molecule	A[a]	B[b]	Q[c]
$(TTF)_{11}[Fe^{III}(CN)_6]_3$•8$H_2O$ (**18•8H_2O**)	A	1.391(3) Å	1.723(3) Å	+0.99
	A	1.391(3) Å	1.723(3) Å	+0.99
	B	1.396(4) Å	1.726(2) Å	+1.03
	B	1.396(4) Å	1.726(2) Å	+1.03
	C	1.400(3) Å	1.721(3) Å	+1.14
	C	1.400(3) Å	1.721(3) Å	+1.14
	D	1.358(7) Å	1.756(5) Å	+0.20
	D	1.358(7) Å	1.756(5) Å	+0.20
	E	1.387(4) Å	1.729(2) Å	+0.88
	E	1.387(4) Å	1.729(2) Å	+0.88
	F	1.380(6) Å	1.732(5) Å	+0.75
$(TTF)_{11}[Co(CN)_6]_3$•8H_2O (**19•8H_2O**)	A	1.384(4) Å	1.724(5) Å	+0.89
	A	1.384(4) Å	1.724(5) Å	+0.89
	B	1.394(6) Å	1.720(5) Å	+1.07
	B	1.394(6) Å	1.720(5) Å	+1.07
	C	1.395(3) Å	1.721(3) Å	+1.07
	C	1.395(3) Å	1.721(3) Å	+1.07
	D	1.383(7) Å	1.721(5) Å	+0.91
	D	1.383(7) Å	1.721(5) Å	+0.91
	E	1.352(4) Å	1.751(2) Å	+0.17
	E	1.352(4) Å	1.751(2) Å	+0.17
	F	1.371(6) Å	1.736(9) Å	+0.58

[a] Central C=C bond distance.
[b] Mean central C-S bond distance.
[c] Q = charge estimated with the formula Q = -17.92 + 23.43*(A/B) from Ref. 94.

Conductivity Measurements

The thermal variation of the electrical conductivity of samples **1** and **3** are displayed in Figure 53. Both compounds show a classical semiconducting behavior with room temperature conductivities of $2.2x10^{-4}$ and $3.0x10^{-4}$ $S.cm^{-1}$ and Arrhenius-like behaviors on decreasing the temperature with activation energies of 305 and 210 meV for samples **1** and **3**, respectively (inset in Figure 53). The low room temperature conductivity and the semiconducting behavior can be easily explained in both cases: in

sample **1** each BEDT-TTF molecule bears an integer charge of +1 whereas sample **3** shows an inhomogeneous charge distribution with $(TMTTF)_2^{2+}$ dimers and isolated neutral TMTTF molecules (see above), precluding the charge delocalization in both cases.

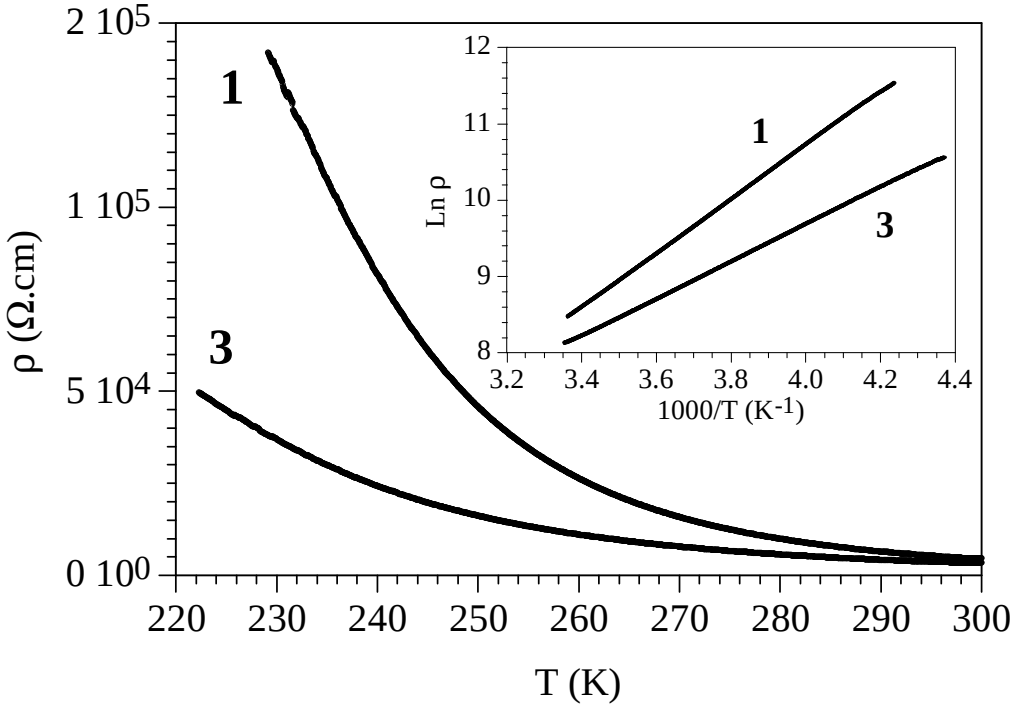

Figure 53. Thermal variation of the resistivity for samples **1** and **3**. Inset shows the Arrhenius plot of both samples.

Conductivity measurements were also conducted on **9** and reveal that the compound is an example of an organic metal, undergoing a metal-to-insulator transition at 110K at 1bar. As demonstrated in Figure 54, measurements conducted at 294 K and 1 bar illustrate that the complex has a room temperature conductivity of 130 $(\Omega \bullet cm)^{-1}$. As the pressure is increased, the room temperature conductivity increases to a maximum of

370 $(\Omega \bullet cm)^{-1}$. These values demonstrate the first time that the *o*-Me_2TTF donor has been used successfully to prepare an organic material which displays metallic conductivity.

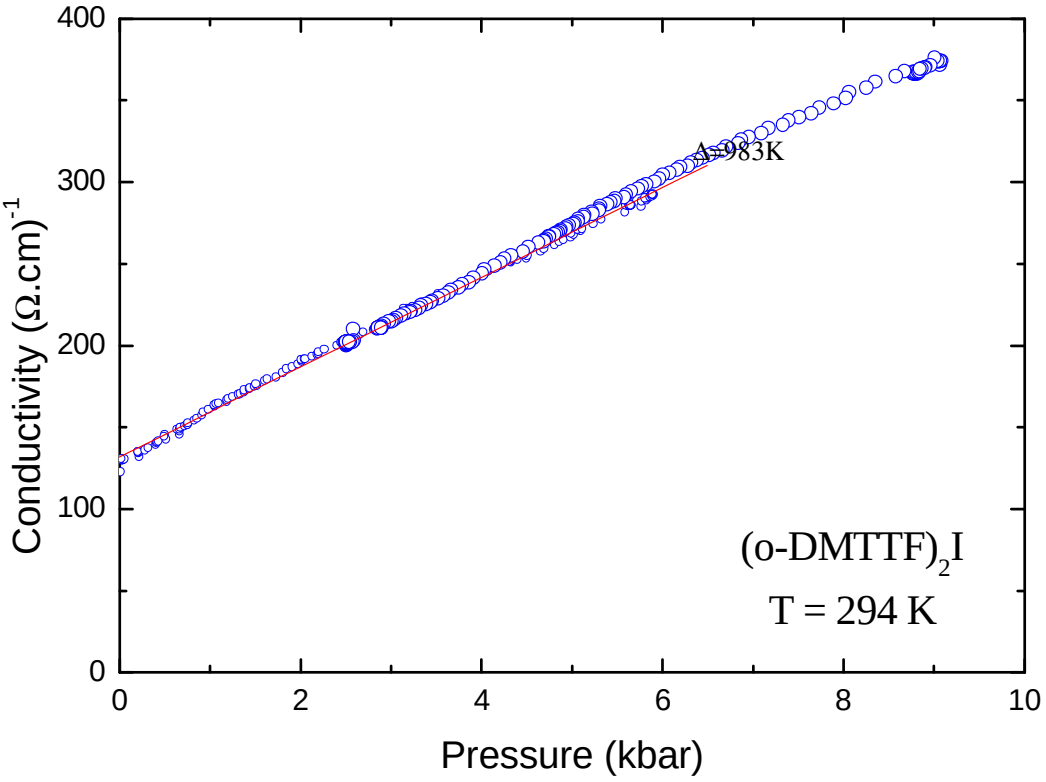

Figure 54. Conductivity values obtained for **9** at 294 K illustrating the increase in conductivity upon increase in pressure.

Magnetic Measurements

In lieu of conductivity measurements, molecular magnetism was used as a qualitative means to search for conductivity, as the presence of a temperature independent paramagnetism (TIP) is indicative of conducting electrons. DC magnetic susceptibility measurements were conducted on **13**, **14**, (**16•2H$_2$O**), and (**18•8H$_2$O**). For **13**, **14**, and (**18•8H$_2$O**), the $[W_6O_{19}]^{2-}$, $[Mo_6O_{19}]^{2-}$, and $[Co(CN)_6]^{3-}$ anions used in the

preparation of those compounds are all diamagnetic, meaning that any resulting magnetic response, will be authored by the organic lattice. In all three cases, no magnetic response from the organic lattice or temperature independent paramagnetism was observed. Such an observation is expected for **13**, **14**, and (**18•8H$_2$O**) as the polyoxometallate salts (**13** and **14**) showed strong charge localization due to σ-type dimers between fully-oxidized *o*-Me$_2$TTF radical cations. A different scenario is observed for the hexacyanocobaltate salt (**18•8H$_2$O**) as the structure does not demonstrate donors in all non-integral oxidation states, but instead shows a mixture of fully-oxidized, partially-oxidized, and neutral donors.

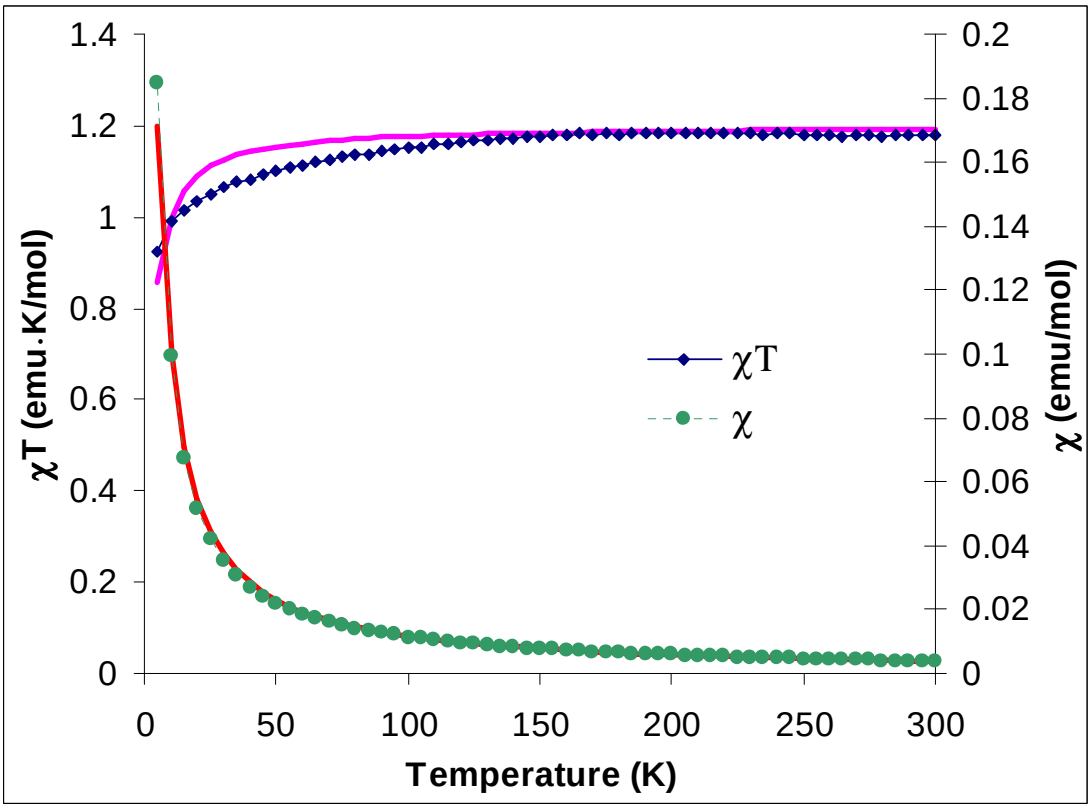

Figure 55. χT vs. T plot for (**16•2H$_2$O**).

The magnetic response for (**16•2H$_2$O**) is interesting, because unlike the previously described salts which contain diamagnetic anions, (**16•2H$_2$O**) utilizes low spin, paramagnetic $Fe^{III}(CN)_6^{3-}$ anions. These strong-field anions possess an S = ½ ground state, facilitated by the presence of a strong ligand field authored by the cyanide ligands around the ferric metal center. The overall χT value of ~1.1 emu•K/mol indicates a paramagnetic response indicative of three, paramagnetic $Fe^{III}(CN)_6^{3-}$ (S = ½) anions (Figure 55). While a paramagnetic response from the anions was observed, no temperature independent paramagnetism from conducting electrons was detected.

Band Diagrams

Theoretical band diagrams calculated using the program CAESAR for **9** (Figure 56) indicate a ¾-filled system (1/4-filled with holes) with no band gap and a Fermi level crossing one of the bands.[92] Such a band diagram is indicative of a system with metallic conductivity. Since compounds **7-11** all have similar stoichiometries, their theoretical band diagrams should also be similar.

The theoretical band diagram for (**18•8H$_2$O**) (Figure 57) was also calculated utilizing CAESAR.[92] In the structure, there are eight crystallographically-independent *o*-Me_2TTF molecules. Application of the inversion center generates sixteen donor molecules, which form a complete conduction plane, and the bands in the band structure, when one considers translations in the (a,c) plane. Based on the stoichiometry of (**18•8H$_2$O**), the sixteen *o*-Me_2TTF donor molecules have a total +12 charge, leaving the remaining upper bands empty. According to the resulting band structure, a large band gap opens, suggesting that (**18•8H$_2$O**) could be a semiconductor.

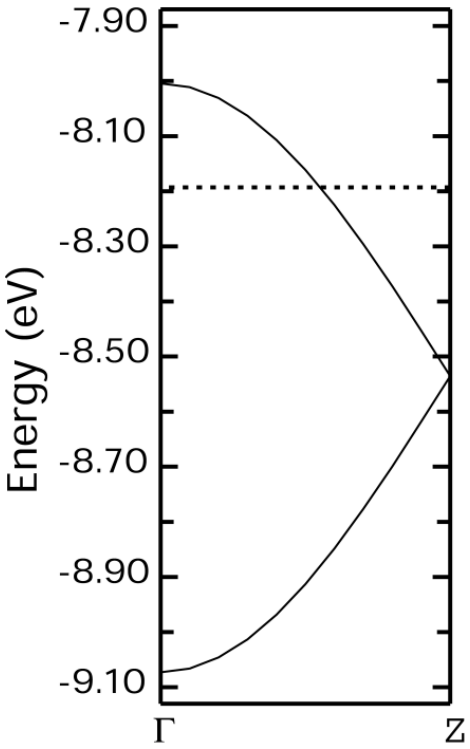

Figure 56. Band structure of **9** where Γ = (0,0,0) and Z = (0,0,c*/2). The dotted line indicates the Fermi level.

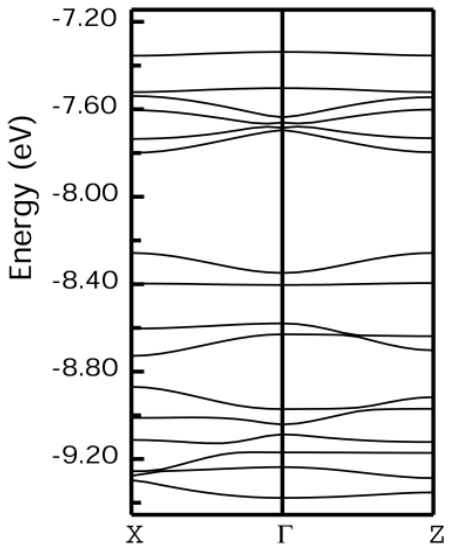

Figure 57. Band structure of (**18•8H_2O**) where Γ = (0,0,0), X = (1,0,0), and Z = (0,0,c*/2).

Conclusions

Electrocrystallized salts have been prepared between various chalcofulvalene donors and various anions of both varying geometry and charge. The chalcofulvalene donors, throughout the series of salts prepared, were found to exist in various oxidation states. Select members of the series contained donors in mixed-valence states while others showed only integral, univalent oxidation states. Other salts, especially those containing anions of more negative charges, such as the cyanometallate or polyoxometallate anions, contain both neutral and fully-ionized donors. Due to the wide range of oxidation states observed, differing levels of transport properties, including semiconducting and metallic conductivity, were observed. In some of the salts, molecular magnetism served as a viable tool to determine the presence of magnetic properties from the inorganic and organic components or as a precursor to conductivity measurements by measuring any temperature independent paramagnetism facilitated by the presence of itinerant electron density in the organic sublattice.

CHAPTER III

PREPARATION OF STABLE TETRATHIAFULVALENE SALTS FOR MATERIALS-BASED METATHESIS REACTIONS

Introduction

Easily oxidized organic molecules such as TTF and its derivatives are important precursors for the preparation of materials that exhibit conducting, optical, magnetic, or a combination of these properties. Often, these materials are encountered as hybrid salts which combine TTF-based radical cations which are essential for the formation of a conducting network with inorganic anions. As discussed in the previous chapter, electrochemical techniques have been successfully used for the preparation of such materials, often generating the radical cations and dications of TTF-like donors (Figure 58) in the course of the experiment. A less investigated alterative to electrochemical methods has been to prepare hybrid materials using metathesis reactions.

Unlike electrochemical preparative techniques where limited solubility has not hindered the preparation of stable salts, metathesis reactions to prepare chalcofulvalenium salts are dependent on the satisfactory solubility of the reactant materials in solvent media. This requirement limits the number of chalcofulvalene donors which can be used, as many of the donors such as BEDT-TTF, BEST, BETS, BET-TTF, and EDT-TTF and similar systems where limited solubility

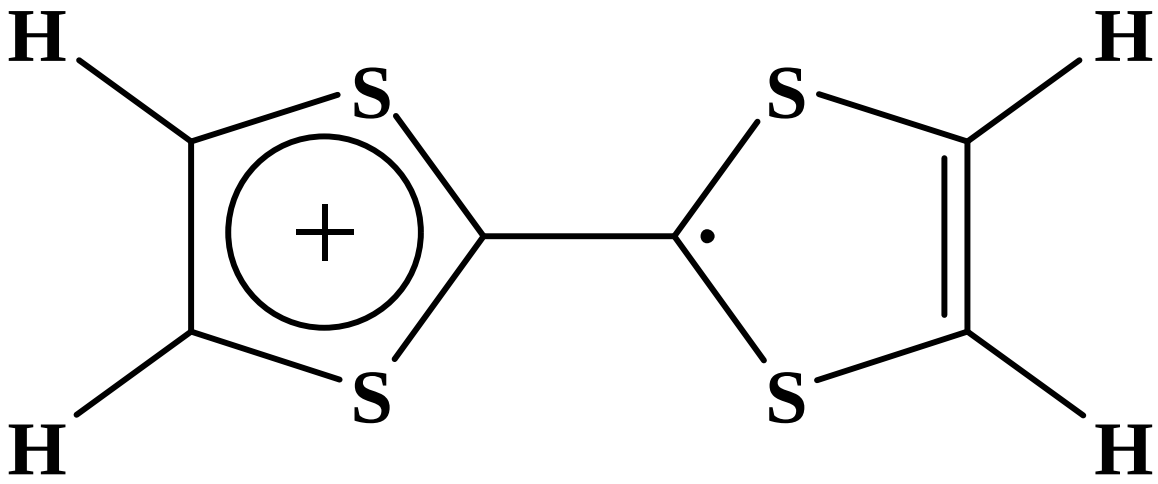

(**a**)

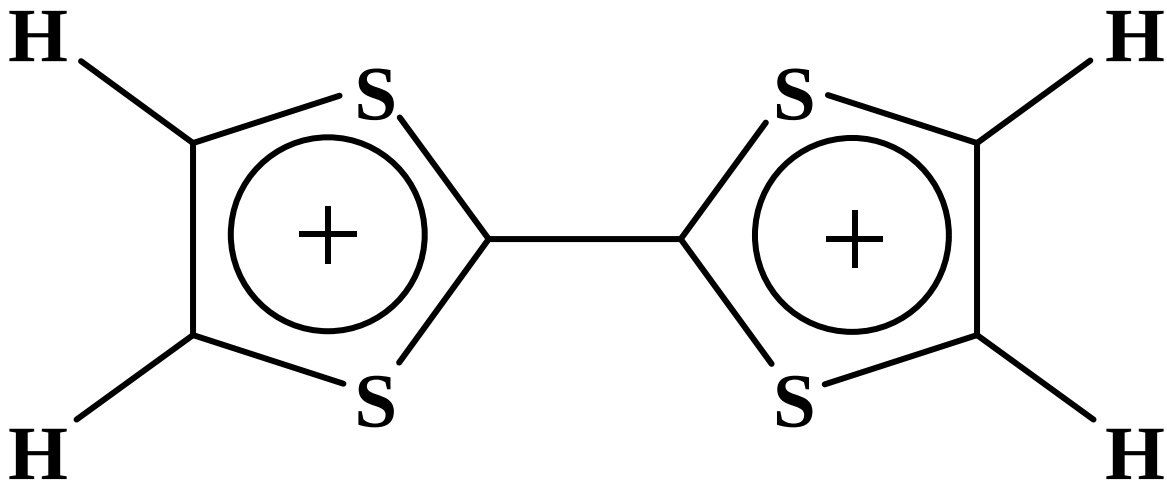

(**b**)

Figure 58. The monocation (**a**) and dication (**b**) of TTF. Donors based on TTF are expected to have the same cationic forms.

renders them inappropriate choices for the preparation of radical cation salts and hybrid systems using metathesis reactions.

First synthesized by Wudl and coworkers in 1975, $(TTF)_3[BF_4]_2$ represented a benchmark in TTF chemistry because, for the first time, a stable, oxidized TTF salt was isolated and used to introduce the TTF radical cation unit into new materials via metathesis techniques.[44] Initial attempts by Wudl and coworkers to prepare a stable salt of oxidized TTF using $AgBF_4$ were unsuccessful as the product could not be successfully separated from colloidal silver.[44] Later attempts using hydrogen peroxide and HBF_4 were successful, yielding $(TTF)_3[BF_4]_2$ as a purple, crystalline solid.

Crystallographic analysis of this purple, crystalline solid was later performed in 1983 by Cassoux and coworkers and revealed dimers of fully-oxidized TTF radical cations separated by neutral TTF donors.[45] The material is soluble in hot acetonitrile and exhibits limited solubility in room-temperature and cold acetonitrile, acetone, and methyl acetate. Despite its relatively limited solubility, $(TTF)_3[BF_4]_2$ has been used to prepare a number of hybrid salts containing TTF-radical cations.[99] Reactions to prepare these hybrid salts using metathesis methods have been limited only to TTF because no stable salts for other donors in the TTF family are known. This chapter outlines work performed as part of this dissertation to prepare stable salts of *o*-Me_2TTF, TMTTF, TTF, and the $[TTF(SCH_2CH_2CN)_4]$ (Figure 59). Air-stable salts of these donors will be useful for introducing radical cations other than $TTF^{\bullet+}$ into hybrid salts using metathesis reactions.

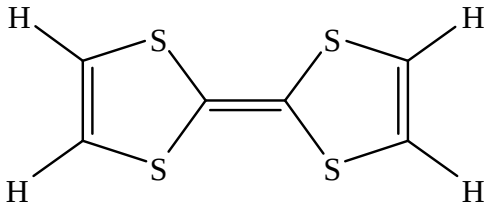

(**a**)

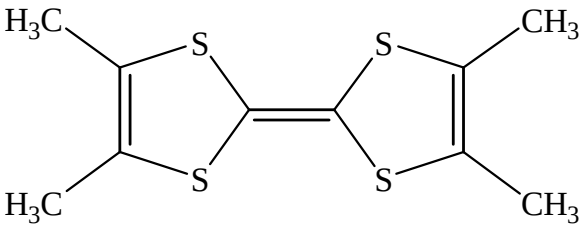

(**b**)

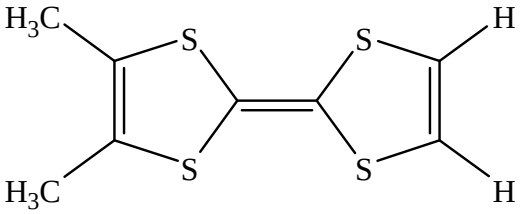

(**c**)

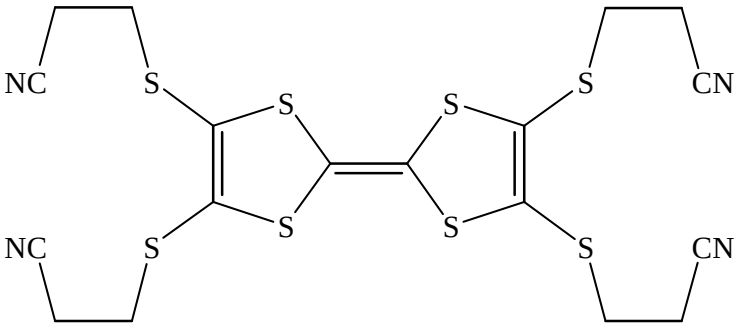

(**d**)

Figure 59. The chalcofulvalene donors TTF (**a**), TMTTF (**b**), *o*-Me_2TTF (**c**), and TTF($SCH_2CH_2CN)_4$ (**d**).

Experimental Section

Preparation of Compounds

All solvents used were dried and freshly distilled prior to use. Dichloromethane and acetonitrile were dried over P_2O_5 and 3Å molecular sieves, respectively. Diethyl ether was passed through an MBRAUN solvent purification system prior to use. TTF($SCH_2CH_2CN)_4$ and the oxidizing agents tris(*p*-bromophenyl)amminium tetra-flouroborate and tris(2,4-dibromophenyl)amminium hexachloroantimonate were prepared according to literature procedures.[100,101] TTF was purchased from Aldrich and used as received without further purification. TMTTF and *o*-Me_2TTF were provided by Prof. Marc Fourmigué and used without additional purification.[84] Unless otherwise noted, all manipulations were performed under an inert atmosphere using a drybox or standard Schlenk-line techniques.

(*o*-Me_2TTF)[BF_4] (1). An orange solution of *o*-Me_2TTF (0.0169g, 7.28 x 10^{-5} mol) dissolved in 10 mL of CH_2Cl_2 was combined with an intensely blue colored solution of tris(*p*-bromophenyl)amminium tetrafluoroborate (0.0439 g, 7.71 x 10^{-5} mol) in 5 mL of CH_2Cl_2. A red precipitate formed instantaneously and the solution was stirred for 5 minutes after which time the solid was collected by filtration and washed with CH_2Cl_2 (2 x 10mL) to remove any unreacted starting material. The solid was dried under vacuum and redissolved in CH_3CN (5 mL) to yield a dark green solution and a white solid. The dark green solution was filtered to remove the amine by-product. Dark green needles were grown from this solution by slow evaporation in air; yield 0.016g (69%).

(TMTTF)[BF_4] (**2**). An orange solution of TMTTF (0.021g, 8.07 x 10^{-5} mol) dissolved in 10 mL of CH_2Cl_2 was combined with a solution of tris(*p*-bromophenyl) amminium tetrafluoroborate (0.0459g, 8.07 x 10^{-5} mol) in CH_2Cl_2 to yield a dark green colored solution which was stirred for 5 minutes. The solution was removed under reduced pressure to yield a dark green solid which was extracted with 5 mL of CH_3CN. The solution was filtered to remove the amine and was evaporated in air which resulted in the formation of dark green needles over the period of two days; yield 0.020g (72%).

$(TTF)_2[SbCl_6]$ (**3**)**.** A yellow solution of TTF (0.024g, 1.17 x 10^{-4} mol) dissolved in 10 mL of CH_2Cl_2 was combined with a green solution of tris(2,4-dibromophenyl)amminium hexachloroantimonate (0.1248g, 1.18 x 10^{-4} mol) in 10 mL of CH_2Cl_2. The combined solutions yielded a red solid which was washed with CH_2Cl_2 (2 x 10 mL) and dried under vacuum. The solid was extracted with CH_3CN (5 mL) and collected by filtration to yield a pale yellow solution which gradually became dark green in color after sitting in air overnight. Dark green platelets grew from the mother liquor over the period of three days; yield 0.041g (65%).

[$TTF(SCH_2CH_2CN)_4$][$SbCl_6$] (**4**)**.** An orange solution of $TTF(SCH_2CH_2CN)_4$ (0.025g, 6.50 x 10^{-5} mol) dissolved in CH_2Cl_2 (10 mL) was combined with a green solution of tris(2,4-dibromophenyl)amminium hexchloroantimonate (0.0692g, 6.57 x 10^{-5} mol) in 10 mL of CH_2Cl_2. Upon addition of the oxidizing agent to the donor solution a dark green solution ensued which was stirred for 5 minutes after which time the solvent was removed under reduced pressure to yield a dark green solid which was extracted with

CH_3CN (5 mL). The solution was filtered to remove the white precipitate of tris(2,4-dibromophenyl)amine and the filtrate was slowly evaporated in air. Dark green platelets grew from the mother liquor after a period of three days; yield 0.033g (83%).

X-ray Crystallographic Details and Structural Solutions

X-ray data for **1**, **2**, and **4** were collected on a Bruker SMART CCD diffractometer at 110±2 K with graphite monochromated Mo-Kα (λ = 0.71073 Å) radiation. The structure for **3** was determined from data collected on a Bruker D8 GADDS system at 110±2K with graphite monochromated Cu-Kα (λ = 1.54178 Å) radiation. The data were corrected for Lorentz and polarization effects. The Bruker SAINT software package was used to integrate the frames and the data were corrected for absorption using the SADABS program.[86,87] Space groups were unambiguously assigned by analysis of symmetry and systematic absences determined by XPREP.[88] The structures were solved by direct methods by the use of the SHELXS-97 program in the Bruker SHELXTL v5.1 software package.[89,90] The final refinements were carried out with anisotropic thermal parameters for all non-hydrogen atoms. Figures for the crystallographic structures were generated using the XSEED program.[91] Crystals for all salts were grown in a similar manner, via slow evaporation from concentrated CH_3CN solutions and secured to a cryoloop using Dow Corning grease and transferred to the liquid nitrogen stream of the diffractometer.

Other Physical Measurements

IR spectra (1600-50 cm-1) were recorded on a computer controlled Nicolet 750 FT-IR spectrophotometer equipped with a TGS/PE detector and silicon beam splitter at 2.0 or 4.0 cm-1 resolution. Electronic absorption spectra were measured on a Hitachi U-2000 spectrophotometer. Electrospray ionization (ESI) mass spectrometry studies were performed on a JEOL HX double-focusing mass spectrometer.

Results and Discussion

Syntheses

The salts of the singly-oxidized donors were prepared by reacting one equivalent of the neutral donor with a stoichiometric quantity of oxidizing agent. In all cases, dark solids resulted upon reactant mixing and solvent removal. Upon subsequent extraction with CH_3CN, formation of intense dark green solutions and white microcrystalline powders occurred which were removed upon filtration. According to various literature reports, dark green is indicative of the singly-oxidized TTF chromophore.[12] The dark green color of the solutions indicates the presence of the singly-oxidized chalcofulavene donor for compounds **1-4**. This conclusion is further corroborated by the presence of the white, microcrystalline powder which is the neutral amine generated upon reduction of the amminium cation from the oxidizing agent. All of the salts are air-stable for prolonged periods of time in both solution and in the solid state.

*(o-Me_2TTF)][BF_4] (**1**) and (TMTTF)[BF_4] (**2**)*

The syntheses for **1** and **2** were performed by reacting CH_2Cl_2 solutions of the neutral donor molecules with CH_2Cl_2 solutions of the oxidizing agent tris(*p*-bromophenyl)amminium tetraflouroborate (Figure 60) in an atmosphere of N_2. After stirring, solvent removal, CH_3CN extraction, and filtration, the resulting dark green solutions were slowly evaporated in air to yield dark green needles of **1** and **2** after a few days.

*(TTF)[$SbCl_6$] (**3**) and [TTF(SCH_2CH_2CN)$_4$][$SbCl_6$] (**4**)*

The syntheses for **3** and **4** were performed by reacting CH_2Cl_2 solutions of the neutral donor molecules with CH_2Cl_2 solutions of the oxidizing agent tris(*p*-bromo-phenyl)amminium hexachloroantimonate (Figure 60) in an atmosphere of N_2. After stirring, solvent removal, CH_3CN extraction, and filtration, the resulting dark green solutions were slowly evaporated in air to yield dark green platelets of **3** and **4** after a few days.

X-ray Structures

The crystals of **1-4** were grown by slow evaporation of concentrated CH_3CN solutions in air. A second method, vapor diffusion of Et_2O into the acetonitrile solutions, also yielded diffraction quality crystals. It has been well established by our group and others that, in the absence of any intermolecular contacts such as π-π or S ••• S interactions, neutral chalcofulvalene donors are non-planar, often exhibiting significant bends of up to 30° along dithiole or diseleno bridges.[12]

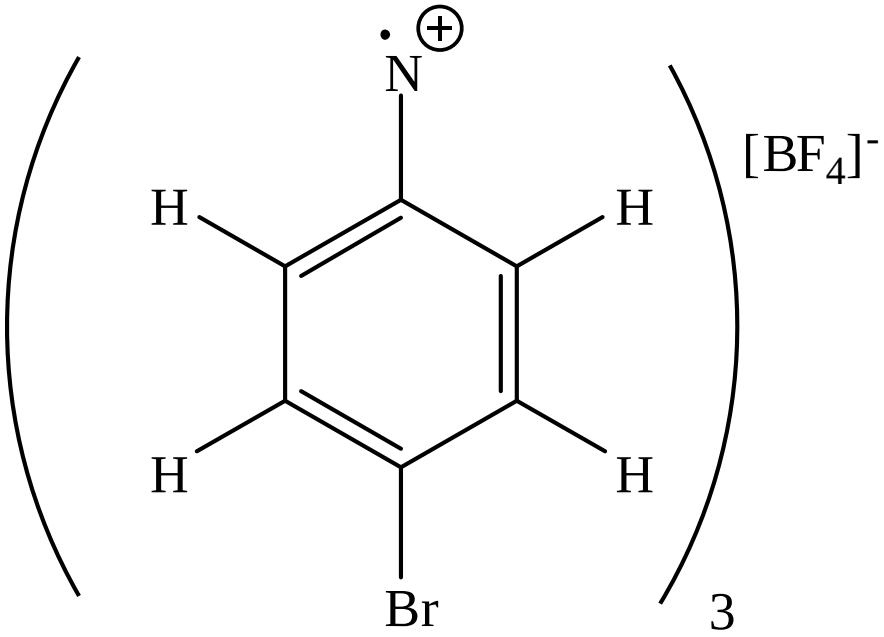

(**a**)

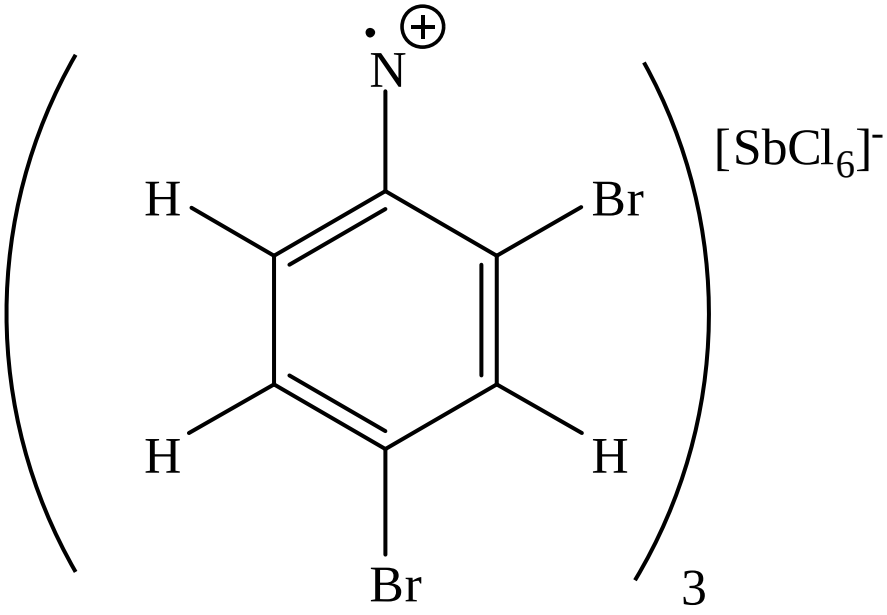

(**b**)

Figure 60. The oxidizing agents tris(p-bromophenyl)amminium tetraflouroborate (**a**) and tris(2,4-dibromophenyl)amminium hexachloroantimonate (**b**).

Upon oxidation of the donor, structural changes in the molecule occur, including the adoption of a planar conformation followed by a lengthening of the central C=C bond and a shortening of the C-S bonds in the central TTF core. These bond distances are the most susceptible to the oxidation state of the donor and have been used by Coppens and coworkers to develop an empirical relationship that can be used to calculate the overall oxidation state of the donor molecule. Upon inspection of these bond distances, it can be ascertained that in all cases the donor molecules have been successfully oxidized to the +1 radical cation state based on the Coppens' formula. With the presence of planar, radical cation salts of TTF-like molecules, another intermolecular interaction occurs in the solid state. Planar, radical cations, such as TTF, have a strong tendency to form dimers in the solid-state via a two-electron bond through direct overlap of their singly-occupied molecular orbitals (SOMOs). An important characteristic of the tetrathiafulvalene molecule is the shape of its SOMO, which is an orbital whose π-character covers the central C_2S_4 motif. The approach of two such radical cations into a face-to-face eclipsed arrangement corresponds to the formation of σ bonding and σ* antibonding combinations of the two SOMOs.[95] With an electron occupancy of two, a strong σ bond between the radicals is formed and the dyadic, dicationic entity becomes fully diamagnetic. X-ray crystallographic and refinement data and the calculated valences for the chalcofulvalenium radical cations in **1-4** are listed in Tables 40 and 41. Selected bond distances are shown in Tables 42-45.

Table 40. X-ray crystallographic information for TTF salts **1-4**.

Compound	(*o*-Me_2TTF)[BF_4] (**1**)	(TMTTF)[BF_4] (**2**)	(TTF)[$SbCl_6$] (**3**)	[TTF($SCH_2CH_2CN)_4$][$SbCl_6$] (**4**)
Formula	$C_8S_4H_8BF_4$	$C_{10}S_4H_{12}BF_4$	$C_6S_4H_4SbCl_6$	$C_{18}S_8H_{16}N_4SbCl_6$
formula weight	319.21	343.23	538.83	879.35
Space group	$P2_1/n$	C2/m	P4/mbm	$P2_1/n$
a, Å	7.010(1)	20.070(4)	11.784(2)	11.452(2)
b, Å	10.902(2)	10.160(2)	11.784(2)	7.323(2)
c, Å	16.164(3)	8.071(2)	11.554(2)	19.112(4)
α, deg	90	90	90	90
β, deg	97.64(3)	100.61(3)	90	102.94(3)
γ, deg	90	90	90	90
volume, $Å^3$	1224.32	1617.62	1604.52	1562.00
Z	4	2	2	2
μ, mm^{-1}	0.80	0.33	2.42	2.94
Temp.	110(2)	110(2)	110(2)	110(2)
Reflns. collected	2777	1958	662	3588
Reflns. I>2σ	2265	1749	599	3264
Parameters	156	115	39	169
Restraints	0	0	0	0
R1[a]	0.0778	0.0653	0.0495	0.0333
wR2[b]	0.1824	0.1896	0.1747	0.0862
Goodness-of-fit[c]	1.060	1.072	0.801	0.573

[a] $R1 = \sum||F_o| - |F_c||/\sum|F_o|$. [b] $wR2 = [\sum [w(F_o^2-F_c^2)^2]/ \sum [w(F_o^2)^2]^{1/2}$

[c] Goodness-of-fit = $[\sum w(|F_o|-|F_c|)^2/(N_{obs}-N_{parameter})]^{1/2}$

Table 41. Comparison of the estimated charges of the donor molecules in salts **1-4**.

salt	**molecule**	**A**[a]	**B**[b]	**Q**[c]
(*o*-Me_2TTF)[BF_4] (**1**)	A	1.386(4) Å	1.721(2) Å	+0.95
(TMTTF)[BF4] (**2**)	A	1.403(3) Å	1.717(5) Å	+1.22
$(TTF)_2[SbCl_6]$ (**3**)	A	1.359(6) Å	1.750(3) Å	+0.28
	B	1.394(7) Å	1.730(4) Å	+0.96
[TTF($SCH_2CH_2CN)_4$][$SbCl_6$] (**4**)	A	1.391(8) Å	1.721(3)Å	+1.06

[a] Central C=C bond distance.

[b] Mean central C-S bond distance.

[c] Q = charge estimated with the formula Q = -17.92 + 23.43*(A/B) from Ref. 94.

Table 42. Bond distances for (*o*-Me_2TTF)][BF_4] (**1**) in Å.

S(1)-C(1)	1.727(3)
S(1)-C(3)	1.722(5)
S(2)-C(2)	1.730(2)
S(2)-C(3)	1.725(4)
S(3)-C(4)	1.720(4)
S(3)-C(5)	1.731(3)
S(4)-C(4)	1.718(3)
S(4)-C(6)	1.732(2)
B(1)-F(1)	1.401(4)
B(1)-F(2)	1.344(4)
B(1)-F(3)	1.323(3)
B(1)-F(4)	1.267(5)
C(1)-C(2)	1.335(4)
C(3)-C(4)	1.386(2)
C(5)-C(6)	1.354(4)
C(5)-C(7)	1.498(3)
C(6)-C(8)	1.505(2)

Table 43. Bond distances for (TMTTF)][BF_4] (**2**) in Å.

S(1)-C(2)	1.749(3)
S(1)-C(3)	1.719(3)
S(2)-C(4)	1.714(4)
S(2)-C(5)	1.731(3)
B(1)-F(1)	1.375(3)
B(1)-F(2)	1.392(4)
B(1)-F(3)	1.389(2)
C(1)-C(2)	1.502(4)
C(3)-C(4)	1.403(6)
C(5)-C(6)	1.501(3)

Table 44. Bond distances for $(TTF)_2[SbCl_6]$ (**3**) in Å.

S(1)-C(1)	1.730(3)
S(1)-C(2)	1.728(5)
S(2)-C(3)	1.740(3)
S(2)-C(4)	1.750(4)
Sb(1)-Cl(1)	2.652(4)
Sb(1)-Cl(2)	2.664(3)
C(1)-C(1a)	1.394(2)
C(4)-C(4a)	1.359(6)

Table 45. Bond distances for $[TTF(SCH_2CH_2CN)_4][SbCl_6]$ (**4**) Å.

S(1)-C(1)	1.724(5)
S(1)-C(2)	1.735(3)
S(2)-C(1)	1.718(2)
S(2)-C(3)	1.745(4)
S(3)-C(2)	1.748(2)
S(3)-C(6)	1.824(8)
S(4)-C(3)	1.754(3)
S(4)-C(9)	1.826(4)
N(1)-C(4)	1.141(2)
N(2)-C(7)	1.142(7)
Sb(1)-Cl(1)	2.382(6)
Sb(1)-Cl(2)	2.355(4)
Sb(1)-Cl(3)	2.362(5)
C(1)-C(1a)	1.391(5)
C(2)-C(3)	1.362(4)
C(4)-C(5)	1.474(5)
C(5)-C(6)	1.538(5)
C(7)-C(8)	1.479(4)
C(8)-C(9)	1.537(6)

This interaction dominates the solid-state structures of **1-3**, in which the *o*-Me_2TTF, TMTTF, and TTF donors form eclipsed dimers indicative of strong σ bond formation. The packing motif in the TTF structure shows a solid-state arrangement with a set of dimers surrounded by a plane of orthogonal dimers. This arrangement is similar to the so-called κ-phase; this phase has produced the largest number of organic superconductors in the TTF family, as well as those with the highest T_c.[101] Despite the structural similarity to the superconducting systems, the arrangement in **3** forms a non-conducting, non-stoichiometric diamagnetic dimeric system. The crystal structure of **4** does not show this strong preference for eclipsed dimer formation, as the steric bulk of the nitrile-protecting groups on **4** prevents close contacts between the radical cations. As a consequence of the formation of strong, eclipsed dimers in the solid-state, high levels of charge localization can occur, leading to low conductivity. This same scenario was observed previously for the $(TTF)_3[BF_4]_2$ structure, in which the formation of eclipsed dimers separated by neutral donor molecules yielded a system exhibiting low conductivity. The solid-state structures for the chalcofulvalenium salts as well as the expanded unit cells illustrating the σ-type dimers in **1** and **2**, the pseudo-κ phase for **3**, and the steric bulk in **4** are shown in Figures 61-68.

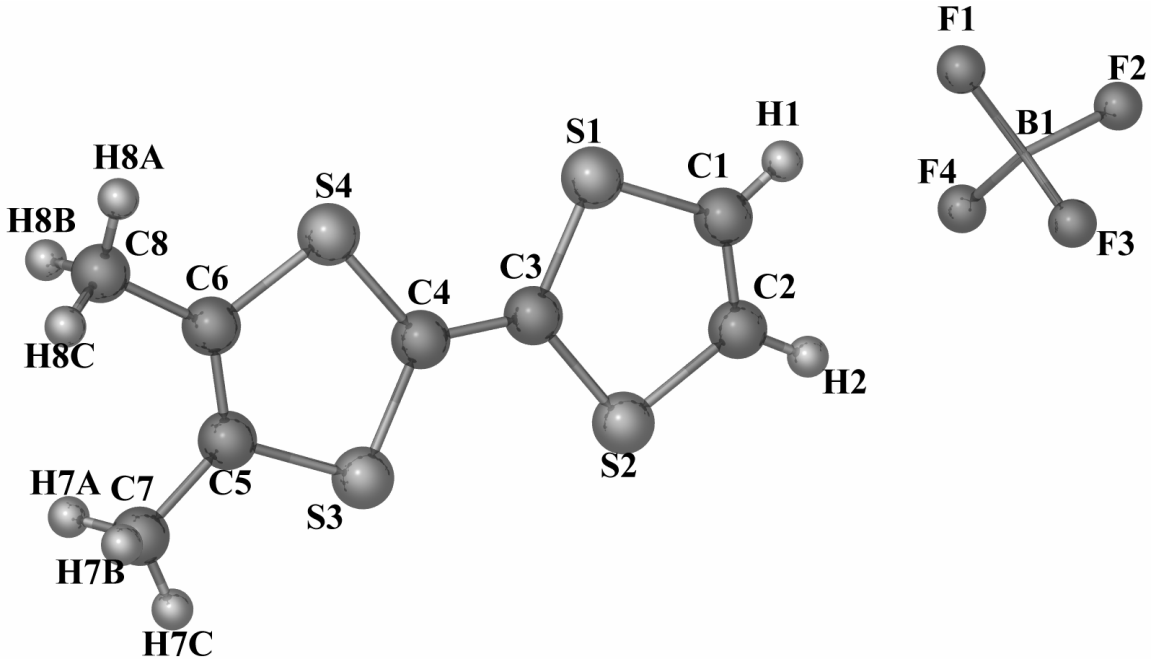

Figure 61. Formula unit of (*o*-Me_2TTF)[BF_4] (**1**).

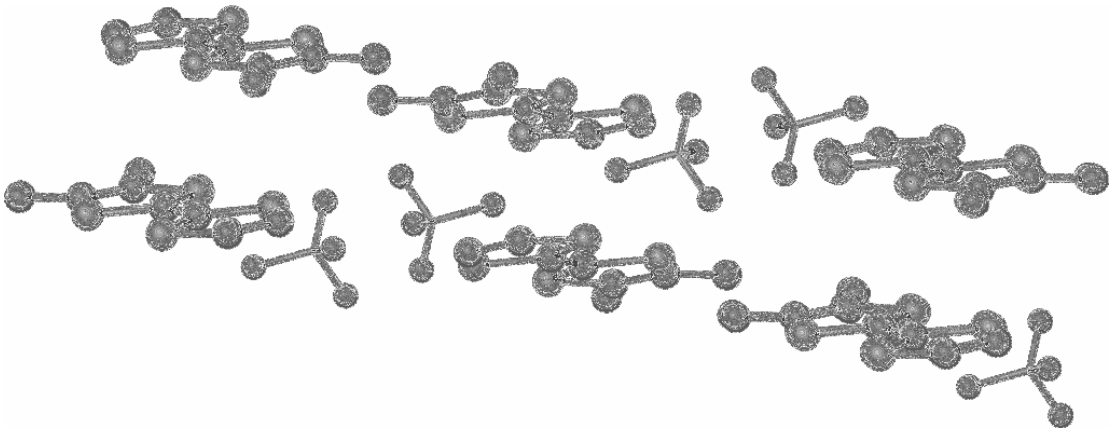

(**a**)

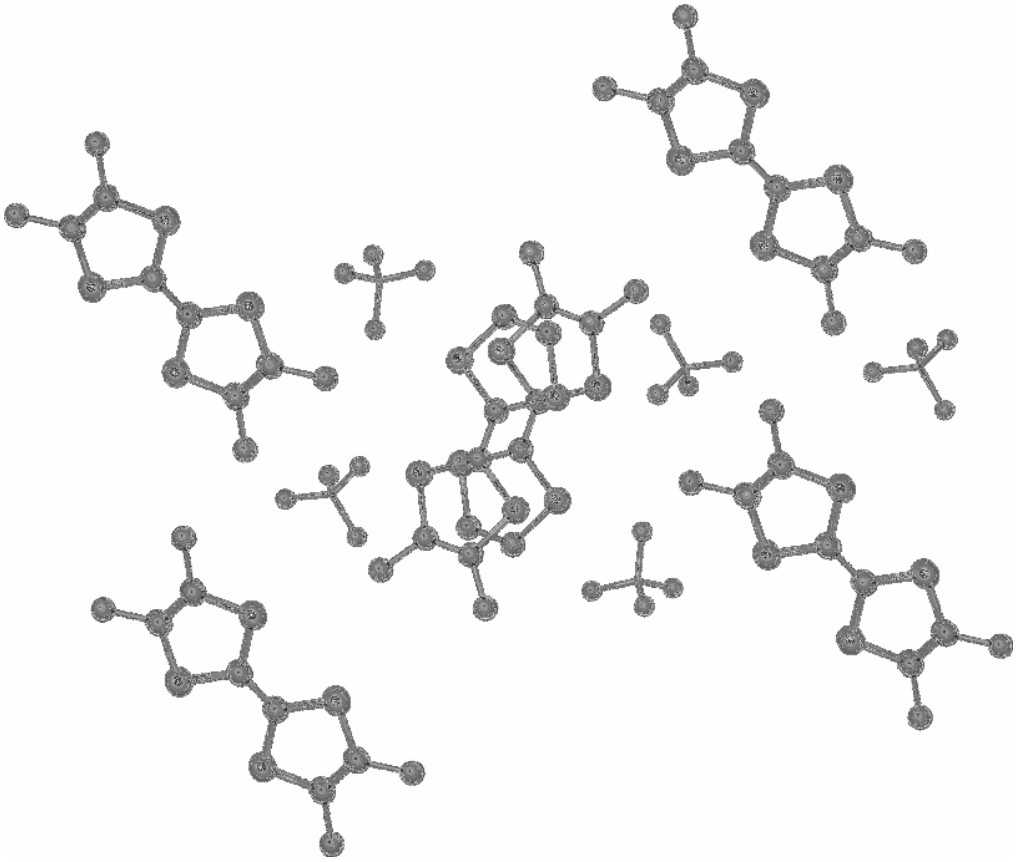

(**b**)

Figure 62. Expanded unit cell for (*o*-Me_2TTF)[BF_4] (**1**) illustrating the formation of eclipsed dimers in the solid state from the side (**a**) and top (**b**). Hydrogen atoms have been omitted for the sake of clarity.

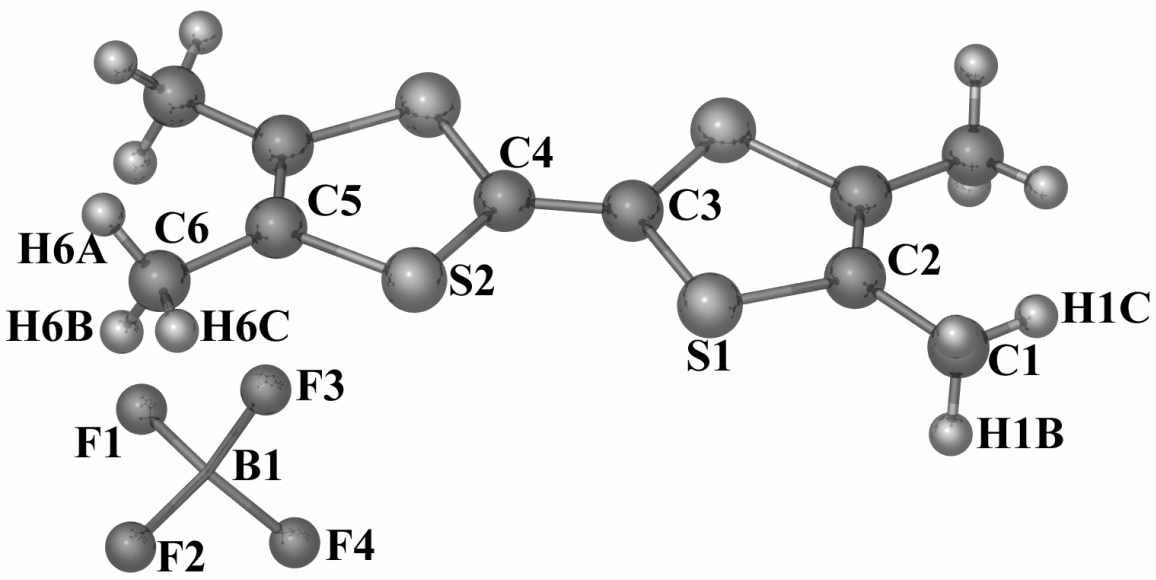

Figure 63. Formula unit of (TMTTF)[BF_4] (**2**).

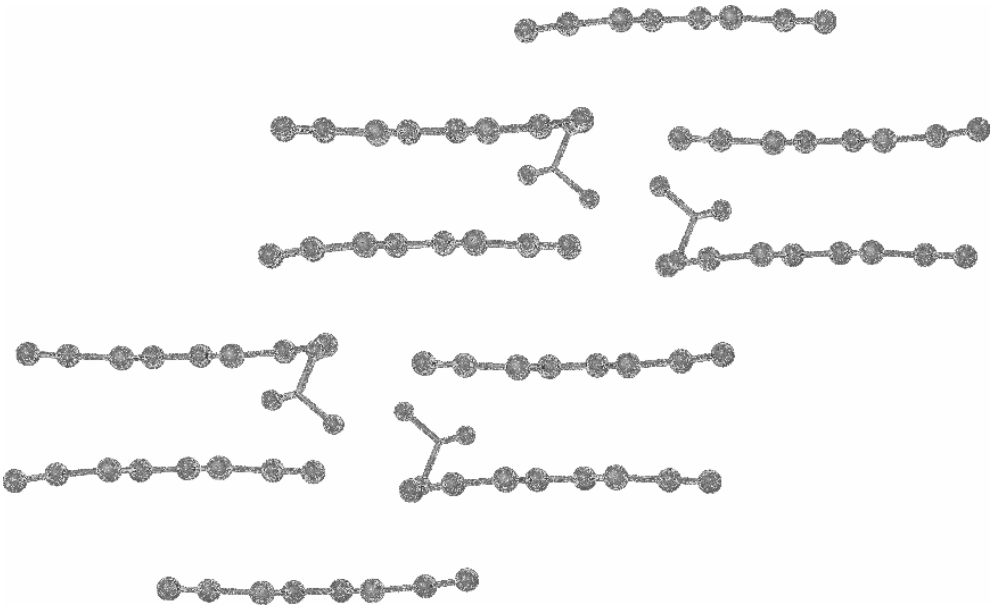

(**a**)

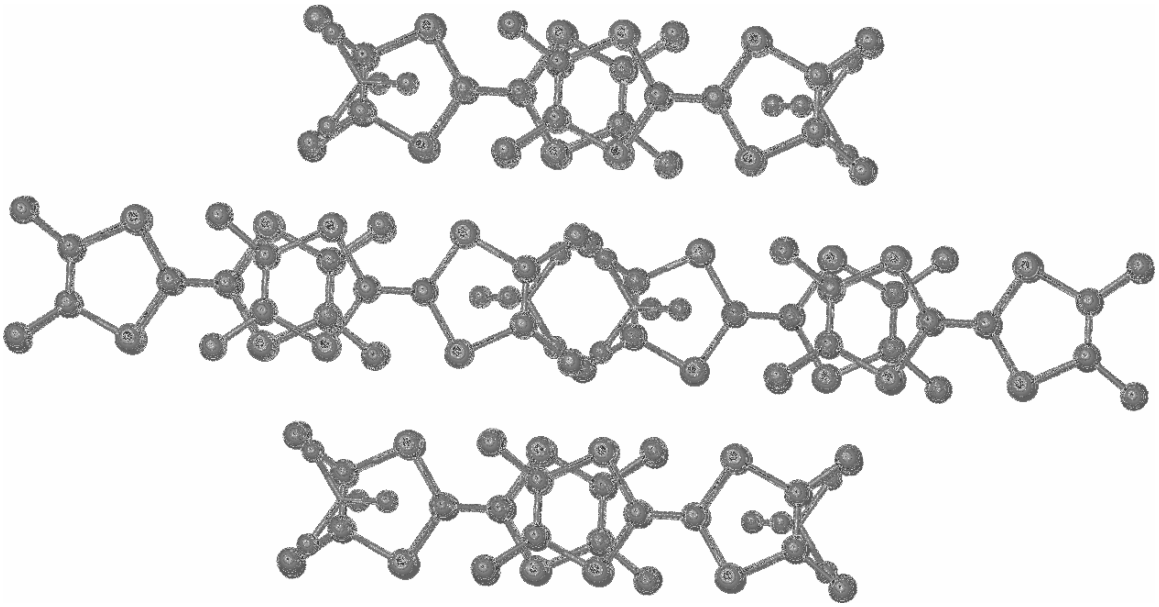

(**b**)

Figure 64. Expanded unit cell for (TMTTF)[BF_4] (**2**) illustrating the formation of eclipsed dimers in the solid state from the side (**a**) and top (**b**). Hydrogen atoms have been omitted for the sake of clarity.

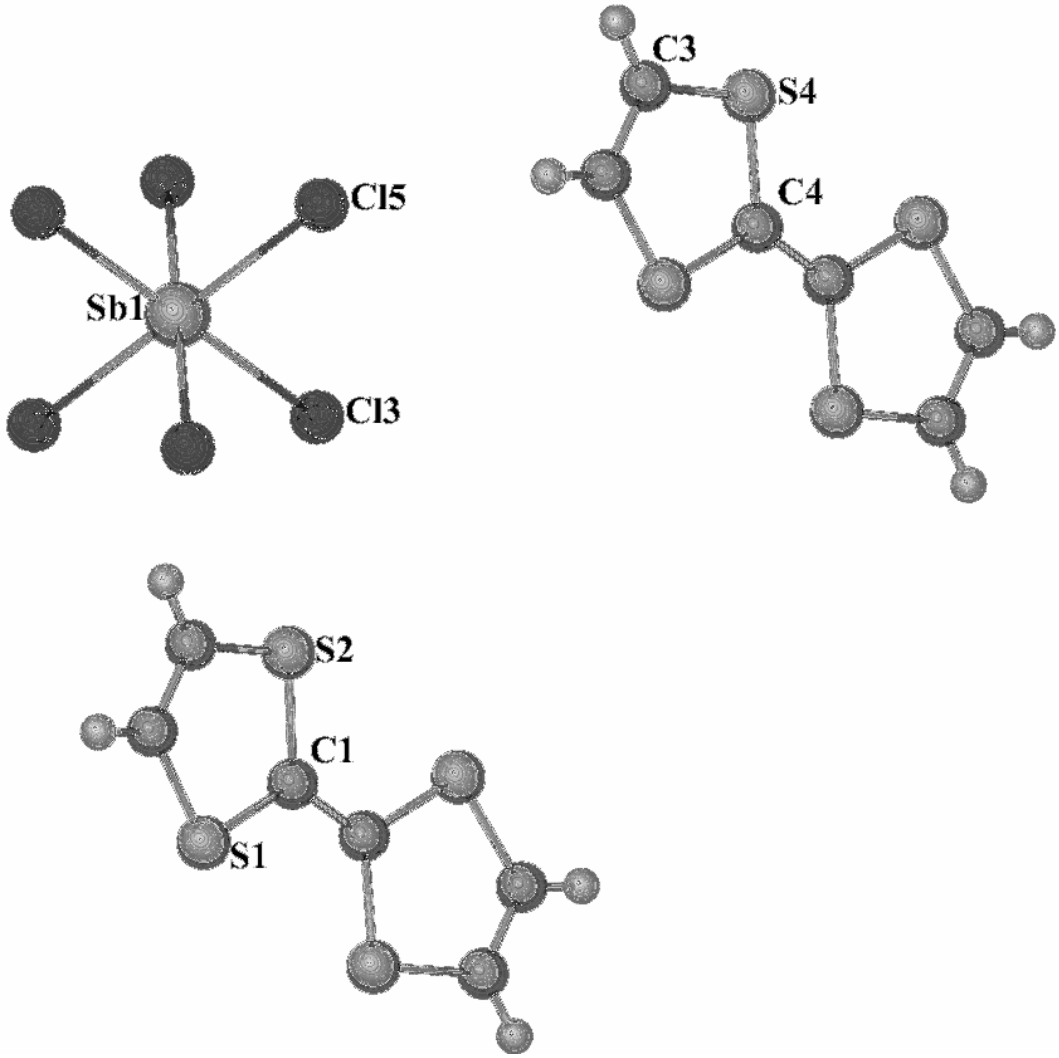

Figure 65. Formula unit of $(TTF)_2[SbCl_6]$ (**3**).

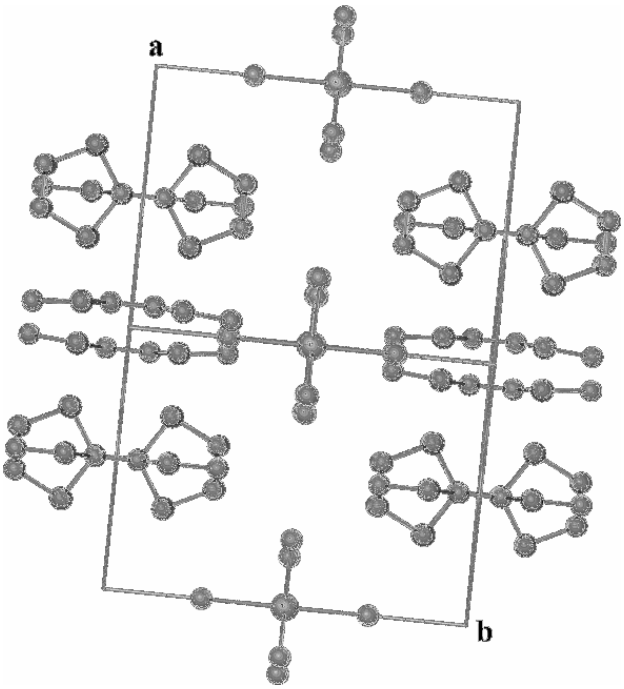

(**a**)

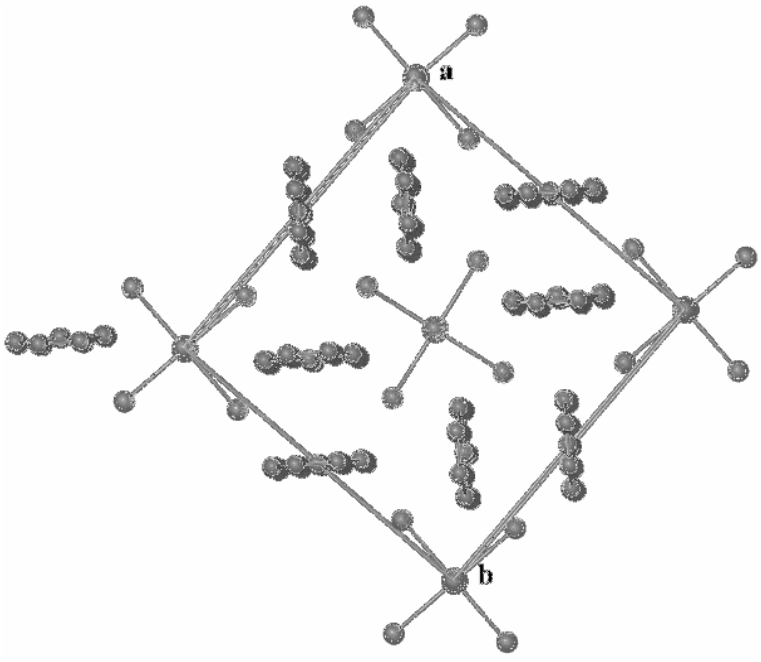

(**b**)

Figure 66. Expanded unit cell for $(TTF)_2[SbCl_6]$ (**3**) illustrating the formation of eclipsed dimers and the pseudo-κ phase in the solid state from the top (**a**) and side (**b**). Hydrogen atoms have been omitted for the sake of clarity.

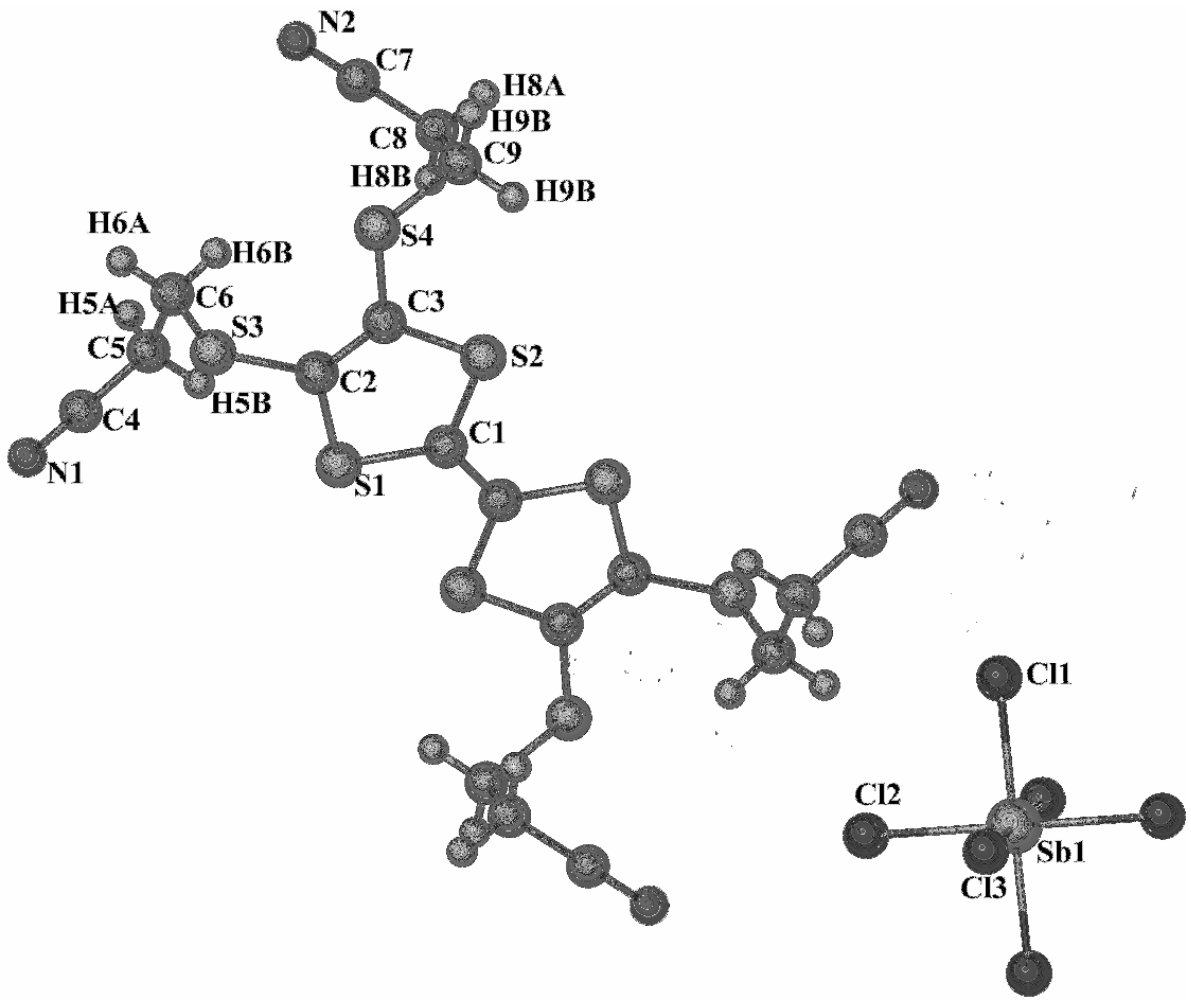

Figure 67. Formula unit of $[TTF(SCH_2CH_2CN)_4][SbCl_6]$ (**4**).

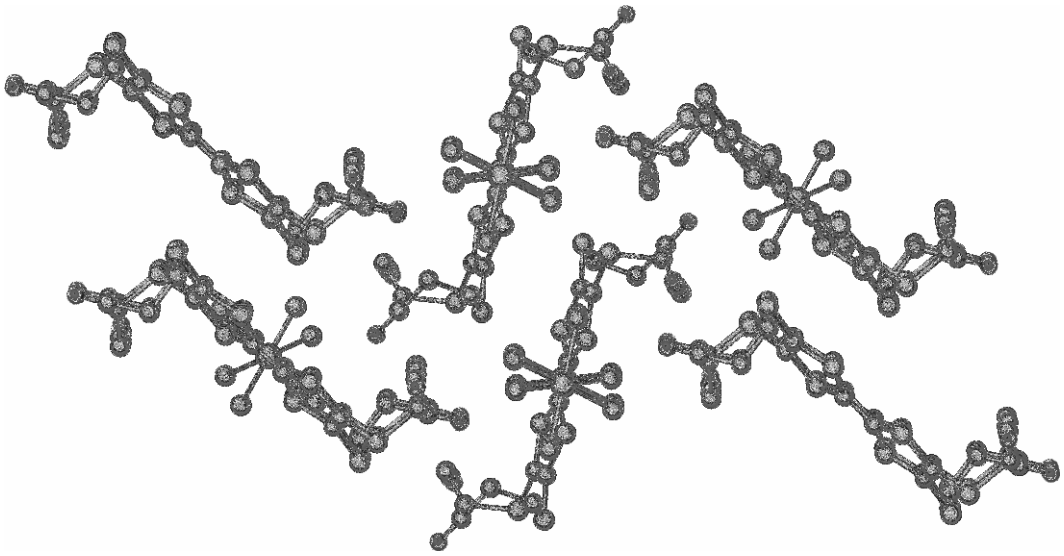

(**a**)

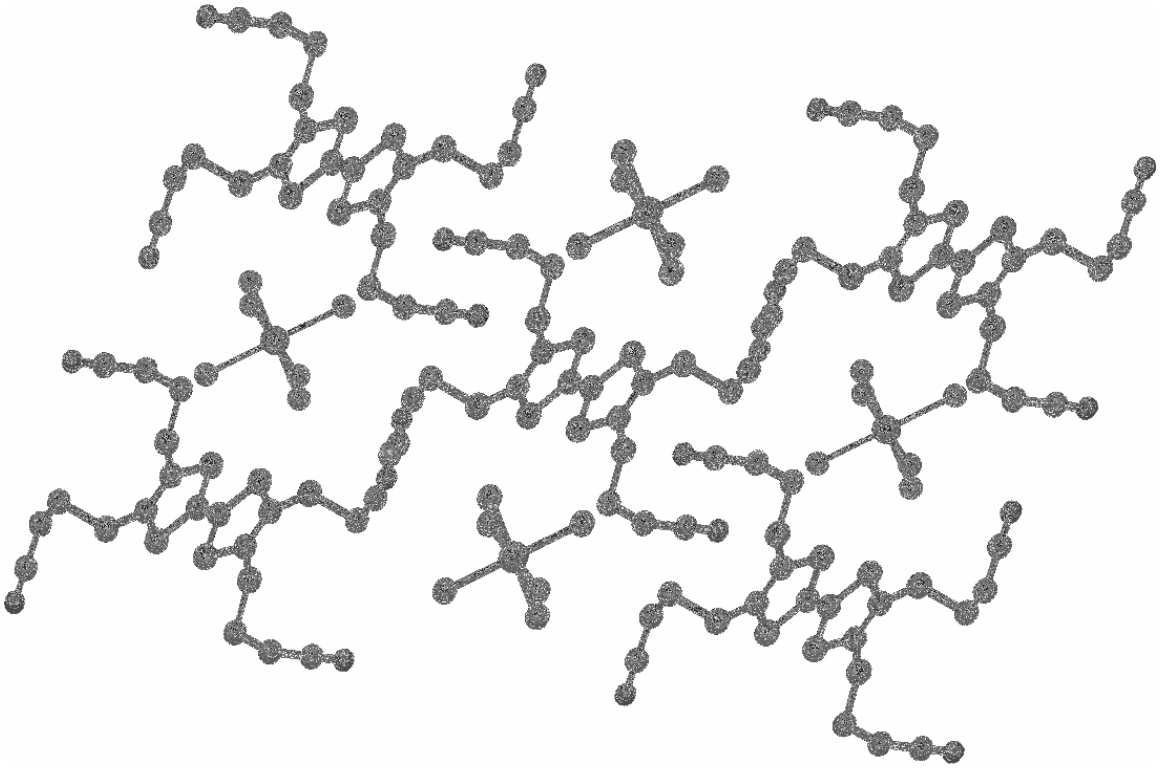

(**b**)

Figure 68. Expanded unit cell of $[TTF(SCH_2CH_2CN)_4][SbCl_6]$ (**4**) illustrating the steric bulk of the nitrile-protecting groups which prevents the formation of eclipsed dimers in the solid-state from the side (**a**) and top (**b**). Hydrogen atoms have been omitted for the sake of clarity.

Spectroscopic Analysis

Electronic Spectral Studies. UV-visible spectral studies were performed on the new compounds as well as the neutral donor molecules. The spectra for the neutral donors are dominated by shoulders between 400 and 430 nm with no features located at lower energies. The spectra for the salts **1-4** donor reveal low energy bands between 600 and 650 nm. These absorptions are similar to those reported by Hünig and coworkers who obtained the radical cation form of TTF by using $Pb(OAc)_4$ as an oxidizing agent.[103] High resolution spectra performed by Torrance and coworkers in CH_3CN revealed resolved peaks and shoulders between 600 and 650 nm. which were assigned to the four lowest symmetry-allowed transitions of the radical cation: $b_{2g} \rightarrow b_{1u}$, $b_{1u} \rightarrow b_{3g}$, $b_{1u} \rightarrow b_{2g}$, and $b_{3g} \rightarrow b_{1u}$.[104] Despite numerous attempts to resolve the low energy bands obtained for the new radical cation salts into their constituent transitions, the individual bands could not be fully identified.

ESI-Mass Spectrometry. The salts of the oxidized donors were investigated by electrospray ionization (ESI) mass spectrometry. For all of the salts, studies were conducted in both the positive and negative modes but they yielded different results depending on the identity of the donor cation. For salt **1**, the spectra showed peaks for the $[salt - BF_4]^+$ (m/z = 232) with no corresponding peak in the negative mode for the $[BF_4]^-$ (m/z = 87). Salt **4** showed more promising results in the positive and negative modes by exhibiting peaks representing $[salt - SbCl_6 - 6H]^+$ (m/z = 543) and $[SbCl_6]^-$ (m/z = 330) respectively. Similar mass spectroscopic analyses were carried out for salts

2 and **3**, but the results did not show any mass peaks indicative of the oxidized donors or their corresponding anions.

Conclusions

Four salts of oxidized TTF derivatives were prepared by reacting the donors with the oxidizing agents tris(*p*-bromophenyl)amminium tetraflouroborate or tris(2,4-dibromophenyl)amminium hexachloroantimonate in CH_2Cl_2. The compounds were characterized by X-ray crystallography, UV-vis-NIR spectroscopy, and ESI-mass spectrometry. The most convincing results for the existence of the monocationic states of the donor molecules were observed from the results of X-ray crystallography and UV-vis spectroscopy. According to the crystallographically determined bond distances, the donor molecules are present in the salts in their radical cation forms. This fact is further confirmed through the use of UV-vis-NIR spectroscopy where low energy bands provide additional evidence for the existence of TTF radical cations. Work is currently underway in order to prepare the salts on a larger scale so that metathesis reactions to prepare new materials can be carried out.

CHAPTER IV

PREPARATION OF NEW ORGANIC TTF-ACCEPTOR COMPLEXES

Introduction

Charge-transfer salts and radical salts containing oxidized species of TTF and its derivatives represent the most numerous and important family of molecular conductors and superconductors, with many examples of molecular metals and superconductors having been reported. Most of the successful examples derive from the radical salt approach, where the overall cationic charge of the oxidized TTF radical cations is counter-balanced by inorganic anions, "innocent" or "electroactive", which represents a successful approach toward multifunctional conductors. In the case of charge transfer salts, a pure organic approach is possible. As mentioned in earlier chapters, the most studied example is that of the 1:1 organic charge complex TTF-TCNQ, which has been the subject of intense research since its discovery in the early 1970s as it was the first example of an organic system that displayed metallic conductivity (500 $S \cdot cm^{-1}$ at 66 K) upon mixing acetonitrile solutions of the neutral molecules.[1] The metallic conductivity occurs as a consequence of two determining factors. The first characteristic is the spontaneous electron transfer which occurred by mixing donors and acceptors of nearly equivalent oxidation and reduction potentials. As a consequence of their similarity in redox potentials, a partial electron transfer occurred between the TTF donor and the TCNQ acceptor which lead to the formation of mixed-valence states for the constituent molecules. The solid-state packing of this material is also very critical as the segregated

stacking motif leads to maximum molecular orbital overlap and the formation of a pathway by which diffuse electron density could be transferred in a facile manner.[2] The necessity of having diffuse electron density being transferred along segregated stacks of partially-oxidized chalcofulvalene donors and its connection to high levels of conductivity in materials is a paradigm in this area of materials chemistry.

In the same vein, other organic acceptors have been systematically investigated, but few detailed studies have been reported, especially for organic acceptors other than nitrile-containing species. The fluorenone family of acceptors (Figure 69) has recently been explored as organic acceptors in the formation of charge-transfer complexes.[105-107] Interest in this area has been heightened by a few examples such as the combination of cyano-derivatives with BEDO-TTF to yield organic metals.[108] Also, nitro-containing derivatives have been combined with trimeric clusters of Au(I) to yield interesting spectroscopic properties.[109] In 1989, Toscano and coworkers prepared a charge-transfer complex between TTF and the organic acceptor 2,7-dinitro-9-fluorenone (DNF) (Figure 70).[48] The properties of this material were later described by the same authors in 1993 who reported that it is an insulator.[49] This can be explained on the basis of the large disparity between their redox potentials, ($E_{1/2}$(TTF) = +0.23 V and $E_{1/2}$(DNF) = -0.68 V), which is expected to lead to a very small effective charge transfer, with both molecules remaining essentially neutral.[49] Due to their electron-withdrawing nature, increasing the number of nitro groups enhances the electron accepting properties of the fluorenone derivatives.[50] Alteration in the reduction potential of the acceptor should have an effect on the electronic properties and packing of the constituent molecules in respective charge transfer salts.

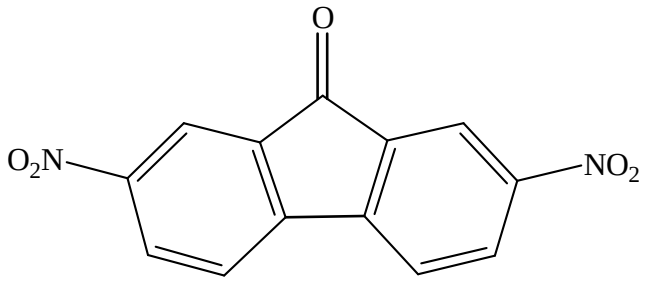

(a) 2,7-dinitro-9-flourenone (DNF) [$E_{1/2}$(red) = -0.68 V]

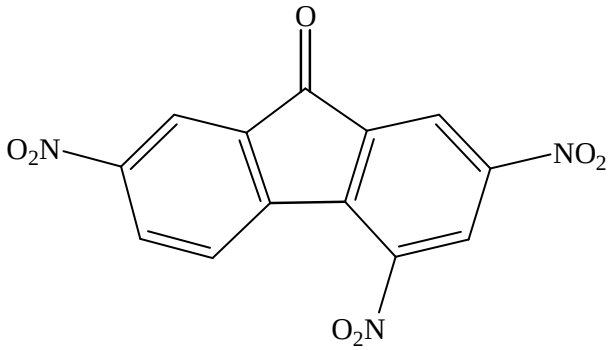

(b) 2,4,7-trinitro-9-flourenone (TRNF) [$E_{1/2}$(red) = -0.42V]

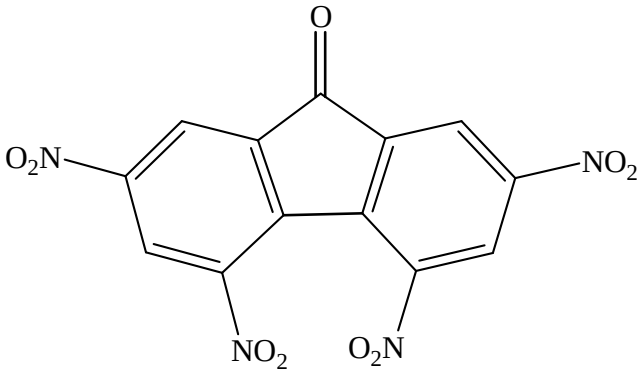

(c) 2,4,5,7-tetranitro-9-flourenone (TENF) [$E_{1/2}$(red) = +0.14V]

Figure 69. The nitroflourenone family of acceptors. The corresponding first reduction potentials for each acceptor are also listed.

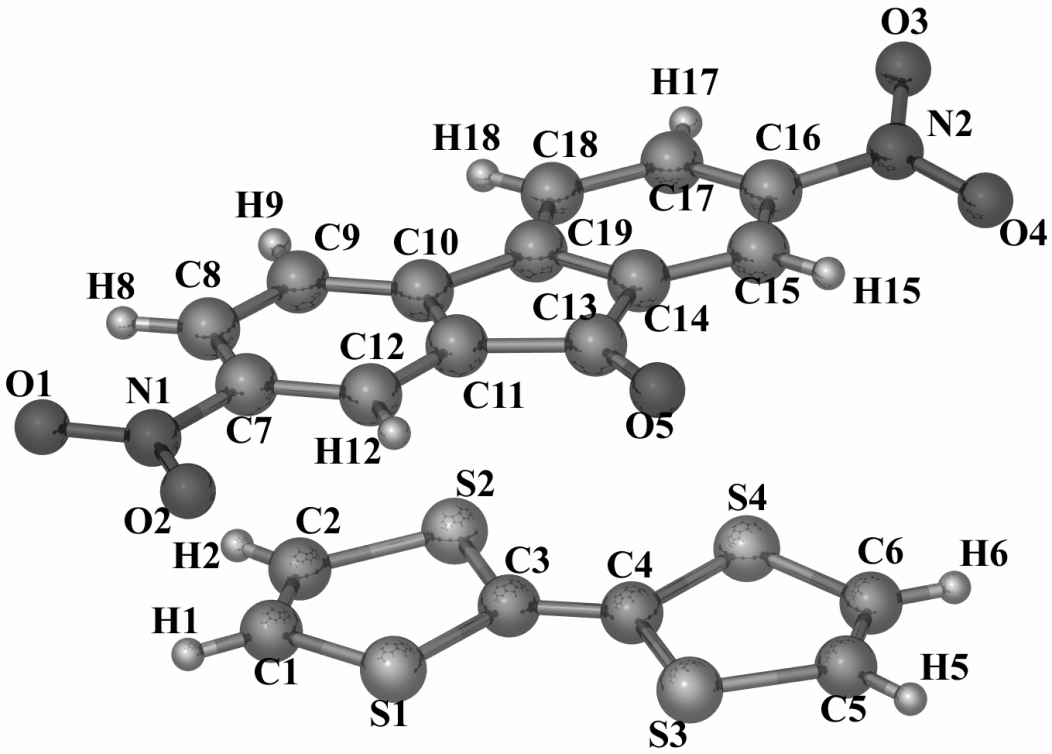

Figure 70. Crystal structure of the charge transfer complex (TTF)[DNF].

In an effort to further study the effect of different organic acceptors, we turned our attention to the organic acceptors HAT-$(CN)_6$ and TCNB. HAT-$(CN)_6$ has seen use as a building block in the preparation of molecule-based magnetic materials as probed by Dunbar and coworkers.[110] Much like TCNQ and its derivatives, the presence of cyanide groups on the triphenylene core could serve as an efficient mode to elucidate the presence of reduced organocyanide acceptors in either solution or solid-state media. Structural and spectroscopic data are available for reduced TCNQ and $TCNQF_4$ in the mono- and extremely air and moisture-sensitive dianionic states generated upon reduction with either one or two equivalents of the powerful reducing agent $(Cp^*)_2Co$.[111] To date, only

information from the cyanide stretching frequencies has offered any information about the reduced states of HAT-$(CN)_6$.[110]

In an effort to explore the ability of these acceptors to generate oxidized states of TTF and its derivatives, one equivalent of TTF, TMTTF and *o*-Me_2TTF donors were reacted with TRNF, TENF, and the organocyanide acceptors HAT-$(CN)_6$ and TCNB. This chapter outlines the preparation of charge-transfer complexes between TTF and some of its derivatives and a description of their properties.

Experimental Section

Preparation of Compounds

All solvents used were used as received. The acceptors TRNF and TENF were provided by Prof. Alan Balch and used without additional purification. The acceptor HAT-$(CN)_6$ was prepared according to literature procedures.[112] TTF was purchased from Aldrich and used without further purification. The donors TMTTF and *o*-Me_2TTF were provided by Prof. Marc Fourmigué.[95] All manipulations were performed in air. The adducts were prepared by reacting one equivalent of the donor molecules with a stoichiometric amount of the nitrofluorenone or organocyanide acceptors. For the preparation of **2-7**, the mixing of concentrated solutions of the donor and acceptor molecules did not lead to the formation of dark green solutions indicative of oxidized TTF donor molecules. The mixing of solutions of TRNF and TTF during the preparation of **1**, showed the formation of a slight dark green color indicating a slight degree of TTF oxidation.

(TTF)[TENF] (**1**)**.** An intensely colored yellow solution of TTF (0.022g, 1.08 x 10^{-4} mol) in a minimum of CH_3CN was added without stirring to a pale yellow solution of TENF (0.038g, 1.046 x 10^{-4} mol) in a minimum of warm CH_3CN. Upon mixing, the solution became slight green in color. Black needle-like crystals of (TTF)[TNNF] (**1**) were harvested from the mother liquor after a period of a couple of ~5 days; yield 0.042g (71%).

(TTF)[TRNF] (**2**)**.** An intensely colored yellow solution of TTF (0.024g, 1.17 x 10^{-4} mol) in a minimum of CH_3CN was added without stirring to a pale yellow solution of TRNF (0.037g, 1.17 x 10^{-4} mol) in a minimum of warm CH_3CN. Upon mixing, the solution showed no change in color. Black block-like crystals of (TTF)[TRNF] (**2**) were harvested from the mother liquor after a period of a couple of ~5 days; yield 0.035g (57%).

(TMTTF)[TRNF] (**3**)**.** An intensely colored yellow solution of TMTTF (0.021g, 8.08 x 10^{-5} mol) in a minimum of CH_2Cl_2 was added without stirring to a pale yellow solution of TRNF (0.025g, 6.67 x 10^{-5} mol) in a minimum of warm CH_3CN. Upon mixing, the solution showed no change in color. Black needle-like crystals of (TMTTF)[TRNF] (**3**) were harvested from the mother liquor after overnight evaporation in air; yield 0.032g (69%).

(TTF)[HAT-$(CN)_6$]•2CH_3CN (**4•2CH_3CN**)**.** An intensely colored yellow solution of TTF (0.021g, 1.03 x 10^{-4} mol) in a minimum of CH_3CN was added without stirring to an

orange solution of HAT-$(CN)_6$ (0.040g, 1.04 x 10^{-4} mol) in a minimum of THF. Upon mixing, the color of the solution became slight brown in color. Brown crystals of (TTF)[HAT-$(CN)_6$]•$2CH_3CN$ (**4**) were harvested from the mother liquor after the period of a week which became a brown powder upon drying; yield 0.028g (47%).

(*o*-Me_2TTF)[HAT-$(CN)_6$] (**5**)**.** In an analogous manner to (**4•$2CH_3CN$**), a CH_2Cl_2 solution of *o*-Me_2TTF (0.024g, 1.03 x 10^{-4} mol) was combined with a THF solution of HAT-$(CN)_6$ (0.040g, 1.05 x 10^{-4} mol). After a period of ~2 weeks, small brown crystals had formed from the mother liquor after slow evaporation in air; yield 0.027g (42%).

(TTF)[TCNB] (**6**)**.** A CH_3CN solution of TTF (0.025g, 1.22 x 10^{-4} mol) was combined with a solution of TCNB (0.021g, 1.22 x 10^{-4} mol) dissolved in a minimum of warm CH_3CN. After a period of ~2 weeks, black block-like crystals formed from the mother liquor after slow evaporation in air; yield 0.029g (63%).

(*o*-Me_2TTF)[TCNB] (**7**)**.** In an analogous manner to (**6**), a CH_3CN solution of *o*-Me_2TTF (0.024g, 1.03 x 10^{-4} mol) was combined with a solution of TCNB (0.021g, 1.22 x 10^{-4} mol) dissolved in a minimum of warm CH_3CN. The solution was concentrated via slow evaporation in air over the period of one month and placed in a freezer at -10^{o}C which resulted in the overnight formation of black needle-like crystals; yield 0.029g (63%).

X-ray Crystallographic Details and Structure Solution

X-ray data for compounds **1**, **2**, and **3** were collected on a Bruker SMART CCD diffractometer at 110±2 K with graphite monochromated Mo-Kα (λ = 0.71073 Å) radiation. The structures for **6** and **7** were determined via data collected on a Bruker APEX II diffractometer at 110±2 K with graphite monochromated Mo-Kα (λ = 0.71073 Å) radiation. The structure for **4** was determined from data collected on a Bruker D8 GADDS system at 110±2K with graphite monochromated Cu-Kα (λ = 1.54178 Å) radiation. The data were corrected for Lorentz and polarization effects. The Bruker SAINT software package was used to integrate the frames and the data were corrected for absorption using the SADABS program.[86,87] Space groups were unambiguously assigned by analysis of symmetry and systematic absences determined by XPREP.[88] The structures were solved by direct methods by the use of the SHELXS-97 program in the Bruker SHELXTL v5.1 software package.[89,90] The final refinements were carried out with anisotropic thermal parameters for all non-hydrogen atoms. Figures for the crystallographic structures were generated using the XSEED program.[91] Crystals for all salts were grown in a similar manner, via slow evaporation from concentrated CH_3CN solutions or mixed CH_2Cl_2 or THF solutions with CH_3CN. All crystals were secured to a cryoloop using Dow Corning grease and transferred to the liquid nitrogen stream of the diffractometer. X-ray crystallographic and refinement data for **1-4**, **6**, and **7** are listed in Tables 46 and 47.

Table 46. X-ray crystallographic data for TTF adducts **1-3**.

Compound	[TTF][TENF] (**1**)	$[TTF]_3[TRNF]_2$ (**2**)	[TMTTF][TRNF] (**3**)
Formula	$C_{19}H_{12}N_4O_9S_4$	$C_{44}H_{22}N_6O_7S_{12}$	$C_{23}H_{17}N_3O_7S_4$
Formula Weight	568.59	1131.44	575.64
Space group	P-1	P-1	P-1
a , Å	7.030(2)	10.607(2)	7.490(2)
b , Å	11.040(2)	10.742(2)	10.030(2)
c , Å	13.690(3)	10.931(2)	16.294(3)
α, deg	92.20(3)	89.45(3)	97.46(3)
β, deg	91.80(3)	83.16(3)	91.85(3)
γ, deg	97.00(3)	75.31(3)	99.20(3)
V, $Å^3$	1093.6(4)	1195.9(4)	1196.3(4)
Z	2	2	2
μ, mm^{-1}	0.500	0.441	0.450
Reflns. collected	2910	3424	3389
Reflns. $I>2\sigma$	2060	2933	1711
R1 [a]	0.0347	0.0358	0.0937
wR2 [b]	0.1341	0.0839	0.2117
quality-of-fit[c]	0.837	1.044	0.950

Table 47. X-ray crystallographic data for (**4•2CH$_3$CN**), **6**, and **7**.

Compound	[TTF][HAT-$(CN)_6$]•$2CH_3CN$ (**4**•$2CH_3$**CN**)	[TTF][TCNB] (**6**)	[o-Me_2TTF][TCNB] (**7**)
Formula	$C_{28}H_{10}N_{14}$	$C_{16}H_6N_4S_4$	$C_{18}H_{10}N_4S_4$
formula weight	542.12	382.49	409.98
Space group	C2	$P2_1/c$	P-1
***a* , Å**	18.892(4)	7.295(2)	6.920(1)
***b* , Å**	7.277(2)	12.162(4)	7.928(2)
***c* , Å**	22.181(4)	9.070(3)	17.454(4)
α, deg	90	90	100.54(3)
β, deg	104.78(3)	94.610(3)	99.67(3)
γ, deg	90	90	97.32(3)
***V*, $Å^3$**	2948.7(1)	802.1(4)	915.6(4)
Z	6	1	2
μ, mm^{-1}	0.367	0.597	0.750
Reflns. collecte	1810	1930	4263
Reflns. $I>2\sigma$	1427	1828	3456
R1 [a]	0.0637	0.0256	0.0325
wR2 [b]	0.1416	0.0713	0.0925
quality-of-fit[c]	1.071	1.058	1.063

[a] $R1 = \sum||F_o| - |F_c||/\sum|F_o|$. [b] $wR2 = [\sum [w(F_o^2-F_c^2)^2]/ \sum [w(F_o^2)^2]]^{1/2}$

[c] Goodness-of-fit = $[\sum w(|F_o|-|F_c|)^2/(N_{obs}-N_{parameter})]^{1/2}$

Other Physical Measurements

IR spectra (1600-50 cm^{-1}) were recorded on a computer controlled Nicolet 750 FT-IR spectrophotometer equipped with a TGS/PE detector and silicon beam splitter at 2.0 or 4.0 cm-1 resolution. Magnetic measurements were performed on a Quantum Design SQUID, MPMS-XL magnetometer. Magnetic susceptibility measurements in the DC mode were carried out at an applied field of 0.1 T in the 2-300 K range.

Results and Discussion

*[TTF][TENF] (**1**) and [TTF][TRNF] (**2**)*

The syntheses for **1** and **2** were performed by combining an intense yellow CH_3CN solution of the neutral TTF donor with pale yellow CH_3CN solutions of the neutral nitrofluourenone acceptors in air without stirring. Upon adding the tetranitrofluorenone (TENF) acceptor to the TTF solution, a slight green color formed indicating the possible presence of TTF radical cations in solution. Addition of trinitrofluorenone (TRNF) to the TTF solution did not yield any detectable green color. The resulting mixed solutions were slowly evaporated in air to yield black needles of **1** and black blocks of **2** over the course of a week.

*[TMTTF][TRNF] (**3**)*

Adduct complex **3** was prepared by adding a pale yellow solution of trinitro-fluorenone in CH_3CN to an orange CH_2Cl_2 solution of TMTTF. The mixed solution was slowly evaporated in air, to yield black needles overnight.

*[TTF][HAT-$(CN)_6$]•$2CH_3CN$ (**4•2CH_3CN**)*

Intensely colored orange solutions of 1,4,5,8,9,12-hexaazatriphenylenehexacarbonitrile (HAT-$(CN)_6$) (Figure 71) in either CH_3CN or THF were combined with a yellow solution of TTF in air without mixing. Upon mixing, a pale brown colored solution ensued which slowly evaporated in air to yield brown needles of (**4•2CH_3CN**) after a period of two weeks.

*[o-Me_2TTF][HAT-$(CN)_6$] (**5**)*

Intensely colored orange solutions of 1,4,5,8,9,12-hexaazatriphenylenehexacarbonitrile (HAT-$(CN)_6$) in either CH_3CN or THF were combined with a yellow solution of TTF in air without mixing to yield a brown solution. Upon mixing, a slight brown color was observed for the solution. The solution was slowly evaporated in air, to yield small brown needles of **5** after a period of two weeks.

*[TTF][TCNB] (**6**) and [o-Me_2TTF][TCNB] (**7**)*

The syntheses of **6** and **7** were performed by combining intensely colored yellow solutions of TTF and *o*-Me_2TTF in CH_3CN with pale yellow solutions of 1,2,4,5-tetracyanobenzene (TCNB) (Figure 71) in CH_3CN in air without stirring. No apparent color change occurred upon mixing the solutions. The resulting yellow solution for **6** was slowly evaporated in air, yielding black blocks of the title compound after a period of two weeks. The resulting solution for **7** was allowed to slowly evaporate in air for one month followed by deposition in a freezer which resulted in the overnight formation of black needle-like crystals.

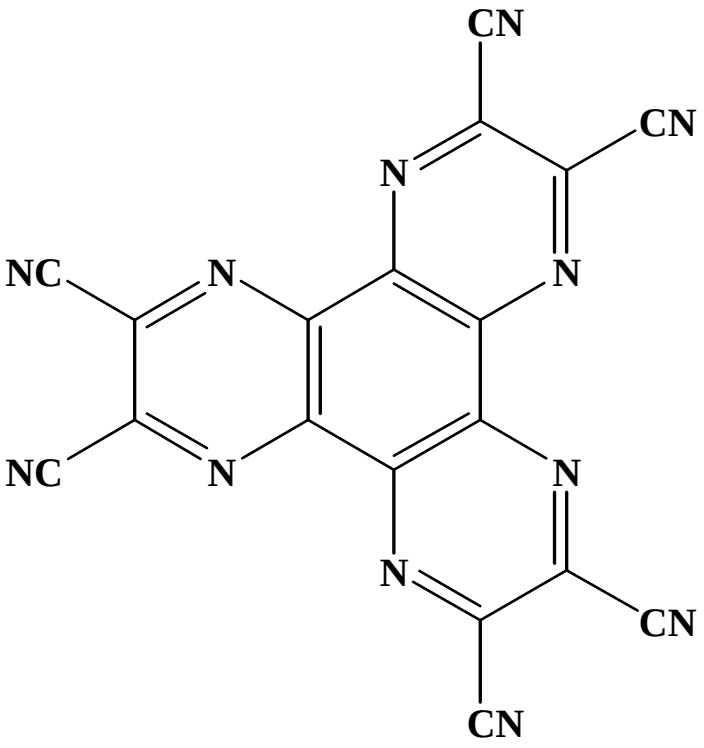

(**a**)

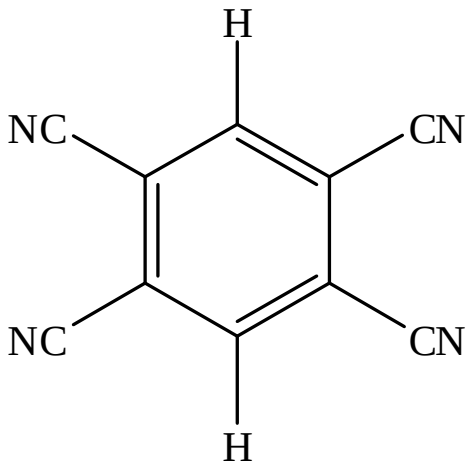

(**b**)

Figure 71. Schematic drawings of the organocyanide acceptors HAT-$(CN)_6$ (**a**) and TCNB (**b**).

Structures

Crystals of **1, 2,** (**4•2CH_3CN**)**, 6,** and **7** were grown by slow evaporation of concentrated CH_3CN solutions in air. Crystals of **3** were grown by slow evaporation of a mixed CH_2Cl_2/CH_3CN solution in air. In all cases, the interaction between donor and acceptor favors the formation of solids with strong intermolecular interactions. These strong intermolecular interactions also dictate the packing in the solid state, wherein, rather than segregated stacks, one observes an alternating integrated stacking of the molecular species. The strength of these and other intermolecular interactions determine the crystal structure of these materials. In most cases, the organic molecules appear with non-integer charge due to the presence of partial charge transfer as estimated from the TTF bonding distances which are very sensitive to its oxidation level. Compound **1** crystallizes in the space group *P-1* and the structure is dominated by 1:1 integrated stacks of donor and acceptor molecules along the *a*-axis forming a 1D chain in a pseudo-tetragonal packing arrangement. The TTF molecules display a slight distortion from planarity by an angle of 7°. From the C-C and C-S bond distances, a charge of +0.18 per TTF molecule can be estimated according to the Coppens method.[94] The nitrofluorenone molecule displays a torsion angle collinear with the axis that bisects the central five-membered ring resulting in a twisted conformation for the central while their constituent nitro groups deviate from planarity. A single nitro group is coplanar with each half of the molecule (torsion angle below 3°), while the second nitro group in each half differs from planarity by torsion angles of 25 and 30°. The solid-state structure of **1** and the packing of the donor and acceptor molecules in the crystal are shown in Figures 72 and 73.

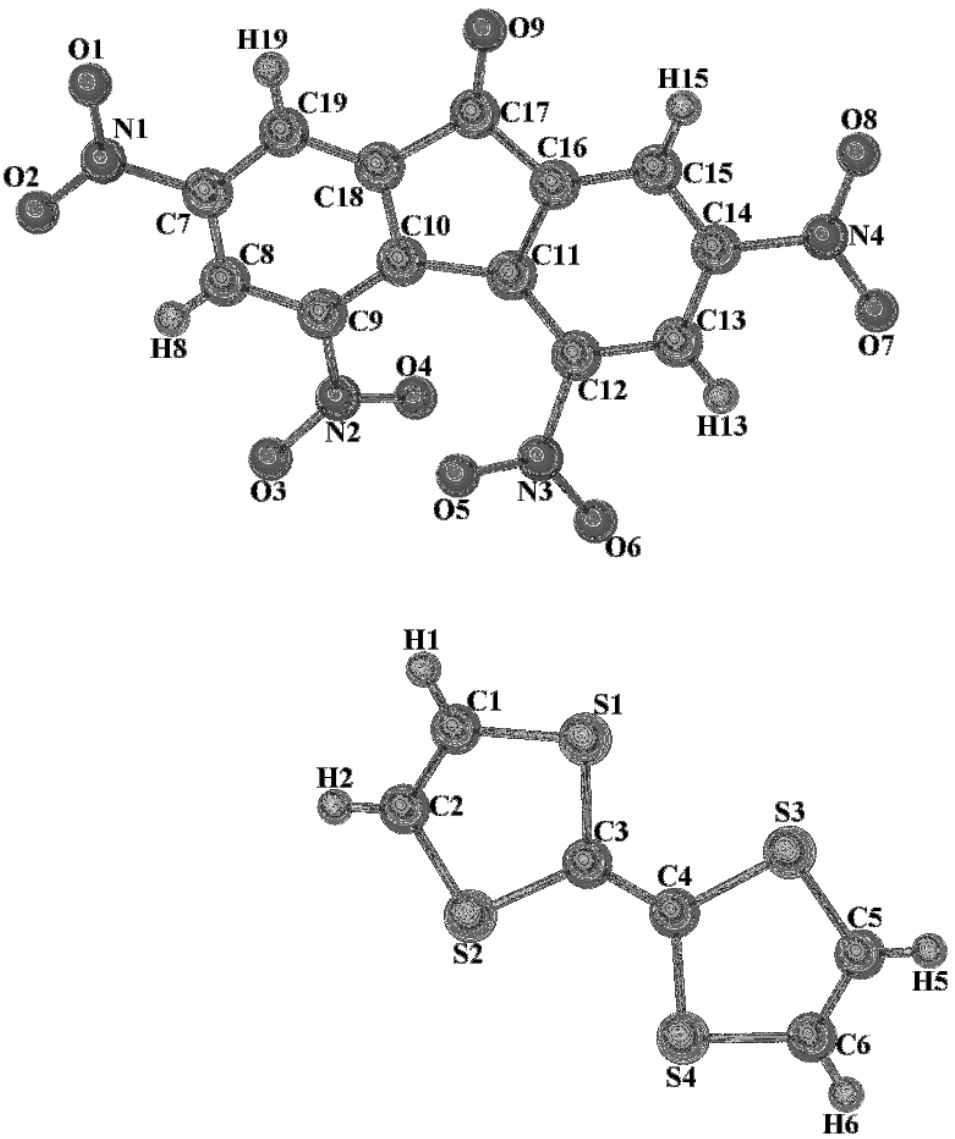

Figure 72. X-ray crystal structure of the [TTF][TENF] adduct (**1**).

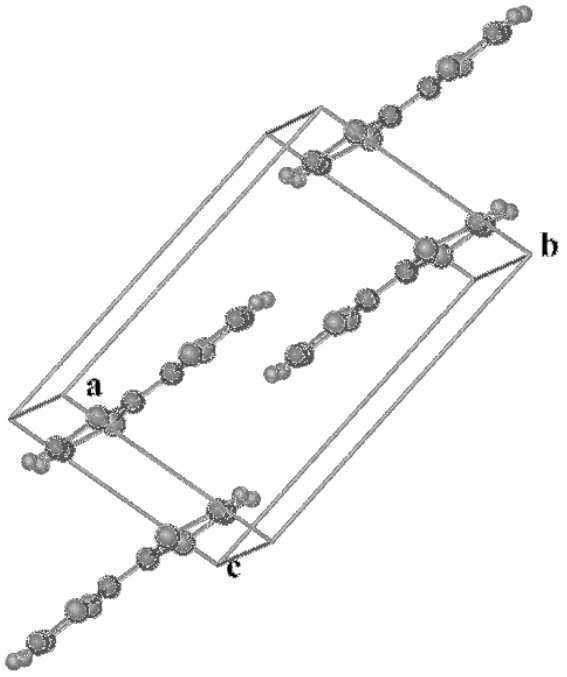

(**a**)

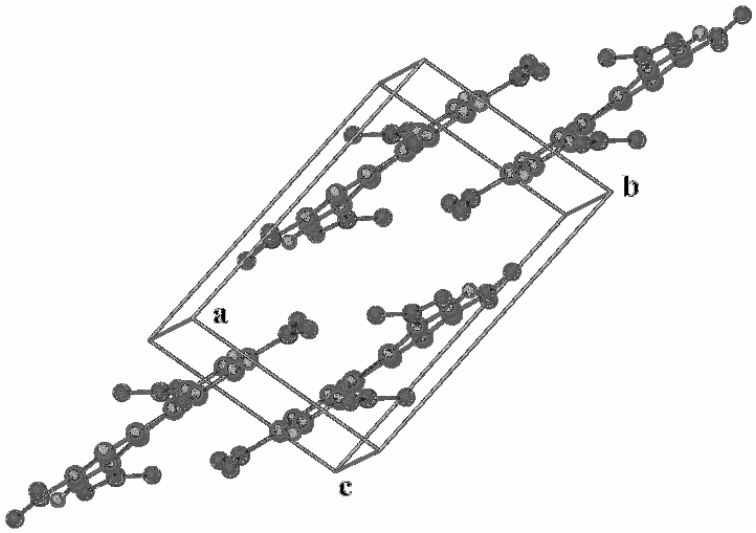

(**b**)

Figure 73. Packing arrangements of **1** illustrating the conformations of the TTF donors (**a**) and fluorenone cores of the TENF acceptor molecules (**b**).

Another interesting feature of the tetranitrofluorenone molecule is the bond length of the carbonyl group defined by C(12) and O(3) is 1.226 Å, whereas the neutral molecule shows a carbonyl bond distance of 1.205 Å. This increase in carbonyl bond distance could be indicative of electron donation from TTF to the carbonyl group of tetranitrofluorenone. There are no close interactions between chains, with all contacts being essentially the sum of the van der Waals radii. There is a weak interaction between adjacent chains between a nitro group and a sulfur atom (O(3)•••S(1) = 2.981(4) Å). Selected bond distances for **1** are shown in Table 48.

Compound **2** crystallizes in the triclinic space group *P-1*, and is characterized by 1D stacks and neutral TTF molecules in a 3:2 stoichiometry. The asymmetric unit contains a single trinitrofluroenone molecule and three half-molecules of TTF (A, B, and C). Two of the three crystallographically independent TTF molecules (A and B) form alternating stacks parallel to the [0 1 -1] direction on the *bc* plane, with a sequence •••A•••TRNF•••B••• TRNF•••. Molecule C appears in the interchain separation with the plane perpendicular to the chains. From the intermolecular bonding distance, there are two neutral TTF molecules (B and C) while molecule A has an estimated charge of +0.30.[94]

Table 48. Bond distances for [TTF][TENF] (**1**) in Å.

S(1)-C(1)	1.771(4)	O(9)-C(17)	1.225(4)
S(1)-C(3)	1.763(4)	C(1)-C(2)	1.350(5)
S(2)-C(2)	1.753(4)	C(3)-C(4)	1.374(5)
S(2)-C(3)	1.793(4)	C(5)-C(6)	1.340(6)
S(3)-C(4)	1.784(4)	C(7)-C(8)	1.388(6)
S(3)-C(5)	1.748(4)	C(7)-C(19)	1.400(6)
S(4)-C(4)	1.763(4)	C(8)-C(9)	1.406(5)
S(4)-C(6)	1.756(4)	C(9)-C(10)	1.415(5)
N(1)-O(1)	1.229(5)	C(10)-C(11)	1.516(5)
N(1)-O(2)	1.246(5)	C(10)-C(18)	1.424(5)
N(1)-C(7)	1.501(5)	C(11)-C(12)	1.411(5)
N(2)-O(3)	1.247(4)	C(11)-C(16)	1.421(5)
N(2)-O(4)	1.244(4)	C(12)-C(13)	1.400(5)
N(2)-C(9)	1.486(5)	C(13)-C(14)	1.397(5)
N(3)-O(5)	1.248(4)	C(14)-C(15)	1.385(5)
N(3)-O(6)	1.236(4)	C(15)-C(16)	1.406(5)
N(3)-C(12)	1.485(5)	C(16)-C(17)	1.499(5)
N(4)-O(7)	1.243(4)	C(17)-C(18)	1.511(5)
N(4)-O(8)	1.239(4)	C(18)-C(19)	1.395(5)
N(4)-C(14)	1.497(5)		

The difference in charges observed for the TTF molecules in the chain are in good agreement with the intermolecular distances. Indeed, the chains do not show a regular stack, with close contacts between molecule A and the TRNF molecules (3.01(5) Å between S1 and the mean plane of the two adjacent TRNF molecules), and much longer for molecule B (3.35(5) and 3.43 Å between S3 and the mean plane of the two adjacent TRNF molecules). Thus the structure can be considered as being composed of sandwiched trimers TRNF•••TTF(A) •••TRNF separated by neutral TTF molecules.

Along the chain, the molecules are related by a center of symmetry, and thus consecutive TRNF molecules show opposite orientations regarding the C=O group and appear with nitro group conformation which exhibit a dihedral angle of 7° which causes them to deviate from the planarity of the fluorenone core. There are no close contacts between stacks or with the neutral and isolated TTF molecule. The closest contacts

between nitro groups and aromatic hydrogen atoms is from adjacent fluorenone molecules (O(4)•••C(18) = 2.832(6) Å), but also between the C=O group with the sulfur atoms from TTF A molecules, the molecules with the highest positive charge (S(1)•••O(7) = 2.904(8) Å). The solid-state structure of **2** and the packing of the donor and acceptor molecules in the crystal are shown in Figures 74 and 75. Selected bond distances for **2** are shown in Table 49.

Compound **3** crystallizes in the space group *P-1* and exhibits a 1:1 stoichiometry. It forms by regular 1D alternating stacks of TMTTF and TRNF along the *a* axis, with a pseudo-hexagonal packing motif. There is only one crystallographically independent neutral TMTTF molecule as estimated from intermolecular bond distances. The interplanar distance is 3.288 Å. The trinitrofluorenone molecule also shows a planar configuration, with torsion angles up to 27° for the central nitro group. Interchain interactions are much weaker, and no significant hydrogen bonding is observed, with the shortest contact appearing between a nitro group and aromatic carbons from fluorenone molecules in adjacent chains (O(4)•••C(19) = 2.844(6) Å). The solid-state structure of **3** and the packing of the donor and acceptor molecules in the crystal are shown in Figures 76 and 77. Selected bond distances for **3** are shown in Table 50.

Compound (**4•2CH$_3$CN**) crystallizes in the space group *C2* and is dominated by integrated 1:1 stacks of TTF donors and HAT-(CN)$_6$ acceptors. From numerous studies on neutral and oxidized chalcofulvalene donors, it has been established by our group and others, that when the TTF donor forms integrated stacks with organic acceptors of non-equivalent redox potentials, intermolecular forces such as π-π or S ••• S interactions become the dominating feature in facilitating nearly-neutral chalcofulvalene donors to adopt a planar conformation.[6,14] Utilizing the Coppens' method, close inspection of the C-C and C-S bond distances reveal that the TTF donor exhibits an overall oxidation state of +0.12.[94] In light of this oxidation state and the appearance of a planar conformation for TTF, it is apparent that TTF engages in π-π interactions with HAT-(CN)$_6$ along the stacking axis. Based on these structural features, TTF and HAT-(CN)$_6$ are approximately neutral.[113] The integrated stacks form along the b-axis and are related to one another by translation along the a-axis. An interesting feature of the structure is that two separate trios of integrated stacks form a V-formation, which intersect at the (1,1,1/2) plane along with interstitial acetonitrile molecules.

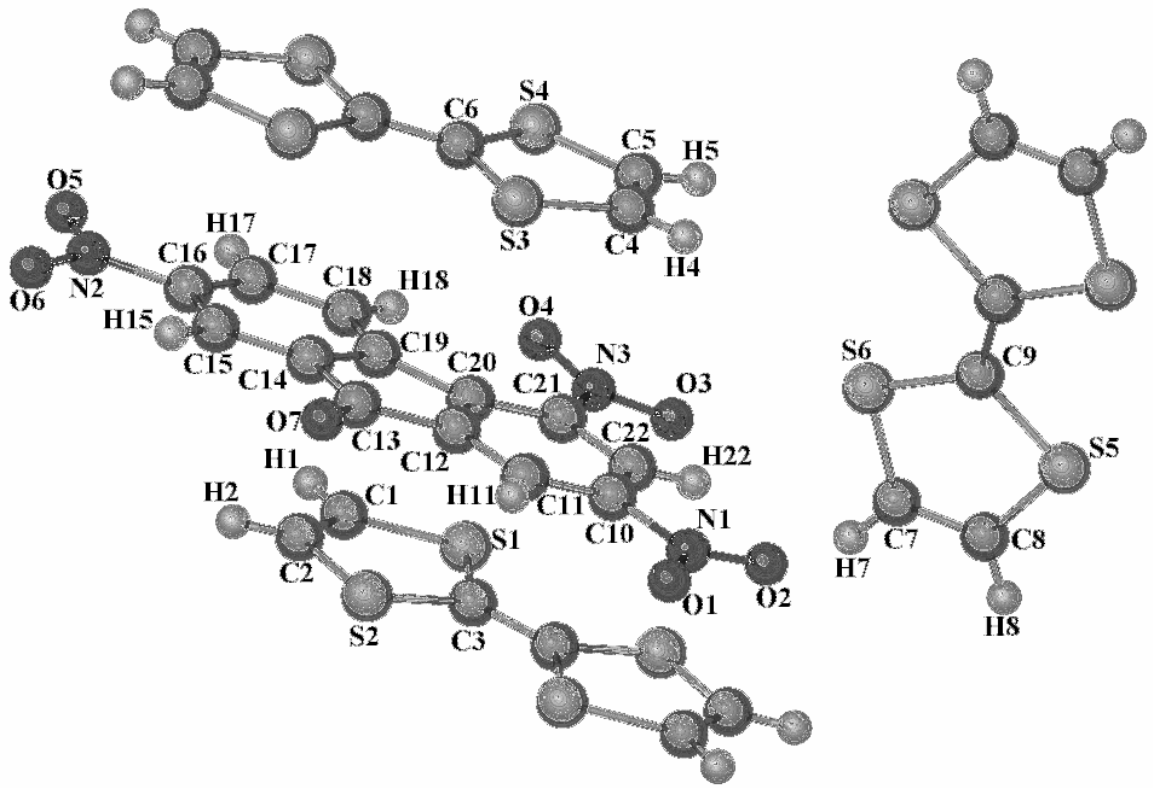

Figure 74. X-ray crystal structure of the [TTF][TRNF] adduct (**2**).

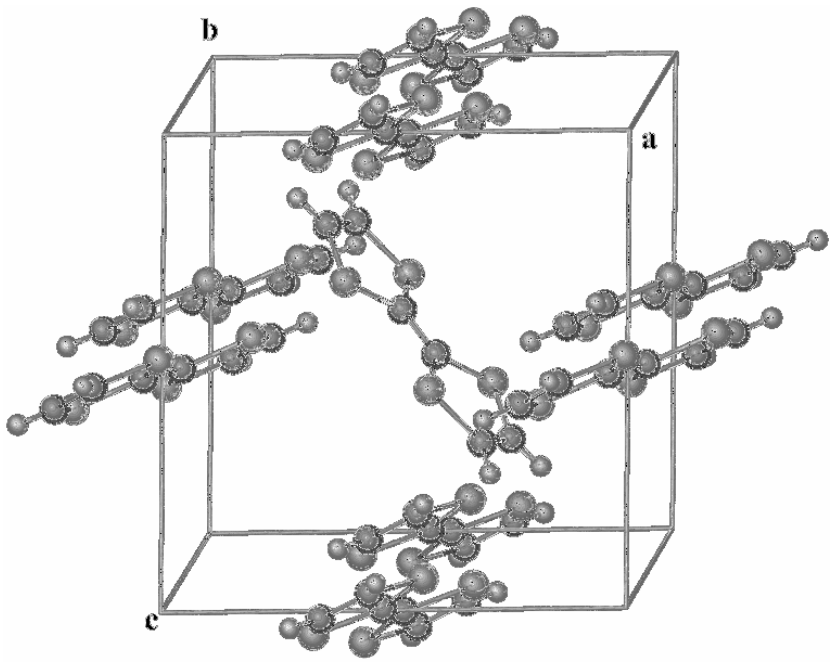

(**a**)

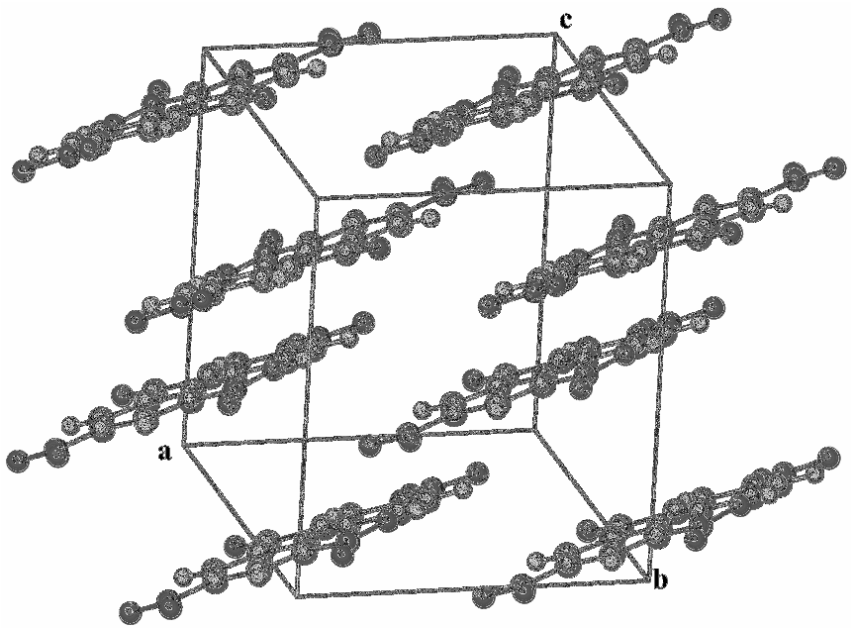

(**b**)

Figure 75. Packing arrangements of **2** illustrating the planar conformation of the TTF donors (**a**) and fluorenone cores of the TRNF acceptor molecules (**b**).

Compound (**4•2CH$_3$CN**) crystallizes in the space group *C2* and is dominated by integrated 1:1 stacks of TTF donors and HAT-(CN)$_6$ acceptors. From numerous studies on neutral and oxidized chalcofulvalene donors, it has been established by our group and others, that when the TTF donor forms integrated stacks with organic acceptors of non-equivalent redox potentials, intermolecular forces such as π-π or S ••• S interactions become the dominating feature in facilitating nearly-neutral chalcofulvalene donors to adopt a planar conformation.[6,14] Utilizing the Coppens' method, close inspection of the C-C and C-S bond distances reveal that the TTF donor exhibits an overall oxidation state of +0.12.[94]

Table 49. Bond distances for [TTF][TRNF] (**2**) in Å.

S(1)-C(1)	1.743(3)	C(1)-C(2)	1.326(4)
S(1)-C(3)	1.756(3)	C(3)-C(3)	1.362(5)
S(2)-C(2)	1.742(3)	C(4)-C(5)	1.327(4)
S(2)-C(3)	1.749(3)	C(6)-C(6)	1.344(6)
S(3)-C(4)	1.741(3)	C(7)-C(8)	1.324(4)
S(3)-C(6)	1.766(3)	C(9)-C(9)	1.335(6)
S(4)-C(5)	1.737(3)	C(10)-C(11)	1.375(4)
S(4)-C(6)	1.764(3)	C(10)-C(22)	1.379(4)
S(5)-C(8)	1.741(3)	C(11)-C(12)	1.378(4)
S(5)-C(9)	1.772(3)	C(12)-C(13)	1.481(4)
S(6)-C(7)	1.744(3)	C(12)-C(20)	1.508(4)
S(6)-C(9)	1.759(3)	C(13)-C(14)	1.483(4)
N(1)-O(1)	1.227(3)	C(14)-C(15)	1.409(4)
N(1)-O(2)	1.224(3)	C(14)-C(19)	1.412(4)
N(1)-C(10)	1.469(4)	C(15)-C(16)	1.377(4)
N(2)-O(5)	1.230(3)	C(16)-C(17)	1.383(4)
N(2)-O(6)	1.223(3)	C(17)-C(18)	1.383(4)
N(2)-C(16)	1.474(4)	C(18)-C(19)	1.387(4)
N(3)-O(3)	1.230(3)	C(19)-C(20)	1.508(4)
N(3)-O(4)	1.210(3)	C(20)-C(21)	1.400(4)
N(3)-C(21)	1.473(3)	C(21)-C(22)	1.387(4)
O(7)-C(13)	1.216(3)		

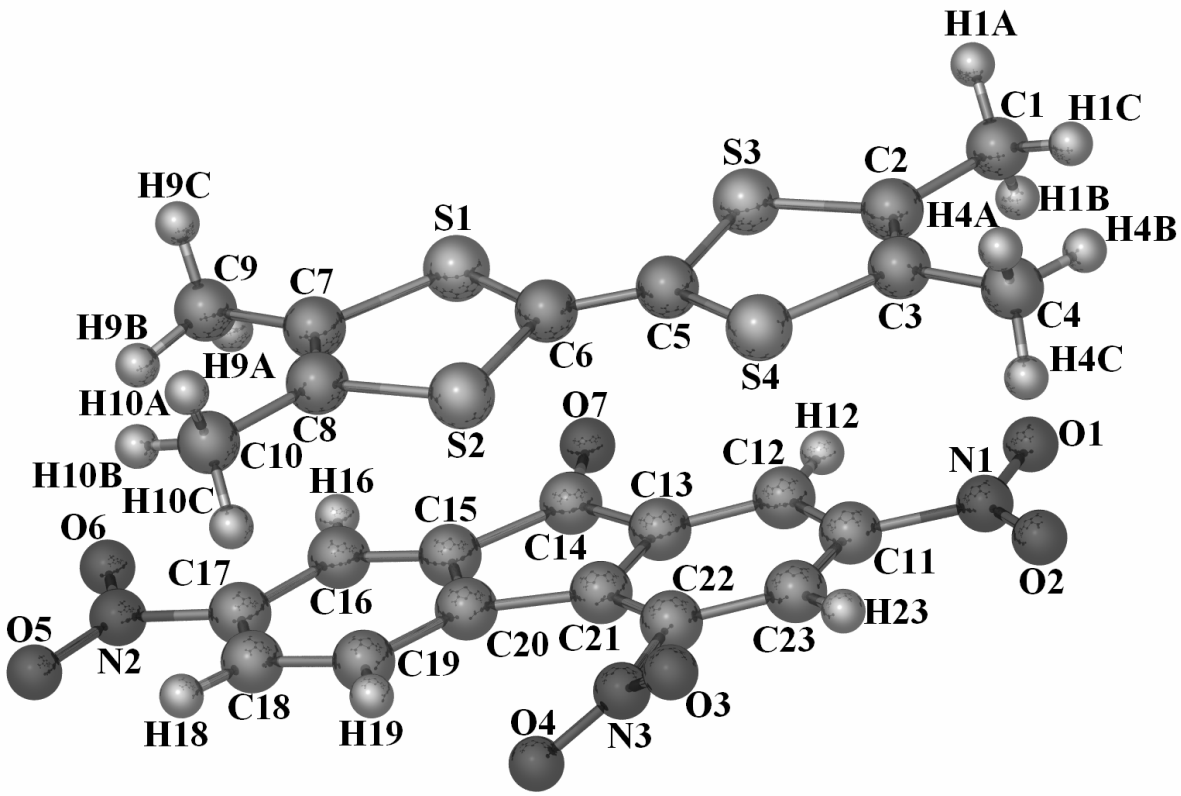

Figure 76. X-ray crystal structure of the [TMTTF][TRNF] adduct (**3**).

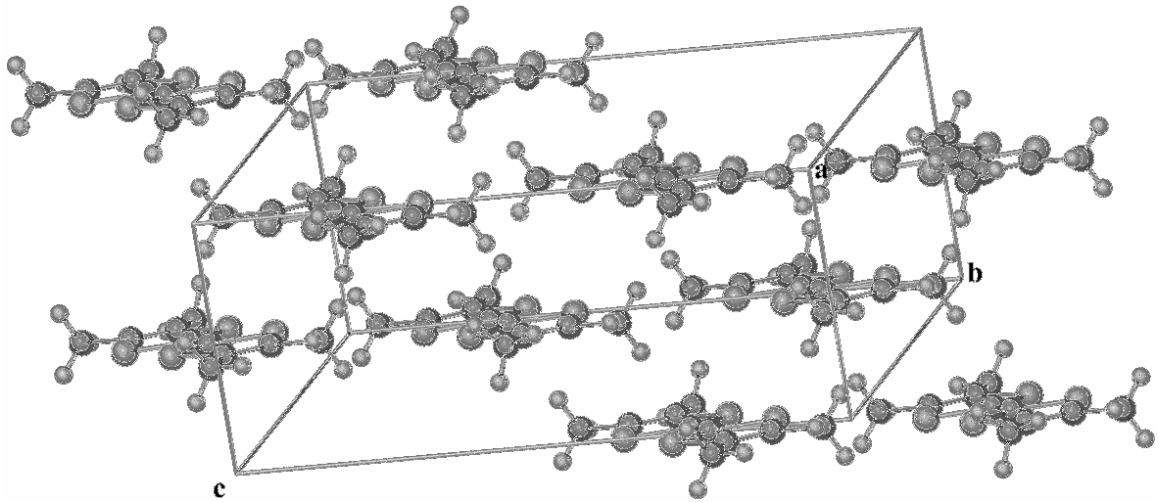

(**a**)

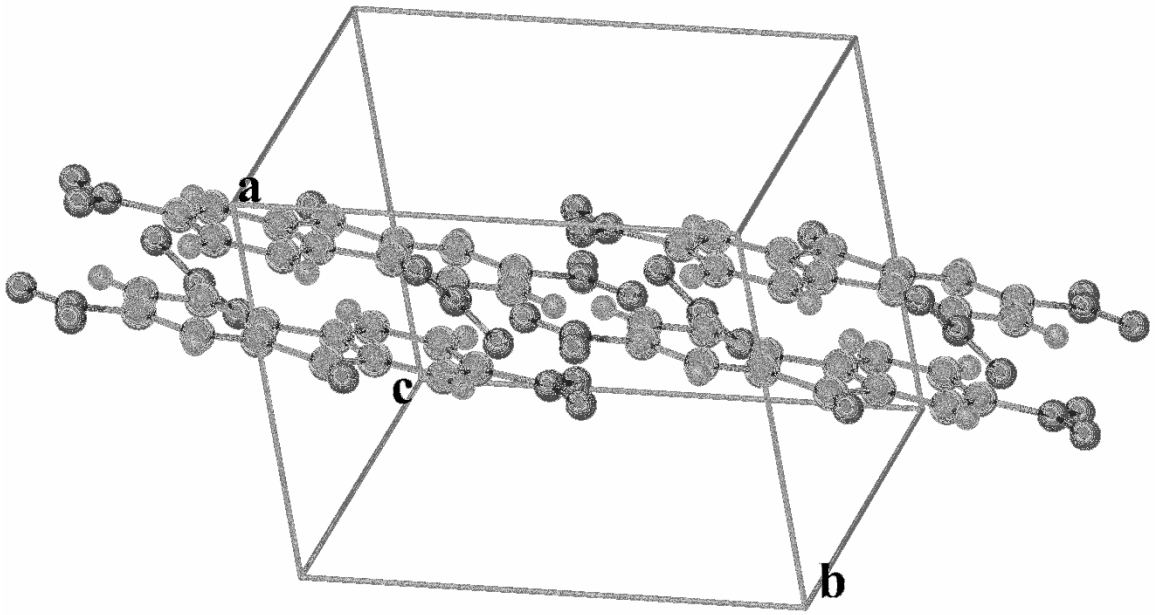

(**b**)

Figure 77. Packing arrangements of **3** illustrating the planar conformation of the TMTTF donors (**a**) and fluorenone cores of the TRNF acceptor molecules (**b**).

In light of this oxidation state and the appearance of a planar conformation for TTF, it is apparent that TTF engages in π-π interactions with HAT-$(CN)_6$ along the stacking axis. Based on these structural features, TTF and HAT-$(CN)_6$ are approximately neutral.[113] The integrated stacks form along the b-axis and are related to one another by translation along the a-axis. An interesting feature of the structure is that two separate trios of integrated stacks form a V-formation, which intersect at the (1,1,1/2) plane along with interstitial acetonitrile molecules. The solid-state structure of (**4•2CH$_3$CN**) and the packing of the donor and acceptor molecules in the crystal are shown in Figures 78 and 79. Selected bond distances for (**4•2CH$_3$CN**) are shown in Table 51.

Compound **6** crystallizes in the monoclinic space group *P2$_1$/c* and consists of integrated stacks of donors and acceptors. As in the case of **4**, the bond distances of TTF as well as those from the cyanide ligands of tetracyanobenzene indicate that both are essentially neutral.[94] Since no charge transfer appears to have taken place, the planarity of TTF can be rationalized on the basis of π-π interactions between the donors and acceptors along the stacking axis, which appears to coincide with the a-axis of the unit cell. Independent stacks are related to one another via translations along the c-axis. Weak to intermediate hydrogen bonding interactions exist in the (1/2,1,1) plane involving $C_{sp}{}^2$-H•••N interactions at distances ranging from a maximum of 2.538 Å to a minimum of 2.372 Å involving the hydrogen atoms C1 and C2 from TTF and nitrogen atoms N1 and N2 from the nitrile group of tetracyanobenzene. The solid-state structure of **6** and the packing of the donor and acceptor molecules in the crystal are shown in Figures 80 and 81. Selected bond distances for **6** are shown in Table 52.

Table 50. Bond distances for [TMTTF][TRNF] (**3**) in Å.

S(1)-C(6)	1.756(8)	C(3)-C(4)	1.492(11)
S(1)-C(7)	1.776(7)	C(5)-C(6)	1.334(11)
S(2)-C(6)	1.781(8)	C(7)-C(8)	1.327(12)
S(2)-C(8)	1.749(9)	C(7)-C(9)	1.509(11)
S(3)-C(2)	1.752(8)	C(8)-C(10)	1.510(11)
S(3)-C(5)	1.775(8)	C(11)-C(12)	1.393(12)
S(4)-C(3)	1.769(8)	C(11)-C(23)	1.370(11)
S(4)-C(5)	1.735(8)	C(12)-C(13)	1.381(11)
N(1)-O(1)	1.229(9)	C(13)-C(14)	1.480(12)
N(1)-O(2)	1.210(9)	C(13)-C(21)	1.394(11)
N(1)-C(11)	1.482(11)	C(14)-C(15)	1.494(10)
N(2)-O(5)	1.219(9)	C(15)-C(16)	1.363(12)
N(2)-O(6)	1.237(9)	C(15)-C(20)	1.412(11)
N(2)-C(17)	1.461(10)	C(16)-C(17)	1.397(11)
N(3)-O(3)	1.221(9)	C(17)-C(18)	1.375(11)
N(3)-O(4)	1.220(9)	C(18)-C(19)	1.362(11)
N(3)-C(22)	1.476(10)	C(19)-C(20)	1.397(11)
O(7)-C(14)	1.224(9)	C(20)-C(21)	1.511(11)
C(1)-C(2)	1.508(10)	C(21)-C(22)	1.393(11)
C(2)-C(3)	1.340(12)	C(22)-C(23)	1.377(11)

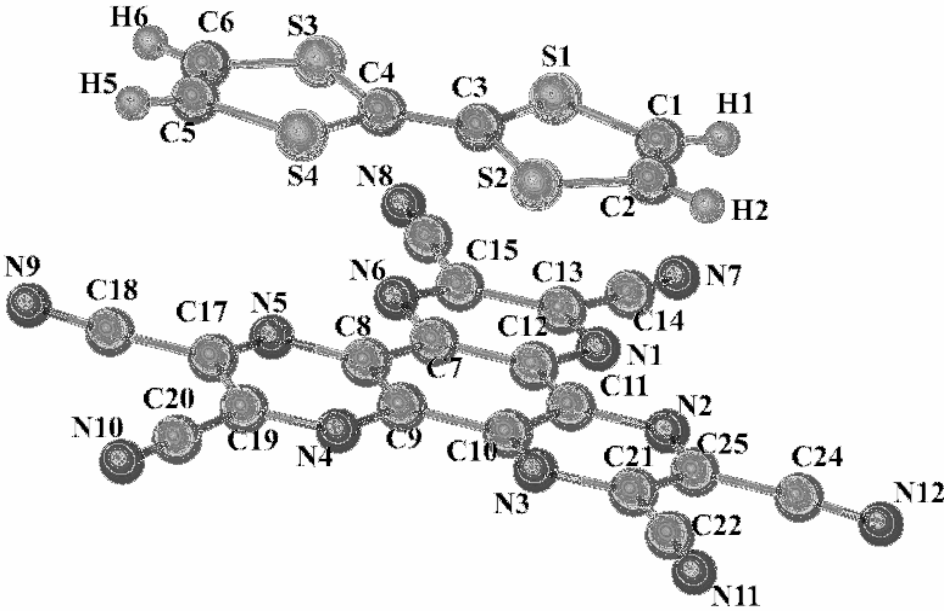

Figure 78. X-ray crystal structure of [TTF][HAT-$(CN)_6$]•2CH_3CN (**4•2CH_3CN**). Interstitial acetonitrile molecules have been removed for the sake of clarity.

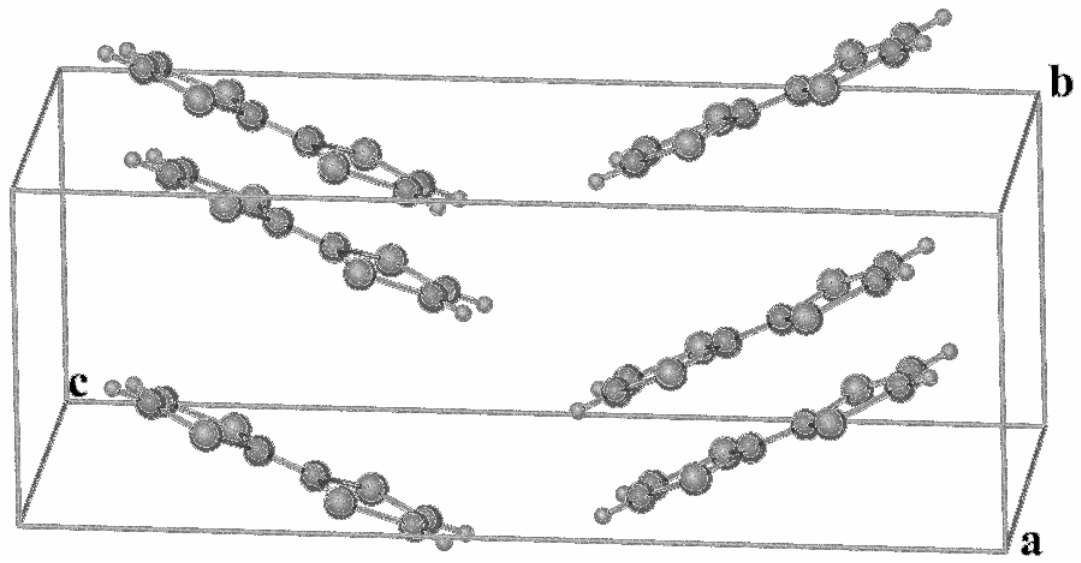

(**a**)

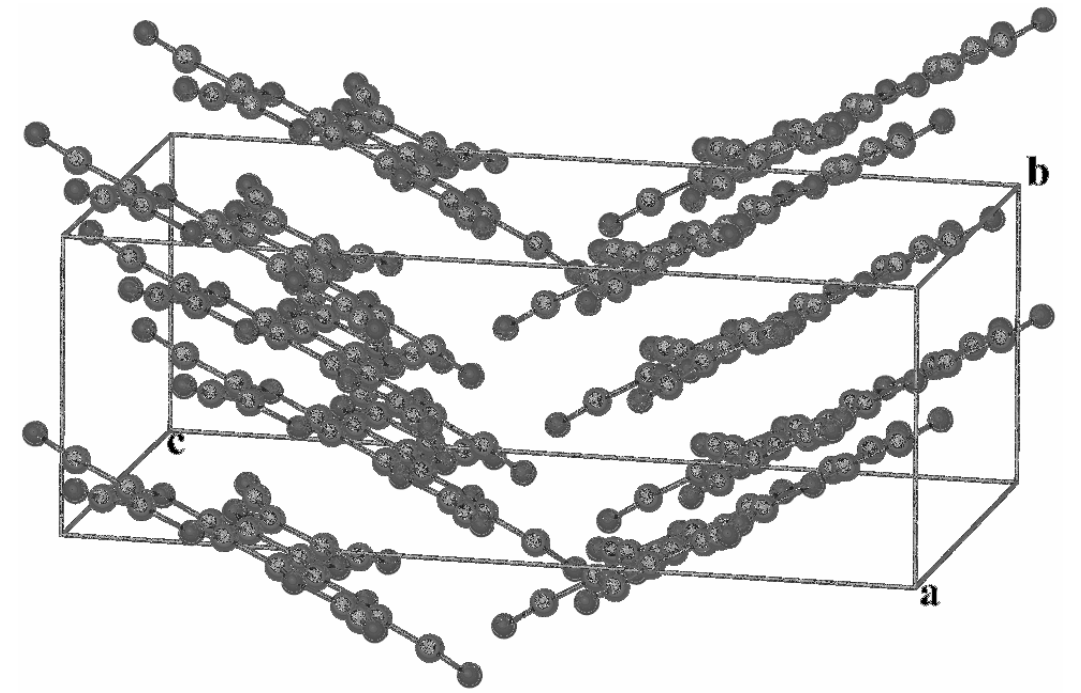

(**b**)

Figure 79. Packing arrangements of (**4•2CH$_3$CN**) illustrating the planar conformation of the TTF donors (**a**) and the HAT-(CN)$_6$ acceptor molecules (**b**).

Table 51. Bond distances for [TTF][HAT-$(CN)_6$]•2CH_3CN (**4•2CH_3CN**) in Å.

S(1)-C(1)	1.74(2)	N(12)-C(24)	1.18(2)
S(1)-C(3)	1.74(2)	N(13)-C(26)	1.11(3)
S(2)-C(2)	1.74(2)	N(14)-C(27)	1.22(6)
S(2)-C(3)	1.78(2)	C(1)-C(2)	1.32(2)
S(3)-C(4)	1.78(2)	C(3)-C(4)	1.35(2)
S(3)-C(6)	1.72(2)	C(5)-C(6)	1.34(2)
S(4)-C(4)	1.80(2)	C(7)-C(8)	1.47(2)
S(4)-C(5)	1.74(2)	C(7)-C(12)	1.42(2)
N(1)-C(12)	1.38(2)	C(8)-C(9)	1.41(2)
N(1)-C(13)	1.33(2)	C(9)-C(10)	1.51(2)
N(2)-C(11)	1.36(2)	C(10)-C(11)	1.44(2)
N(2)-C(23)	1.34(2)	C(11)-C(12)	1.41(2)
N(3)-C(10)	1.31(2)	C(11)-C(22)	1.14(2)
N(3)-C(21)	1.37(2)	C(13)-C(14)	1.48(2)
N(4)-C(9)	1.38(2)	C(13)-C(15)	1.44(2)
N(4)-C(19)	1.37(2)	C(15)-C(16)	1.46(2)
N(5)-C(8)	1.35(2)	C(17)-C(18)	1.46(3)
N(5)-C(17)	1.32(2)	C(17)-C(19)	1.40(2)
N(6)-C(7)	1.40(2)	C(19)-C(20)	1.49(3)
N(6)-C(15)	1.32(2)	C(21)-C(22)	1.46(3)
N(7)-C(14)	1.10(2)	C(21)-C(23)	1.41(2)
N(8)-C(16)	1.15(2)	C(23)-C(24)	1.48(3)
N(9)-C(18)	1.17(3)	C(25)-C(26)	1.48(3)
N(10)-C(20)	1.13(2)	C(27)-C(28)	1.13(6)

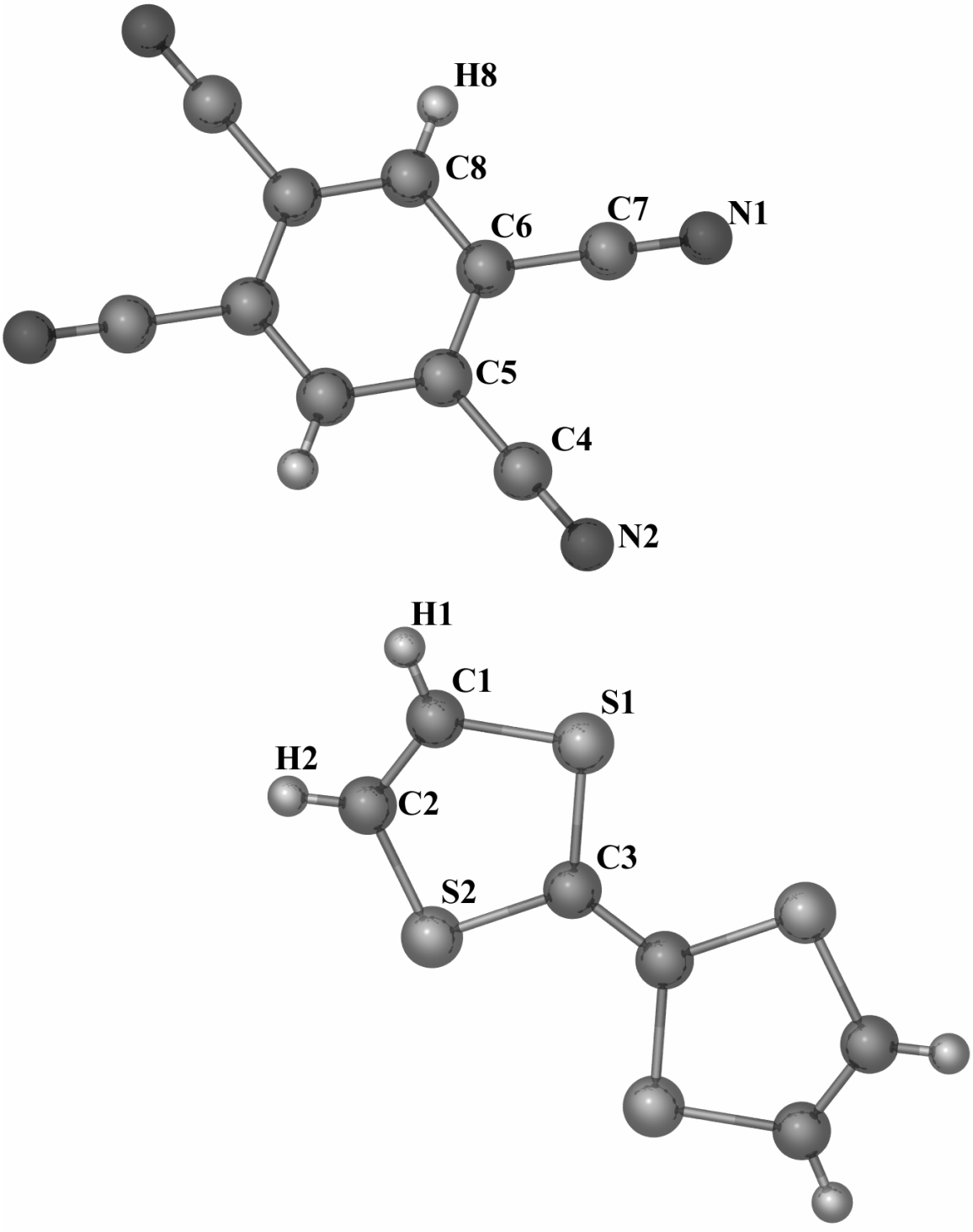

Figure 80. X-ray crystal structure of the [TTF][TCNB] adduct (**6**).

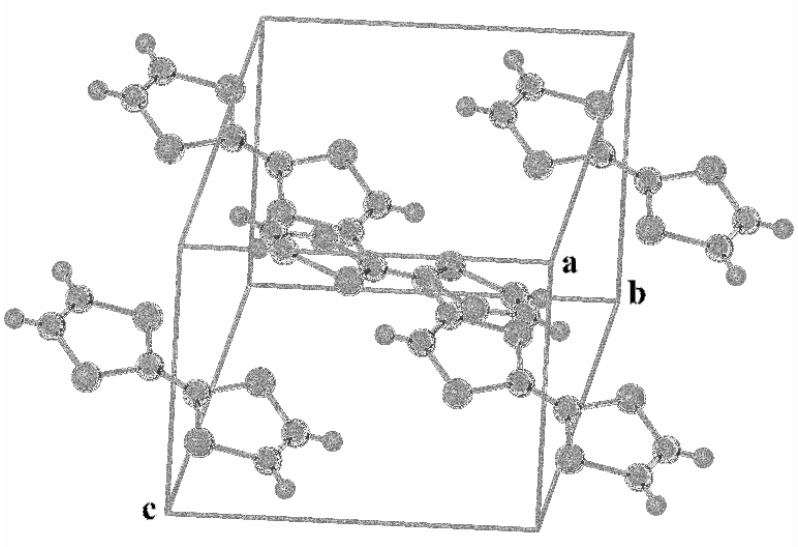

(**a**)

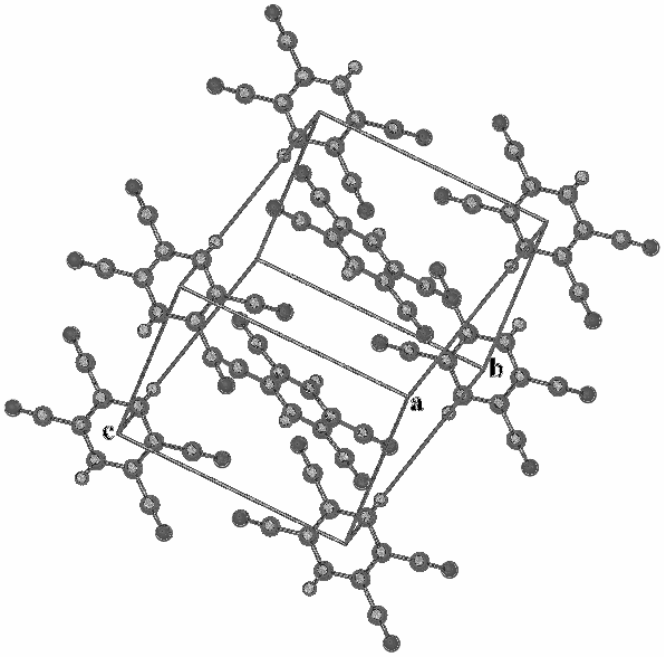

(**b**)

Figure 81. Solid-state contents of **6** illustrating the planar conformation of the TTF donors (**a**) and the TCNB acceptor molecules (**b**).

Table 52. Bond distances for [TTF][TCNB] (**6**) in Å.

S(1)-C(1)	1.740(2)
S(1)-C(3)	1.755(2)
S(2)-C(2)	1.743(2)
S(2)-C(3)	1.755(2)
N(1)-C(7)	1.143(3)
N(2)-C(4)	1.143(3)
C(1)-C(2)	1.334(3)
C(3)-C(3)	1.350(3)
C(4)-C(5)	1.439(2)
C(5)-C(8)	1.387(2)
C(5)-C(6)	1.407(2)
C(6)-C(7)	1.438(2)
C(6)-C(8)	1.389(2)

Compound **7** crystallizes in the triclinic space group *P-1* forming integrated stacks in the solid-state. According to closer inspection of the structure, the integrated stacks from along the a axis and exist in the (1,0,1) plane. No hydrogen bonding appears to exist in the structure between the C_{sp}^2 and C_{sp}^3-hybridized carbons from the *o*-Me_2TTF donors and TCNB acceptors. Based on redox-sensitive bond distances, no charge transfer has occurred, suggesting that the onset of planarity from the *o*-Me_2TTF donor molecules can be explained by π-π interactions. The solid-state structure of **7** and the packing of the donor and acceptor molecules in the crystal are shown in Figures 82 and 83. Selected bond distances for **7** are shown in Table 53.

Spectroscopic Analyses

Infrared Spectral Studies. With the presence of bridging carbonyl and terminal cyanide groups, infrared spectroscopy is a viable method to determine the level of reduction in the

organic acceptors. Suspensions of (**4•2CH$_3$CN**) and **5** in Nujol allowed for probing of the cyanide stretching vibrations which revealed a small level of reduction. According to literature reports, neutral HAT-(CN)$_6$ exhibits a cyanide stretching vibration at 2243 cm^{-1}.[113] In a manner similar to TCNQ and TCNQF$_4$, the shifting of cyanide stretching vibrations to lower frequencies in HAT-(CN)$_6$ would indicate reduction as electron donation into the π*-orbitals of the cyanide ligands increases their bond lengths facilitating a lowering of their corresponding vibration frequency. Upon spectroscopic analyses, adducts (**4•2CH$_3$CN**) and **5** showed cyanide stretching vibrations of 2240 cm^{-1} and 2239 cm^{-1} in their individual spectra. These results indicate there is no electron donation into the π*-orbitals of the cyanide ligands and that the HAT-(CN)$_6$ acceptors are neutral. Due to the disparity between the redox potentials of TTF and the nitrofluorenone acceptors the other complexes were not subjected to infrared anaylsis as they should only show stretching vibrations indicative of neutral donors.

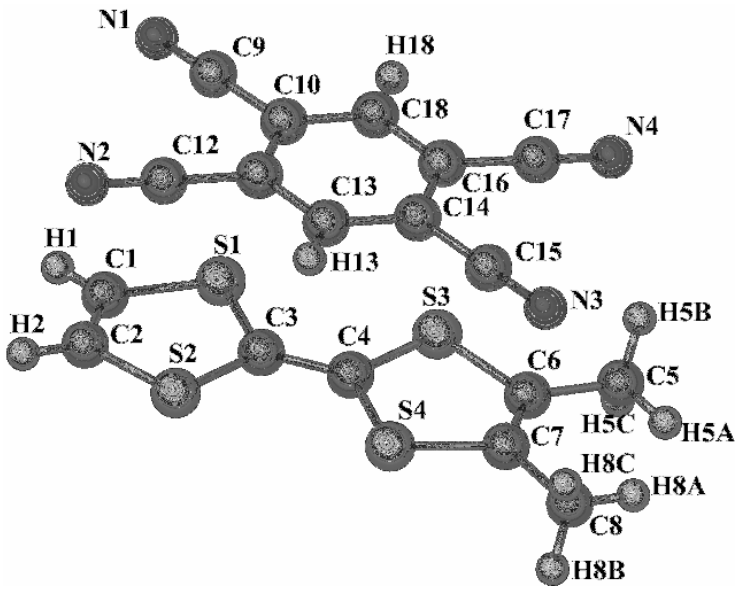

Figure 82. X-ray crystal structure of the [*o*-Me$_2$TTF][TCNB] adduct (**7**).

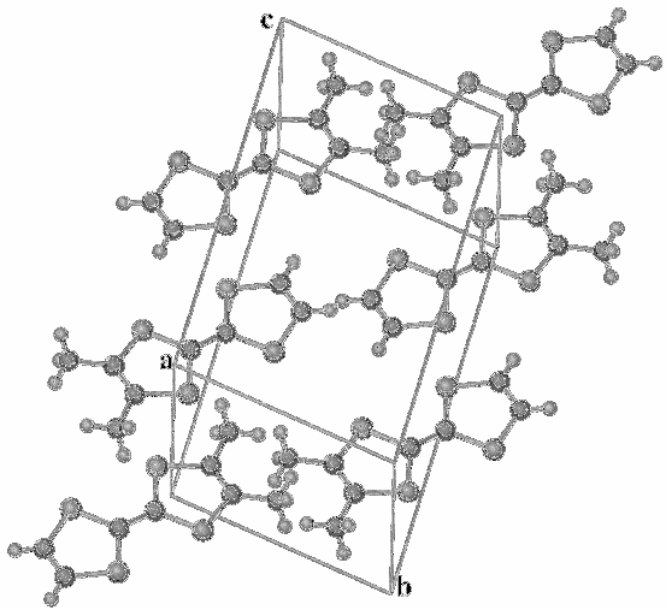

(**a**)

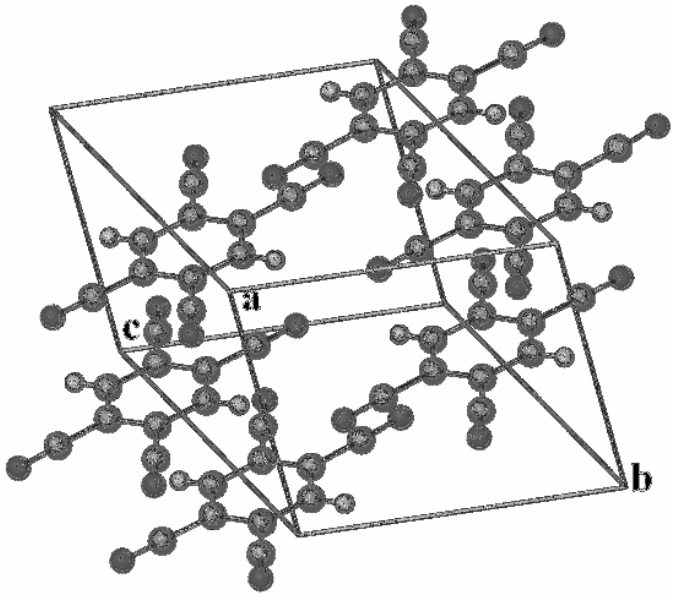

(**b**)

Figure 83. Solid-state contents of **7** illustrating the planar conformation of the o-Me_2TTF donors (**a**) and the TCNB acceptor molecules (**b**).

Table 53. Bond distances for [*o*-Me_2TTF][TCNB] (**7**) in Å.

S(1)-C(1)	1.743(2)
S(1)-C(3)	1.756(2)
S(2)-C(2)	1.736(2)
S(2)-C(3)	1.760(2)
S(3)-C(4)	1.751(2)
S(3)-C(6)	1.763(2)
S(4)-C(4)	1.754(2)
S(4)-C(7)	1.758(2)
N(1)-C(9)	1.145(2)
N(2)-C(12)	1.143(2)
N(3)-C(15)	1.144(2)
N(4)-C(17)	1.141(2)
C(1)-C(2)	1.318(3)
C(3)-C(4)	1.342(2)
C(5)-C(6)	1.495(2)
C(6)-C(7)	1.334(2)
C(7)-C(8)	1.500(2)
C(9)-C(10)	1.440(2)
C(10)-C(11)	1.407(2)
C(10)-C(18)	1.386(2)
C(11)-C(12)	1.440(2)
C(11)-C(13)	1.388(2)
C(13)-C(14)	1.390(2)
C(14)-C(15)	1.440(2)
C(14)-C(16)	1.405(2)
C(16)-C(17)	1.438(2)
C(16)-C(18)	1.389(2)

Magnetic Susceptibility

Molecular Magnetism. DC magnetic susceptibility measurements on adducts **1** and (**4•2CH$_3$CN**), representative examples for the nitrofluorenone and the organocyanide family of acceptors, revealed that both were diamagnetic. The behavior for **1** and (**4•2CH$_3$CN**) can be rationalized on the basis of the structural and spectroscopic evidence. As discussed earlier, the TTF donor and TRNF and HAT-(CN)$_6$ acceptors were found to be neutral, with the solid-state structures being dominated by the presence of weak intermolecular interactions, instead of charge transfer. With the combined lack of charge transfer, hole formation on the TTF Fermi surface, and close S•••S interactions due to the integrated stacks of donors and acceptors, the materials are insulators and do not exhibit temperature independent paramagnetism due to the presence of conducting electrons. Since the other complexes, whose preparation was outlined in this chapter, showed features indicative of neutral donor and acceptor molecules, they were excluded from magnetic susceptibility analysis.

Conclusions

The products of the direct reactions between TTF, *o*-Me$_2$TTF, and TMTTF with the acceptors TENF, TRNF, HAT-(CN)$_6$, and TCNB were analyzed by a X-ray crystallography, IR spectroscopy, and molecular magnetism, which reveal that there has been little to no charge transfer between the donor and acceptor molecules. In all compounds, the crystal packing consists of alternating donor•••acceptor stacks and the degree of charge transfer appears to depend on the solid state structure, controlled mostly by π-π and other very weak intermolecular interactions.

It is surprising to note that the strongest electron donor, tetranitrofluorenone, does not yield the product with the most efficient charge transfer. The compound combining TTF with TRNF formed a complex where the overall charge on TTF was +0.3.[94] The reason for this is believed to be structural, as two trinitrofluorenone molecules are accepting electron density from a single TTF donor, resulting in the formation of trimers with close interactions while the other structures, are dominated by regular chains. In all cases, structural evidence showed alterations in TTF reminiscent of slight oxidation, but the dominating feature of the stacks most likely responsible for the onset of planarity are the intermolecular π-π interactions between the donors and acceptors within the integrated stacks and not oxidation of the TTF moiety. Apart from the interesting structural features controlling the degree of charge transfer from the TTF molecules, the weak charge transfer found in all cases renders these compounds diamagnetic insulators.

CHAPTER V

PREPARATION OF SUPRAMOLECULAR STACKS CONTAINING INORGANIC DONORS AND ORGANIC ACCEPTORS

Introduction

An active area of research for over three decades has been the study of charge transfer complexes that display interesting conducting and spectroscopic properties.[114] In this realm, purely organic complexes have shown interesting, electronic and charge transfer properties. Another approach has been to prepare hybrid organic-inorganic materials whereby d-π interactions enhance those properties. Most notably, one especially fascinating result has been the preparation of metal-containing charge transfer compounds involving the complex $[Ni(dmit)_2]^{2-}$ (dmit = 2-thioxo-1,3-dithiole-4,5-dithiolate), which undergoes partial oxidation and forms superconducting salts with open- and closed-shell organic cations.[115] Intermolecular interactions govern the conducting nature of these materials, with the most significant contribution to these interactions being interactions between the diffuse π-orbital on sulfur and the metal d-orbitals.[115] Additionally, depending on the stacking pattern of the donors and acceptors, varying degrees of conductivity can be achieved. If the donors and acceptors assemble in segregated stacks, metallic or superconducting states can be achieved. If the resulting solid-state packing yields integrated stacks, semi-conducting or insulating states are obtained. This behavior has been demonstrated by several organic and metal-containing donor-acceptor extended chain species.[117] Based on their spectroscopic properties, an

interesting application of these metal-containing charge transfer complexes are their use in solar cells as photosensitizing dyes for wide band gap semiconductors.[118]

An initial report in 2003 by the combined groups of Professor Kim Dunbar at Texas A&M University and Professor Mohammad Omary at the University of North Texas described new supramolecular stacks combining inorganic donors of general formula M(dbbpy)(dmid) (M = Pt, Pd; dbbpy = 4,4'di-*tert*-butyl-2,2'-bipyridine; dmid = 2-oxo-1,3-dithiole-4,5-dithiolate) with the organocyanide acceptors TCNQ, $TCNQF_4$, and TCNE.[68] The interest in these systems was to probe their optoelectronic properties in solution and in the solid state. A similar system was prepared when the same donor was also combined with the acceptor DM-DCNQI (Figure 84).

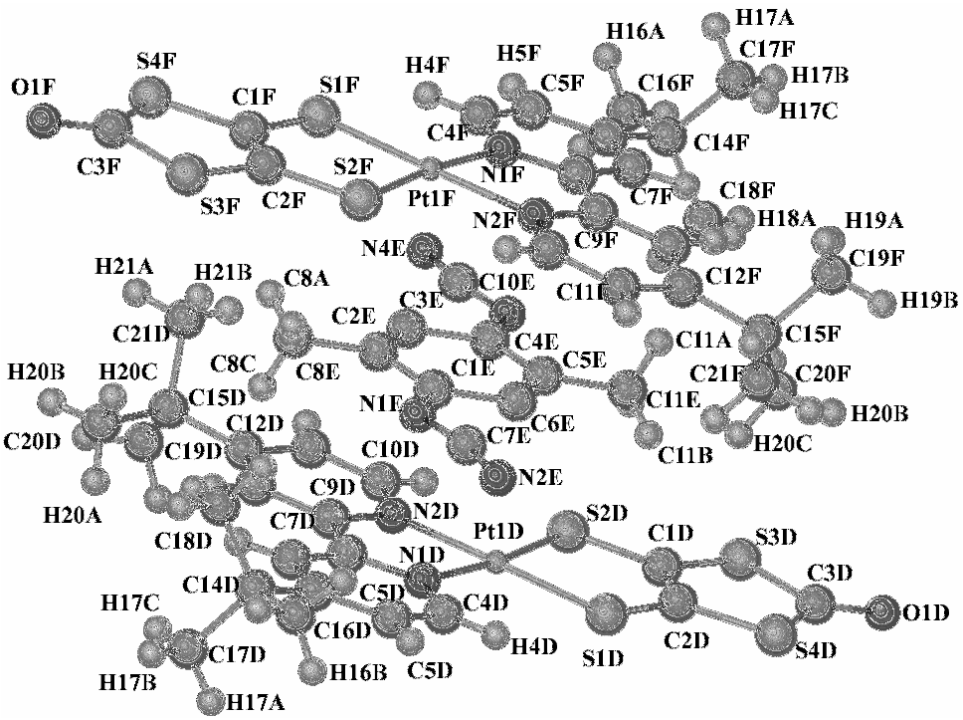

Figure 84. X-ray structure of the stack formed between Pt(dbbpy)(dmid) and the organocyanide acceptor DM-DCNQI.

It was found that in the absence of traditional anchoring groups such as carboxylates, phosphonates, or sulfonates, the peripheral cyanide group on the acceptor molecules were apparently able to serve as a suitable anchoring ligand in the presence of the metal complex.[68] Despite this interesting discovery, it was found that these supramolecular systems suffered from reduced performance as compared to the Ru(II)-pyridyl systems.[57] It was rationalized that the reason for the lower performance of these supramolecular systems is a consequence of the organocyanide acceptors being unable to inject an electron into the conduction band of the semiconductor. Facile electron injection into the conduction band of the semiconductor occurs if the first reduction potential of the former is more negative then the latter.[68] Upon inspection of the first reduction potentials of the organocyanide acceptors ($E_{1/2}$(red) for TCNQ = +0.34 V, $E_{1/2}$(red) for $TCNQF_4$ = +0.55V, and $E_{1/2}$(red) for TCNE = +0.12 V), none were more negative than the first reduction potential of TiO_2's conduction band (-0.78 V). In an effort to overcome this situation, we synthesized three new supramolecular systems containing the inorganic molecule Pt(dbbpy)(tdt) (tdt = 3,4-toluenedithiolate) and the organic acceptors DNF, TRNF, and TENF were prepared. The three supramolecular systems were characterized by X-ray crystallography and cyclic voltammetry at Texas A&M. UV-VIS-NIR studies were conducted by Joshua Hudson of Prof. Omary's group and reveal that strong charge transfer interactions occur in the case of the complexes formed with the TENF acceptor.

Experimental Section

Syntheses

All solvents were dried and freshly distilled prior to use. Dichloromethane and benzene were dried over P_2O_5 and sodium-potassium/benzophenone respectively. Pt(dbbpy)(tdt) was prepared according to literature procedures.[66] DNF was purchased from TCI and used as received without further purification. The organic acceptors TRNF and TENF were provided by Prof. Alan Balch. Compounds **2-4** were prepared by layering CH_2Cl_2 solutions of Pt(dbbpy)(tdt) with solutions of the organic acceptor in a 2:1 solution of CH_2Cl_2/C_6H_6. The flask was then covered with aluminum foil and left undisturbed for a period of approximately one week. The resulting dark blue/black solution was then exposed to slow evaporation under nitrogen atmosphere to yield dark blue/black needles of the three supramolecular stacked systems. All of the crystallized supramolecular systems were obtained using a 2:1 ratio of D:A molecules. Adducts **2-4** were analyzed by X-ray crystallography and cyclic voltammetry. As part of this collaborative project with the University of North Texas, spectroscopic studies were carried out in the laboratories of Prof. Mohammad Omary. A second phase of the complex between Pt(dbbpy)(tdt) and TENF (**5**) was prepared by Joshua Hudson, a student in the laboratory of Prof. Omary, utilizing the same preparative conditions as those utilized for **2-4**, with the exception of the 1:1 ratio of donor:acceptor molecules. The compounds appear to be air and moisture-stable, as the resulting solid product from each mixture maintains its dark blue/black color in light and in an ambient atmosphere. Crystalline quality for the samples diminishes over a period of a few days presumably due to the loss of solvent from the crystalline matrix.

[Pt(dbbpy)(tdt)][DNF]•0.5C_6H_6 (2•0.5C_6H_6). Under a nitrogen atmosphere a dark purple solution of Pt(dbbpy)(tdt) (0.0154 g, 2.4 x 10^{-4} mol) in 5 mL of CH_2Cl_2 was layered with a pale yellow solution of DNF (0.0034 g, 1.2 x 10^{-4} mol) in 10 mL of a 1:1 solution of CH_2Cl_2. The tube was carefully covered in aluminum foil and allowed to stand undisturbed for a period of one week. The resulting black solution was subjected to slow evaporation under nitrogen which resulted in the formation of dark blue/black needles of [Pt(dbbpy)(tdt)] [DNF]•0.5C_6H_6 (**2•0.5C_6H_6**) which formed over the course of one week.

[Pt(dbbpy)(tdt)][TRNF]•C_6H_6 (3•C_6H_6). In a manner similar to that used for **2**, a dark purple solution of Pt(dbbpy)(tdt) (0.0154 g, 2.4 x 10^{-4} mol) in 5mL of CH_2Cl_2 was layered with a pale yellow solution of TRNF (0.0039 g, 1.2 x 10^{-4} mol) in a 1:1 solution of CH_2Cl_2/C_6H_6. Dark blue/black needles of [Pt(dbbpy)(tdt)][TRNF]•C_6H_6 (**3•C_6H_6**) formed over the period of 10 days.

[Pt(dbbpy)(tdt)]$_2$[TENF]•2C_6H_6 (4•2C_6H_6). By using a procedure similar to that used to prepare **2** and **3**, Pt(dbbpy)(tdt) (0.0154 g, 2.4 x 10^{-4} mol) and TENF (0.0045 g, 1.2 x 10^{-4} mol) were combined and isolated as dark blue/black needles of [Pt(dbbpy)(tdt)]$_2$ [TENF]•2C_6H_6 (**4•2C_6H_6**) after a period of seven days.

[Pt(dbbpy)(tdt)][TENF]•C_6H_6 (5•C_6H_6). By utilizing the same synthetic procedure as those listed for **2-4**, a 1:1 ratio of Pt(dbbpy)tdt and TENF were combined and slowly

evaporated under argon for several days to a final volume of 5 mL where black crystals formed from the mother liquor.

X-ray Crystallographic Details

X-ray data for Pt(dbbpy)(tdt) (**1•H_2O**), [Pt(dbbpy)(tdt)][DNF] (**2•0.5C_6H_6**), [Pt(dbbpy)(tdt)] [TRNF] (**3•C_6H_6**), [Pt(dbbpy)(tdt)]$_2$[TENF] (**4•2C_6H_6**) were collected on a Bruker D8 GADDS system at 110±2K with graphite monochromated Cu-Kα (λ = 1.54178 Å) radiation. The data were corrected for Lorentz and polarization effects. The Bruker SAINT software package was used to integrate the frames and the data were corrected for absorption using the SADABS program.[87,88] The structures were solved by direct methods by the use of the SHELXS-97 program in the Bruker SHELXTL v5.1 software package.[89,90] The final refinement was carried out with anisotropic thermal parameters for all non-hydrogen atoms except for the atoms of the interstitial solvent molecules. Hydrogen atoms were placed in calculated positions. The final thermal ellipsoid plots for all compounds were generated using the XSEED program.[91]

X-ray data for (**5•C_6H_6**) was collected on a Bruker SMART APEX II CCD-based diffractometer and a Mo Kα fine-focus sealed tube (λ = 0.71073 Å) with a graphite monochromator operated at 50 kV, 30 mA at 100 K at the University of North Texas with the help of Dr. Xiaoping Wang. The data frames for each compound were integrated with the available APEX2 software using a narrow-frame algorithm. The structures were solved and refined using the SHELXTL program package. The disordered moieties were refined accordingly with distance constraints. All nonhydrogen atoms were refined anisotropically. Hydrogen atoms were assigned calculated positions and allowed to ride

on the attached carbon atoms in final structure refinements. The molecular structures for all three compounds were checked using PLATON. Crystallographic parameters for (**1•4H_2O),** (**2•0.5C_6H_6**), (**3•C_6H_6**)**,** (**4•2C_6H_6**), and (**5•C_6H_6**) are listed in Tables 54 and 55.

Other Physical Measurements

Cyclic voltammetry experiments were carried out at a scan rate of either 100 or 200 mV/s on a CH Instruments Electrochemical Analyzer in 0.1 or 0.2 M solutions of doubly-recrystallized $TBAPF_6$ in CH_2Cl_2 at a Pt disk working electrode with a Ag/AgCl reference and a Pt counter electrode.

UV-VIS-NIR measurements were carried out using a Perkin Elmer Lambda 900 in Suprasil quartz cuvettes with 1mm, 10mm, and 100mm path lengths. The solid reflectance data were collected using the LabSphere integrating sphere accessory to the Lambda 900. The titrations were performed by measuring out 7.7mg of Pt(dbbpy)tdt in several vials to this an aliquot of stock nitrofluorenone solution was added and this was diluted to 25 mL to give exact molar ratios used in the titrations.

Magnetic measurements were performed on a Quantum Design SQUID, MPMS-XL magnetometer. Magnetic susceptibility measurements in the DC mode were carried out at an applied field of 0.1 T in the 2-300 K range.

Table 54. X-ray crystallographic and refinement data for Pt(dbbpy)(tdt)•4H_2O (**1•4H_2O**)

Compound	Pt(tbtrpy)(tdt)•4H_2O (**1•4H_2O**)
Formula	$PtS_2N_4O_4C_{25}H_{38}$
formula weight	689.78
Space group	$P2_1/c$
a, Å	7.373(2)
b, Å	18.533(4)
c, Å	18.754(4)
α, deg	90
β, deg	90.25(3)
γ, deg	90
volume, Å^3	2562.5(9)
Z	4
μ, mm^{-1}	7.092
Temp.	110(2)
Reflns. collected	5962
Reflns. I>2σ	3785
Parameters	219
Restraints	0
R1[a]	0.1275
wR2[b]	0.2899
Goodness-of-fit[c]	1.129

Table 55. X-ray crystallographic and refinement data for (**2•0.5C_6H_6**), (**3•C_6H_6**), (**4•2C_6H_6**), and (**5•C_6H_6**).

Compound	[Pt(dbbpy)(tdt)][DNF]•0.5C_6H_6 (**2•0.5C_6H_6**)	[Pt(dbbpy)(tdt)][TRNF]•C_6H_6 (**3•C_6H_6**)	[Pt(dbbpy)(tdt)]$_2$[TENF]•C_6H_6 (**4•C_6H_6**)	[Pt(dbbpy)(tdt)][TENF]•C_6H_6 (**5•C_6H_6**)
Formula	$C_{41}H_{39}N_4O_5PtS_2$	$C_{44}H_{41}N_5O_7PtS_2$	$C_{75}H_{76}N_8O_9Pt_2S_4$	$C_{41}H_{37}N_6O_9PtS_2$
formula weight	926.97	1011.03	1751.86	1016.98
Space group	P-1	Fdd2	P2(1)/n	P2(1)/n
a, Å	11.298(2)	52.430(6)	11.257(2)	23.128(2)
b, Å	13.599(3)	48.844(6)	26.004(5)	7.164(6)
c, Å	13.964(3)	6.799(8)	24.165(5)	25.474(2)
α, deg	75.51(3)	90	90	90
β, deg	86.77(3)	90	92.19(3)	109.19(2)
γ, deg	69.05(3)	90	90	90
volume, Å^3	1938.6(7)	17410(4)	7069(2)	7069(2)
Z	2	16	4	4
μ, mm^{-1}	3.776	7.381	8.918	3.690
Temp.	110(2)	110(2)	110(2)	110(2)
Reflns. collected	8499	5787	10095	41047
Reflns. I>2σ	7282	4708	3004	7294
R1[a]	0.0347	0.0545	0.0971	0.0480
wR2[b]	0.0653	0.1324	0.1831	0.1076
Goodness-of-fit[c]	0.997	1.003	0.913	1.041

[a] $R1 = \sum||F_o| - |F_c||/\sum|F_o|$. [b] $wR2 = [\sum [w(F_o^2-F_c^2)^2]/ \sum [w(F_o^2)^2]^{1/2}$

[c] Goodness-of-fit = $[\sum w(|F_o|-|F_c|)^2/(N_{obs}-N_{parameter})]^{1/2}$

Results and Discussion

Pt(dbbpy)(tdt) (1)

The synthesis of **1** was carried out in collaboration with researchers at the University of North Texas under a dry atmosphere of N_2 according to literature procedures. An initial attempt to prepare single crystals of this compound was performed by layering saturated, intensely colored purple solutions of **1** in CH_2Cl_2 with an excess of isomeric hexanes. After one week, the solution was exposed to slow evaporation under nitrogen. Dark purple needles formed over the course of one week. The solid-state crystal structure and selected bond distances for (**1•4H$_2$O**) are presented in Figure 85 and Table 56 respectively.

X-ray Crystallographic Studies

The four supramolecular stacks are all defined by donor-acceptor interactions in the solid-state. An important characteristic used to determine the onset of charge transfer is the interplanar distance between the molecules. An inspection of the solid-state structures reveals interplanar distances < 3.7 Å that are well within the range for π-interactions. Despite these interactions that indicate a degree of partial charge transfer between the donor and acceptor molecules, no differences in bond distances of the constituent molecules were noted.

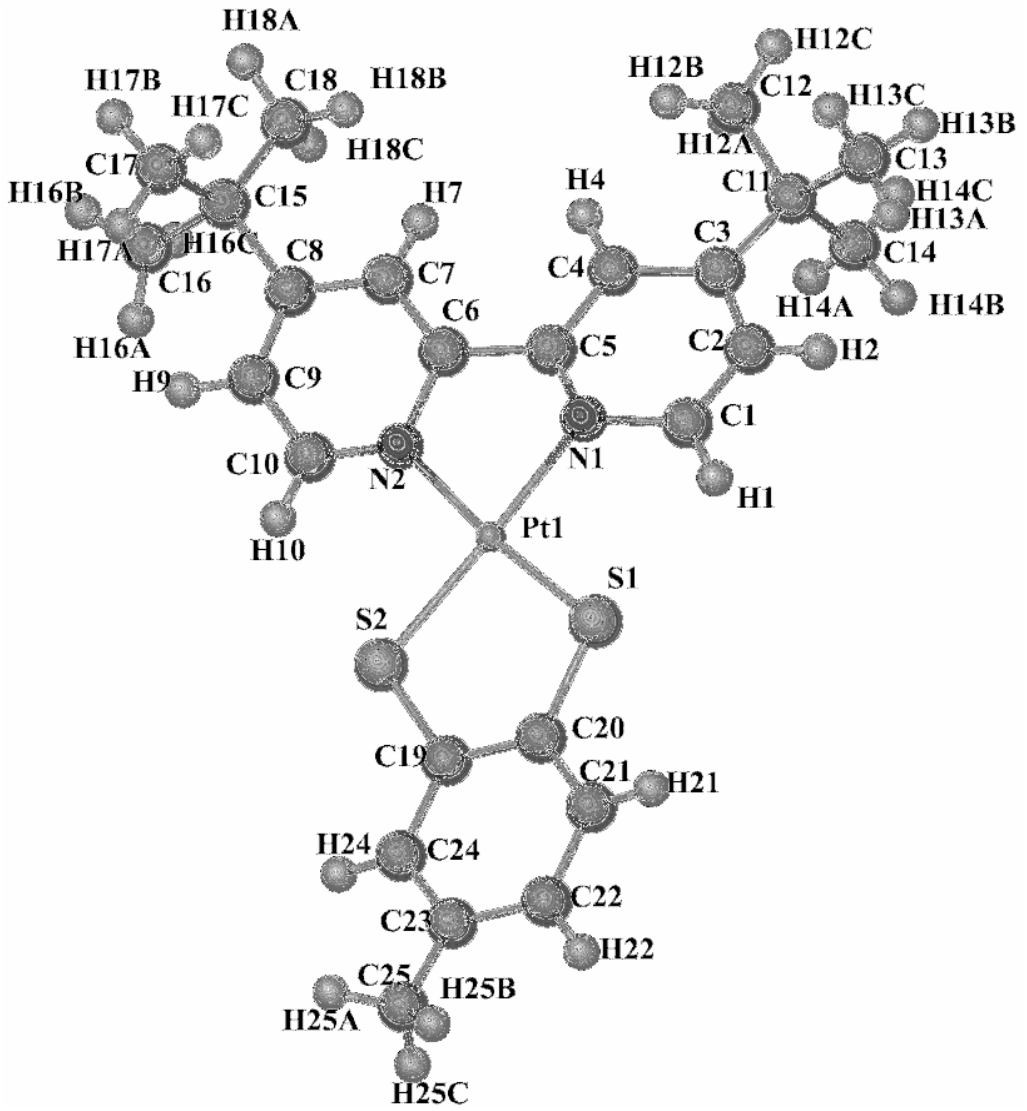

Figure 85. X-ray crystal structure of the donor Pt(dbbpy)(tdt) • $4H_20$ (**1•4H_2O**). Interstitial water molecules have been removed for the sake of clarity.

Table 56. Bond distances for Pt(dbbpy)(tdt)•4H_2O (**1•4H_2O**) in Å.

Pt(1)-S(1)	2.241(9)	C(7)-C(8)	1.31(4)
Pt(1)-S(2)	2.232(9)	C(8)-C(9)	1.34(4)
Pt(1)-N(1)	2.03(2)	C(8)-C(15)	1.61(4)
Pt(1)-N(2)	2.01(2)	C(9)-C(10)	1.39(4)
S(1)-C(20)	1.72(4)	C(11)-C(12)	1.50(5)
S(2)-C(19)	1.78(6)	C(11)-C(13)	1.49(5)
N(1)-C(1)	1.40(3)	C(11)-C(14)	1.54(4)
N(1)-C(5)	1.33(4)	C(15)-C(16)	1.48(4)
N(2)-C(6)	1.40(3)	C(15)-C(17)	1.58(5)
N(2)-C(10)	1.22(4)	C(15)-C(18)	1.47(4)
C(1)-C(2)	1.36(5)	C(19)-C(20)	1.39(6)
C(2)-C(3)	1.36(5)	C(19)-C(24)	1.42(8)
C(3)-C(4)	1.44(5)	C(20)-C(21)	1.47(6)
C(3)-C(11)	1.47(4)	C(21)-C(22)	1.39(7)
C(4)-C(5)	1.39(4)	C(22)-C(23)	1.40(8)
C(5)-C(6)	1.42(4)	C(23)-C(24)	1.42(9)
C(6)-C(7)	1.41(4)	C(23)-C(25)	1.38(11)

Compound (**2•0.5C_6H_6**) crystallizes in the space group *P-1*. The structure is dominated by the donor and acceptor molecules being stacked in a 1:1 ratio. The DNF acceptor molecule is situated directly above the donor which allows for more orbital overlap between the acceptor and the M-tdt unit. Studies by Eisenberg and coworkers commencing in 1989 and later in 1996 illustrated, by spectroscopic methods, that the HOMO for the M(diimine)(dithiolate) family of inorganic donors is composed of this unit.[58,66] The X-ray crystal structure for (**2•0.5C_6H_6**) and the contents of its unit cell are is depicted in Figures 86 and 87. Bond distances for (**2•0.5C_6H_6**) are presented in Table 57.

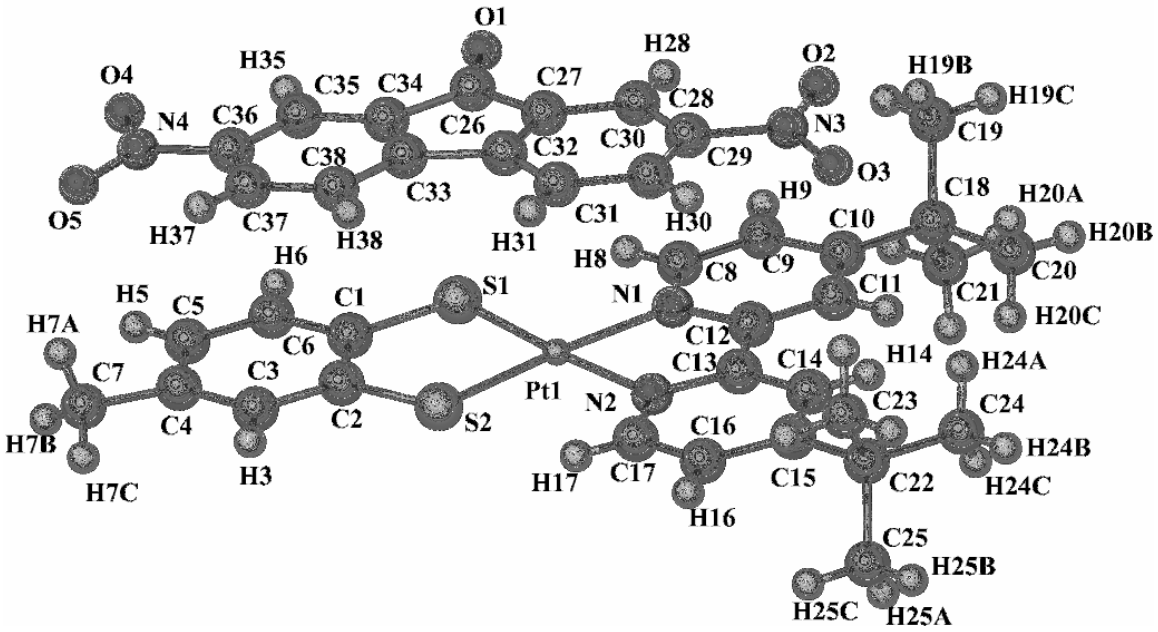

Figure 86. X-ray crystal structure for [Pt(dbbpy)(tdt)] [DNF]•0.5C_6H_6 (**2•0.5C_6H_6**). Interstitial benzene molecules have been omitted for the sake of clarity.

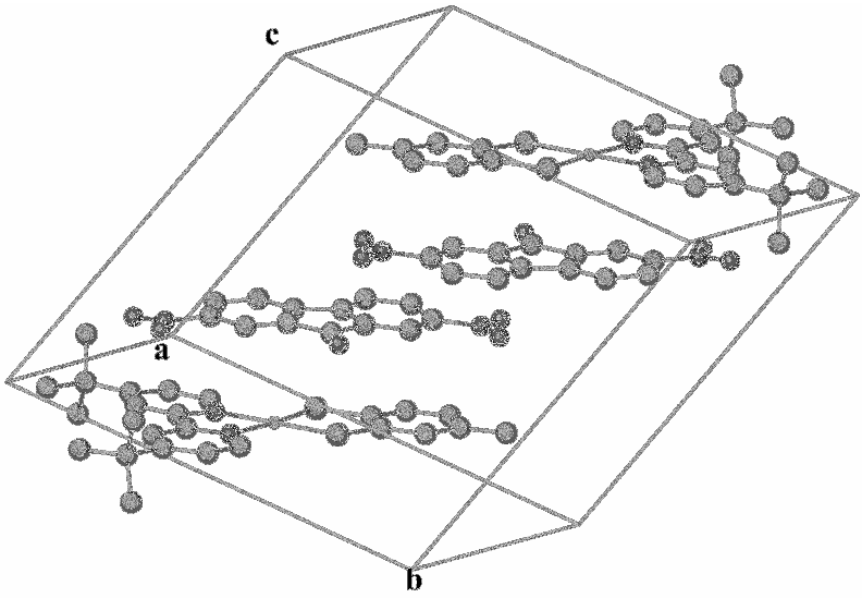

Figure 87. Contents of the unit cell for **2•0.5C_6H_6** illustrating the one-dimensional stacking motif for the donor and acceptor molecules. Hydrogen atoms and interstitial benzene molecules have been removed for the sake of clarity.

Table 57. Bond distances for [Pt(dbbpy)(tdt)][DNF]•0.5C_6H_6 (**2•0.5C_6H_6**) in Å.

Pt(1)-N(1)	2.080(3)	C(12)-C(13)	1.480(5)
Pt(1)-N(2)	2.066(3)	C(13)-C(14)	1.402(5)
Pt(1)-S(1)	2.2861(11)	C(14)-C(15)	1.411(5)
Pt(1)-S(2)	2.2735(12)	C(15)-C(16)	1.415(5)
S(1)-C(1)	1.796(4)	C(16)-C(17)	1.389(5)
S(2)-C(2)	1.786(4)	C(18)-C(19)	1.541(5)
N(1)-C(8)	1.356(5)	C(18)-C(20)	1.541(5)
N(1)-C(12)	1.389(5)	C(18)-C(21)	1.559(5)
N(2)-C(13)	1.374(4)	C(10)-C(18)	1.547(5)
N(2)-C(17)	1.361(4)	C(22)-C(23)	1.550(5)
N(3)-O(3)	1.241(5)	C(22)-C(24)	1.548(6)
N(3)-C(29)	1.496(5)	C(22)-C(25)	1.547(6)
N(4)-C(36)	1.497(5)	C(15)-C(22)	1.541(5)
O(1)-C(26)	1.226(5)	C(26)-C(27)	1.506(6)
O(2)-N(3)	1.234(5)	C(27)-C(28)	1.400(5)
O(4)-N(4)	1.234(4)	C(27)-C(32)	1.416(5)
O(5)-N(4)	1.243(4)	C(28)-C(29)	1.390(6)
C(1)-C(2)	1.403(5)	C(29)-C(30)	1.395(6)
C(2)-C(3)	1.416(5)	C(30)-C(31)	1.402(5)
C(3)-C(4)	1.398(6)	C(31)-C(32)	1.394(6)
C(4)-C(5)	1.412(6)	C(32)-C(33)	1.510(5)
C(4)-C(7)	1.525(7)	C(33)-C(34)	1.405(5)
C(5)-C(6)	1.393(5)	C(34)-C(35)	1.402(5)
C(1)-C(6)	1.420(5)	C(26)-C(34)	1.514(5)
C(8)-C(9)	1.393(5)	C(33)-C(38)	1.397(5)
C(9)-C(10)	1.414(5)	C(35)-C(36)	1.400(5)
C(10)-C(11)	1.390(5)	C(36)-C(37)	1.398(5)
C(11)-C(12)	1.409(5)	C(37)-C(38)	1.402(5)

The solid state structures for (**3•C_6H_6**) and (**4•2C_6H_6**) crystallize in the space groups *Fdd2* and *$P2_1/n$* respectively. Both compounds are dominated by maximum orbital overlap allowing for orbital interactions between the HOMO of the donor molecule and the π-orbitals of the acceptor molecules, but are different with respect to the ratio of donor and acceptor molecules. The X-ray structure for (**3•C_6H_6**) revealed a 1:1 ratio of the donor and acceptor molecules, whereas the structure for (**4•2C_6H_6**) exhibits a 2:1 ratio of D:A molecules wherein the TRNF molecule is sandwiched between the donor molecules. In the absence of the TRNF acceptor, the donor molecules are stacked head-to-tail in an eclipsed orientation. The X-ray crystal structures for and the contents of the unit cells for (**3•C_6H_6**), (**4•2C_6H_6**), and (**5•C_6H_6**) are depicted in Figures 88-93. Bond distances for these supramolecular systems are presented in Table 58-60.

Electrochemical Studies

Cyclic voltammetric studies of (**2•0.5C_6H_6**), (**3•C_6H_6**)**,** and (**4•2C_6H_6**) reveal two irreversible oxidations at +0.49 V and +0.90V which can be attributed to the oxidation of the M-tdt unit. Compound (**2•0.5C_6H_6**) shows two reversible reductions at -0.68 V and -0.90 V which can be attributed to the two reductions of the DNF acceptor. A third reduction at -1.30 V, which is irreversible, is assigned to reduction of the dbbpy ligand. Compound (**3•C_6H_6**) exhibits the same irreversible oxidations as (**2•0.5C_6H_6**) and reversible reductions, presumably acceptor-based, that occur at -0.42 V and -0.68 V. The experimental cutoff for the electrochemical analysis of (**3•C_6H_6**) was stopped at -1.0 V preventing the observation of the third, reversible acceptor-based reductions and the dbbpy ligand reduction.

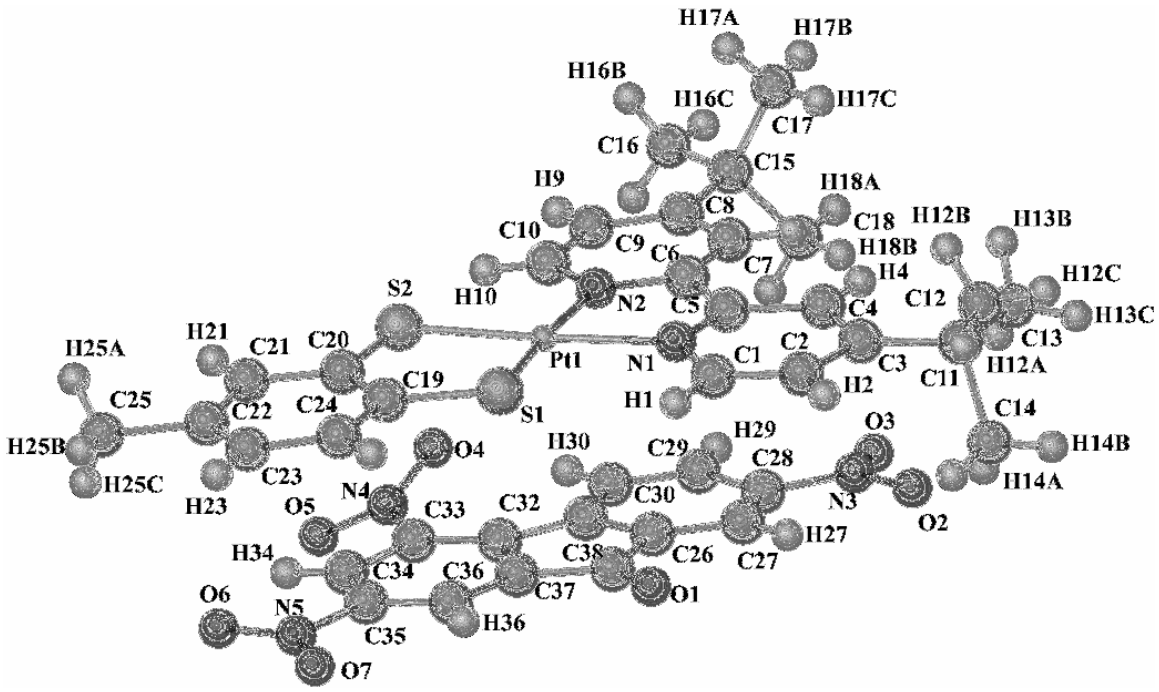

Figure 88. X-ray crystal structure of [Pt(dbbpy)(tdt)][TRNF]•C_6H_6 (**3•C_6H_6**). Interstitial benzene molecules have been omitted for the sake of clarity.

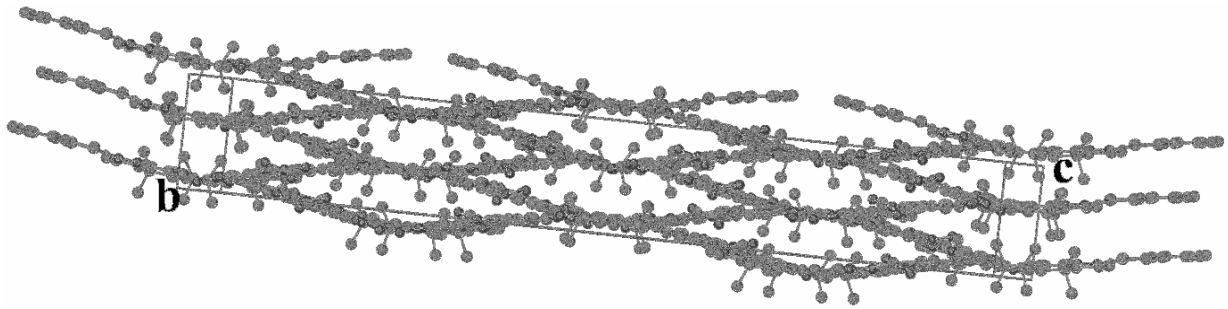

Figure 89. Contents of the unit cell for (**3•C_6H_6**) illustrating the stacking motif. Hydrogen atoms and interstitial benzene molecules have been removed for the sake of clarity.

Table 58. Bond distances for [Pt(dbbpy)(tdt)][TRNF]•C_6H_6 (**3•C_6H_6**) in Å.

Pt(1)-S(2)	2.261(3)	C(11)-C(14)	1.43(2)
S(1)-C(19)	1.728(16)	C(15)-C(16)	1.53(2)
S(2)-C(20)	1.750(18)	C(15)-C(17)	1.52(2)
N(1)-C(1)	1.365(18)	C(15)-C(18)	1.508(19)
N(1)-C(5)	1.301(17)	C(19)-C(20)	1.38(2)
N(2)-C(6)	1.381(17)	C(19)-C(24)	1.38(2)
N(2)-C(10)	1.371(17)	C(20)-C(21)	1.44(2)
N(3)-O(2)	1.267(19)	C(21)-C(22)	1.48(3)
N(3)-O(3)	1.209(18)	C(22)-C(23)	1.31(3)
N(3)-C(28)	1.452(19)	C(22)-C(25)	1.58(2)
N(4)-O(4)	1.244(16)	C(23)-C(24)	1.38(2)
N(4)-O(5)	1.260(15)	C(26)-C(27)	1.394(18)
N(4)-C(33)	1.441(17)	C(26)-C(31)	1.434(18)
N(5)-O(6)	1.248(16)	C(27)-C(28)	1.36(2)
N(5)-O(7)	1.203(15)	C(29)-C(28)	1.39(2)
N(5)-C(35)	1.460(19)	C(29)-C(30)	1.36(2)
O(1)-C(38)	1.195(15)	C(30)-C(31)	1.369(19)
C(1)-C(2)	1.350(19)	C(31)-C(32)	1.473(18)
C(2)-C(3)	1.377(2)	C(32)-C(33)	1.343(19)
C(3)-C(4)	1.411(2)	C(32)-C(37)	1.480(18)
C(3)-C(11)	1.520(2)	C(33)-C(34)	1.394(18)
C(4)-C(5)	1.459(2)	C(34)-C(35)	1.331(19)
C(5)-C(6)	1.433(2)	C(35)-C(36)	1.371(18)
C(6)-C(7)	1.381(2)	C(36)-C(37)	1.366(18)
C(7)-C(8)	1.398(2)	C(38)-C(26)	1.487(17)
C(8)-C(9)	1.376(2)	C(38)-C(37)	1.460(18)
C(8)-C(15)	1.52(2)		

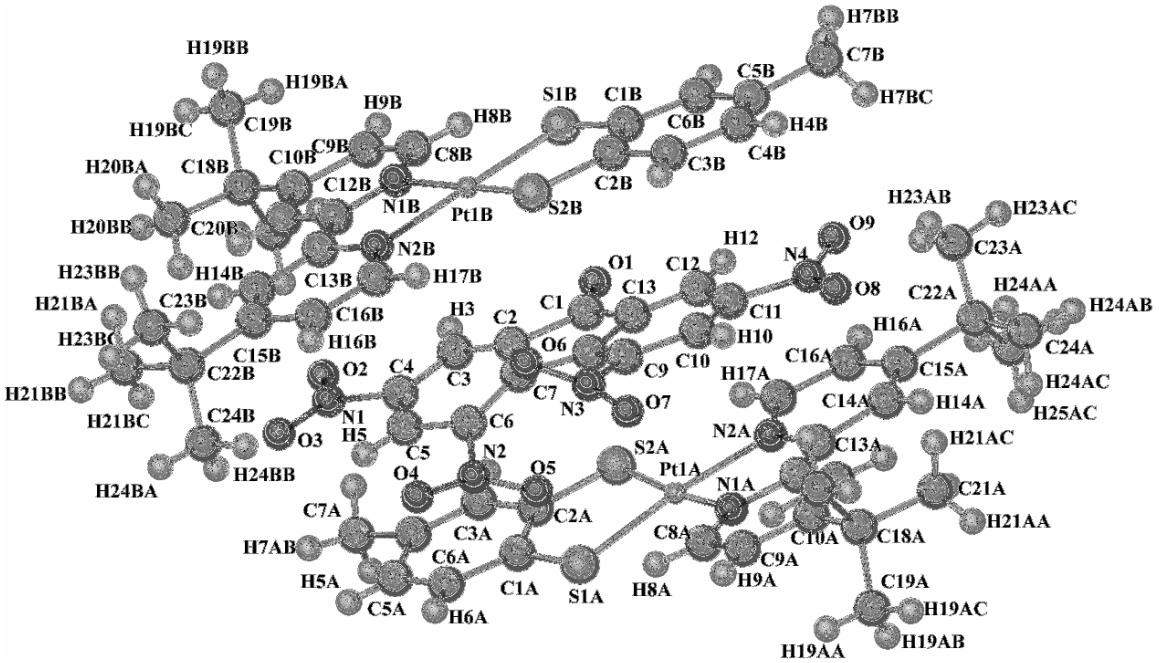

Figure 90. X-ray crystal structure of $[Pt(dbbpy)(tdt)]_2[TENF]\bullet 2C_6H_6$ (**4•2C$_6$H$_6$**). Interstitial benzene molecules have been omitted for the sake of clarity.

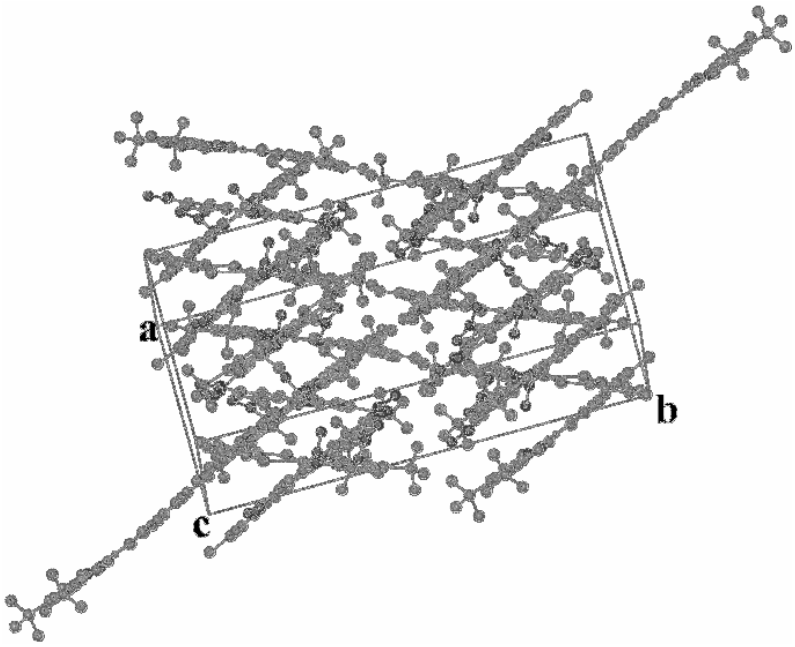

Figure 91. Contents of the unit cell for (**4•2C$_6$H$_6$**) illustrating the stacking motif. Hydrogen atoms and interstitial benzene molecules have been removed for the sake of clarity.

Table 59. Bond distances for $[Pt(dbbpy)(tdt)]_2[TENF]\cdot 2C_6H_6$ (**4•2C$_6$H$_6$**) in Å.

Pt(1A)-N(1A)	2.04(2)	O(4)-N(2)	1.207(3)
Pt(1A)-N(2A)	2.10(2)	O(5)-N(2)	1.207(3)
Pt(1B)-N(1B)	2.14(2)	O(6)-N(3)	1.207(3)
Pt(1B)-N(2B)	2.09(2)	O(7)-N(3)	1.207(3)
Pt(1A)-S(1A)	2.248(7)	O(8)-N(4)	1.207(3)
Pt(1A)-S(2A)	2.261(8)	C(1)-C(2)	1.50(4)
Pt(1B)-S(1B)	2.263(8)	C(1)-C(13)	1.43(4)
Pt(1B)-S(2B)	2.272(8)	C(1A)-C(2A)	1.43(4)
S(1A)-C(1A)	1.75(3)	C(1A)-C(6A)	1.43(4)
S(1B)-C(1B)	1.73(3)	C(1B)-C(2B)	1.35(4)
S(2B)-C(2B)	1.67(3)	C(1B)-C(6B)	1.46(4)
S(2A)-C(2A)	1.67(4)	C(1S)-C(2S)	1.40(4)
N(1)-C(4)	1.527(9)	C(1S)-C(6S)	1.40(4)
N(1A)-C(8A)	1.36(3)	C(2)-C(3)	1.24(3)
N(1A)-C(12A)	1.36(3)	C(2)-C(7)	1.43(3)
N(2)-C(6)	1.525(9)	C(2A)-C(3A)	1.37(4)
N(2A)-C(13A)	1.36(3)	C(2B)-C(3B)	1.40(4)
N(2A)-C(17A)	1.32(3)	C(2S)-C(3S)	1.43(4)
N(1B)-C(8B)	1.31(3)	C(3)-C(4)	1.36(3)
N(1B)-C(12B)	1.32(3)	C(3A)-C(4A)	1.34(4)
N(2B)-C(13B)	1.35(3)	C(3B)-C(4B)	1.39(4)
N(2B)-C(17B)	1.207(3)	C(3S)-C(4S)	1.27(4)
N(3)-C(9)	1.525(9)	C(4)-C(5)	1.34(3)
N(4)-O(9)	1.207(3)	C(4A)-C(5A)	1.42(4)
N(4)-C(11)	1.527(9)	C(4A)-C(7A)	1.52(4)
O(1)-C(1)	1.22(4)	C(4B)-C(5B)	1.30(4)
O(2)-N(1)	1.207(3)	C(4S)-C(5S)	1.42(4)
O(3)-N(1)	1.207(3)	C(5)-C(6)	1.36(3)

Table 59. Continued.

C(5A)-C(6A)	1.35(4)	C(12)-C(13)	1.31(4)
C(5B)-C(6B)	1.47(4)	C(12A)-C(13A)	1.43(4)
C(5B)-C(7B)	1.53(5)	C(12B)-C(13B)	1.44(3)
C(5S)-C(6S)	1.29(4)	C(13A)-C(14A)	1.48(4)
C(6)-C(7)	1.35(3)	C(13B)-C(14B)	1.38(3)
C(7)-C(8)	1.48(4)	C(14A)-C(15A)	1.26(4)
C(7S)-C(8S)	1.38(5)	C(14B)-C(15B)	1.41(3)
C(7S)-C(12S)	1.39(4)	C(15A)-C(16A)	1.41(4)
C(8)-C(9)	1.42(4)	C(15A)-C(22A)	1.62(4)
C(8)-C(13)	1.42(4)	C(15B)-C(16B)	1.40(3)
C(8A)-C(9A)	1.38(3)	C(15B)-C(22B)	1.56(4)
C(8B)-C(9B)	1.31(4)	C(16A)-C(17A)	1.42(4)
C(8S)-C(9S)	1.37(5)	C(16B)-C(17B)	1.38(3)
C(9)-C(10)	1.41(4)	C(18A)-C(19A)	1.540(2)
C(9A)-C(10A)	1.39(4)	C(18A)-C(20A)	1.545(2)
C(9B)-C(10B)	1.50(4)	C(18A)-C(21A)	1.537(2)
C(9S)-C(10S)	1.37(4)	C(18B)-C(19B)	1.57(4)
C(10)-C(11)	1.27(4)	C(18B)-C(20B)	1.47(3)
C(10A)-C(11A)	1.38(4)	C(18B)-C(21B)	1.52(4)
C(10A)-C(18A)	1.69(5)	C(18C)-C(20C)	1.537(2)
C(10A)-C(18C)	1.41(4)	C(18C)-C(21C)	1.540(2)
C(10B)-C(11B)	1.35(3)	C(18C)-C(19C)	1.544(2)
C(10B)-C(18B)	1.50(4)	C(22A)-C(23A)	1.62(4)
C(10S)-C(11S)	1.38(5)	C(22A)-C(24A)	1.42(4)
C(11)-C(12)	1.32(4)	C(22A)-C(25A)	1.45(4)
C(11A)-C(12A)	1.32(3)	C(22B-C(23B)	1.62(4)
C(11B)-C(12B)	1.38(3)	C(22B)-C(24B)	1.56(4)
C(11S)-C(12S)	1.37(4)	C(22B)-C(25B)	1.48(4)

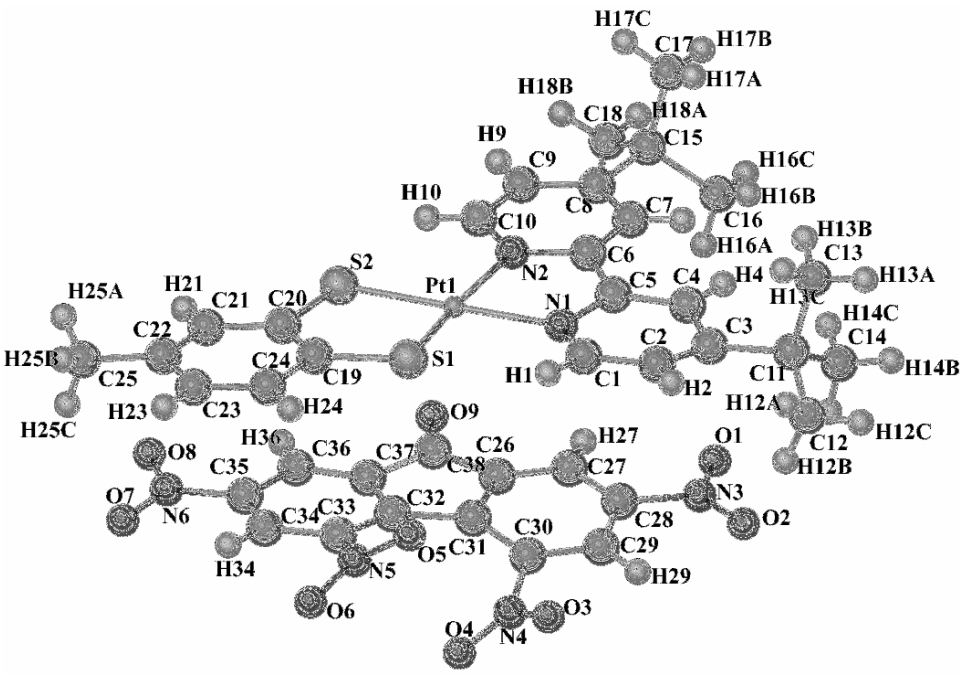

Figure 92. X-ray crystal structure of [Pt(dbbpy)(tdt)][TENF]•C_6H_6 (**5•C_6H_6**). Interstitial benzene molecules have been omitted for the sake of clarity.

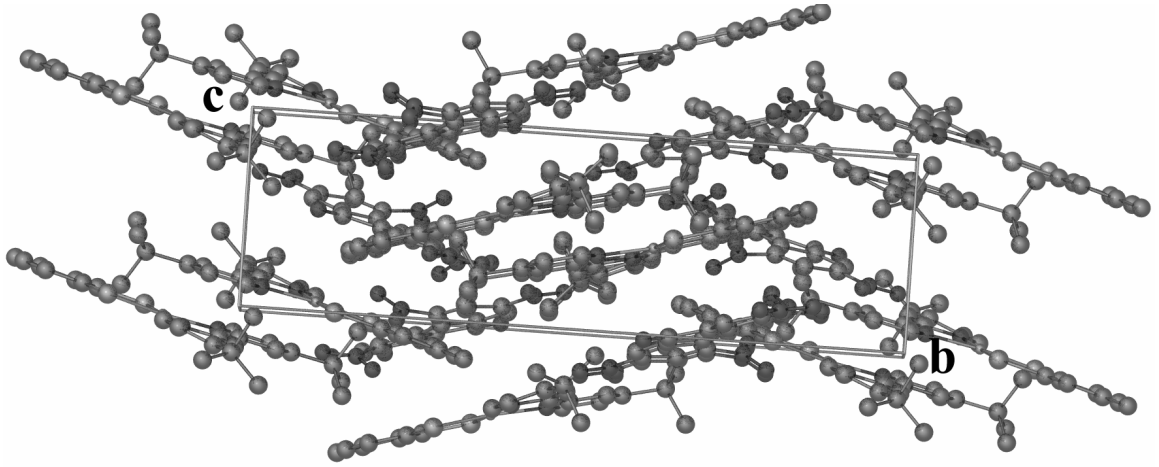

Figure 93. Contents of the unit cell for (**5•C_6H_6**) illustrating the intermolecular stacking motif via top views (**a**) and side views (**b**). Hydrogen atoms and interstitial benzene molecules have been removed for the sake of clarity.

Table 60. Bond distances for [Pt(dbbpy)(tdt)][TENF]•C_6H_6 (**5•C_6H_6**) in Å.

Pt(1)-S(1)	2.243(4)	C(9)-C(10)	1.390(3)
Pt(1)-S(2)	2.251(4)	C(11)-C(12)	1.536(3)
Pt(1)-N(1)	2.052(2)	C(11)-C(13)	1.536(5)
Pt(1)-N(2)	2.085(2)	C(11)-C(14)	1.541(7)
N(1)-C(1)	1.349(3)	C(15)-C(16)	1.565(8)
N(1)-C(5)	1.390(6)	C(15)-C(17)	1.503(4)
N(2)-C(6)	1.390(5)	C(15)-C(18)	1.562(9)
N(2)-C(10)	1.390(6)	S(1)-C(19)	1.722(8)
N(3)-C(28)	1.500(4)	S(2)-C(20)	1.799(6)
N(3)-O(2)	1.244(5)	C(19)-C(20)	1.378(5)
N(3)-O(1)	1.222(2)	C(19)-C(24)	1.413(7)
N(4)-C(30)	1.459(2)	C(20)-C(21)	1.405(3)
N(4)-O(3)	1.233(3)	C(21)-C(22)	1.374(5)
N(4)-O(4)	1.217(6)	C(22)-C(23)	1.417(2)
N(5)-C(33)	1.477(7)	C(23)-C(24)	1.355(4)
N(5)-O(5)	1.231(6)	C(22)-C(25)	1.474(6)
N(5)-O(6)	1.223(8)	C(26)-C(27)	1.370(2)
N(6)-C(33)	1.471(5)	C(26)-C(31)	1.408(3)
N(6)-O(7)	1.213(2)	C(26)-C(38)	1.478(8)
N(6)-O(8)	1.234(2)	C(27)-C(28)	1.378(6)
O(9)-C(38)	1.211(3)	C(28)-C(29)	1.371(3)
C(1)-C(2)	1.378(6)	C(29)-C(30)	1.379(5)
C(2)-C(3)	1.396(8)	C(30)-C(31)	1.401(6)
C(3)-C(4)	1.390(6)	C(31)-C(32)	1.478(5)
C(3)-C(11)	1.539(8)	C(32)-C(33)	1.393(7)
C(4)-C(5)	1.390(7)	C(32)-C(37)	1.410(2)
C(5)-C(6)	1.384(2)	C(33)-C(34)	1.388(5)
C(6)-C(7)	1.390(2)	C(34)-C(35)	1.375(6)
C(7)-C(8)	1.390(5)	C(35)-C(36)	1.390(5)
C(8)-C(9)	1.390(9)	C(36)-C(37)	1.364(8)
C(8)-C(15)	1.597(2)	C(37)-C(38)	1.501(2)

Compound (**4•2C_6H_6**) illustrates similar anodic behavior as the previous systems and shows a cathodic behavior similar to that of the pure TENF acceptor with the first and second reversible oxidations in (**3•C_6H_6**) occurring at -0.20 and -0.65 V. In a fashion similar to (**3•C_6H_6**) the electrochemical range of the experiment for (**4•2C_6H_6**) was halted at -1.0 V which prevented the observation of the other acceptor-based reduction waves and the dbbpy ligand reduction. It is important to note that our experimental interest was in the observation of the first-reduction potential of the acceptor as this value was central to our selection of the nitrofluorenone acceptors and not the reduction of the diimine ligand. For all compounds, halting the electrochemical experiments at -1.0 V made the observation of the acceptors reduction potential possible. The electrochemical potentials for (**2•0.5C_6H_6**), (**3•C_6H_6**), and (**4•2C_6H_6**) are listed in Table 61 and the voltammograms are represented by Figures 94-96.

Table 61. Summary of electrochemical potentials for (**2•0.5C_6H_6**), (**3•C_6H_6**), and (**4•2C_6H_6**) in volts.[a,b]

compound	$E_{1/2}$(ox), donor	$E_{1/2}$(red), acceptor
[Pt(dbbpy)(tdt)][DNF]•0.5C_6H_6 (**2**•0.5C_6H_6)	+0.49	-0.70
	+0.90	-0.90
[Pt(dbbpy)(tdt)][TRNF]•C_6H_6 (**3**•C_6H_6)	+0.50	-0.42
	+0.88	-0.68
[Pt(dbbpy)(tdt)]$_2$[TENF]•2C_6H_6 (**4**•2C_6H_6)	+0.48	+0.18
	+0.86	-0.25

[a] Values are volts vs.Ag/AgCl, Pt disk electrode in 0.1 M $TBAPF_6/CH_2Cl_2$ at a scan rate of 100 mV/s.

[b] Experimental runs were stopped at a lower limit of -1.0 V. This prevented the observation of the dbbpy ligand-based reduction and the observation of an additional cathodic response from the TRNF and TENF acceptors.

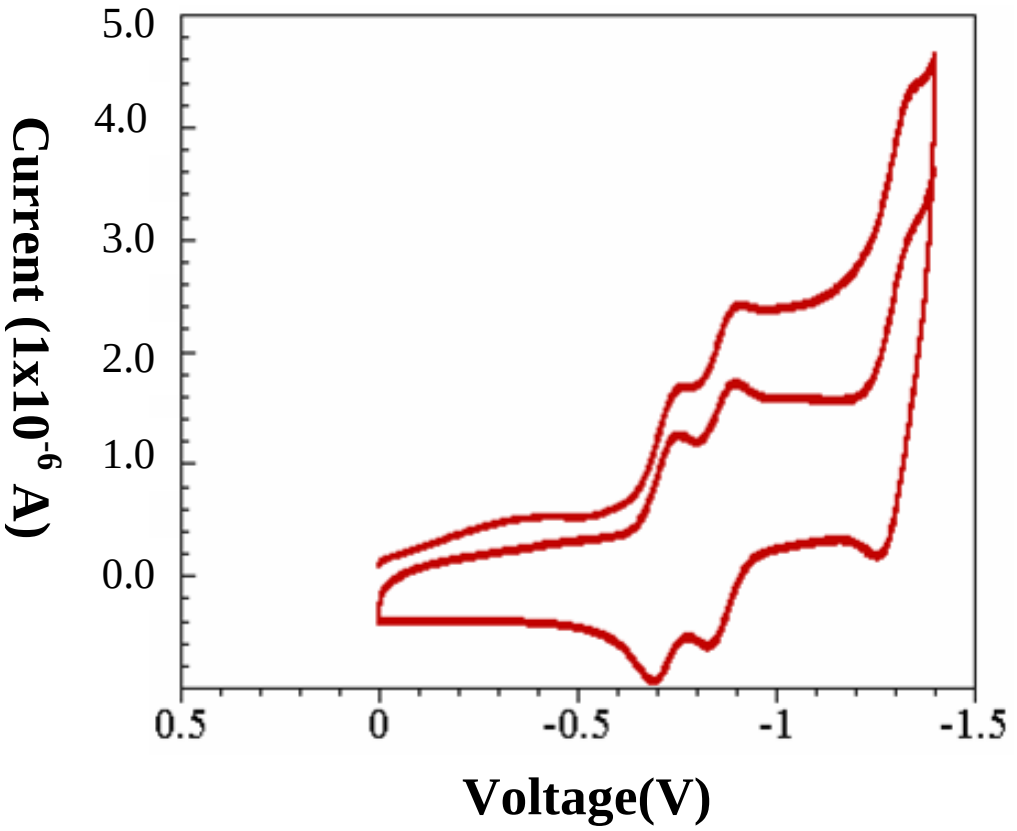

Figure 94. Cyclic voltammogram for (**2•0.5C_6H_6**) performed in a 0.1 M $TBAPF_6$ solution prepared from CH_2Cl_2 at a scanning potential of .2 V/s against Ag/AgCl reference electrode using a Pt disk working electrode and a Pt wire counter electrode.

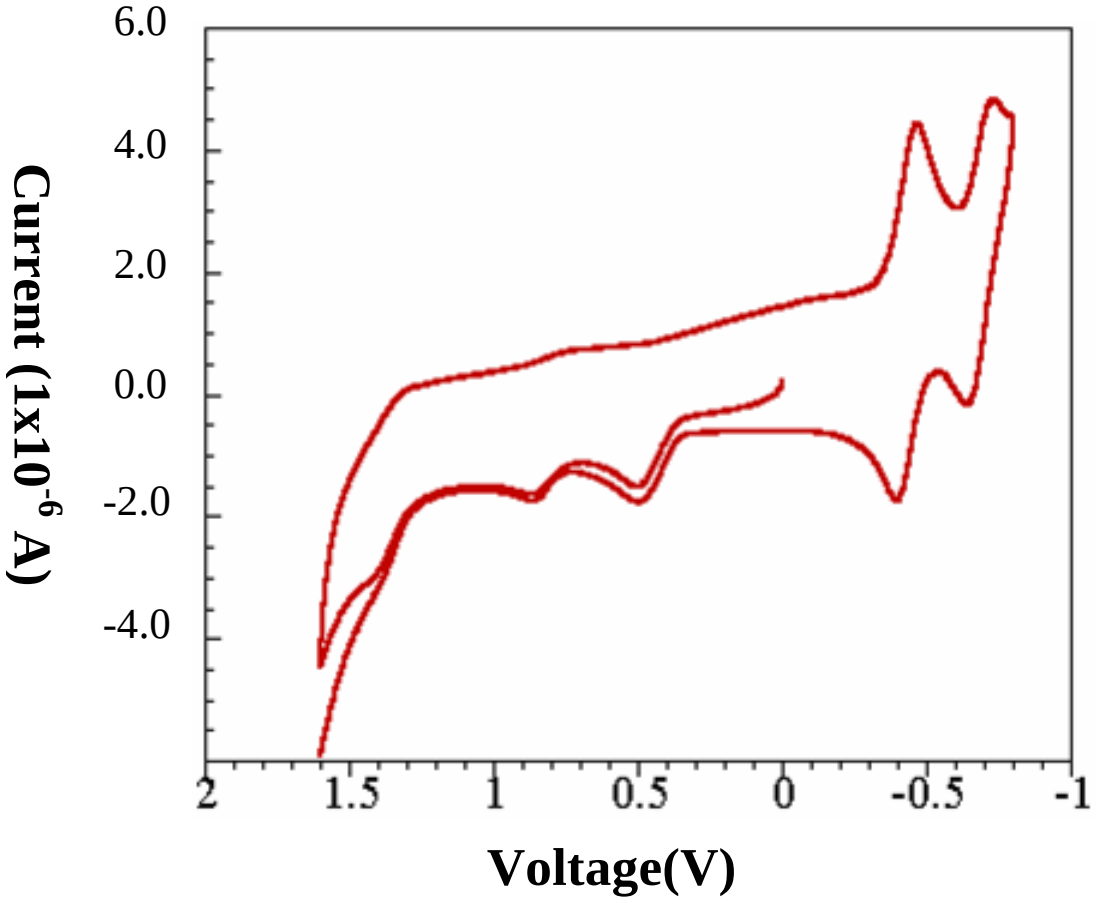

Figure 95. Cyclic voltammogram for (**3•C_6H_6**) performed in a 0.1 M $TBAPF_6$ solution prepared from CH_2Cl_2 at a scanning potential of .2 V/s against Ag/AgCl reference electrode using a Pt disk working electrode and a Pt wire counter electrode.

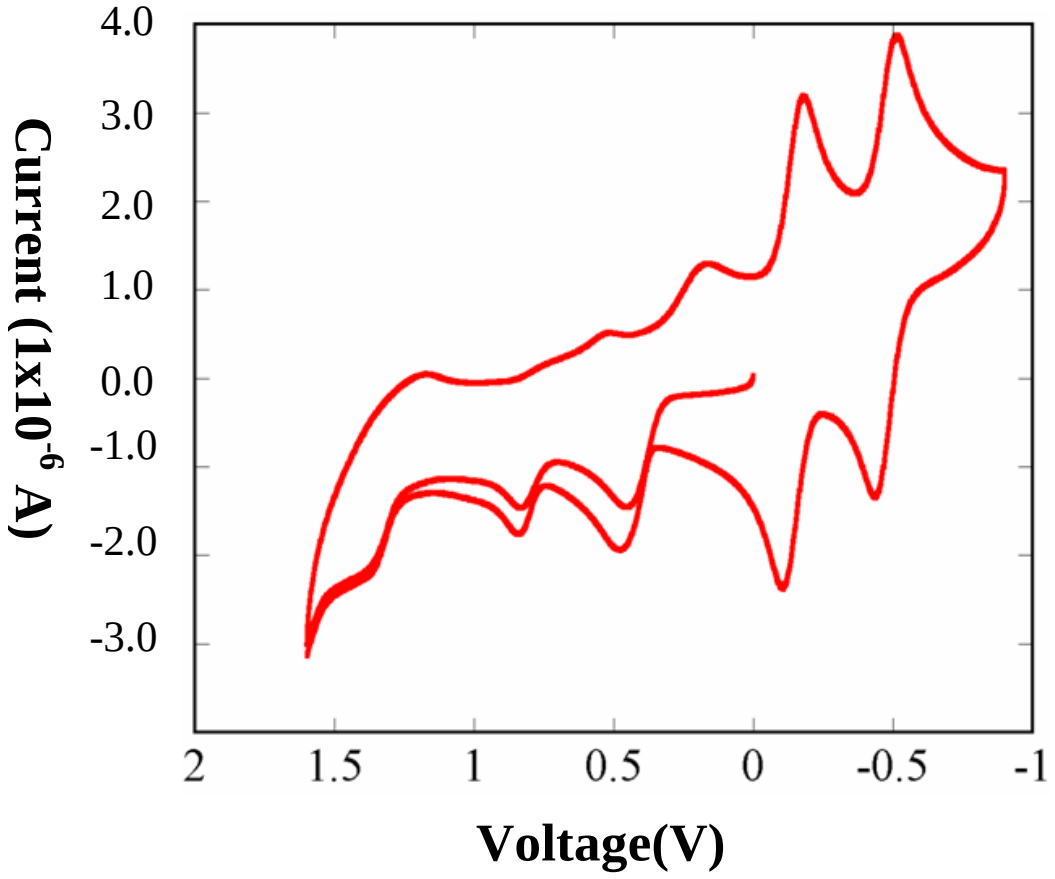

Figure 96. Cyclic voltammogram for (**4•2C_6H_6**) performed in a 0.1 M $TBAPF_6$ solution prepared from CH_2Cl_2 at a scanning potential of .2 V/s against Ag/AgCl reference electrode using a Pt disk working electrode and a Pt wire counter electrode.

Spectroscopic Studies

The UV-VIS-NIR spectra for complexes (**2•0.5C_6H_6**), (**3•C_6H_6**), and (**5•C_6H_6**) were performed at room temperature using an exact amount of Pt(dbbpy)tdt and adding in an exact amount of nitrofluorenone from a stock solution then diluting to 25 mL. The resulting solutions were used immediately to collect the spectral data. For the solid spectral data the solutions used for UV-VIS-NIR were mixed together and the volume reduced under reduced pressure. The solution was then reconstituted to 25mL by addition of dichloromethane and benzene. The solutions were allowed to slowly evaporate under argon. The resultant solid crystalline product was collected and placed on a Whatman filter paper. The filter paper was used as the substrate for reflectance measurements for the solids. The UV-VIS-NIR data for (**2•0.5C_6H_6**) show very little change in the low energy region beyond the CT band of the Pt(dbbpy)tdt (Figures 97 and 98). The 1 cm cuvette measurements reveal very little change in the extinction coefficients of the Pt(dbbpy)tdt which would be expected if there were significant interactions in solution. However in the solid state there is evidence that there is some interaction between DNF and Pt(dbbpy)tdt. The solid state reflectance data for the powder show no growth of a new band in the low energy region below the CT of the Pt(dbbpy)tdt. This is attributed to the weak interactions between the DNF and the Pt(dbbpy)(tdt) which make the CT less favored.

The absorption spectra for the titration of Pt(dbbpy)(tdt) with TRNF are shown in Figure 99. The spectra show that there is a much stronger interaction between the TRNF and Pt(dbbpy)tdt. This is evident by the growth of a new absorption band in the 825 nm region. This band grows in intensity with increasing concentration of TRNF. The band is very strong in the reflectance spectrum of the solids. The solution data at 825 nm was fit using the method of Benesi and Hildebrand (Figure 100).[119] The equilibrium constant is 553 and the extinction coefficient is 102 mol^{-1} cm^{-1}. The trinitrofluorenone is a slightly stronger acceptor compared to the DNF but weaker than the TENF.

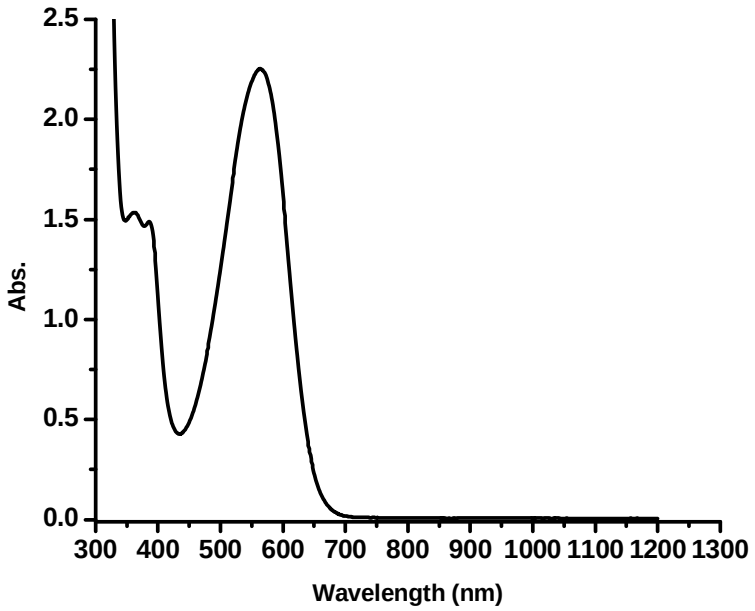

Figure 97. Absorption spectrum for Pt(dbbpy)(tdt) in CH_2Cl_2 at RT in a 1cm cuvette showing the CT band and no NIR bands. (5 x 10^{-4} M).

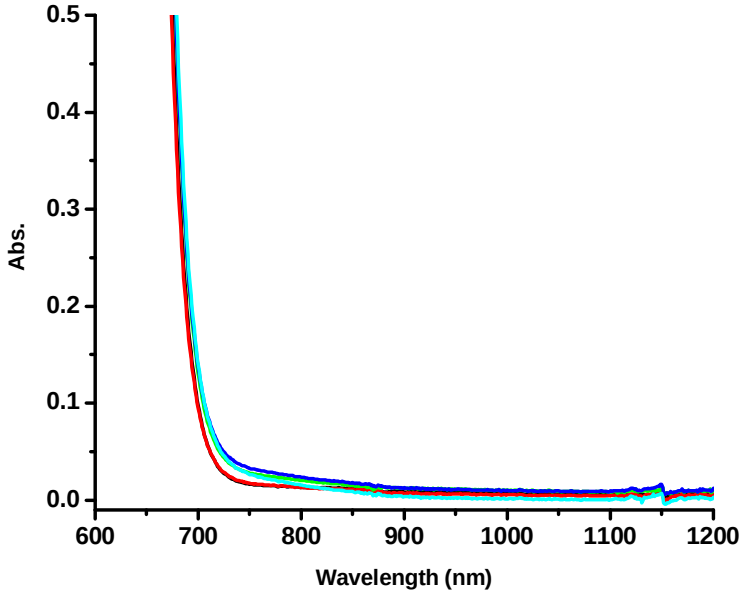

Figure 98. Absorption spectra for Pt(dbbpy)(tdt) titrated with DNF, showing almost no change in the visible or NIR range.

The 1 cm cuvette measurements show only slight fluctuations in the CT band of the Pt(dbbpy)tdt that are within the experimental error. The new band at 825 nm is attributed to the CT of the complex [Pt(dbbpy)(tdt)] [TRNF] in solution. The TRNF being a weaker acceptor than the TENF should have less affinity to the electron rich Pt(dbbpy)(tdt). The extinction coefficient is higher than that found for the TENF adduct though which contributes to the intensity of the CT even though there is less complex in solution. The TENF adduct shows a very strong band at 950 nm that grows larger with each addition of the TENF (Figure 101). The titration data was fit using the same method as **2** (Figure 102) revealing a higher equilibrium constant K = 6,080 which is indicative of the TENFs strong attraction to the electron rich Pt(dbbpy)(tdt). The adduct has an extinction coefficient of 32.89 M^{-1} cm^{-1} that is most evident in the solid spectra in which

this lower energy band is a dominant feature in Figure 102. The evidence of such strong interactions between Pt(diimine)(dithiolate) complexes and strong electron acceptors has been previously reported.[68]

The diffuse reflectance data, Figure 103, show that the complexes exist in the solid state. The CT band due to the complex is readily seen in the spectra as a dominant absorption, which extends the absorption range far into the NIR region compared to the Pt(dbbpy)(tdt) alone and the free nitrofluorenone's which shows no absorptions beyond 450 nm.

The absorption data indicate that the stronger the acceptor the more likely a new band will be seen in the spectra. The amount of new complex in solution, is dependant upon the concentration of the acceptor, exist in equilibrium with the free components in solution. Therefore it is difficult to see the band in a 1 cm cuvette. The data in the solid state should be dependant upon the stacking mode as well therefore the data shown is for samples whose structure was determined prior to collecting the data. In the solutions however one cannot the stoichiometry of the complex, which in this case is assumed to be 1:1.

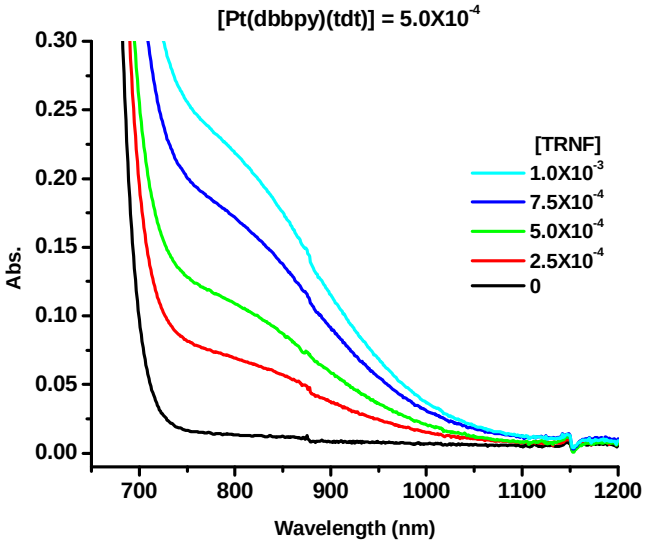

Figure 99. Absorption spectra showing the new CT band growth during the titration experiment for [Pt(dbbpy)(tdt)] [TRNF] in CH_2Cl_2 in a 10cm cuvette at RT.

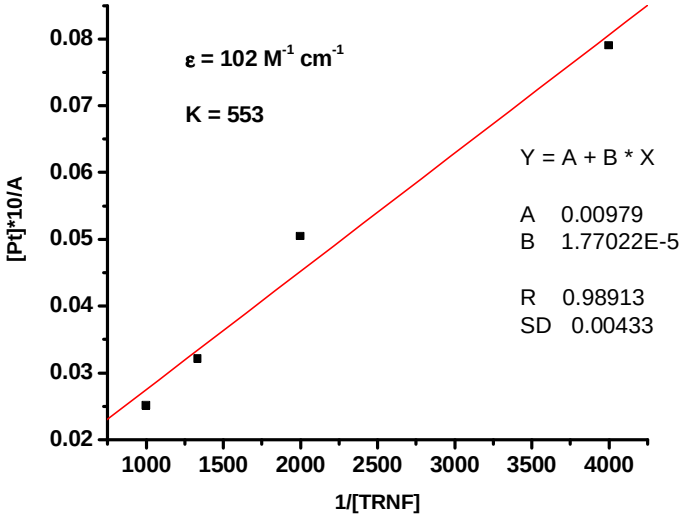

Figure 100. Benesi-Hildebrand plot for titrations of Pt(dbbpy)(tdt) with TRNF in CH_2Cl_2 at RT in a 10 cm cuvette for the absorption at 825 nm.

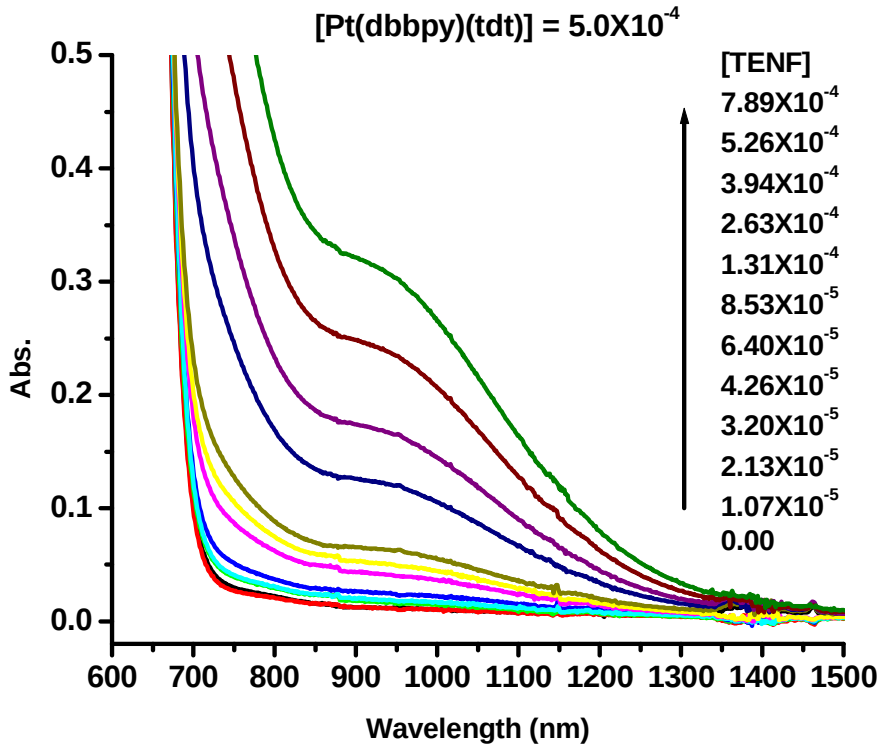

Figure 101. Absorption spectra showing the new CT band growth during the titration experiment for [Pt(dbbpy)(tdt)] [TENF] in CH_2Cl_2 in a 10cm cuvette at RT.

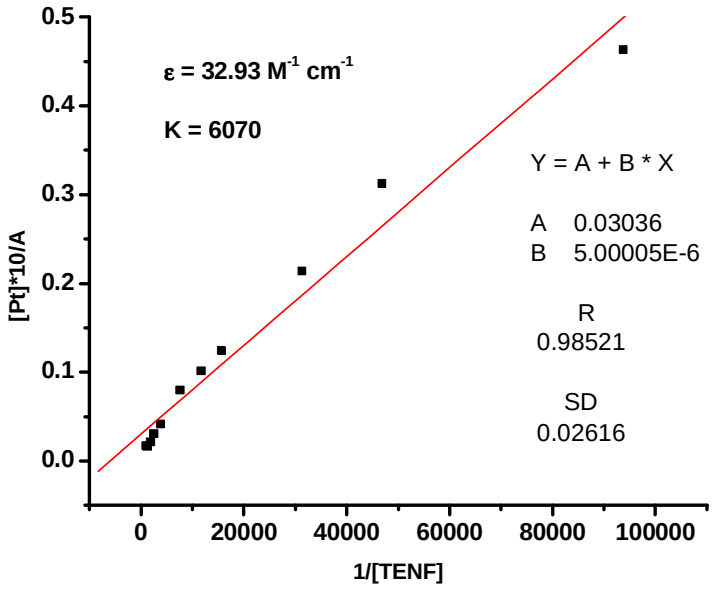

Figure 102. Benesi-Hildebrand plot for titrations of Pt(dbbpy)(tdt) with TENF in CH_2Cl_2 at RT in a 10 cm cuvette for the absorption at 950 nm.

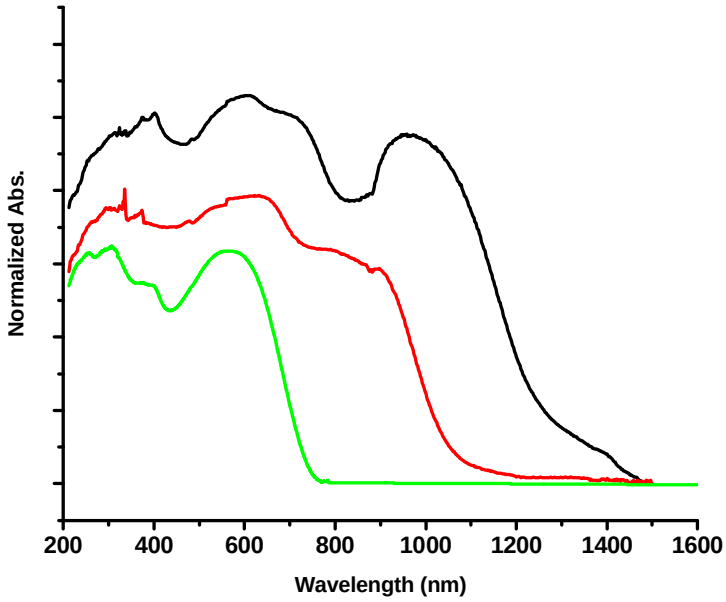

Figure 103. Solid state diffuse reflectance data for **5** (*top*), **2**(*middle*), and Pt(dbbpy)(tdt) (**1**) (*bottom*) showing the strong absorptions in the NIR region.

Magnetic Measurements

DC magnetic susceptibility measurements were done on samples of (**3•C_6H_6**) and (**5•C_6H_6**) in search of temperature independent paramagnetism indicative of conducting electrons. Despite seeing interactions between the donor and acceptor molecules, indicated in the Benesi-Hildebrand plots for (**3•C_6H_6**) and (**5•C_6H_6**), no TIP values were found to exist. In order to determine to the exact level of conductivity in the complexes, two- or four-probe conductivity measurements are planned in due course.

Conclusions

Four supramolecular adducts of the inorganic donor Pt(dbbpy)(tdt) with the nitrofluorenone family of acceptors were prepared by layering CH_2Cl_2 solutions of the donors with C_6H_6 solutions of the acceptors. Electrochemical analysis of the compounds revealed potentials indicative of the individual reagents as expected, while UV-VIS-NIR and diffuse reflectance measurements revealed interactions between Pt(dbbpy)(tdt) and the organic donors TRNF and TENF. Similar analysis for Pt(dbbpy)(tdt) and DNF revealed no formation of low-energy bands extending into the NIR, indicating little to no interaction between the constituent molecules.

In the real of solar energy systems low band gap dyes are ideal. For a solar cells based on SnO_2 or TiO_2, it is unknown if the nitrofluorenone will bind to surface of the semiconductor. The ability to bind to a surface is circumvented when the species is used in a photovoltaic device where the complex is deposited as a thin film or the components can be deposited as separate layers. The whole class of complexes should be great starting points for a new breed of solar cell dyes and conductors.

CHAPTER VI

X-RAY CRYSTALLOGRAPHIC AND ELECTROCHEMICAL STUDIES OF Pt-TRIIMINE SALTS*

Introduction

$[Pt(terpy)Cl]^+$ salts have received considerable attention in the last few years due to their applicability to DNA intercalation, protein probing, and inorganic spectroscopy.[120-124] This broad-reaching applicability to different branches of chemistry has been determined to be dependent on the open coordination sites of the molecule and its potential water solubility. The pioneering work of McMillan and coworkers led to the discovery of the rich spectroscopic behavior of the $[Pt(triimine)X]^+$ class of molecules with X^- = Cl^-, NCS^-, OMe^-, or OH^- which were found to exhibit near-UV and short-wavelength visible absorptions which were assigned to spin-allowed metal-to-ligand transitions (^{1}MLCT); the emission bands have been attributed to spin-forbidden transitions (^{3}MLCT). Interesting spectroscopic and photophysical behavior has been observed in these molecules when other substituted terpyridine ligands as well as other triimine ligands and even different X and Y groups have been utilized. Along with the spectroscopic studies of these compounds, Yam and coworkers undertook studies of the structural and electrochemical properties of these salts.[70,71] Compututional studies of the $[Pt(triimine)X]^+$ family of molecules revealed that, much like the Pt(diimine)(dithiolate)

*Part of the data from this chapter is reprinted with permission from "Coarse and Fine Tuning of the Electronic Energies of Triimineplatinum(II) Square-Planar Complexes", 2006. *Inorganic Chemistry*, 45, pgs. 2770-2772, Copyright 2006 American Chemical Society.

molecules studied extensively by Eisenberg and coworkers, the HOMO of these molecules consists of a hybrid molecular orbital incorporating contributions from the atomic orbitals of both the metal and the ligand "X".[66] The LUMO of these triimine molecules, is dominated by contributions from the chelating nitrogen-containing ligand. The solid-state structures presented to date by Yam and coworkers are all dominated by divalent platinum atoms in a distorted square-planar environment. This specific ligation mode is caused by the bite angles of the tris(t-butyl-terpyridine) ligand, which causes alteration of the typical angles of 90 and 180°. Yam and coworkers also provided a benchmark for beginning to understand the electrochemistry of the $[Pt(triimine)X]^+$ family of compounds. According to their work, there were two reversible reductions attributed to the terpyridyl ligand, which showed little to no alteration in their respective $E_{1/2}$ values regardless of the substituents present on the pyridyl rings.[70] An irreversible oxidation wave attributed to the Pt(II) → Pt(III) process was also located and found to depend on the fourth ligand in the coordination sphere of the cationic unit. The oxidation wave for the complexes studied by Yam and coworkers were found to occur at more positive potentials for complexes with less electron rich alkynyl ligands. When considering the research of McMillan and Yam who were interested in the spectroscopic behavior and how these behaviors could be tailored for biological studies, it is possible that the spectroscopic response could be extended to applications such as solar energy conversion, electrical conductivity, molecular magnetism, donor-acceptor chemistry, and supramolecular assemblies.

The previous chapter dealt with work from the combined groups of the Prof. Kim Dunbar at Texas A&M University and that of Prof. Mohammad Omary at the University

of North Texas where inorganic Pt(diimine)(dithiolate) donors were combined with organic donors to prepare potential photosensitizing dyes for colloidal semiconductors composed of TiO_2. Analysis of the conversion efficiencies of the adsorbed dyes showed poor conversion and was attributed to a mismatch of the electrochemical potentials between the organic acceptor and the conduction band of the semiconductor. To circumvent this problem, the $[Pt(triimine)X]^+[TCNQ]^-$ family of salts were used to target solar cells composed of SnO_2, as the singly-reduced TCNQ acceptor necessary to neutralize the cationic charge from the square-planar unit exhibits a reduction potential that is closer to the electrochemical potential of this semiconductor. Through the combined efforts of both research groups, the solid-state structures for a several members of the $[Pt(triimine)X]^+$ family have been obtained. Additionally, cyclic voltammetry has been used to obtain the oxidation and reduction potentials for each of the members which support the order of charge transfer bands observed via spectroscopy conducted by the Omary group. Due to the fact that my responsibilities in this joint effort did not focus on the preparation and spectroscopic data, limited discussion related to these topics will be presented. A discussion of the solid-state structures and some of their corresponding electrochemical properties will be presented in order to demonstrate the systematic variation of both the X and Y ligands and counterions in this family of salts.

Experimental Section

All solvents used in the growth of X-ray quality single crystals were dried and freshly distilled prior to use. Dichloromethane and acetonitrile were dried over P_2O_5 and 3Å molecular sieves, respectively. Hexanes and diethyl ether were passed through an

MBRAUN solvent purification system prior to use. Crystal growth was carried out under a nitrogen atmosphere employing standard Schlenk-line techniques unless otherwise noted.

X-ray Crystallographic Details and Structure Solution

X-ray data for salts **1**, **2, 4, 5,** and **6** were collected on a Bruker SMART 1000 CCD diffractometer at 110±2 K. Salts **3**, **7,** and **8** were collected on a Bruker SMART APEX diffractometer also at 110±2 K. All X-ray data for the above listed salts were collected using graphite monochromated Mo-Kα (λ = 0.71073 Å) radiation. Due to the small size of the crystals, structures for **9-11** were determined from data collected on a Bruker D8 GADDS system at 110±2K with graphite monochromated Cu-Kα (λ = 1.54178 Å) radiation. The data were corrected for Lorentz and polarization effects. The Bruker SAINT software package was used to integrate the frames and the data were corrected for absorption using the SADABS program.[86,87] Space groups were unambiguously assigned by analysis of symmetry and systematic absences determined by XPREP.[88] The structures were solved by direct methods by the use of the SHELXS-97 program in the Bruker SHELXTL v5.1 software package.[89,90] The final refinements were carried out with anisotropic thermal parameters for all non-hydrogen atoms. Figures for the crystallographic structures were generated using the XSEED program.[91]

Other Physical Measurements

Cyclic voltammetry experiments were carried out at a scan rate of either 100 or 200 mV/s on a CH Instruments Electrochemical Analyzer in 0.1 or 0.2 M solutions of doubly-recrystallized $TBAPF_6$ in CH_2Cl_2 at a Pt disk working electrode with a Ag/AgCl reference and a Pt counter electrode.

Results and Discussion

*[Pt(tbtrpy)Cl][Cl] (**1**), [Pt(tbtrpy)(4-mbt)][BF_4] (**5**), and [Pt(tbtrpy)OH][TCNQ] (**9•2H_2O**)*

The syntheses of **1**, **2**, and **9** were performed in collaboration with researchers at the University of North Texas and were reported previously.[125] Yellow and red blocks of **1** and **2** respectively were grown by layering concentrated CH_2Cl_2 solutions of the solutions with an isomeric mixture of hexanes. Dark green needles of **9** were grown by slow evaporation of a concentrated CH_2Cl_2 solution in air.

*[Pt(tbtrpy)Cl][BF_4] (**2**) and [Pd(tbtrpy)Cl][BF_4] (**3**)*

The syntheses of **2** and **3** were prepared by metathesis of the starting materials with potassium or sodium salts of $[BF_4]^-$ with the starting materials [Pt(tbtrpyCl][Cl] and [Pd(tbtrpy)Cl][Cl]. Pale yellow blocks of the salts were prepared by diffusion of hexanes into concentrated CH_2Cl_2 solutions of **2** and **3** respectively.

*[Pt(tbtrpy)NCS][BF_4] (**4•CH_2Cl_2**), [Pt(tbtrpy)(2,5-dmeobt)][BF_4] (**6**), [Pt(tbtrpy)(snap)][BF_4] (**7•H_2O**), and [Pt(tbtrpy)(SO_2ph)][BF_4] (**8**)*

The salts **4** and **6-8** were prepared via slight modifications of the preparative procedure for **5**. Red blocks for all of the salts were prepared by layering CH_2Cl_2 solutions with an isomeric mixture of hexanes. The solid-state structure of **8** is an oxidation by-product of the intended synthetic target [Pt(tbtrpy)(sph)][BF_4].

*[Pt(tbtrpy)Cl][TCNQ] (**11•2CH_2Cl_2**), and [Pt(tbtrpy)CN][TCNQ] (**12•2CH_3CN**)*

Compounds **11** and **12** were found to be the result of ligand substitution into the coordination sphere of [Pt(tbtrpy(4-mbt)][TCNQ]. Dark green needles of **9** were grown by slow evaporation of CH_2Cl_2 solutions of the title compound. Dark green needles of **11** and **12** were grown by vapor diffusion of Et_2O into solutions of [Pt(tbtrpy)(4-mbt)][TCNQ] in CH_2Cl_2 and CH_3CN respectively.

X-ray Crystallography

A unifying feature present in the structures is the presence of distorted square-planar geometry around the platinum or palladium metal centers due to the presence of the tris-chelating tris(*t-butyl*)terpyridine ligand which occupies three of the four metal coordination sites. When looking at all of the crystallized tris(*t-butyl*)terpyridine salts, the coordination of this heteroatomic ligand forces two of the angles to become acute, while the remaining angles adopt obtuse values. The *t-butyl* groups on the pyridyl rings, added to enhance solubility, display typical angles of ~109.5°, indicative of tetrahedral groups possessing a sp^3-hybridized carbon atom.

*[Pt(tbtrpy)Cl][Cl] (**1**), [Pt(tbtrpy)Cl][BF_4] (**2**), and [Pd(tbtrpy)Cl][BF_4] (**3**)*

As stated above, **1-3** show distorted square-planar geometry where the acute angles adopt intermediate values between 80 and 81°, while the obtuse angles display values ranging from 99-101°. Salt **1** crystallizes in the monoclinic space group $P2_1/c$ while the structures for **2** and **3** are isostructural, crystallizing in the monoclinic space group $P2_1/n$. The bond distances between the transition metal center and nitrogen atoms in **1** and **3** are similar in distance for all of the salts. For **1**, the bond distances for Pt(1)-N(1) and Pt(1)-N(3) are 2.031(4) and 2.028(2) Å respectively. In salts **2** and **3**, the bond distances show values of 2.017(4) Å/2.037(2) Å and 2.016(2) Å/2.032(3) Å respectively, maintaining the similarity between these experimentally determined bond distances which was initially described in **1**.

Unlike the bonding between the nitrogen atoms and transition metal center, which resulted in the formation of bonds of equivalent distance trans to one another, the bond distances between nitrogen 2 and the metal is shorter than those involving nitrogen atoms 1 and 3. In the former bonding scenario, the bond existing between nitrogen 2 and the platinum/ palladium center is located trans to the metal-chlorine bond. Due to the enhanced electronegativity of the chlorine atom, there is a shortening of the metal-N(2) bond distance, a characteristic observed in all of the salts with distances of 1.936(4), 1.938(4), and 1.922(2) Å respectively for **1-3**. The latter two salts contain $[BF_4]^-$ to neutralize the charge of the square-planar cationic unit in the salts. For those systems, all tetrafluoroborate B-F bond distances are approximately 1.400 Å in length with bond angles of ~109.5°, characteristics of this tetrahedral anion. Crystallographic parameters for **1-3** are listed in Table 62. The X-ray crystal structures for **1-3** are depicted in Figures 104-106. The corresponding bond distances are presented in Tables 63-65.

Table 62. X-ray crystallographic and refinement data for **1-3.**

Compound	[Pt(tbtrpy)Cl][Cl] (**1**)	[Pt(tbtrpy)Cl][BF_4] (**2**)	[Pd(tbtrpy)Cl][BF_4] (**3**)
Formula	$PtCl_2N_3C_{27}H_{35}$	$PtClN_3C_{27}H_{35}BF_4$	$PdClN_3C_{27}H_{35}BF_4$
formula weight	666.19	718.22	629.16
Space group	$P2_1/c$	$P2_1/n$	$P2_1/n$
a, Å	15.874(3)	12.651(9)	12.670(3)
b, Å	13.128(26)	16.572(11)	16.570(3)
c, Å	17.699(4)	13.217(8)	13.290(3)
α, deg	90	90	90
β, deg	112.61(3)	92.07(2)	92.17(3)
γ, deg	90	90	90
volume, Å^3	3404.98	2769	2788.43
Z	4	4	4
μ, mm^{-1}	4.31	4.07	0.89
Temp.	110(2)	110(2)	110(2)
Reflns. collected	8146	6867	3979
Reflns. I>2σ	7194	4771	3791
Parameters	370	344	343
Restraints	0	0	0
R1[a]	0.0631	0.0432	0.0263
wR2[b]	0.2033	0.1111	0.1043
Goodness-of-fit[c]	1.019	1.080	0.950

[a] $R1 = \sum||F_o| - |F_c||/\sum|F_o|$. [b] $wR2 = [\sum [w(F_o^2-F_c^2)^2]/ \sum [w(F_o^2)^2]]^{1/2}$

[c] Goodness-of-fit = $[\sum w(|F_o|-|F_c|)^2/(N_{obs}-N_{parameter})]^{1/2}$

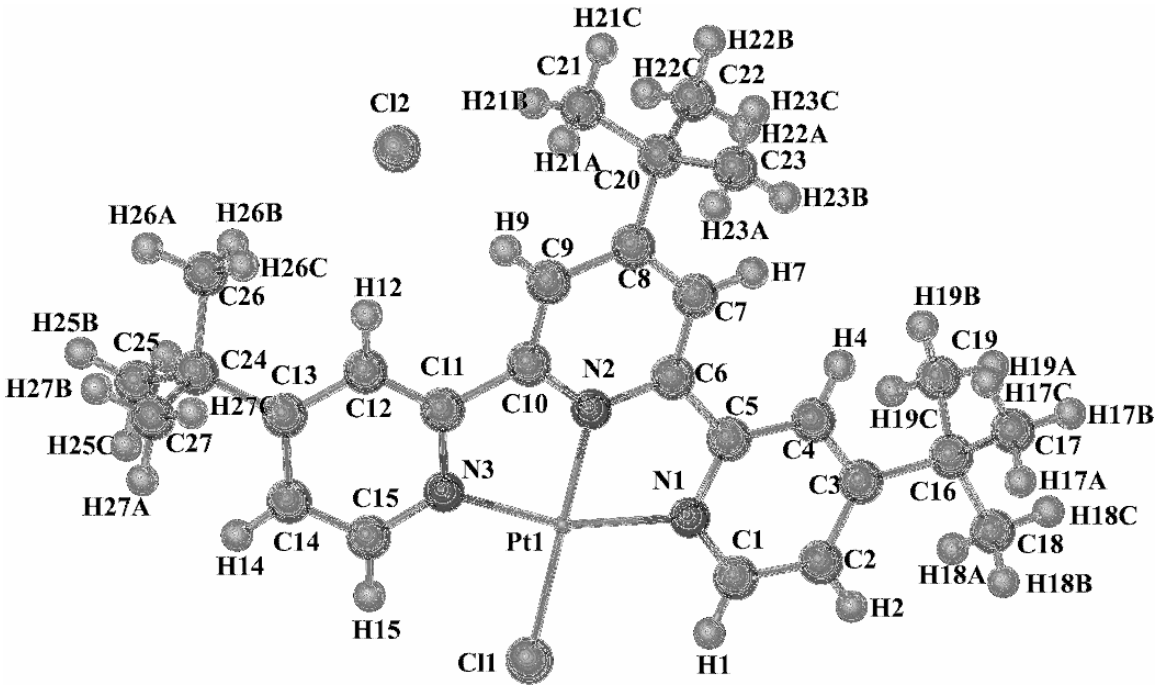

Figure 104. X-ray crystal structure of [Pt(tbtrpy)Cl][Cl] (**1**). Interstitial solvent molecules have been eliminated for the sake of clarity.

Table 63. Bond distances for [Pt(tbtrpy)Cl][Cl] (**1**) in Å.

Pt(1)-Cl(1)	2.299(2)	C(8)-C(9)	1.403(9)
Pt(1)-N(1)	2.031(4)	C(8)-C(20)	1.526(2)
Pt(1)-N(2)	1.936(4)	C(9)-C(10)	1.378(3)
Pt(1)-N(3)	2.028(2)	C(10)-C(11)	1.489(4)
N(1)-C(1)	1.337(3)	C(11)-C(12)	1.376(3)
N(1)-C(5)	1.369(7)	C(12)-C(13)	1.411(5)
N(2)-C(6)	1.348(2)	C(13)-C(14)	1.389(7)
N(2)-C(10)	1.342(2)	C(13)-C(24)	1.532(6)
N(3)-C(11)	1.367(3)	C(14)-C(15)	1.389(5)
N(3)-C(15)	1.339(2)	C(16)-C(17)	1.532(3)
C(1)-C(2)	1.386(3)	C(16)-C(18)	1.541(2)
C(2)-C(3)	1.394(4)	C(16)-C(19)	1.533(5)
C(3)-C(4)	1.402(3)	C(20)-C(21)	1.536(3)
C(3)-C(16)	1.528(8)	C(20)-C(22)	1.530(7)
C(4)-C(5)	1.378(8)	C(20)-C(23)	1.533(8)
C(5)-C(6)	1.483(2)	C(24)-C(25)	1.521(4)
C(6)-C(7)	1.387(2)	C(24)-C(26)	1.530(3)
C(7)-C(8)	1.407(5)	C(24)-C(27)	1.532(8)

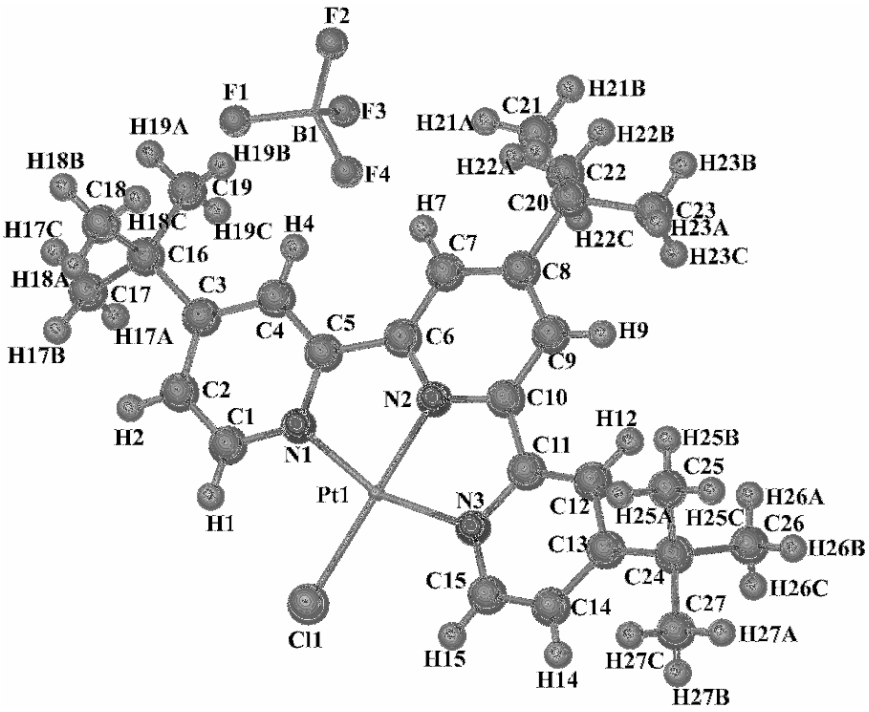

Figure 105. X-ray crystal structure of [Pt(tbtrpy)Cl][BF_4] (**2**). Hydrogen atoms and interstitial solvent molecules have been eliminated for the sake of clarity.

Table 64. Bond distances for [Pt(tbtrpy)Cl][BF_4] (**2**) in Å.

Pt(1)-Cl(1)	2.295(2)	C(6)-C(7)	1.386(2)
Pt(1)-N(1)	2.017(4)	C(7)-C(8)	1.384(5)
Pt(1)-N(2)	1.938(4)	C(8)-C(9)	1.393(9)
Pt(1)-N(3)	2.016(2)	C(8)-C(20)	1.537(2)
B(1)-F(1)	1.390(8)	C(9)-C(10)	1.373(3)
B(1)-F(2)	1.407(2)	C(10)-C(11)	1.471(4)
B(1)-F(3)	1.379(6)	C(11)-C(12)	1.372(3)
B(1)-F(4)	1.378(6)	C(12)-C(13)	1.386(5)
N(1)-C(1)	1.356(3)	C(13)-C(14)	1.384(7)
N(1)-C(5)	1.354(7)	C(13)-C(24)	1.534(6)
N(2)-C(6)	1.336(2)	C(14)-C(15)	1.381(5)
N(2)-C(10)	1.343(2)	C(16)-C(17)	1.534(3)
N(3)-C(11)	1.388(3)	C(16)-C(18)	1.524(2)
N(3)-C(15)	1.323(2)	C(16)-C(19)	1.531(5)
C(1)-C(2)	1.367(3)	C(20)-C(21)	1.506(3)
C(2)-C(3)	1.391(4)	C(20)-C(22)	1.540(7)
C(3)-C(4)	1.416(2)	C(20)-C(23)	1.527(6)
C(3)-C(16)	1.538(8)	C(24)-C(25)	1.540(4)
C(4)-C(5)	1.372(8)	C(24)-C(26)	1.507(3)
C(5)-C(6)	1.489(2)	C(24)-C(27)	1.489(8)

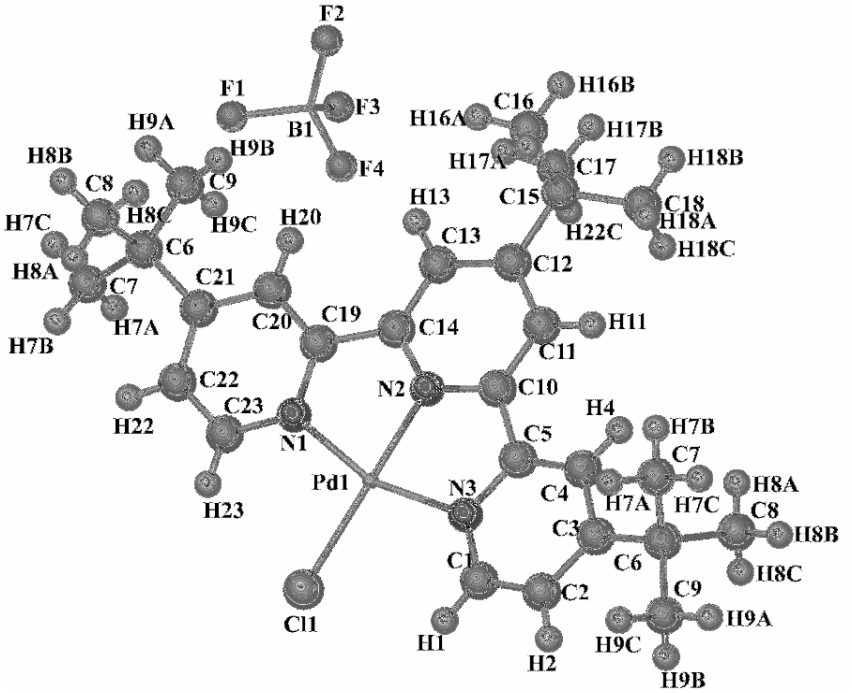

Figure 106. X-ray crystal structure of [Pd(tbtrpy)Cl][BF_4] (**3**). Hydrogen atoms and interstitial solvent molecules have been eliminated for the sake of clarity.

Table 65. Bond distances for [Pd(tbtrpy)Cl][BF_4] (**3**) in Å.

Pd(1)-N(1)	2.037(2)	C(6)-C(7)	1.533(5)
Pd(1)-N(2)	1.922(2)	C(6)-C(8)	1.536(5)
Pd(1)-N(3)	2.032(3)	C(6)-C(9)	1.523(5)
Pd(1)-Cl(1)	2.275(9)	C(10)-C(11)	1.372(4)
F(1)-B(1)	1.392(4)	C(11)-C(12)	1.399(4)
F(2)-B(1)	1.379(4)	C(12)-C(13)	1.390(4)
F(3)-B(1)	1.386(4)	C(12)-C(15)	1.527(4)
F(4)-B(1)	1.394(4)	C(13)-C(14)	1.373(4)
N(1)-C(19)	1.365(4)	C(14)-C(19)	1.479(4)
N(1)-C(23)	1.331(4)	C(15)-C(16)	1.541(5)
N(2)-C(10)	1.340(4)	C(15)-C(17)	1.516(5)
N(2)-C(14)	1.339(4)	C(15)-C(18)	1.520(4)
N(3)-C(1)	1.337(4)	C(19)-C(20)	1.373(4)
N(3)-C(5)	1.360(4)	C(20)-C(21)	1.398(4)
C(1)-C(2)	1.368(5)	C(21)-C(22)	1.386(4)
C(2)-C(3)	1.383(5)	C(22)-C(23)	1.378(5)
C(3)-C(4)	1.396(4)	C(21)-C(24)	1.523(4)
C(3)-C(6)	1.536(5)	C(24)-C(25)	1.538(5)
C(4)-C(5)	1.377(4)	C(24)-C(26)	1.515(5)
C(5)-C(10)	1.481(4)	C(24)-C(27)	1.510(5)

*[Pt(tbtrpy)NCS][BF_4] (**4•CH_2Cl_2**)*

The solid-state structure of (**4•CH_2Cl_2**) crystallizes in the triclinic space group *P-1* and displays structural features similar to those seen in the previously discussed salts. One of these characteristics is the presence of a distorted square-planar coordination environment around the platinum metal center. As a direct consequence of this distorted geometry, imposed by the tris(*t-butyl*)terpyridine ligand, two of the angles become acute with values of 80.91° and 81.63° respectively. While these angles become acute, in order to maintain the required 360° among the four constituent angles, the remaining angles become obtuse with values of 97.62° and 99.89°. Closer inspection of the platinum-heteroatom bond distances reveal a behavior similar to those observed in salts **1-3**. The bonds which formed between platinum and nitrogen atoms 1 and 3 had distances of 2.004(4) Å and 2.018(4) Å respectively illustrating the presence of equivalent electronegativity between the platinum and these nitrogen atoms. Contrary to this observed behavior, the bond between platinum and nitrogen 2 is much shorter, having a distance of 1.936(4) Å. Other features of this salt include the coordination of the ancillary thiocyanate ligand, present in this salt in the isothiocyanate coordination mode. This particular linkage, indicating ligation to the metal through the ligand's nitrogen atom versus its sulfur has been observed in several coordination compounds including the photoactive compound Ru(dcbpy)$(NCS)_2$.[57] As its charge compensating anion, **4** utilizes the tetrahedral anion $[BF_4]^-$. All B-F bond distances (~1.400 Å in length) and angles (~109.5°) are equivalent with reported values for this anion. Crystallographic parameters for **4** are listed in Table 66. The X-ray crystal structure and bond distances for **4** are depicted in Figure 107 and Tables 67.

Table 66. X-ray crystallographic and refinement data for [Pt(tbtrpy)NCS][BF_4]•CH_2Cl_2 (**4•CH_2Cl_2**).

Compound	[Pt(tbtrpy)NCS][BF_4]•CH_2Cl_2 (**4•CH_2Cl_2**)
Formula	$PtN_4C_{29}H_{37}BF_4Cl_2$
formula weight	793.21
Space group	P-1
a, Å	13.455(1)
b, Å	15.008(1)
c, Å	17.165(1)
α, deg	65.65(4)
β, deg	82.83(5)
γ, deg	979.96(4)
volume, Å^3	3104.1(4)
Z	2
μ, mm^{-1}	10.299
Temp.	110(2)
Reflns. collected	8377
Reflns. I>2σ	6620
Parameters	748
Restraints	0
R1[a]	0.0265
wR2[b]	0.0595
Goodness-of-fit[c]	0.935

[a] $R1 = \sum||F_o| - |F_c||/\sum|F_o|$. [b] $wR2 = [\sum [w(F_o^2-F_c^2)^2]/ \sum [w(F_o^2)^2]^{1/2}$

[c] Goodness-of-fit = $[\sum w(|F_o|-|F_c|)^2/(N_{obs}-N_{parameter})]^{1/2}$

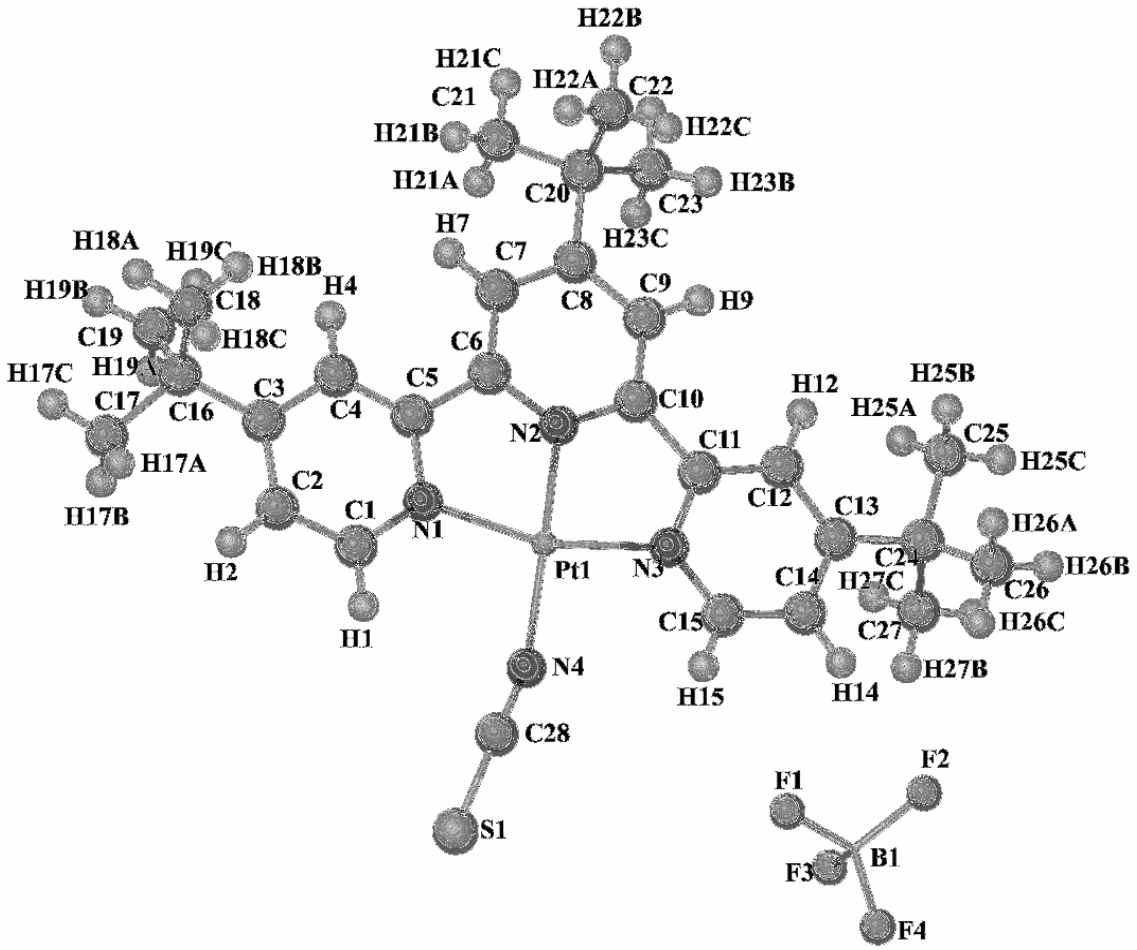

Figure 107. X-ray crystal structure of [Pt(tbtrpy)NCS][BF_4]•CH_2Cl_2 (**4•CH_2Cl_2**). Interstitial dichloromethane molecules have been eliminated for the sake of clarity.

Table 67. Bond distances for [Pt(tbtrpy)NCS][BF_4]•CH_2Cl_2 (**4•CH_2Cl_2**) in Å.

Pt(1)-N(2)	1.936(4)	N(7)-C(39)	1.376(5)
Pt(1)-N(4)	2.009(4)	N(7)-C(43)	1.345(5)
Pt(1)-N(3)	2.009(4)	N(8)-C(56)	1.136(6)
Pt(1)-N(1)	2.018(4)	F(1)-B(1)	1.374(6)
Pt(2)-N(6)	1.924(4)	F(2)-B(1)	1.396(6)
Pt(2)-N(8)	1.996(4)	F(3)-B(1)	1.390(6)
Pt(2)-N(7)	2.008(4)	F(4)-B(1)	1.388(6)
Pt(2)-N(5)	2.022(4)	F(5)-B(2)	1.387(6)
S(1)-C(28)	1.634(6)	F(6)-B(2)	1.395(6)
S(2)-C(56)	1.627(5)	F(7)-B(2)	1.401(6)
N(1)-C(1)	1.339(5)	F(8)-B(2)	1.385(7)
N(1)-C(5)	1.369(6)	C(1)-C(2)	1.380(6)
N(2)-C(6)	1.345(6)	C(2)-C(3)	1.398(6)
N(2)-C(10)	1.353(5)	C(3)-C(4)	1.415(6)
N(3)-C(11)	1.371(6)	C(3)-C(16)	1.507(6)
N(3)-C(15)	1.343(6)	C(4)-C(5)	1.362(6)
N(4)-C(28)	1.130(6)	C(5)-C(6)	1.480(6)
N(5)-C(29)	1.332(5)	C(6)-C(7)	1.387(6)
N(5)-C(33)	1.372(5)	C(7)-C(8)	1.406(6)
N(6)-C(34)	1.349(5)	C(8)-C(9)	1.401(6)
N(6)-C(38)	1.355(6)	C(8)-C(20)	1.533(6)

Table 67. Continued.

C(9)-C(10)	1.383(6)	C(33)-C(34)	1.476(6)
C(10)-C(11)	1.483(6)	C(34)-C(35)	1.376(6)
C(11)-C(12)	1.387(6)	C(35)-C(36)	1.395(6)
C(12)-C(13)	1.394(6)	C(36)-C(37)	1.401(6)
C(13)-C(14)	1.396(6)	C(36)-C(48)	1.527(6)
C(14)-C(15)	1.385(6)	C(37)-C(38)	1.385(6)
C(14)-C(15)	1.385(6)	C(38)-C(39)	1.475(6)
C(16)-C(17)	1.537(6)	C(39)-C(40)	1.375(6)
C(16)-C(18)	1.532(6)	C(40)-C(41)	1.405(6)
C(16)-C(19)	1.539(7)	C(41)-C(42)	1.383(6)
C(20)-C(21)	1.533(6)	C(42)-C(43)	1.373(6)
C(20)-C(22)	1.524(6)	C(44)-C(45)	1.511(7)
C(20)-C(23)	1.548(6)	C(44)-C(46)	1.545(7)
C(24)-C(25)	1.532(7)	C(44)-C(47)	1.520(7)
C(24)-C(26)	1.550(6)	C(48)-C(49)	1.540(6)
C(24)-C(27)	1.524(6)	C(48)-C(50)	1.523(6)
C(29)-C(30)	1.366(6)	C(48)-C(51)	1.539(6)
C(30)-C(31)	1.392(6)	C(52)-C(53)	1.536(6)
C(31)-C(32)	1.404(6)	C(52)-C(54)	1.525(6)
C(31)-C(44)	1.528(6)	C(52)-C(55)	1.535(6)
C(32)-C(33)	1.379(6)		

*[Pt(tbtrpy)(4-mbt)][BF4] (**5**), [Pt(tbtrpy)(2,5-dmeobt)][BF$_4$] (**6**), [Pt(tbtrpy)(snap)][BF$_4$] (**7•H$_2$O**), and [Pt(tbtrpy)(SO$_2$ph)][BF$_4$] (**8**)*

The solid-state structures for salts **5, 6,** (**7•H$_2$O**)**,** and **8** show strong similarity in their cationic units as all are dominated by the coordination of tris(t-butyl)terpyridine to a divalent platinum metal center. All salts display a distorted square-planar environment around the platinum metal center. This distortion, facilitated by the tris-chelating ligand, forces two of the surrounding angles to adopt acute values, in the range 81-82°. In order to maintain the prerequisite 360° bond angle environment, the remaining angles adopt obtuse values around 99-102°. In a manner similar to the previously-reported salts, bonds between platinum and nitrogen atoms 1 and 3 are similar in length (~2.020(6) Å) for **5-8**. The platinum-nitrogen 2 bond is much shorter in all cases (~1.960(5) Å), authored by the presence of a net dipole caused by the enhanced electronegativity of the ancillary ligand trans to nitrogen 2. As their charge compensating anion, **5-8** utilize the tetrahedral anion $[BF_4]^-$. All B-F bond distances (~1.400 Å in length) and angles (~109.5°) are equivalent with reported values for this anion. All pyridyl rings of the heteroatomic ligand show common aromatic bond distances while the t-butyl groups in the para position reveal bond angles indicative of this group's central sp^3-hybridized carbon atom. Despite these structural similarities, salts **5, 6,** (**7•H$_2$O**)**,** and **8** possess different arylthiolate ancillary ligands, which leads to different space groups for the compounds. Salts **5** and (**7•H$_2$O**) crystallize in the orthorhombic space groups *Pca2$_1$* and *Pbca* respectively. Salt **6** crystallizes in the monoclinic space group *P2$_1$/c* and **8** crystallizes in the triclinic space group *P-1*. The bond distances for the various Pt-S bond distances are ~2.3 Å for all systems, displaying values similar to measured bond distances in the well-known

Pt(diimine)(dithiolate) family of compounds. All aromatic rings in these arylthiolate ligands display C-C bond distance values of ~1.4 Å, similar to established values for bonds in aromatic rings. Among the most interesting feature observed in the structural elucidation of **5, 6,** (**7•H_2O**)**,** and **8**, is presence of two S=O bonds in **8**. Initially prepared with benzenthiolate as its ancillary ligand, the ligand became oxidized to the sulfinate via oxygen exposure in either its initial preparation or crystal growth. This is not unusual and has been documented by Cocker and Bachman in their studies of the photochemical and chemical oxidation of M(bpy)(bdt) [M = Ni, Pd, and Pt; bdt = benzenedithiolate] complexes.[126] In the presence of ambient light and atmospheric conditions, mono- and disulfinate complexes were generated and crystallographically characterized. Similar products were also generated by reacting the diimine-dithiolene complexes with strong oxidants such as concentrated H_2O_2. The formation of the sulfinate complex from the [Pt(tbtrpy)(sph)][BF_4] salt illustrates that the observed photochemical oxidation of metal diimine-dithiolene complexes can be extended to the tbtrpy/arylthiolate salts. Crystallographic parameters for **5, 6,** (**7•H_2O**)**,** and **8** are listed in Table 68. The X-ray crystal structure and bond distances for these structures are depicted in Figure 108-111 and Tables 69-72 respectively.

Table 68. X-ray crystallographic and refinement data for **5, 6, (7•H_2O),** and **8.**

Compound	[Pt(tbtrpy)(4-mbt)][BF_4](**5**)	[Pt(tbtrpy)(2,5-dmeobt)][BF_4] (**6**)	[Pt(tbtrpy)(snap)][BF_4]•H_2O (**7**)	[Pt(tbtrpy)(SO_2ph)][BF_4] (**8**)
Formula	$PtSN_3C_{34}H_{42}BF_4$	$PtSN_3O_2C_{35}H_{44}BF_4$	$PtSN_3OC_{37}H_{43}BF_4$	$PtSN_3O_2C_{33}H_{40}BF_4$
formula weight	806.28	852.28	859.28	824.25
Space group	$Pca2_1$	$P2_1/c$	Pbca	P-1
a, Å	20.910(12)	13.382(2)	18.535(4)	9.989(4)
b, Å	19.829(13)	13.976(3)	17.508(4)	13.459(6)
c, Å	15.930(9)	19.235(4)	24.488(5)	13.559(6)
α, deg	90	90	90	94.702(9)
β, deg	90	105.19(3)	90	105.465(9)
γ, deg	90	90	90	111.55((8)
volume, $Å^3$	6604.78	3473.55	7946.60	1600.80
Z	4	4	4	2
μ, mm^{-1}	4.36	5.23	4.93	4.51
Temp.	110(2)	110(2)	110(2)	110(2)
Reflns. collected	13346	7963	5712	7712
Reflns. I>2σ	10224	6894	4876	6592
Parameters	809	435	541	403
Restraints	1	0	0	0
R1[a]	0.0427	0.0362	0.1013	0.0507
wR2[b]	0.0982	0.0767	0.2157	0.1127
Goodness-of-fit[c]	1.056	1.001	1.114	1.079

[a] $R1 = \sum||F_o| - |F_c||/\sum|F_o|$. [b] $wR2 = [\sum [w(F_o^2-F_c^2)^2]/ \sum [w(F_o^2)^2]^{1/2}$

[c] Goodness-of-fit = $[\sum w(|F_o|-|F_c|)^2/(N_{obs}-N_{parameter})]^{1/2}$

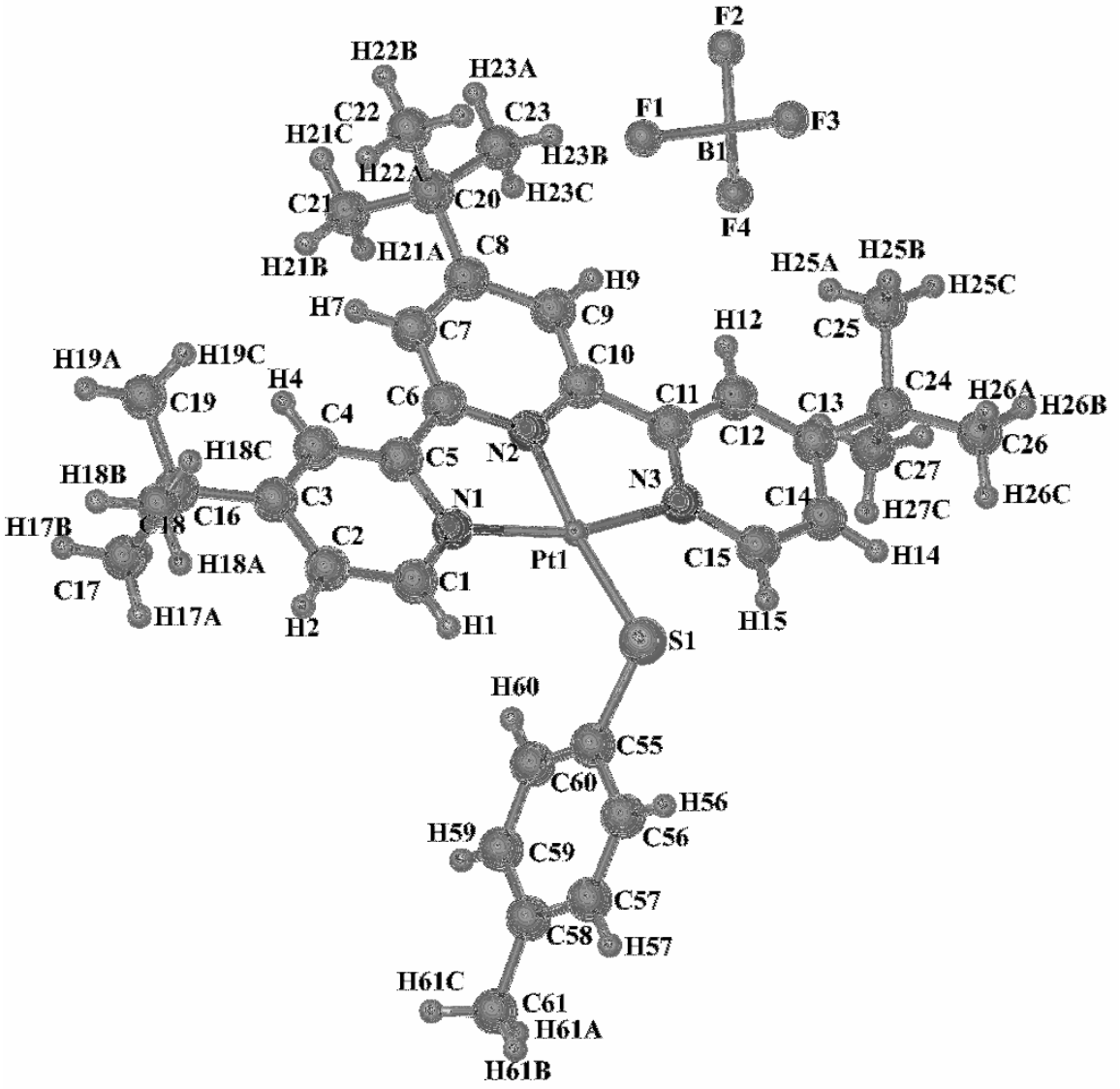

Figure 108. X-ray crystal structure of [Pt(tbtrpy)(4-mbt)][BF_4] (**5**).

Table 69. Bond distances for [Pt(tbtrpy)(4-mbt)][BF_4] (**5**) in Å.

Pt(1)-N(2)	1.95(1)	C(16)-C(18)	1.52(2)
Pt(1)-N(1)	2.02(7)	C(16)-C(17)	1.53(1)
Pt(1)-N(3)	2.04(8)	C(20)-C(23)	1.50(1)
Pt(1)-S(1)	2.31(3)	C(20)-C(21)	1.51(1)
Pt(2)-N(5)	1.98(8)	C(20)-C(22)	1.55(1)
Pt(2)-N(6)	2.02(9)	C(24)-C(27)	1.52(1)
Pt(2)-N(4)	2.04(8)	C(24)-C(26)	1.53(2)
Pt(2)-S(2)	2.32(3)	C(24)-C(25)	1.55(1)
S(1)-C(55)	1.77(9)	C(28)-C(29)	1.36(1)
S(2)-C(62)	1.77(1)	C(29)-C(30)	1.37(1)
F(1)-B(1)	1.45(2)	C(30)-C(31)	1.40(1)
F(2)-B(1)	1.43(2)	C(30)-C(43)	1.53(1)
F(3)-B(1)	1.34(2)	C(31)-C(32)	1.38(1)
F(4)-B(1)	1.26(2)	C(32)-C(33)	1.47(1)
F(5)-B(2)	1.29(2)	C(33)-C(34)	1.40(1)
F(6)-B(2)	1.38(1)	C(34)-C(35)	1.38(1)
F(7)-B(2)	1.40(2)	C(35)-C(36)	1.42(1)
F(8)-B(2)	1.39(1)	C(35)-C(47)	1.55(1)
N(1)-C(1)	1.36(1)	C(36)-C(37)	1.37(1)
N(1)-C(5)	1.40(1)	C(37)-C(38)	1.52(1)
N(2)-C(10)	1.35(1)	C(38)-C(39)	1.37(1)
N(2)-C(6)	1.36(1)	C(39)-C(40)	1.39(1)
N(3)-C(15)	1.34(1)	C(40)-C(41)	1.39(1)
N(3)-C(11)	1.40(1)	C(40)-C(51)	1.53(1)
N(4)-C(32)	1.35(1)	C(41)-C(42)	1.37(2)
N(4)-C(28)	1.35(1)	C(43)-C(46)	1.51(1)
N95)-C(37)	1.31(1)	C(43)-C(44)	1.54(1)
N(5)-C(33)	1.36(1)	C(43)-C(45)	1.55(1)

Table 69. Continued.

N(4)-C(32)	1.35(1)	C(41)-C(42)	1.37(2)
N(4)-C(28)	1.35(1)	C(43)-C(46)	1.51(1)
N95)-C(37)	1.31(1)	C(43)-C(44)	1.54(1)
N(5)-C(33)	1.36(1)	C(43)-C(45)	1.55(1)
N(6)-C(42)	1.35(1)	C(47)-C(49)	1.50(2)
N(6)-C(38)	1.36(1)	C(47)-C(50)	1.53(2)
C(1)-C(2)	1.41(1)	C(47)-C(48)	1.55(1)
C(2)-C(3)	1.40(1)	C(51)-C(54)	1.50(1)
C(3)-C(4)	1.39(1)	C(51)-C(53)	1.52(1)
C(3)-C(16)	1.53(1)	C(51)-C(52)	1.55(2)
C(4)-C(5)	1.35(1)	C(55)-C(60)	1.36(1)
C(5)-C(6)	1.49(1)	C(55)-C(56)	1.44(1)
C(6)-C(7)	1.36(1)	C(56)-C(57)	1.38(1)
C(7)-C(8)	1.40(1)	C(57)-C(58)	1.37(1)
C(8)-C(9)	1.42(1)	C(58)-C(59)	1.40(1)
C(8)-C(20)	1.54(1)	C(58)-C(61)	1.51(1)
C(9)-C(10)	1.36(1)	C(59)-C(60)	1.38(1)
C(10)-C(11)	1.48(1)	C(62)-C(63)	1.35(1)
C(11)-C(12)	1.36(1)	C(62)-C(67)	1.43(1)
C(12)-C(13)	1.39(1)	C(63)-C(64)	1.38(1)
C(13)-C(14)	1.39(1)	C(64)-C(65)	1.35(2)
C(13)-C(24)	1.53(1)	C(65)-C(66)	1.39(2)
C(14)-C(15)	1.36(1)	C(65)-C(68)	1.50(2)
C(16)-C(19)	1.52(1)	C(66)-C(67)	1.41(1)

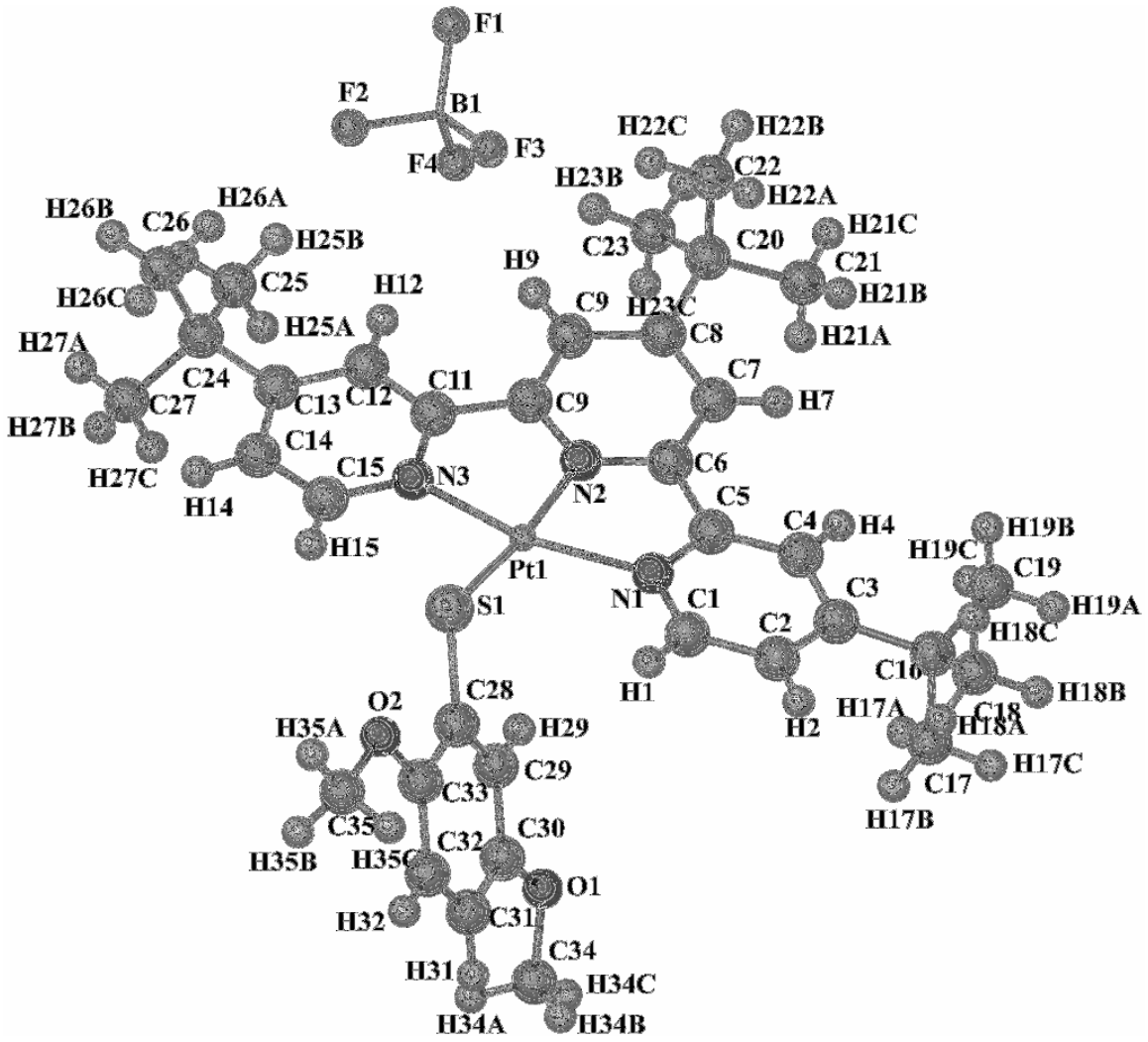

Figure 109. X-ray crystal structure of [Pt(tbtrpy)(2,5-dmeobt)][BF_4] (**6**).

Table 70. Bond distances for [Pt(tbtrpy)(2,5-dmeobt)][BF_4] (**6**) in Å.

Pt(1)-S(1)	2.316(2)	C(7)-C(8)	1.398(5)
Pt(1)-N(1)	2.033(4)	C(8)-C(9)	1.404(9)
Pt(1)-N(2)	1.962(4)	C(8)-C(20)	1.527(2)
Pt(1)-N(3)	2.029(2)	C(9)-C(10)	1.381(3)
B(1)-F(1)	1.364(8)	C(10)-C(11)	1.475(4)
B(1)-F(2)	1.349(2)	C(11)-C(12)	1.386(3)
B(1)-F(3)	1.387(6)	C(12)-C(13)	1.394(5)
B(1)-F(4)	1.392(6)	C(13)-C(14)	1.398(7)
N(1)-C(1)	1.347(3)	C(13)-C(24)	1.525(6)
N(1)-C(5)	1.379(7)	C(14)-C(15)	1.370(5)
N(2)-C(6)	1.337(2)	C(16)-C(17)	1.538(3)
N(2)-C(10)	1.343(2)	C(16)-C(18)	1.531(2)
N(3)-C(11)	1.371(3)	C(16)-C(19)	1.524(5)
N(3)-C(15)	1.343(2)	C(20)-C(21)	1.535(3)
S(1)-C(28)	1.742(2)	C(20)-C(22)	1.535(7)
O(1)-C(30)	1.367(2)	C(20)-C(23)	1.536(8)
O(1)-C(34)	1.424(3)	C(24)-C(25)	1.522(4)
O(2)-C(33)	1.383(2)	C(24)-C(26)	1.533(3)
O(2)-C(35)	1.405(2)	C(24)-C(27)	1.536(8)
C(1)-C(2)	1.384(3)	C(28)-C(29)	1.384(4)
C(2)-C(3)	1.395(4)	C(28)-C(33)	1.424(3)
C(3)-C(4)	1.400(2)	C(29)-C(30)	1.390(8)
C(3)-C(16)	1.525(8)	C(30)-C(31)	1.393(7)
C(4)-C(5)	1.381(8)	C(31)-C(32)	1.371(6)
C(5)-C(6)	1.475(2)	C(32)-C(33)	1.392(6)
C(6)-C(7)	1.387(2)		

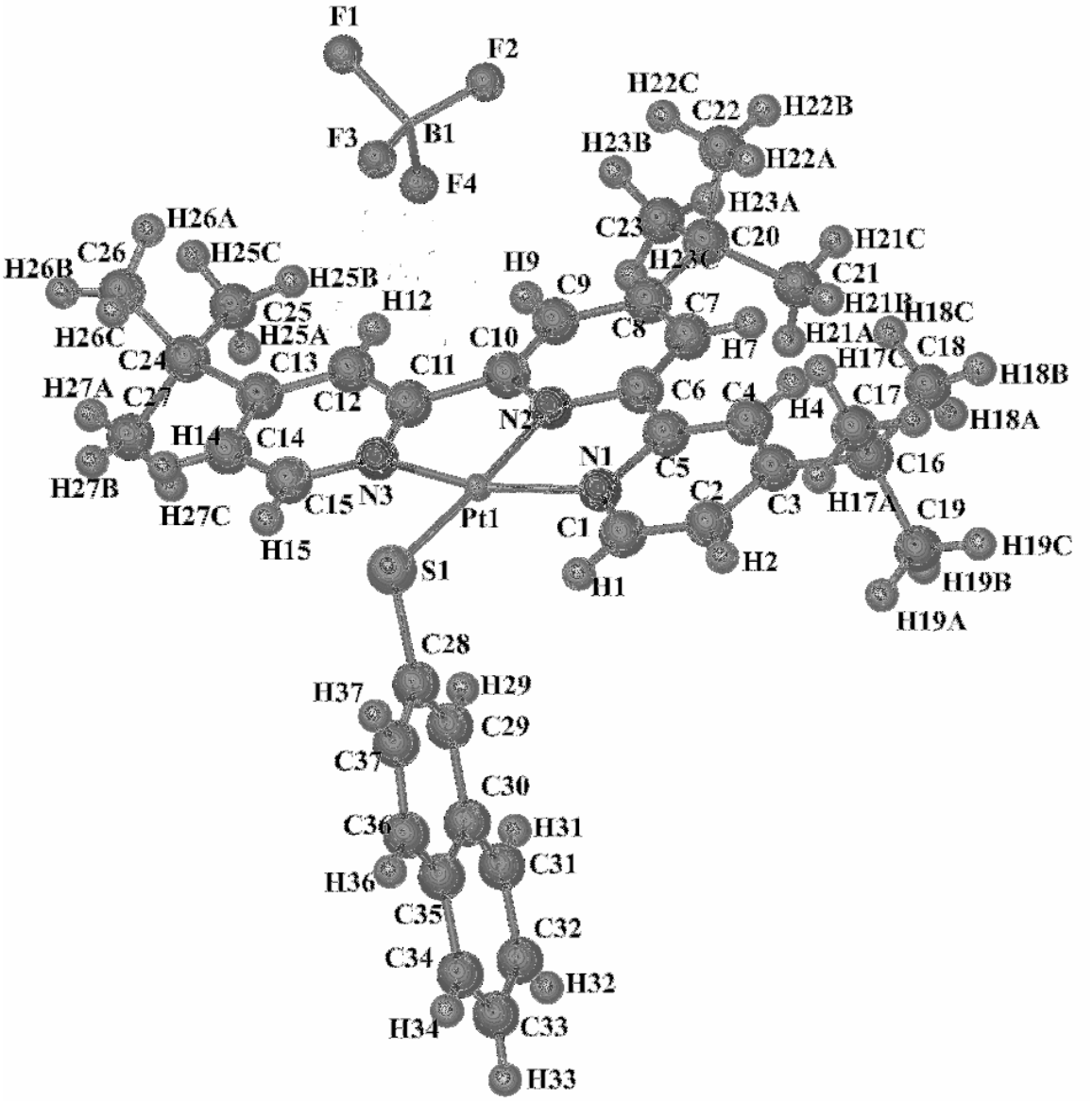

Figure 110. X-ray crystal structure of [Pt(tbtrpy)(snap)][BF_4]•H_2O (**7•H_2O**). Interstitial water molecules have been eliminated for the sake of clarity.

Table 71. Bond distances for [Pt(tbtrpy)(snap)][BF_4]•H_2O (**7•H_2O**) in Å.

Pt(1)-N(2)	1.98(1)	C(10)-C(11)	1.50(2)
Pt(1)-N(1)	2.00(1)	C(11)-C(12)	1.33(2)
Pt(1)-N(3)	2.01(1)	C(12)-C(13)	1.41(3)
Pt(1)-S(1)	2.31(6)	C(13)-C(14)	1.35(3)
S(1)-C(28)	1.71(3)	C(13)-C(24)	1.55(3)
N(1)-C(1)	1.35(2)	C(14)-C(15)	1.42(3)
N(1)-C(5)	1.39(2)	C(16)-C(17)	1.51(3)
N(2)-C(6)	1.35(2)	C(16)-C(18)	1.49(3)
N(2)-C(10)	1.35(2)	C(16)-C(19)	1.50(3)
N(3)-C(11)	1.39(2)	C(20)-C(21)	1.47(3)
N(3)-C(15)	1.32(2)	C(20)-C(22)	1.54(4)
F(1)-B(1)	1.34(3)	C(20)-C(23)	1.51(3)
F(2)-B(1)	1.42(3)	C(24)-C(25)	1.47(3)
F(3)-B(1)	1.33(4)	C(24)-C(26)	1.49(3)
F(4)-B(1)	1.29(3)	C(24)-C(27)	1.51(3)
C(1)-C(2)	1.34(3)	C(28)-C(29)	1.36(4)
C(2)-C(3)	1.40(3)	C(28)-C(37)	1.48(3)
C(3)-C(4)	1.39(2)	C(29)-C(30)	1.42(3)
C(3)-C(16)	1.56(2)	C(30)-C(31)	1.35(3)
C(4)-C(5)	1.39(2)	C(30)-C(35)	1.46(3)
C(5)-C(6)	1.47(2)	C(31)-C(32)	1.40(4)
C(6)-C(7)	1.37(2)	C(32)-C(33)	1.43(3)
C(7)-C(8)	1.39(2)	C(33)-C(34)	1.38(4)
C(8)-C(9)	1.39(2)	C(34)-C(35)	1.44(4)
C(8)-C(20)	1.56(3)	C(35)-C(36)	1.39(4)
C(9)-C(10)	1.35(2)	C(36)-C(37)	1.35(4)

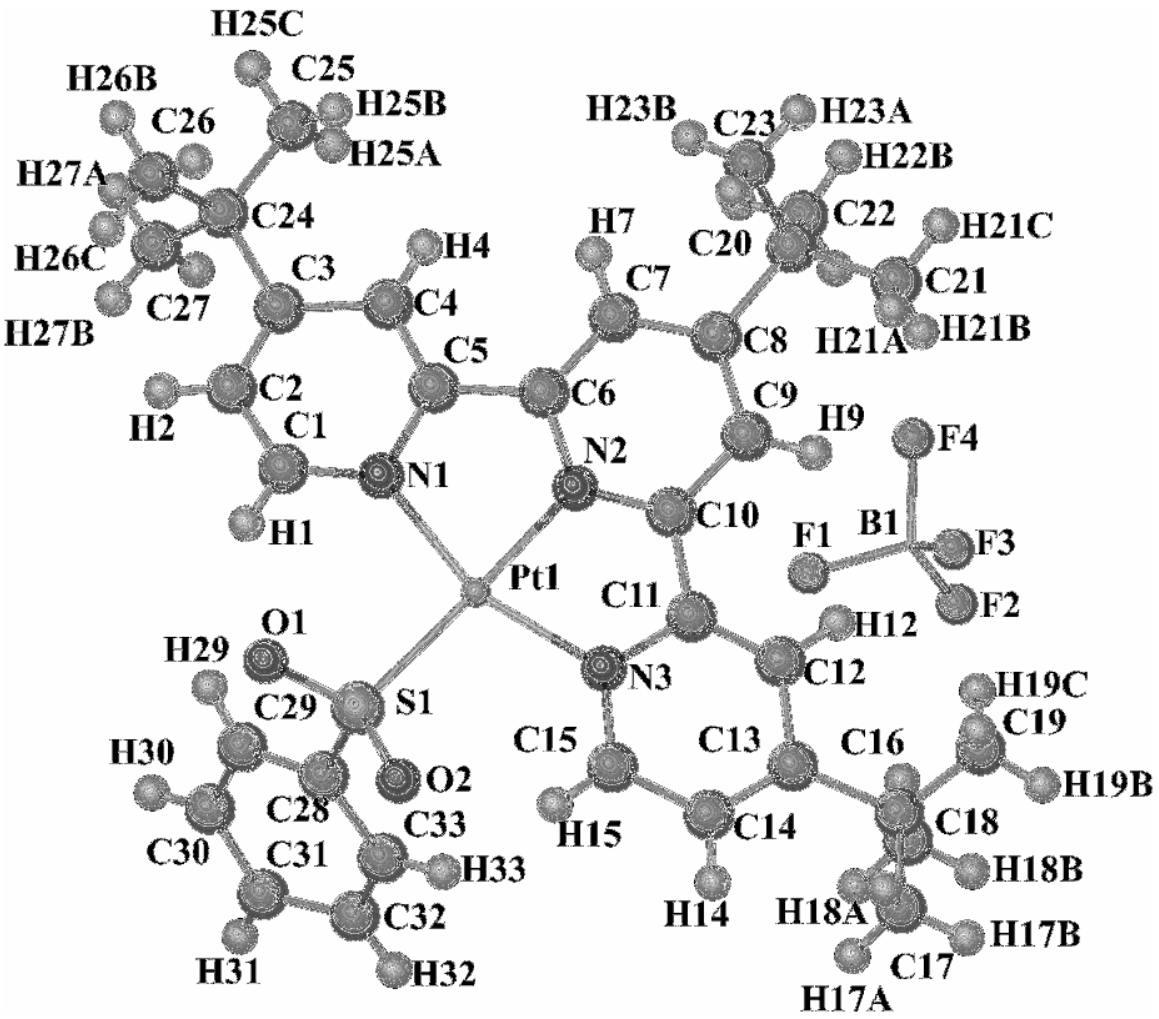

Figure 111. X-ray crystal structure of [Pt(tbtrpy)(SO_2ph)][BF_4] (**8**).

Table 72. Bond distances for [Pt(tbtrpy)(SO_2ph)][BF_4] (**8**) in Å.

Pt(1)-N(1)	2.039(5)	C(7)-C(8)	1.402(8)
Pt(1)-N(2)	1.962(5)	C(8)-C(9)	1.416(8)
Pt(1)-N(3)	2.041(5)	C(8)-C(20)	1.524(9)
Pt(1)-S(1)	2.2709(18)	C(9)-C(10)	1.364(9)
S(1)-O(1)	1.438(7)	C(10)-C(11)	1.485(8)
S(1)-O(2)	1.457(6)	C(12)-C(13)	1.397(9)
S(1)-C(28)	1.799(5)	C(13)-C(14)	1.397(10)
B(1)-F(1)	1.344(10)	C(13)-C(24)	1.517(9)
B(1)-F(2)	1.388(9)	C(14)-C(15)	1.374(10)
B(1)-F(3)	1.360(9)	C(16)-C(17)	1.538(9)
B(1)-F(4)	1.364(10)	C(16)-C(18)	1.544(9)
N(1)-C(1)	1.343(8)	C(16)-C(19)	1.513(9)
N(1)-C(5)	1.363(8)	C(20)-C(21)	1.516(9)
N(2)-C(6)	1.353(8)	C(20)-C(22)	1.542(10)
N(2)-C(10)	1.355(8)	C(20)-C(23)	1.534(9)
N(3)-C(11)	1.368(8)	C(24)-C(25)	1.531(11)
N(3)-C(15)	1.344(8)	C(24)-C(26)	1.524(11)
C(1)-C(2)	1.376(9)	C(24)-C(27)	1.537(11)
C(1)-C(12)	1.375(9)	C(28)-C(29)	1.390
C(2)-C(3)	1.384(9)	C(28)-C(33)	1.390
C(3)-C(4)	1.391(8)	C(29)-C(30)	1.390
C(3)-C(16)	1.526(8)	C(30)-C(31)	1.390
C(4)-C(5)	1.368(8)	C(31)-C(32)	1.390
C(5)-C(6)	1.480(8)	C(32)-C(33)	1.390
C(6)-C(7)	1.367(9)		

[Pt(tbtrpy)(OH)][TCNQ]•2H_2O ***(9•2H_2O)****, [Pt(tbtrpy)(Cl)] [TCNQ]•2CH_2Cl_2* ***(10•2CH_2Cl_2)****, and [Pt(tbtrpy)(CN)][TCNQ]•2CH_3CN* ***(11•2CH_3CN)***

The solid-state structures for salts (**9•2H_2O**), (**10•2CH_2Cl_2**), and (**11•2CH_3CN**) crystallize in triclinic, orthorhombic, and monoclinic space groups. Salt (**10•2CH_2Cl_2**) crystallize in the triclinic space group *P-1*, while (**9•2H_2O**) crystallizes in the orthorhombic space group *Pbcn*, and (**11•2CH_3CN**) crystallizes in the monoclinic space group $P2_1/c$. The cationic platinum unit possesses a distorted square-planar environment with angles ranging from 80.4-102.3°. As with the other crystallographically characterized salts, the distances between the platinum metal center and nitrogen atoms 1 and 3 are approximately equivalent in distance at ~2.00 Å. Upon their initial preparation, salts (**9•2H_2O**)**,** (**10•2CH_2Cl_2**)**,** and (**11•2CH_3CN**) were prepared by Joyce Chen at the University of North Texas with arylthiolate ancillary ligands. During the course of crystallization, these ligands were replaced by OH^-, Cl^-, and CN^- in (**9•2H_2O**)**,** (**10•2CH_2Cl_2**)**,** and (**11•2CH_3CN**) respectively. Platinum is known to undergo an associative mechanism, forming a five-coordinate transition state before returning to its standard four-coordinate environment. It is uncertain whether platinum undergoes an A or I_a mechanism, but this metal is known to form five-coordinate intermediates. Beside the presence of solvent fragments in the platinum coordination sphere, another interesting feature of (**9•2H_2O**)**,** (**10•2CH_2Cl_2**)**,** and (**11•2CH_3CN**) is the use of the reduced organocyanide acceptor TCNQ as the charge-compensating anion. The ultimate goal of these salts has been to target them for use in solar cells. In an initial attempt to prepare photosensitizing dyes with neutral diimine/dithiolate donors and organocyanide acceptors, poor photoconversion efficiencies were obtained, presumably due to reduced

electron injection into the TiO_2 conduction band due to fact that the first reduction potential of the acceptor is lower than the semiconductor conduction band. Ultimately, incorporation of the pre-reduced acceptor as the charge-compensating anion in each salt would allow these systems to be useful as dyes for solar cells composed of the semi-conductor SnO_2 as its conduction band lies at a potential lower than the first reduction potential of the stable organocyanide radical. Inspection of the quinone and exocyclic bond distances were used by Kistenmacher and coworkers to establish an empirical relationship to calculate the overall valence of the TCNQ acceptor and its derivatives.[127] Close inspection of these crystallographically-determined distances suggest the further reduction of the acceptor to a $(1+\delta)^-$ state.[128] Unlike the other TCNQ salts, the structure for (**9•2H_2O**) is dominated by a 1:1 stack of donors and acceptors along the c-axis with close interplanar distances of 3.502 Å. Crystallographic parameters for (**9•2H_2O**), (**10•2CH_2Cl_2**), and (**11•2CH_3CN**) are listed in Table 73. The X-ray crystal structure and bond distances for these structures are depicted in Figure 112-114 and Tables 74-76 respectively.

Table 73. X-ray crystallographic and refinement data for (**9•2H_2O**), (**10•2CH_2Cl_2**), and (**11•2CH_3CN**).

Compound	[Pt(tbtrpy)(OH)][TCNQ]•2H_2O (**9•2H_2O**)	[Pt(tbtrpy)(Cl)][TCNQ]•2CH_2Cl_2 (**10•2CH_2Cl_2**)	[Pt(tbtrpy)(CN)][TCNQ]•2CH_3CN (**11•2CH_3CN**)
Formula	$PtO_2N_7C_{39}H_{44}$	$PtN_7Cl_5C_{43}H_{43}$	$PtN_{10}C_{45}H_{45}$
formula weight	837.32	1027.17	920.35
Space group	Pbcn	P-1	$P2_1/c$
a, Å	13.84(3)	11.706(2)	12.556(3)
b, Å	23.17(4)	13.591(3)	13.827(3)
c, Å	23.38(4)	13.748(3)	23.500(5)
α, deg	90	72.31(3)	90
β, deg	90	84.92(3)	92.31(3)
γ, deg	90	66.13(3)	90
volume, Å^3	7498.67	1903.98	4076.54
Z	8	2	4
μ, mm^{-1}	3.79	4.16	3.89
Temp.	110(2)	110(2)	110(2)
Reflns. collected	6625	7136	6574
Reflns. I>2σ	4357	5849	5124
Parameters	457	394	498
Restraints	7	2	0
R1[a]	0.1008	0.0523	0.0791
wR2[b]	0.1949	0.1167	0.1625
Goodness-of-fit[c]	1.243	1.096	1.104

[a] $R1 = \sum||F_o| - |F_c||/\sum|F_o|$. [b] $wR2 = [\sum [w(F_o^2-F_c^2)^2]/ \sum [w(F_o^2)^2]^{1/2}$

[c] Goodness-of-fit $= [\sum w(|F_o|-|F_c|)^2/(N_{obs}-N_{parameter})]^{1/2}$

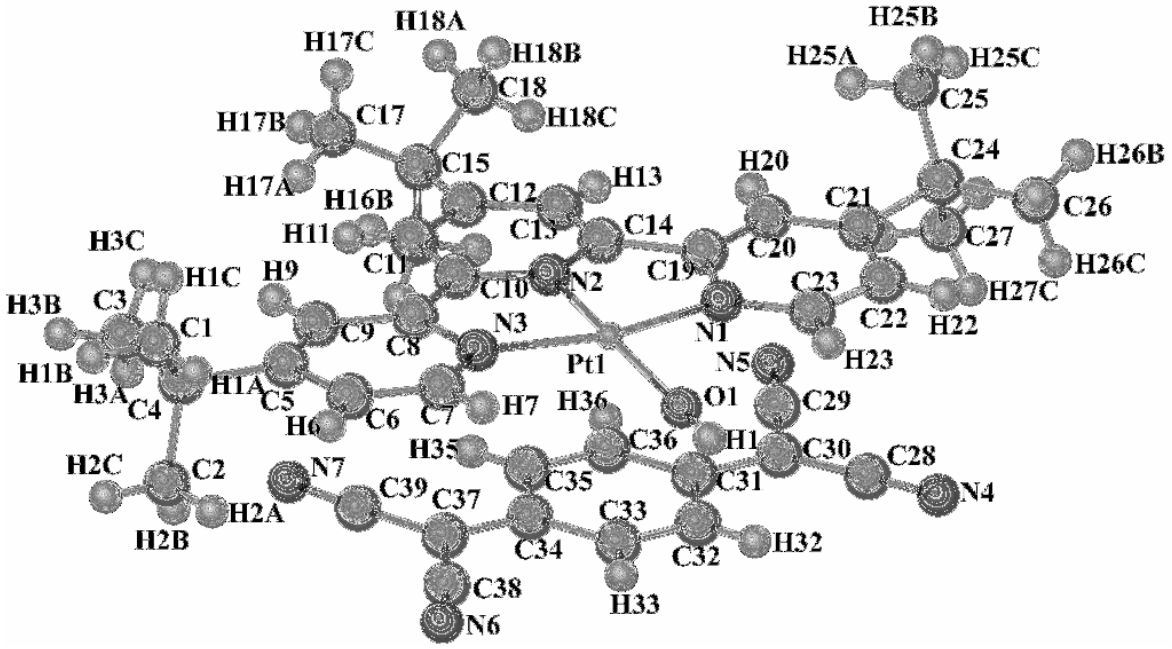

Figure 112. X-ray crystal structure of [Pt(tbtrpy)OH][TCNQ]•2H_2O (**9•2H_2O**). Interstitial water molecules have been eliminated for the sake of clarity.

Table 74. Bond distances for [Pt(tbtrpy)OH][TCNQ]•2H_2O (**9•2H_2O**) in Å.

Pt(1)-O(1)	2.236(2)	C(11)-C(12)	1.451(3)
Pt(1)-N(1)	1.987(4)	C(12)-C(13)	1.296(5)
Pt(1)-N(2)	1.956(4)	C(13)-C(14)	1.353(8)
Pt(1)-N(3)	2.004(2)	C(13)-C(24)	1.553(4)
N(1)-C(1)	1.351(3)	C(14)-C(15)	1.346(3)
N(1)-C(5)	1.359(6)	C(16)-C(17)	1.570(3)
N(2)-C(6)	1.342(5)	C(16)-C(18)	1.508(3)
N(2)-C(10)	1.335(6)	C(16)-C(19)	1.436(5)
N(3)-C(11)	1.354(7)	C(20)-C(21)	1.465(3)
N(3)-C(15)	1.357(8)	C(20)-C(22)	1.353(7)
N(4)-C(37)	1.136(9)	C(20)-C(23)	1.428(7)
N(5)-C(36)	1.133(2)	C(24)-C(25)	1.483(2)
N(6)-C(38)	1.155(2)	C(24)-C(26)	1.510(3)
N(7)-C(39)	1.134(2)	C(24)-C(27)	1.482(8)
C(1)-C(2)	1.354(3)	C(28)-C(29)	1.426(3)
C(2)-C(3)	1.382(4)	C(28)-C(38)	1.448(8)
C(3)-C(4)	1.409(3)	C(28)-C(39)	1.403(3)
C(3)-C(16)	1.547(5)	C(29)-C(30)	1.443(8)
C(4)-C(5)	1.361(7)	C(30)-C(31)	1.352(5)
C(5)-C(6)	1.549(4)	C(31)-C(32)	1.405(6)
C(6)-C(7)	1.337(2)	C(32)-C(33)	1.419(8)
C(7)-C(8)	1.378(5)	C(33)-C(34)	1.353(4)
C(8)-C(9)	1.405(9)	C(32)-C(35)	1.441(8)
C(8)-C(20)	1.564(2)	C(35)-C(36)	1.394(6)
C(9)-C(10)	1.316(3)	C(35)-C(37)	1.406(5)
C(10)-C(11)	1.499(7)		

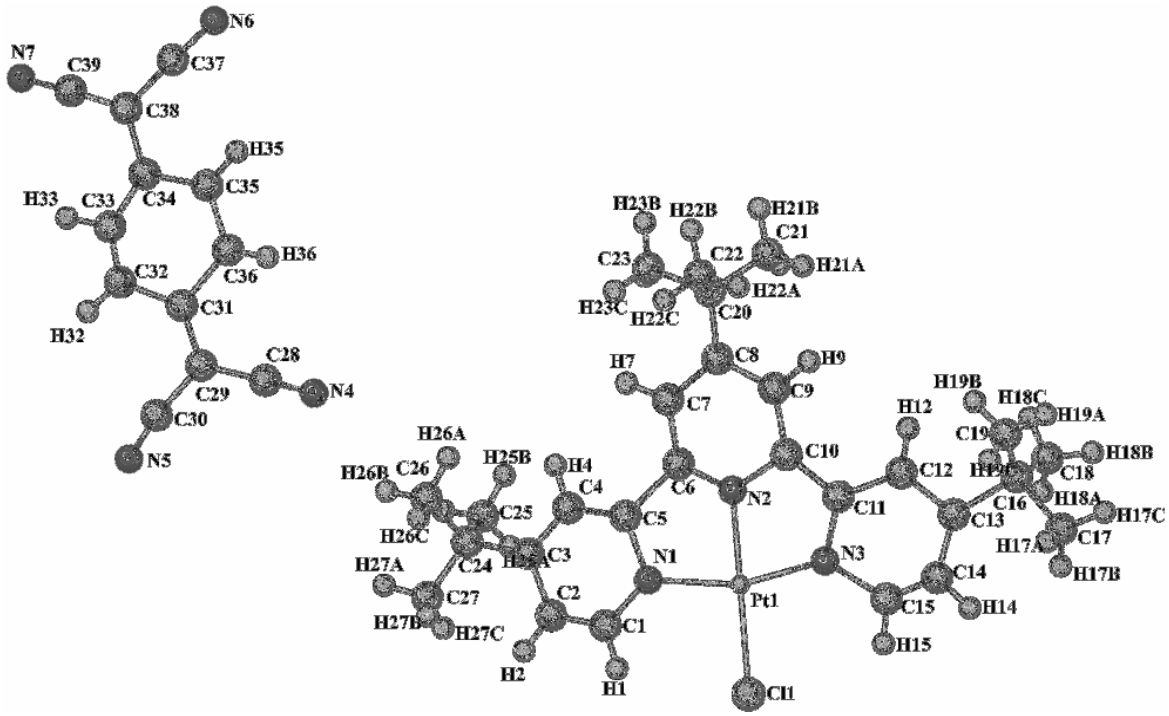

Figure 113. X-ray crystal structure of [Pt(tbtrpy)Cl][TCNQ]•2CH_2Cl_2 (**10•2CH_2Cl_2**). Interstitial dichloromethane molecules have been eliminated for the sake of clarity.

Table 75. Bond distances for [Pt(tbtrpy)Cl][TCNQ]•2CH_2Cl_2 (**10•2CH_2Cl_2**) in Å.

Pt(1)-Cl(1)	2.276(2)	C(11)-C(12)	1.318(3)
Pt(1)-N(1)	1.980(4)	C(12)-C(13)	1.402(5)
Pt(1)-N(2)	1.847(4)	C(13)-C(14)	1.451(7)
Pt(1)-N(3)	2.101(2)	C(13)-C(24)	1.476(6)
N(1)-C(1)	1.364(3)	C(14)-C(15)	1.639(5)
N(1)-C(5)	1.306(7)	C(16)-C(17)	1.570(3)
N(2)-C(6)	1.407(2)	C(16)-C(18)	1.483(2)
N(2)-C(10)	1.237(2)	C(16)-C(19)	1.595(5)
N(3)-C(11)	1.370(3)	C(20)-C(21)	1.637(3)
N(3)-C(15)	1.159(2)	C(20)-C(22)	1.615(7)
N(4)-C(28)	1.117(2)	C(20)-C(23)	1.556(8)
N(5)-C(30)	1.113(2)	C(24)-C(25)	1.709(4)
N(6)-C(38)	1.201(2)	C(24)-C(26)	1.591(3)
N(7)-C(39)	1.263(2)	C(24)-C(27)	1.532(8)
C(1)-C(2)	1.497(3)	C(28)-C(29)	1.508(3)
C(2)-C(3)	1.289(4)	C(29)-C(30)	1.413(8)
C(3)-C(4)	1.463(3)	C(29)-C(31)	1.341(8)
C(3)-C(16)	1.587(8)	C(31)-C(32)	1.532(5)
C(4)-C(5)	1.4058)	C(31)-C(36)	1.532(8)
C(5)-C(6)	1.381(2)	C(32)-C(33)	1.482(3)
C(6)-C(7)	1.395(2)	C(33)-C(34)	1.412(6)
C(7)-C(8)	1.407(5)	C(34)-C(35)	1.333(4)
C(8)-C(9)	1.434(9)	C(34)-C(37)	1.468(2)
C(8)-C(20)	1.597(2)	C(35)-C(36)	1.190(8)
C(9)-C(10)	1.391(3)	C(37)-C(38)	1.278(6)
C(10)-C(11)	1.554(4)	C(37)-C(39)	1.263(9)

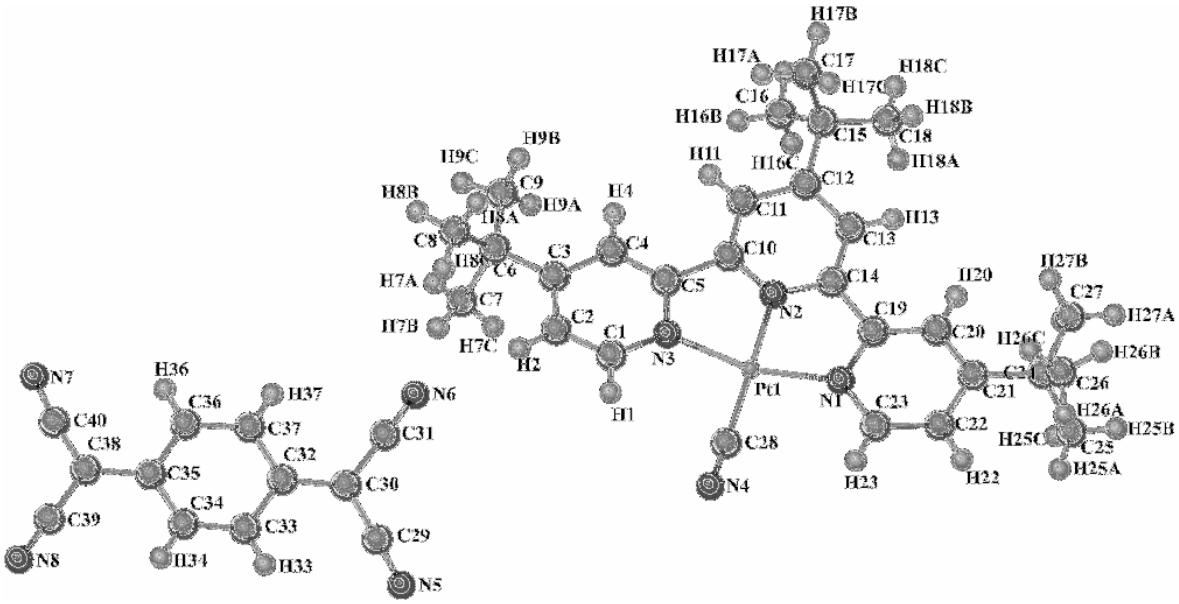

Figure 114. X-ray crystal structure of [Pt(tbtrpy)CN][TCNQ]•2CH_3CN (**11•2CH_3CN**). Interstitial acetonitrile molecules have been eliminated for the sake of clarity.

Table 76. Bond distances for [Pt(tbtrpy)CN][TCNQ]•2CH_3CN (**11•2CH_3CN**) in Å.

Pt(1)-C(4)	1.980(2)	C(12)-C(13)	1.419(5)
Pt(1)-N(1)	1.964(4)	C(12)-C(15)	1.571(3)
Pt(1)-N(2)	1.949(4)	C(13)-C(14)	1.375(7)
Pt(1)-N(3)	1.999(2)	C(15)-C(16)	1.499(8)
N(1)-C(19)	1.411(3)	C(15)-C(17)	1.540(4)
N(1)-C(23)	1.343(6)	C(15)-C(18)	1.455(9)
N(2)-C(10)	1.324(5)	C(19)-C(20)	1.373(5)
N(2)-C(14)	1.323(4)	C(20)-C(21)	1.366(3)
N(3)-C(1)	1.340(3)	C(21)-C(22)	1.410(7)
N(3)-C(5)	1.340(7)	C(21)-C(24)	1.524(2)
N(5)-C(29)	1.158(2)	C(22)-C(23)	1.396(8)
N(6)-C(31)	1.161(2)	C(24)-C(25)	1.570(2)
N(7)-C(40)	1.139(5)	C(24)-C(26)	1.545(3)
N(8)-C(39)	1.193(4)	C(24)-C(27)	1.534(3)
N(28)-C(4)	1.161(2)	C(29)-C(30)	1.420(8)
C(1)-C(2)	1.352(8)	C(30)-C(31)	1.450(6)
C(2)-C(3)	1.396(7)	C(30)-C(32)	1.352(5)
C(3)-C(6)	1.506(4)	C(32)-C(33)	1.446(8)
C(3)-C(28)	1.403(5)	C(32)-C(37)	1.424(3)
C(5)-C(10)	1.495(3)	C(33)-C(34)	1.342(4)
C(5)-C(28)	1.400(9)	C(34)-C(35)	1.374(6)
C(6)-C(7)	1.595(2)	C(35)-C(36)	1.434(2)
C(6)-C(8)	1.498(3)	C(35)-C(38)	1.416(9)
C(6)-C(9)	1.535(7)	C(36)-C(37)	1.399(6)
C(10)-C(11)	1.390(7)	C(38)-C(39)	1.473(2)
C(11)-C(12)	1.446(8)	C(38)-C(40)	1.313(5)

Electrochemical Studies

Cyclic voltammetry experiments were carried out at a scan rate of either 100 or 200 mV/s on a CH Instruments Electrochemical Analyzer in either 0.1 or 0.2 M solutions of doubly-recrystallized $TBAPF_6$ in CH_2Cl_2 at a Pt disk working electrode with a Ag/AgCl reference and a Pt counter electrode.

The electrochemical properties of **1** (Figure 115) show a ligand centered reduction ascribed to the tbtrpy ligand. The first cathodic couple occurs at -0.9 V and appears to be reversible. The second cathodic couple occurs at -1.5 V and is irreversible. There is no anodic response upon scanning indicating that, unlike the work of Yam and coworkers, who first presented electrochemical studies on the terpyridine family of salts, there are no metal centered oxidations. There are expected to be no ligand-centered oxidations as the chloride ligand in the coordination sphere of platinum is electrochemically innocent.

Upon closer inspection of the cyclic voltammogram of (**4•CH_2Cl_2**) (Figure 116), only ligand centered cathodic waves are observed at -0.9 and -1.3 V respectively. The former cathodic couple appears to be reversible while the latter appears to be irreversible. As in the case of **1**, there are no ligand- or metal-centered oxidations indicating that the isocyanate ligand, much like the ancillary chloride ligand in **1** is also electrochemically innocent. Considering the attributes of voltammograms for **1** and (**4•CH_2Cl_2**), salts **2** and **3** should show only terpyridine-based reductions as both **2** and **3** possess electrochemically-innocent ligands and counter anions.

The voltammograms for salts **5** (Figure 117)**, 6,** and (**7•H_2O**) (Figure 118) are interesting because for the first-time ligand centered oxidations are seen. Also, the cyclic voltammogram for the salt $[Pt(tbtrpy)(sph)][BF_4]$ is presented (Figure 119).

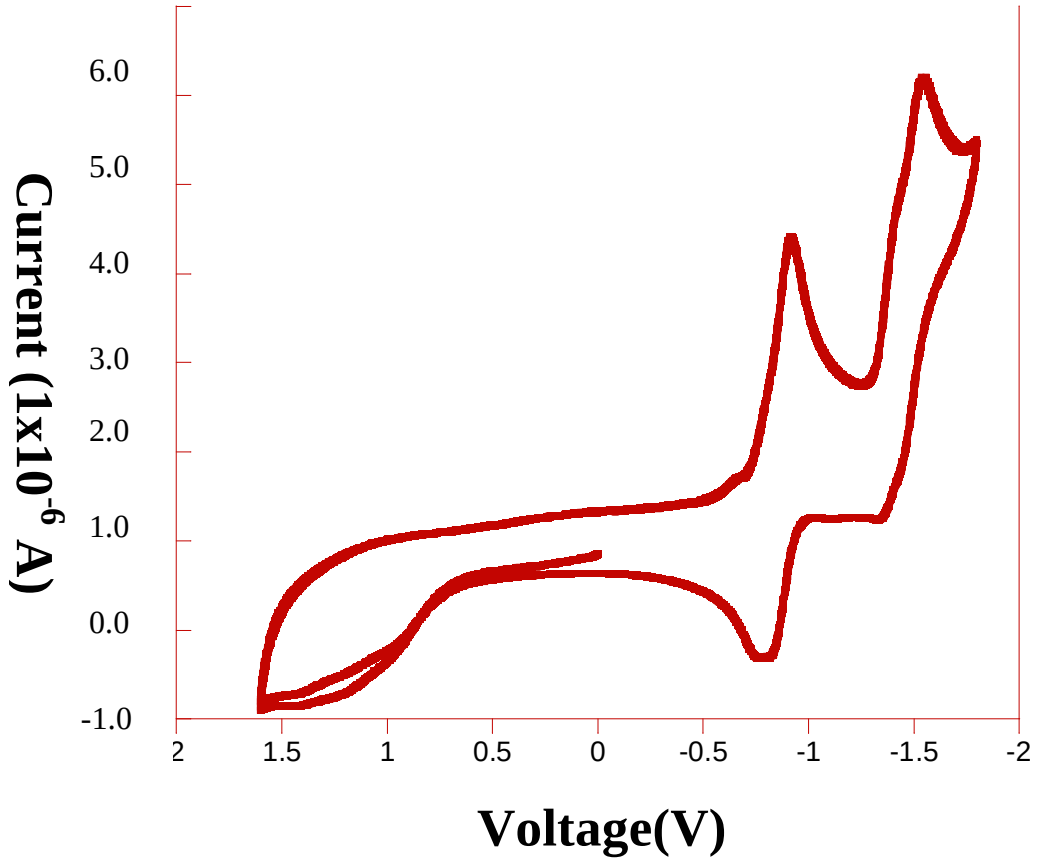

Figure 115. Cyclic voltammogram for [Pt(tbtrpy)Cl][Cl] (**1**) performed in a 0.1 M $TBAPF_6$ solution prepared from CH_2Cl_2 at a scanning potential of .2 V/s against Ag/AgCl reference electrode using a Pt disk working electrode and a Pt wire counter electrode.

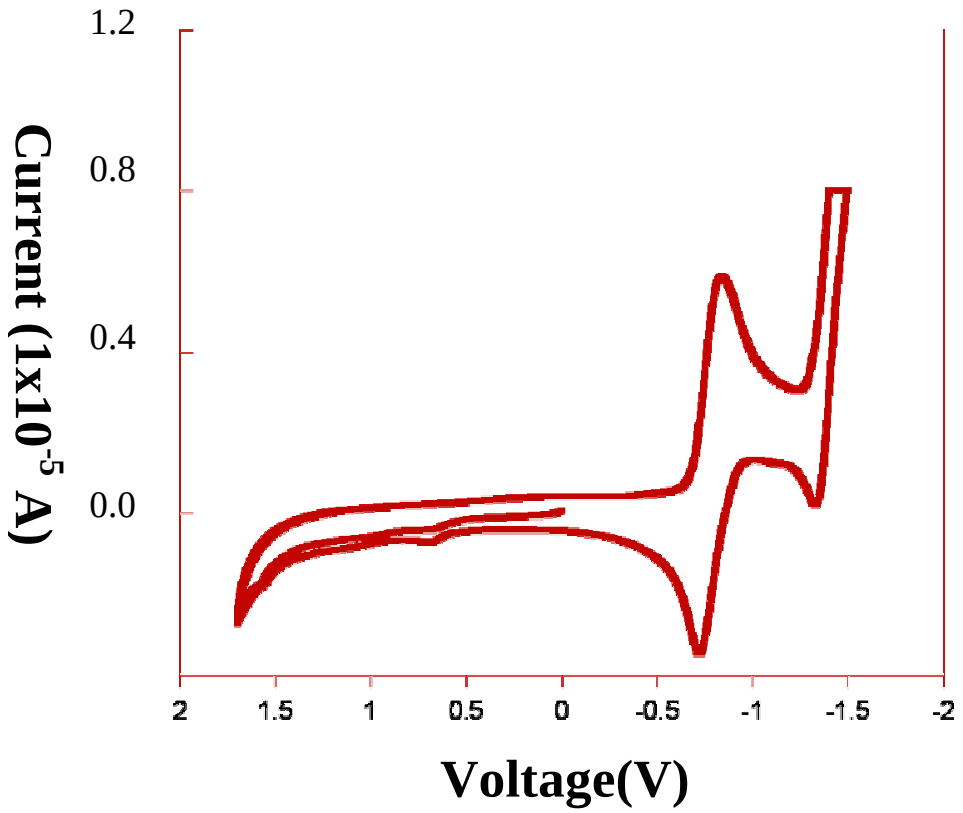

Figure 116. Cyclic voltammogram for [Pt(tbtrpy)(NCS)][BF_4] (**4•CH_2Cl_2**) done in a 0.1 M $TBAPF_6$ solution prepared from CH_2Cl_2 at a scanning potential of .2 V/s against Ag/AgCl reference electrode using a Pt disk working electrode and a Pt wire counter electrode.

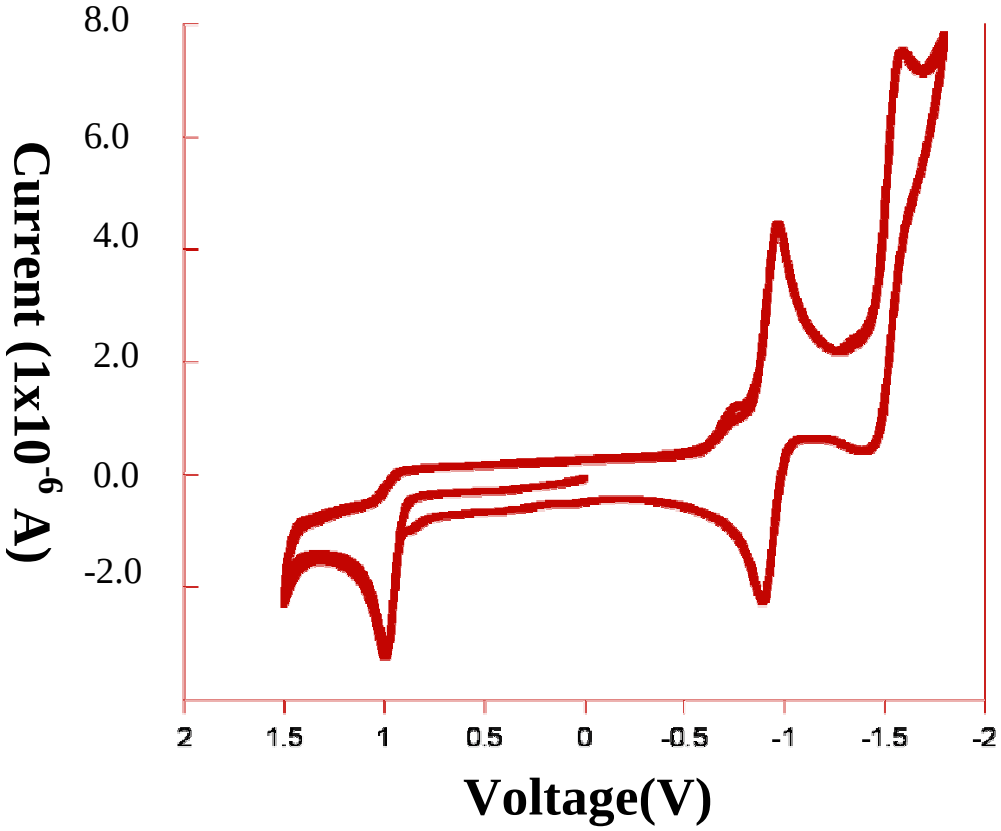

Figure 117. Cyclic voltammogram for [Pt(tbtrpy)(4-mbt)][BF_4] (**5**) done in a 0.1 M $TBAPF_6$ solution prepared from CH_2Cl_2 at a scanning potential of .2 V/s against Ag/AgCl reference electrode using a Pt disk working electrode and a Pt wire counter electrode.

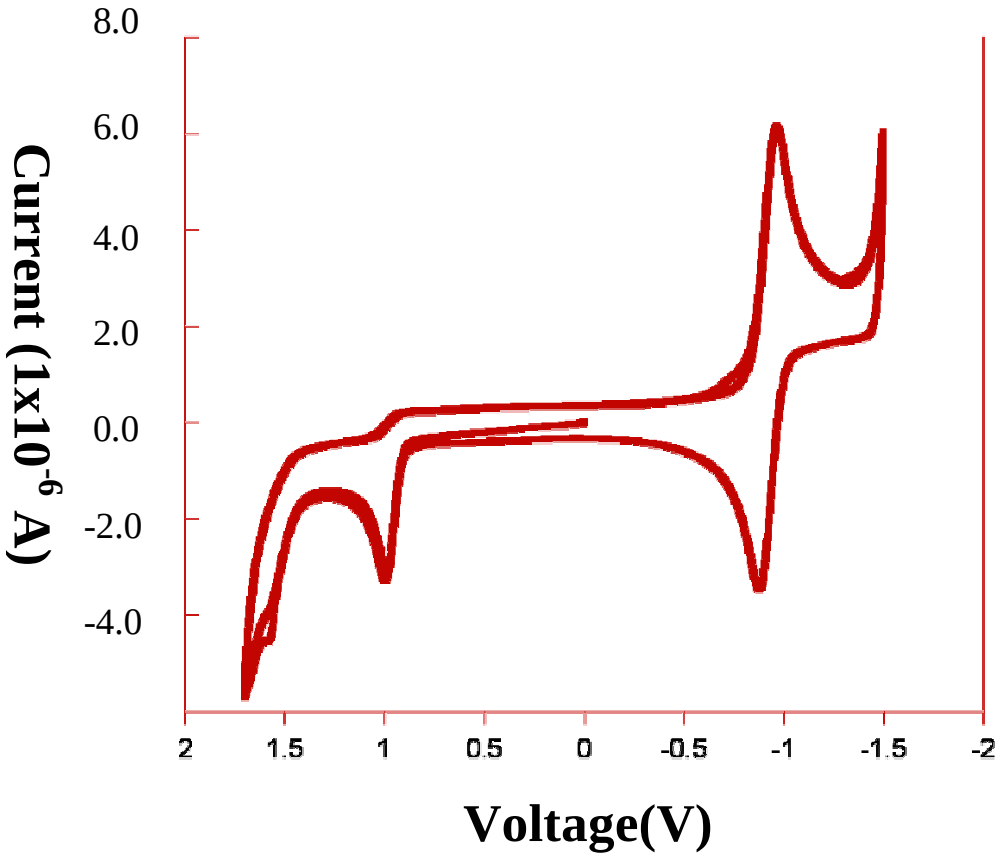

Figure 118. Cyclic voltammogram for [Pt(tbtrpy)(snap)][BF_4] (**7•H_2O**) done in a 0.1 M $TBAPF_6$ solution prepared from CH_2Cl_2 at a scanning potential of .2 V/s against Ag/AgCl reference electrode using a Pt disk working electrode and a Pt wire counter electrode.

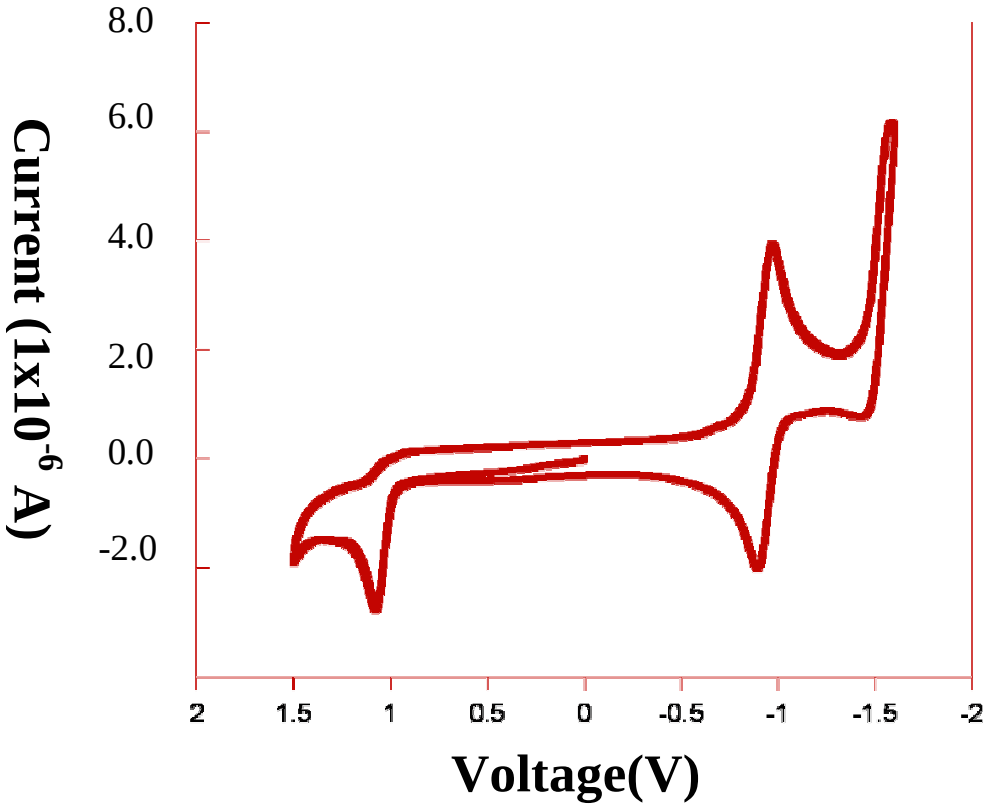

Figure 119. Cyclic voltammogram for [Pt(tbtrpy)sph][BF_4] done in a 0.1 M $TBAPF_6$ solution prepared from CH_2Cl_2 at a scanning potential of .2 V/s against Ag/AgCl reference electrode using a Pt disk working electrode and a Pt wire counter electrode.

Much like the previously described salts, these four salts show ligand centered cathodic couples at -0.9 and -1.5 V respectively. In a similar manner to the previously described voltammograms, the former redox couple is reversible while the latter was irreversible. Unlike the previous salts, there are irreversible oxidations at potentials between +0.98 and +1.1 V attributed to the oxidation of the ancillary thiolate ligand. These results are interesting upon considering the results of Yam and coworkers who claimed that the irreversible oxidations observed at ~+1.0 V were caused by the Pt(II)→ Pt(III) process. In the previously described salts where redox-innocent ancillary ligands were incorporated into the coordination sphere of platinum, no metal-based oxidations were observed. If the primary contributor to the observed anodic waves was the metal ion, a response would have been observed despite the presence of electrochemically innocent ligands.

The cyclic voltammogram for [Pt(tbtrpy)NCS][TCNQ] (Figure 120) presents a rich electrochemical nature, as it incorporates the TCNQ radical anion as the counterion. This organic acceptor is known to exist as a free species in the integral oxidation states of -1 and -2 as well as in the non-integral oxidation state of -0.5 in materials. Upon inspection of the cyclic voltammogram for this salt, terpyridine-centered cathodic waves were observed a -0.9 and -1.5 V respectively and like the preceding salts, the former wave is reversible while the latter is irreversible. The selection of the initial scanning potential at 0.0 V was critical because this potential lies between the first and second reduction potentials of TCNQ. The cathodic wave observed at -0.5 V is due to the reduction of TCNQ from its radical anion to its dianion. The first cathodic wave, also reversible in nature at +0.20 V is caused by

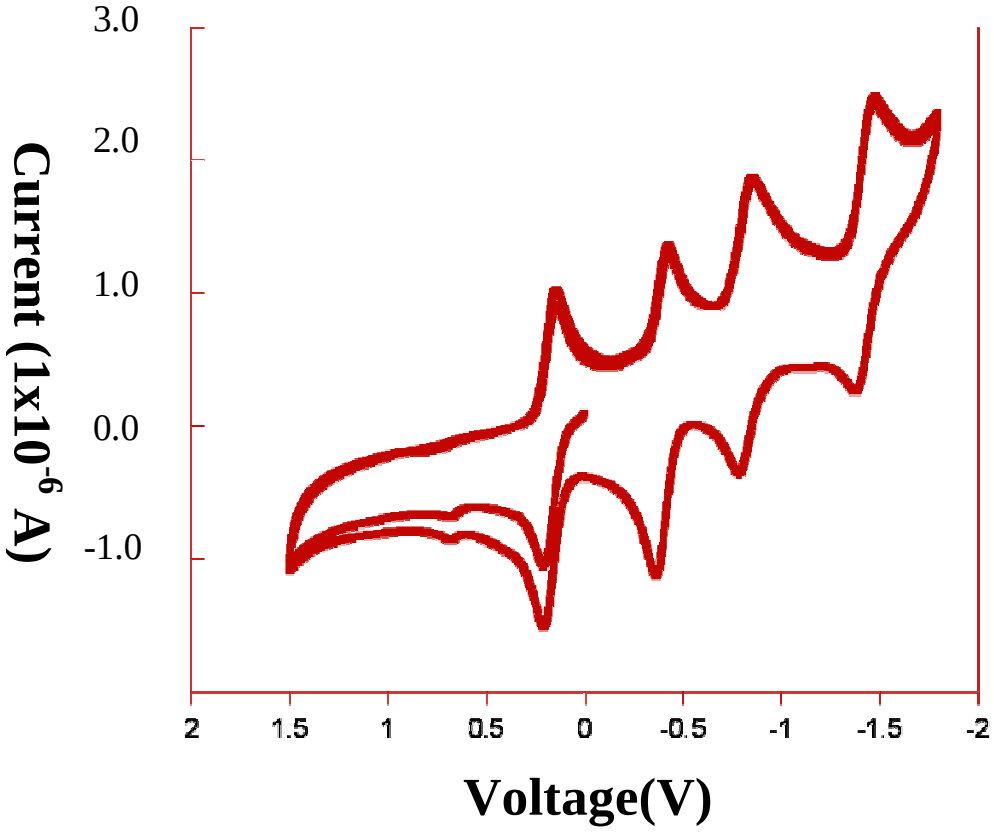

Figure 120. Cyclic voltammogram for [Pt(tbtrpy)(NCS)][TCNQ] done in a 0.1 M $TBAPF_6$ solution prepared from CH_2Cl_2 at a scanning potential of .2 V/s against Ag/AgCl reference electrode using a Pt disk working electrode and a Pt wire counter electrode.

the reduction of neutral TCNQ to its radical anion. No oxidation waves due to ligand- or metal-based processes are observed. Eventually, the incorporation of TCNQ radicals into salts containing arylthiolate ligands is the intended synthetic target. Based on the knowledge obtained thus far with salts containing electrochemically innocent ancillary ligands and counter ions as well as those salts involving redox-active thiolate ligands, the intended synthetic targets should show three separate electrochemical processes due to by the terpyridine ligand, the thiolate ligand, and TCNQ separately. Unfortunately, the TCNQ salts (**9•2H_2O**), (**10•2CH_2Cl_2**), and (**11•2CH_3CN**), obtained as by-products from crystallization attempts involving arylthiolate/TCNQ salts, do not contain thiolate ligands and should show separate cathodic waves from the terpyrdine ligand and TCNQ.

Conclusions

New platinum-terpyridine salts have been prepared in conjunction with the laboratory of Dr. Mohammad Omary and his students at the University of North Texas. The compounds were crystallized and their electrochemical properties were analyzed via cyclic voltammetry at Texas A&M. Among the salts prepared are those which possess thiolate ancillary ligands that display charge transfer bands red-shifted from those with chloride. Additional salts have been prepared which contain the reduced organocyanide acceptor TCNQ that, based on bond distances, exhibit additional reduction to a $(1+\delta)^-$ oxidation state. The absorption spectra for these salts show π-π^* transitions red-shifted from the charge transfer bands of the salts.

CHAPTER VII

CONCLUSIONS

The preparation of compounds containing sulfur donors is attractive because, of the level of electronic communication observed in compounds integrating this element. In this dissertation, the use of sulfur has been probed in the preparation of conducting materials such as those which possess oxidized TTF-like donors. The use of electrochemical and chemical oxidation pathways were the methods by which the oxidation of sulfur or selenium containing donors were oxidized to yield salts containing the donors' radical cation forms.[13] The use of sulfur-containing thiolate ligands have also seen use in the materials realm for preparing materials where a spectroscopic response at lower energies is beneficial.[68]

Various salts containing the donors TTF, *o*-Me_2TTF, TMTTF, BEDT-TTF, BPDT-TTF, and TMTSF were prepared utilizing various anions including spherical, tetrahedral, octahedral, bimetallic, cyanometallate, polyoxometallate, and metal(bis-dithiolene) anions. The primary method by which these compounds were characterized was X-ray crystallography. All of these systems revealed stacking of the radical cations, dominated by close intermolecular S•••S contacts. In the case of radical cation salts obtained between TTF and *o*-Me_2TTF and the cyanometallate anions, ornate networks of hydrogen bonds between interstitial water molecules and the cyanometallate anions were found to exist. The most interesting results existed between *o*-Me_2TTF and the anions Cl^-, Br^-, I^-, $[BF_4]^-$, and $[PF_6]^-$, and represent the first examples whereby salts were electrochemically prepared with donors in non-integral oxidation states. Among these salts, the salts prepared between the halide and tetrafluoroborate anions offered an

unprecedented packing of mixed-valence *o*-Me_2TTF donors. Based on crystallographic symmetry, the stacks are uniform and one-dimensional with intermolecular S•••S contacts at distances <3.5Å and show metallic conductivity to 110K. The salt with $[PF_6]^-$ presents a structural motif seen in the Bechgaard family of salts, where slight dimerization of the donor molecules occur in the solid state.[13] Conductivity measurements were also performed on salts containing the metal-metal bond containing dianion $[Re_2Cl_8]^{2-}$ and the donors BEDT-TTF and TMTSF and reveal that these compounds are weak semiconductors. In lieu of conductivity measurements, molecular magnetism was utilized as a qualitative means to observe itinerant electron density attributable to conducting electrons. In the cases of the *o*-Me_2TTF salts with the polyoxometallate anions $[W_6O_{19}]^{2-}$ and $[Mo_6O_{19}]^{2-}$, no TIP values were found, indicating that these compounds were diamagnetic insulators. Similar results were seen when molecular magnetism was used to probe samples of *o*-Me_2TTF with $[Co(CN)_6]^{3-}$.

Soluble, radical cation salts of TTF and some of its derivatives for use in metathesis reactions were prepared by reacting solutions of ammonium oxidizing agents with solutions of neutral donors. The salts were characterized by mass spectroscopy, UV-VIS spectroscopy, and X-ray crystallography and reveal that in the cases studied between oxidant solutions and the donors *o*-Me_2TTF, TMTTF, TTF, and $TTF(SCH_2CH_2CN)_4$, stable, soluble salts could be prepared.

Compounds were also prepared between TTF and the tri- and tetranitrofluorenone acceptors. A complex was also prepared between TMTTF and trinitrofluorenone. These preparations served as a method to prepare salts similar to TTF-TCNQ by utilizing chemical oxidation. Initial reports by Toscano and coworkers in 1989 revealed that the

dinitrofluorenone acceptor, with a first reduction potential of -0.78 V was capable of oxidizing TTF to an oxidation state of +0.20. In order to prepare a complex where more facile redox reactions could occur between the donor and acceptor, tetranitrofluorenone with a first-reduction potential of +0.14V was reacted with TTF. In order to further probe reactions between TTF and its derivatives and the nitrofluorenone family, TTF and TMTTF were reacted with trinitrofluorenone. Reactions between TTF and *o*-Me_2TTF with the organocyanide acceptors HAT-$(CN)_6$ and TCNB were also done. X-ray crystallography revealed in all cases the presence of integrated stacks of donors and acceptors. Infrared spectroscopy and revealed that very little to no spontaneous redox reactions occurred. Finally, molecular magnetism showed no temperature independent paramagnetism, showing that the systems were diamagnetic insulators.

The concept of course and fine-tuning of the spectroscopic response through the use of ligand coordination and integration of organic acceptors has seen limited use in materials applications. A second generation of hybrid inorganic/organic charge transfer systems were prepared utilizing Pt(dbbpy)(tdt) and the nitrofluorenone family of acceptors. Using a 2:1 ratio of donor:acceptor yielded a 2:2 phase with dintrofluorenone, a 1:1 phase with trinitrofluorenone, and a 2:1 phase with tetranitro-fluorenone. When the ratio was switched to 1:1, only a variation in the obtained stoichiometry of the donor/acceptor complex with tetranitrofluorenone was seen as another phase was obtained where the donor and acceptor molecules existed in a 1:1 ratio, instead of the previously obtained 2:1 phase. Infrared spectroscopy of the complexes suggests a partial electron transfer between the donor and acceptor. Through careful titration of solutions of the acceptor into dilute solutions of the donor, equilibrium constants were calculated

and strong interactions were found to exist between the donor and the tetranitrofluorenone acceptor. Also, solid-state diffuse reflectance spectroscopy revealed low energy transitions for the tri- and tetranitro complexes which make them suitable choices for materials based applications, such as solar cells or organic photovoltaic devices. Cyclic voltammetry measurements showed features indicative of the pure components.

Another class of compounds which could serve as another generation of photosensitizing dyes are the platinum-terpyridine salts. Much like the hybrid inorganic/organic supramolecular stacks, the spectroscopic response can be tuned to lower energies through the incorporation of ancillary, monodentate thiolate ligands. In order to balance the charge of the platinum, cationic unit, spectroscopically innocent anions such as Cl^- and $[BF_4]^-$ were used. The use of pre-reduced organic acceptors, such as $TCNQ^{\bullet -}$, serves a two-fold purpose. First, the radical anion balances the cationic charge of the platinum-terpyridine unit. Secondly, as seen in the case of the supramolecular stacks utilizing organocyanide acceptors, low energy transitions extending into the NIR-region resulted.[68] The terpyridine compounds with platinum showed a tunability level similar to that observed in complexes with Pt(diimine)(dithiolate) compound. Electrochemical measurements revealed reversible ligand-based reductions and thiolate-based oxidations. Electrochemical processes attributed to TCNQ were also observed.

REFERENCES

1 (a) Manriquez, J.M.; Yee, G.T.; McLean, R.S.; Epstein, A.J.; Miller, J.S. *Science*, **1991**, *252*, 1415. (b) Pei, Y.; Kahn, O.; Nakatani, K.; Codjovi, E.; Mathionère, C.; Sletten, J. *J. Am. Chem. Soc.* **1991**, *113*, 6558. (c) Cornelissen, J.P.; Le Loux, R.; Jansen, J.; Haasnoot, J.G.; Reedjik, J.; Horn, E.; Spek, A.L.; Pomarède, B.; Legros, J.P.; Reefman, D. *J. Chem. Soc. Dalton Trans.* **1992**, 2911. (d) Serroni, S.; Denti, G.; Campagna, S.; Juris, A.; Ciano, M.; Balzani, V. *Angew. Chem. Int. Ed. Engl.* **1992**, *31*, 1493. (e) Kollmar, C.; Kahn, O. *Acc. Chem. Res.* **1993**, *26*, 259. (f) Miller, J.S.; Epstein, A.J. *Angew. Chem. Int. Ed. Engl.* **1994**, *33*, 385. (g) O. Khan, *Molecular Magentism*, VCH, New York 1993. (h) Pomarède, B.;Garreau, B.; Malfante, I.; Valade, L.; Cassoux, P.; Legros, J.P.; Audouard, A.; Brossard, L.; Ulmet, J.P.; Doublet, M.L.; Canadell, E. *Inorg. Chem.* **1994**, *33*, 3401. (i) Stumpf, H.O.; Pei, Y.; Michaut, C.; Kahn, O.; Renard, J.R.; Ouahab, L. *Chem. Mater.* **1994**, *6*, 257. (j) Kaim, W. Moscherosch, M. Coord. Chem. Rev. **1994**, *129*, 157. (k) *The Physics and Chemistry of Organic Superconductors* ed. Saito, G.; Kagoshima, S. Springer, Berlin, 1990. (l) Wudl, F. *Acc. Chem. Res.* **1984**, *17*, 227. (m) Williams, J.M.; Wang, H.H.; Emge, T.J.; Geiser, U.; Beno, M.A.; Leung, P.C.W.; Carlson, K.D.; Thorn, R.J.; Schultz, A.J.; Whangbo, M.H. in *Prog. Inorg. Chem.*, ed. Lippard, S.J. Wiley, New York, 1987, vol.35, p. 51.

2 Davidson, A.; Boubekeur, K.; Pènicaud, A.; Auban, P.; Lenoir, C.; Batail, P.; Hervé, G. *J. Chem. Soc. Chem. Comm.* **1989**, 1373. (b) Pènicaud, A.; Boubekeur, K.; Batail, P.; Canadell, E.; Auban-Senzier, P.; Jerome, D. *J. Am. Chem. Soc.* **1993**, *115*, 4101. (c) Coulon, C.; Livage, C.; Gonzalez, L.; Boubekeur, K.; Batail, P. *J. Phys. 1*, **1993**, *3*, 1. (d) Coronado, E.; Gómez-García, C.J. *Comments Inorg. Chem.* **1995**, *17*, 255. (e) Gómez-García, C.J.; Giménez-Saiz, C.; Triki, S.; Coronado, E.; Magueres, P.L.; Ouahab, L.; Ducasse, L.; Sourisseau, C.; Delhaes, P.; *Inorg. Chem.* **1995**, *34*, 4139. (f) Galán-Mascarós, J.R.; Giménez-Saiz, C.; Triki, S.; Gómez-García, C.J.; Coronado, E.; Ouahab, L. *Angew. Chem. Int. Ed. Engl.* **1995**, *34*,1460. (g) Coronado, E.; Galán-Mascarós, J.R.; Giménez-Saiz, C.; Gómez-García, C.J.; Triki, S. *J. Am. Chem. Soc.* **1998**, *120*, 4671. (h) Kobayashi, H.; Tomita, H.; Naito,T.; Kobayashi, A.; Sakai, F.; Watanabe, T.; Cassoux, P. *J. Am. Chem. Soc.* **1996**, *118*, 368.

3 Kurmoo, M.; Graham, A.W.; Day, P.; Coles, S.J.; Hursthouse, M.B.; Caulfield, J.L.; Singleton, J.; Pratt, F.L.; Hayes, W.; Ducasse, L.; Guinneau, P. *J. Am. Chem. Soc.* **1995**, *117*, 12209.

4 Coronado, E.; Galán-Mascarós, J.R.; Gómez-Garcia, C.J.; Laukhin, V. *Nature*, **2000**, *408*, 447.

5 (a) Ishikawa, A.; Fischer, Ø. *Solid State Commun.* **1977**, *23*, 37. (b) Lynn, J.W.; Shirane, G.; Thomlinson, W.; Sheldon, R.N. *Phys. Rev. Lett.* **1981**, *46*, 368.

6 (a) Fertig, W.A.; Johnston, D.C.; DeLong, L.E.; McCallum, R.W.; Maple, M.B.; Matthias, B.T. *Phys. Rev. Lett.* **1977**, *38*, 987. (b) Moncton, D.E.; McWhann, D.B.; Schmidt, P.H.; Shirane, G.; Thomlinson, W.; Maple, M.B.; MacKay, H.B.; Woolf, L.D.; Fisk, Z.; Johnston, D.C. *Phys. Rev. Lett.* **1980**, *45*, 2060.

7 Beauchamp, K.M.; Spalding, G.C.; Huber, W.H.; Goldman, A.M. *Phys. Rev. Lett.* **1994**, *73*, 2752.

8 Wudl, F.; Smith, G.M.; Hufnagel, E.J. *Chem. Comm.* **1970**, 1453.

9 (a) Salahub, D.R.; Messmer, R.P. Herman, F. *Phys. Rev. B* **1976**, *13*, 4252. (b) Tanaka, H.; Okano, Y.; Kobayashi, H.; Suzuki, W.; Kobayashi, A. *Science* **2001**, *291*, 285. (c) Kobayashi, A.; Okano, Y.; Kobayashi, H. *J. Phys. Soc. Jpn.* **2006**, *75*, 051002-1. (d) Abboud, K.A.; Clevenger, M.B.; de Oliviera, G.F.; Talham, D.R. *J. Chem. Soc,. Chem. Comm.* **1993**, 1560.

10 (a) Ferraris, J.; Cowan, D.O.; Walatka, V.J.; Perlstin, J.H. *J. Am. Chem. Soc.* **1973**, *95*, 948. (b) Coleman, L.B.; Cohen, M.J.; Sandmand, D.J.; Yamagishi, F.G.; Garito, A.F.; Heeger, A.J. *Solid State Commun.* **1973**, *12*, 1135.

11 Phillips, T.E.; Kistenmacher, J.; Ferraris, J.P.; Cowan, D.O. *Chem. Comm.* **1973**, 471.

12 Williams, J.M.; Ferraro, J.R.; Thorn, R.J.; Carlson, K.D.; Geiser, U.; Wang, H.H.; Kini, A.M.; Whangbo, M-H. *Organic Superconductors*, Prentice Hall, Englewood Cliffs, New Jersey, 1992.

13 (a) Fourmigué, M.; Uzelmeier, C.E.; Boubekeur, K.; Bartley, S.L.; Dunbar, K.R. *J. Organomet. Chem.* **1997**, *529*, 343. (b) Smucker, B.W.; Dunbar, K.R. *Dalton Trans.* **2000**, 1309. (c) Uzelmeier, C.E.; Smucker, B.W.; Reinheimer, E.W.; Shatruk, M.; O'Neal, A.; Fourmigué, M.; Dunbar, K.R. *Dalton Trans.* **2006**, 5259. (d) Avarvari, N.; Fourmigué, M. *Chem. Comm.* **2004**, 1300. (e) Avarvari, N.; Martin, D.; Fourmigué, M. *J. Organomet. Chem.* **2002**, *643-644*, 292. (f) Gouverd, C.; Biaso, F.; Cataldo, L.; Berclaz, T.; Geoffrey, M.; Levillain, E.; Avarvari, N.; Fourmigué, M.; Sauvage, F.X.; Wartelle, C. *Phys. Chem. Chem. Phys.* **2005**, *7*, 85. (g) Kobayashi, A.; Fujiwara, E.; Kobayashi, H. *Chem. Rev.* **2004**, *104*, 5243.

14 Bechgaard, K.; Jacobsen, C.S.; Mortensen, K.; Pedersen, H.J.; Thorup, N. *Solid State Commun.* **1980**, *33*, 1119.

15 Parkin, S.S.P.; Engler, E.M.; Schumaker, R.R.; Lagier, R.; Lee, V.Y.; Scott, J.C.; Greene, R.L. *Phys. Rev. Lett.* **1983**, *50*, 270.

16 Bechgaard, K.; Carneiro, K.; Rasmussen, F.B.; Olsen, M. *J. Am. Chem. Soc.* **1981**, *103*, 2440.

17 Mori, T. *Bull. Chem. Soc. Jpn.* **1998**, *71*, 2509.

18 (a) Alberola, A.; Coronado, E.; Galán-Mascarós, J.R.; Giménez-Saiz, C.; Gómez-García, C.J. *J. Am. Chem. Soc.* **2003**, *125*, 10774.

19 Day, P.; Kurmoo, M.; Mallah, T.; Marsden, I.R.; Friend, R.H.; Pratt, F.L.; Hayes, W.; Chasseau, D.; Gaulthier, J.; Bravic, G.; Ducasse, L. *J. Am. Chem. Soc.* **1992**, *114*, 10722.

20 Coronado, E.; Falvello, L.R.; Galán-Mascarós, J.R.; Giménez-Saiz, C.; Gómez-García, C.J.; Laukhin, V.N.; Pérez-Benítez, A.; Rovira, C.; Veciana, J. *Adv. Mater.* **1997**, *9*, 984.

21 Kobayashi, H.; Tomita, H.; Naito, T.; Kobayashi, A.; Sakai, F.; Watanabe, T.; Cassoux, P. *J. Am. Chem. Soc.* **1996**, *118*, 368.

22 Le Magueres, P.; Ouahab, L.; Briard, P.; Even, J.; Bertault, M.; Toupet, L.; Ramos, J.; Gómez-García, C.J.; Delhaes, P. *Mol. Cryst. Liq. Cryst.* **1997**, *305*, 479.

23 (a) Clemente-León, M.; Coronado, E.; Galán-Mascarós, J.R.; Gómez-García, C.J.; Fabre, J.M. *Synth. Met.* **1999**, *103*, 2279. (b) Clemente-León, M.; Coronado, E.; Galán-Mascarós, J.R.; Giménez-Saiz, C.; Gómez-García, C.J.; Ribera, E.; Vidal-Gancedo, J.; Rovira, C.; Canadell, E.; Laukhin, V. *Inorg. Chem.* **2001**, *40*, 3526.

24 (a) Clemente-León, M.; Coronado, E.; Galán-Mascarós, J.R.; Gómez-García, C.J.; Rovira, C.; Laukhin, V.N. *Synth. Met.* **1999**, *103*, 2339. (b) Clemente-León, M.; Coronado, E.; Galán-Mascarós, J.R.; Giménez-Saiz, C.; Gómez-García, C.J.; Fabre, J.M.; Mousdis, G.A.; Papavassiliou, G.C. *J. Solid State Chem.* **2002**, *168*, 616.

25 Bouherour, S.; Ouahab, L.; Peńa, O.; Padiou, J.; Grandjean, D. *Acta. Cryst.* **1989**, *C45*, 371.

26 (a) Pressprich, M.R.; White, M.A.; Vekhter, Y.; Coppens, P. *J. Am. Chem. Soc.* **1994**, *116*, 5233. (b) Carducci, M.D.; Pressprich, M.R.; Coppens, P. *J. Am. Chem. Soc.* **1997**, *119*, 2669.

27 Yu, H.; Zhu, D. *Physica C* **1997**, *282*, 1893.

28 Gener, G.; Canadell, E.; Kashanov, S.S.; Zorina, L.V.; Shibaeva, R.P.; Kushch, L.A.; Yagubskii, E.B. *Solid State Commun.* **1999**, *111*, 329.

29 Kushch, L.; Buratov, L.; Tkacheva, V.; Yagubskii, E.; Zorina, L.; Khasanov, S.; Shibaeva, R. *Synth. Met.* **1999**, *102*, 1646.

30 Coronado, E.; Gómez-García, C.J. *Chem. Rev.* **1998**, *98*, 273.

31 Triki, S.; Ouahab, L.; Padiou, J.; Grandjean, D. *J. Chem. Soc., Chem. Comm.* **1989**, 1068.

32 (a) Bellitto, C.; Attanasio, D.; Bonamico, M.; Fares, V. Imperatori, P.; Patrizio, S. *Mater. Res. Soc. Symp. Proc.* **1990**, *173*, 143. (b) Attanasio, D.; Bellitto, C.; Bonamico, M.; Fares, V.; Imperatori, P. *Gazz. Chim. Ital.* **1991**, *121*, 155.

33 Triki, S.; Ouahab, L.; Grandjean, D.; Fabre, J.M. *Acta Cryst.* **1991**, *C47*, 1371.

34 Triki, S.; Ouahab, L.; Halet, J.F.; Peña, O.; Padiou, J.; Grandjean, D.; Garrigou-Lagrange, C.; Delhaes, P. *J.Chem. Soc., Dalton Trans.* **1992**, 1217.

35 (a) Gómez-García, C.J.; Ouahab, L.; Giménez-Saiz, C.; Triki, S.; Coronado, E.; Delhaes, P. *Angew. Chem., Int. Ed. Engl.* **1994**, *33*, 223. (b) Gómez-García, C.J.; Giménez-Saiz, C.; Triki, S.; Coronado, E.; Le Magueres, P.; Ouahab, L.; Ducasse, L.; Sourisseau, C.; Delhaes, P. *Inorg. Chem.* **1995**, *34*, 4139. (c) Gómez-García, C.J.; Giménez-Saiz, C.; Triki, S.; Coronado, E.; Ducasse, L.; Le Magueres, P.; Ouahab, L. *Synth. Met.* **1995**, *70*, 783. (d) Galán-Mascarós, J.R.; Giménez-Saiz, C.; Triki, S.; Gómez-García, C.J.; Coronado, E.; Ouahab, L. *Angew. Chem., Int. Ed. Engl.* **1995**, *34*, 1460. (e) Coronado, E.; Galán-Mascarós, J.R.; Giménez-Saiz, C.; Triki, S.; Delhaes, P. *Mol. Cryst. Liq. Cryst.* **1995**, *274*, 89. (f) Coronado, E.; Galán-Mascarós, J.R.; Giménez-Saiz, C.; Gómez-García, C.J.; Triki, S. *J. Am. Chem. Soc.* **1998**, *120*, 4671. (g) Clemente-León, M.; Coronado, E.; Galán-Mascarós, J.R.; Giménez-Saiz, C.; Gómez-García, C.J.; Fernández-Otero, T. *J. Mater. Chem.* **1998**, *8*, 309.

36 Coronado, E.; Galán-Mascarós, J.R.; Giménez-Saiz, C.; Gómez-García, C.J.; Falvello, L.R.; Delhaés, P. *Inorg. Chem.* **1998**, *37*, 2183.

37 Coronado, E.; Galán-Mascarós, J.R.; Giménez-Saiz, C.; Gómez-García, C.J.; Rovira, C.; Tarrés, J.; Triki, S.; Veciana, J. *J. Mater. Chem.* **1998**, *8*, 313.

38 Triki, S.; Ouahab, L.; Grandjean, D.; Amiel, J.; Garrigou-Lagrange, C.; Delhaes, P.; Fabre, J.M. *Synth. Met.* **1991**, *41-43*, 2589.

39 Triki, S.; Ouahab, L.; Fabre, J.M. *Acta Cryst.* **1994**, *C50*, 219.

40 Triki, S.; Ouahab, L.; Grandjean, D.; Canet, R.; Garrigou-Lagrange, C.; Delhaes, P. *Synth. Met.* **1993**, *55-57*, 2028.

41 Coronado, E.; Galán-Mascarós, J.R.; Giménez-Saiz, C.; Gómez-García, C.J.; Laukhin, V.N. *Adv. Mater.* **1996**, *8*, 801.

42 Coronado, E.; Galán-Mascarós, J.R.; Gómez-García, C.J.; Ensling, J.; Gütlich, P. *Chem. Eur. J.* **2000**, *6*, 552.

43 Le Maguerès, P.; Ouahab, L.; Golhen, S.; Grandjean, D.; Peña, O.; Jegaden, J.-C.; Gómez-García, C.J.; Delhaès, P. *Inorg. Chem.* **1994**, *33*, 5180.

44 Wudl, F. *J. Am. Chem. Soc.* **1975**, *97*, 1962.

45 Lagros, J.P.; Bousseau, M.; Valade, L.; Cassoux, P. *Mol. Cryst. Liq. Cryst.* **1983**, *100*, 181.

46 Coronado, E.; Galán-Mascarós, J.R.; Giménez-Saiz, C.; Gómez-García, C.J.; Ruiz-Perez, C. *Eur. J. Inorg. Chem.* **2003**, 2290.

47 Okawa, H.; Mitsumi, M.; Ohba, M.; Kodera, M.; Matsumoto, N. *Bull. Chem. Soc. Jpn.* **1994**, *67*, 2139.

48 Soriano-García, M.; Toscano, R.A.; Robles-Martínez, J.G.; Salmerón-Valverde, A.; Lezama-Ramírez, R. *Acta. Cryst.* **1989**, *C45*, 1442.

49 Salmerón-Valverde, A.; Robles-Martínez, J.G.; Lezama-Ramírez, R.; Juárez-Posadas, J.; Zehe, A.; Soriano-García, M.; Toscano, R.A. *Synth. Met.* **1993**, *58*, 73.

50 Loufy, R.O.; Hsiao, C.K.; Ong, B.S.; Keoshkerian, B. *Can. J. Chem.* **1984**, *62*, 1877.

51 Meyer, T.J. *Acc. Chem. Res.* **1989**, *22*, 163.

52 Pelizzetti, E.; Serpone, F. *Homogeneous and Heterogeneous Photocatalysts*; Pelizzeti, E., Serpone, N., Ed.; D. Reidel Publishing: Dordrecht, Holland, 1985.

53 Cheng, L.-T.; Tam, W.; Eaton, D.F. *Organometallics* **1990**, *9*, 2856.

54 Prasad, P.N.; Reinhardt, B.A. *Chem. Mater.* **1990**, *2*, 660.

55 Friedman, A.E.; Chambron, J.-C.; Sauvage, J.-P.; Turro, N.J.; Barton, J.K. *J. Am. Chem. Soc.* **1990**, *112*, 4960.

57 O'Regan, B.; Grätzel, M. *Nature* **1991**, *353*, 737.

58 Zuleta, J.A.; Chesta, C.A.; Eisenberg, R. *J. Am. Chem. Soc.* **1989**, *111*, 8916.

59 Chan, C.-W.; Cheng, L.-K.; Che, C.-M. *Coord. Chem. Rev.* **1994**, *132*, 87.

60 Blanton, C.B.; Murtaza, Z.; Shaver, R.J.; Rillemma, D.P. *Inorg. Chem.* **1992**, *31*, 3230.

61 Maestri, M.; Sandrini, D.; Balzani, V.; von Zelewsky, A.; Deuschel-Cornioley, C.; Jolliet, P. *Helv. Chim. Acta* **1988**, *71*, 1053.

62 Chan, C.-W.; Lai, T.F.; Che, C,-M.; Peng, S.-M. *J. Am. Chem. Soc.* **1993**, *115*, 11245.

63 Aldridge, T.K.; Stacy, E.M.; McMillin, D.R. *Inorg. Chem.* **1994**, *33*, 722.

64 Chan, C.-W.; Che, C.-M.; Cheng, M.-C.; Wang, Y. *Inorg. Chem.* **1992**, *31*, 4874.

65 Yam, V.W.-W.; Hui, C.-K.; Yu, S.-Y.; Zhu, N. *Inorg. Chem.* **2004**, *43*, 812.

66 Cummings, S.D.; Eisenberg, R. *J. Am. Chem. Soc.* **1996**, *118*, 1949.

67 Islam, A.; Sugihara, H,; Hara, K.; Singh, L.-P; Katoh, R.; Yanagida, M.; Takahasi, Y.; Murata, S.; Arakawa, H. *Inorg. Chem.* **2001**, *40*, 5371.

68 Smucker, B.W.; Hudson, J.M.; Omary, M.A.; Dunbar, K.R. *Inorg. Chem.* **2003**, *42*, 4714.

69 (a) Lippard, S.J. *Acc. Chem. Res.* **1978**, *11*, 211. (b) Howe-Grant, M.; Lippard, S.J. *Biochemistry* **1979**, *18*, 5762.

70 (a) Kwok, W.M.; Phillips, D.L.; Yeung, P.K.-K.; Yam, V.W.-W. *J. Phys. Chem. A* **1997**, *101*, 9286. (b) Yam, V.W.-W.; Tao, C.-H.; Zhang, L.; Wong, K.M.-C.; Cheung, K.-K. *Organometallics* **2001**, *20*, 453. (c) Yam, V.W.-W.; Tang, R.P.-L.; Wong, K.M.-C.; Cheung, K.-K. *Organometallics* **2001**, *20*, 4476.

71 Wong, K.M.-C.; Tang, W.-S.; Chu, B.W.-K.; Zhu, N.; Yam, V.W.-W. *Organometallics* **2004**, *23*, 3459.

72 Yam, V.W.-W.; Wong, K.M.-C.; Zhu, N. *J. Am. Chem. Soc.* **2002**, *124*, 6506.

73 Coronado, E.; Day, P. *Chem. Rev.* **2004**, *104*, 5419.

74 Coronado, E.; Galán-Mascarós, J.R.; Gómez-García, C.J. *J.Chem. Soc., Dalton Trans.* **2000**, 205.

75 Martin, L.; Turner, S.S.; Day, P.; Giuonneau, P.; Howard, J.A.K.; Uriuchi, M.; Yakushi, K. *J. Mater. Chem.* **1999**, *9*, 2731.

76 (a) Triki, S.; Bérézovsky, F.; Pala, J.S.; Riou, A.; Molinié, P. *Synth. Met.* **1999**, *103*, 1974. (b) Triki, S.; Bérézovsky, F.; Pala, J.S.; Gómez-García, C.J.; Coronado, E.; Costuas, K.; Halet, J.F. *Inorg. Chem.* **2001**, *40*, 5127.

77 Kepert, C.J.; Kurmoo, M.; Day, P. *Inorg. Chem.* **1997**, *36*, 1128.

78 Fettoui, M.; Ouahab, L.; Perrin, A.; Grandjean, D.; Fabre, J.M. *Acta Cryst.* **1991**, *C47*, 2457.

79 Alemida, M.; Henriques, R.T. In *Handbook of Organic Conductive Molecules and Polymers. Volume 1: Charge-transfer Salts, Fullerenes and Photoconductors*; Nalwa, H.S., Ed.; John Wiley & Sons Ltd.: New York, 1997; Chapter 2, p 87.

80 Chi,X.; Scott, B.; Lawes, G.; Ramirez, A.P. *J. Chem. Cryst.* **2004**, *34*, 249.

81 (a) Alcacer, L.; Novais, H.; Pedroso, F.; Flandrois, S.; Colon, C.; Chasseau, D.; Caultier, J. *Solid State Commun.* **1980**, *35*, 945. (b) Underhill, A.E.; Tonge, J.S.; Clemenson, P.I.; Wang, H.-H.; Williams, J.M. *Mol. Cryst. Liq. Cryst.* **1985**, *125*, 439. (c) Reith, W.; Polborn, K.; Amberger, E. *Angew. Chem. Int. Ed. Engl.* **1988**, *27*, 699.

82 Mori, H.; Hirabayashi, I.; Tanaka, S.; Mori, T.; Maruyama, Y. *Synth. Met.* **1995**, *70*, 1177.

83 Fourmigué, M.; Krebs, F.C.; Larsen, J. *Synthesis* **1993**, 509.

84 Cotton, F.A.; Curtis, N.F.; Johnson, B.F.G.; Robinson, W.R. *Inorg. Chem.* **1965**, *4*, 326.

85 Che, M.; Fournier, M.; Launay, J.-P. *J. Chem. Phys.* **1979**, *71*, 1954.

86 Siemens Corp., Analytical X-Ray Instruments Inc., Madison, WI, 1994-1996.

87 G.M. Sheldrick, SADABS, Program for Siemens area detector absorption correction, University of Göttingen, Germany, 1996.

88 G.M. Sheldrick, XPREP, Program for space group determination, University of Göttingen, Germany, 1996.

89 G.M. Sheldrick, SHELXS-97, Program for crystal structure determination, University of Göttingen, Germany, 1997.

90 G.M. Sheldrick, SHELXTL, An integrated system for solving refining and displaying crystal structures from diffraction data (Revision 5.1), University of Göttingen, Germany, 1985.

91 Barbour, L.J. *J. Supramol. Chem.* **2001**, *1*, 189.

92 Whangbo, M. -H.; Hoffmann, R. *J. Am. Chem. Soc.*, 1978, **100**, 6093.

93 (a) Coronado, E.; Galán-Mascarós, J.R.; Gómez-García, C.J.; Laukhin, V. *Nature* **2000**, *408*, 447. (b) Alberola, A.; Coronado, E.; Galán-Mascarós, J.R.; Giménez-Saiz, C.; Gómez-García, C.J. *J. Am. Chem. Soc.* **2003**, *125*, 10774. (c) Coronado, E.; Galán-Mascarós, J.R.; Gómez-García, C.J.; Murcia-Martínez, A.; Canadell, E. *Inorg. Chem.* **2004**, *43*, 8072. (d) Coronado, E.; Galán-Mascarós, J.R.; Gómez-García, C.J.; Martínez-Ferrero, E.; van Smaalen, S. *Inorg. Chem.* **2004**, *43*, 4808. (e) Clemente-León, M.; Coronado, E.; Galan-Mascarós, J.R.; Giménez-Saiz, C.; Gómez-García, C.J.; Ribera, E.; Vidal-Gancedo, J.; Rovira, C.; Canadell, E.; Laukhin, V. Inorg. *Chem.* **2001**, *40*, 3526. (f) Clemente-León, M.; Coronado, E.; Galán-Mascarós, J.R.; Gómez-García, C.J.; Rovira, C.; Laukhin, V.N. *Synth. Metals* **1999**, *103*, 2339. (g) Clemente-León, M.; Coronado, E.; Galán-Mascaros, J.R.; Giménez-Saiz, C.; Gómez-García, C.J.; Fabre, J.M. *Synth. Metals* **1999**, *103*, 2279. (h) Kobayashi, H.; Tomita, H.; Naito, T.; Kobayashi, A.; Sakai, F.;

Watanabe, T.; Cassoux, P. *J. Am. Chem. Soc.* **1996**, *118*, 368. (i) Kurmoo, M.; Graham, A.W.; Day, P.; Coles, S.J.; Hursthouse, M.B.; Caulfield, J.L.; Singleton, J.; Pratt, F.L.; Hayes, W.; Ducasse, L.; Guionneau, P. *J. Am. Chem. Soc.* **1995**, *117*, 12209. (j) Bousseau, M.; Valade, L.; Legros, J.P.; Cassoux, P.; Garbauskas, M.; Interrante, L.V. *J. Am. Chem. Soc.* **1986**, *108*, 1908. (k) Perruchas, S.; Boubekeur, K.; Auban-Senzier, P. *J. Mater. Chem.* **2004**, *14*, 3509. (l) Kazheva, O.N.; Alexandrov, G.G.; Dyachenko, O.A.; Zinenko, T.N.; Kravchenko, A.V.; Staroub, V.A.; Khotkevich, A.V. *Synth. Metals* **2006**, *156*, 251; (m) Chi, X.; Scott, B.; Lawes, G.; Ramirez, A.P. *J. Chem. Cryst.* **2004**, *34*, 249.

94 Umland, T.C.; Allie, S.; Kuhlmann, T.; Coppens, P. *J. Phys. Chem.* **1987**, *92*, 6456.

95 Fourmigué, M.; Batail, P. *Chem. Rev.* **2004**, *104*, 5379.

96 Cotton, F.A.; Harris, C.B. *Inorg. Chem.* **1965**, *4*, 330.

97 Mhanni, A.; Ouahab, L.; Grandjean, D. *Acta Cryst.* **1993**, *C49*, 1187.

98 Dolbecq, A.; Guirauden, A.; Fourmigué, M.; Boubekeur, K.; Batail, P.; Rohmer, M.M.; Bénard, M.; Sallé, M.; Blanchard, P. *J.Chem. Soc., Dalton Trans.* **1999**, 1241.

99 Wudl, F.; Kaplan, M.L. *Inorg. Synthesis* **1979**, *19*, 27.

100 Svenstrup, N.; Rasmussen, K.M.; Hansen, T.K.; Becher, J. *Synthesis* **1994** 809.

101 (a) Bell, F.A.; Ledwith, A.; Sherrington, D.C. *J. Chem. Soc.* **1969** 2719. (b) Yueh, W.; Bauld, N.L. *J. Am. Chem. Soc.* **1995**, *117*, 5671.

102 Williams, J.M.; Ferraro, J.R.; Thorn, R.J.; Carlson, K.D.; Geiser, U.; Wang, H.H.; Kini, H.M.; Whangbo, M.H. In *Organic Superconductors. Synthesis, Structure, Properties and Theory*; Grimes, R.N., Ed.; Prentice Hall: Englewood Cliffs, NJ, 1992 264-287.

103 Hünig, S.; Schlaf, H.; Kiesslick, G.; Schentzow, D. *Tet. Lett.* **1969** 2271.

104 Torrance, J.B.; Scott, B.A.; Weber, B.; Kaufman, F.B.; Seiden, P.E. *Phys. Rev. B* **1979**, *19*, 730.

105 Perepichka, I.F.; Kuz'mina, L.G.; Perepchika, D.F.; Bryce, M.R.; Goldenberg, L.M.; Popov, A.F.; Howard, J.A.K. *J. Org. Chem.* **1998**, *63*, 6484.

106 Perepichka, I.F.; Popov, A.F.; Orekhova, T.V.; Bryce, M.R.; Andrievskii, A.M.; Batsanov, A.S.; Howard, J.A.K.; Sokolov, N.I. *J. Org. Chem.* **2000**, *65*, 3053.

107 Kuz'mina, L.G.; Perepichka, I.F.; Perepchika, D.F.; Howard, J.A.K.; Bryce, M.R. *Cryst. Reports* **2002**, *47*, 251.

108 Horiuchi, S.; Yamochi, H.; Saito, G.; Sakaguchi, K.; Kusunoki, M. *J. Am. Chem. Soc.* **1996**, *118*, 8604.

109 Olmstead, M.M.; Jiang, F.; Attar, S.; Balch, A.L. *J. Am. Chem. Soc.* **2001**, *123*, 3260.

110 Szalay, P.S.; Galán-Mascarós, J.R.; Clerac, R.; Dunbar, K.R. *Synth. Met.* **2001**, *122* 535.

111 (a) Miller, J.S.; Zhang, J.H.; Reiff, W.M.; Dixon, D.A.; Preston, L.D.; Reis Jr., A.H.; Gebert, E.; Extine, M.; Troup, J.; Epstein, A.J.; Ward, M.D. *J. Phys. Chem.* **1987**, *91*, 4344; (b) Dixon, D.A.; Calabrese, J.C.; Miller, J.S. *J. Phys. Chem.* **1989**, *93*, 2284.

112 Rademacher, J.; Kanakarajan, K.; Czarnik, A.W. *Synthesis* **1994** 378.

113 Szalay, P.S.; Galán-Mascarós, J.R.; Schottel, B.L.; Bacsa, J.; Peréz, L.M.; Ichimura, A.S.; Chouai, A.; Dunbar, K.R. *J. Cluster Sci.* **2004**, *15*, 503.

114 (a) Ferraris, J.; Cowan, D.O.; Walatka, V.V.; Perlstein, J.H. *J. Am. Chem. Soc.* **1973**, *95*, 948. (b) Coleman, L.B.; Cohen, M.J.; Sandman, D.J.; Yamagishi, F.G.; Garito, A.F.; Heeger, A.J. *Solid State Commun.* **1973**, *12*, 1125.

115 (a) Bousseau, M.; Valade, L.; Legros, J.-P.; Cassoux, P.; Garbauskas, M.; Interrante, L.V. *J. Am. Chem. Soc.* **1986**, *108*, 1908. (b) Brossard, L.; Bousseau, M.; Ribault, M.; Valade, L.; Cassoux, P. *C.R. Acad. Sci. 2* **1986**, *302*, 205. (c) Cassoux, P.; Valade, L.; Kobayashi, H.; Kobayashi, A.; Clark, R.A.; Underhill, A.E. *Coord. Chem. Rev.* **1991**, *110*, 115. (d) Cassoux, P. *Coord. Chem. Rev.* **1999**, *185-186*, 213.

116 Alvarez, S.; Vicente, R.; Hoffman, R. *J. Am. Chem. Soc.* **1985**, *107*, 6253.

117 Shaik, S.S. *J. Am. Chem. Soc.* **1982**, *104*, 5328. (b) McConnell, H.M.; Hoffman, B.M.; Metzger, R.M. *Proc. Natl, Acad. Sci. U.S.A.* **1965**, *53*, 46. (c) Miller, H.S.; Epstein, A.J. *J. Am. Chem. Soc.* **1987**, *109*, 3850. (d) Tanaka, H.; Okano, Y.; Kobayashi, H.; Suzuki, W.; Kobayashi, A. *Science* **2001**, *291*, 285. (e) Bigoli, F.; Deplano, P.; Mercuri, M.L.; Pellinghelli, M.A.; Pilia, L.; Pintus, G.; Serpe, A.; Trogu, E.F. *Inorg. Chem.* **2002**, *41*, 5324. (f) Coomber, A.T.; Beljonne, D.; Friend, R.H.; Brédas, J.K.; Charlton, A.; Robertson, N.; Underhill, A.E.; Kurmoo, M.; Day, P. *Nature* **1996**, *380*, 144. (g) Robertson, N.; Cronin, L. *Coord. Chem. Rev.* **2002**, *227*, 93.

118 For a review on the topic, see: Kalyanasundaram, K.; Grätzel, M. Efficient Photovoltaic Solar Cells Based on Dye Sensitization of Nanocrystalline Oxide Films. In *Optoelectronic Properties of Inorganic Compounds*; Roundhill, D.M., Fackler, J.P., Jr., Eds.; Plenum Press: New York, 1999; Chapter 5.

119 Benesi, H.A.; Hildebrand, J.H. *J. Am. Chem. Soc.* **1949**, *71*, 2703.

120 McMillin, D.R.; Moore, J.J. *Coord. Chem. Rev.* **2002**, *229*, 113.

121 Willison, S.A.; Jude, H.; Antonelli, R.M.; Rennekamp, J.M.; Eckert, N.A.; Bauer, J.A.K.; Connick, W.B. *Inorg. Chem.***2004**, *43*, 2548.

122 Lai, S.-W.; Chan, M.C.W.; Cheung, K.-K.; Che, C.-M. *Inorg. Chem.* **1999**, *38*, 4262.

123 Rakhimov, R.D.; Weinstein, Yu. A.; Lileeva, E.V.; Zheligovskaya, N.N.; Mel'nikov, M. Ya.; Butin, K.P. *Russ. Chem. Bull.* **2003**, *52*, 1150.

124 (a) McFadyen, W.D.; Wakelin, L.P.G.; Roos, I.A.G.; Leopold, V.A. *J. Med. Chem.* **1985**, *28*, 1113. (b) Ratilla, E.M.A.; Brothers, H.M.; Kostic, N.M. *J. Am. Chem. Soc.* **1987**, *109*, 4592.

125 Chen, W.H.; Reinheimer, E.W.; Dunbar, K.R.; Omary, M.A. *Inorg. Chem.* **2006**, *45*, 2770.

126 Cocker, T.M.; Bachean, R.E. *Inorg. Chem.* **2001**, *40*, 1550.

127 Emge, T.J.; Maxfield, M.; Cowan, D.O.; Kistenmacher, T.J. *Mol. Cryst. Liq. Cryst.* **1981**, *65*, 161.

128 Miyasaka, H.; Campos-Fernandez, C.S.; Clerac, R.; Dunbar, K.R. *Angew. Chem. Int. Ed.* **2000**, 39, 3831.

VITA

Eric Wade Reinheimer was born in Mt. Pleasant, MI and later moved at the age of two to Midland, TX where he spent the formative years of his life. In 1989, he and his family moved to southern California where he graduated from Etiwanda High School in 1995. In June of 2000, he received his B.S. degree in Chemistry from California State Polytechnic University, Pomona. In June of 2002, he received his M.S. degree in Chemistry also from California State Polytechnic University, Pomona. He began his doctoral studies under the supervision of Dr. Kim Dunbar at Texas A&M University in July of 2002. He received his Ph.D. in Chemistry from Texas A&M University in December of 2007.

Eric will be moving back to southern California where he will accept a National Institute of Health postdoctoral fellowship under the supervision of Dr. Douglas Rees conducting research on the enzyme nitrogenase at the California Institute of Technology in Pasadena beginning September 1, 2007.

Eric can always be reached at 12311 Daisy Ct., Etiwanda, CA, 91739.